

## PUBLISHER

On Behalf of Textile and Apparel Research  
Application Center

Faruk BOZDOĞAN

## EDITOR IN CHIEF

Arif Taner ÖZGÜNEY  
arif.taner.ozguney@ege.edu.tr

## ASSOCIATE EDITORS

Mehmet KÜÇÜK  
mehmet.kucuk@ege.edu.tr

Pelin SEÇİM KARAKAYA  
pelinsecim@mail.ege.edu.tr

## EDITORIAL BOARD

Ahmet ÇAY

Aslı DEMİR

Gözde ERTEKİN

Hale KARAKAŞ

Hüseyin Aksel EREN

Pınar ÇELİK

## ENGLISH EDITING SERVICE

Mengü Noyan ÇENGEL

## SCIENTIFIC ADVISORY BOARD

Andrej DEMŠAR

Arzu MARMARALI

Bojana VONČINA

Bülent ÖZİPEK

E. Perrin AKÇAKOCA KUMBASAR

Ender BULGUN

Esen ÖZDOĞAN

Hüseyin KADOĞLU

Mirela BLAGA

Nilgün ÖZDİL

Oktay PAMUK

Ozan AVIŇÇ

Peter J. HAUSER

Recep EREN

Rıza ATAV

Savvas G. VASSILIADIS

Turan ATILGAN

## ABSTRACTING / INDEXING

Science Citation Index Expanded (SCIE)

Scopus

WOS

EBSCO

Ulakbim

## TYPESETTING AND PRINTING

AK-MAT Matbaacılık Yayıncılık Kır. Malz. San. Tic. Ltd. Şti  
Barbaros Mah. Refik Tulga Cd. No: 13, Bornova – İzmir  
akmatlimited@gmail.com Tel: 0 232 444 28 23

Printed Date: 29 June, 2022

**The Relief Effects of Thermoplastic Structured-Shrunken  
Yarns on Woven Fabrics**

Elif Kurtuldu Dönmez, Nesrin Önlü ..... 87

***Bacillus aryabhatai* SMNCH17-07 Strain: First Isolation and  
Characterization from Textile Wastewater with Evaluation of Its  
Decolorization Ability against Azo Dyes**

Safiye Elif Korcan, Kübra Çitekçi, Büşra Aydın,  
Ahmed Badri Abed, Gülderen Uysal Akkuş ..... 99

**Effects of Age, Body Region and Mineral Contents on the Fleece  
Characteristics of Central Anatolian Merino Sheep**

Sedat Behrem, Mahmut Keskin, Sabri Gül, Engin Ünay, Abdülkadir Erişek ... 108

**Flame Retardant and Antibacterial Coating on Cotton Fabric by  
Layer-by-Layer Assembly With Huntite-Hydromagnesite,  
Ammonium Polyphosphate, Chitosan and Aptes**

Nurhan OnarÇamlıbel, Emre Koç ..... 115

**Design and Development of an Innovative Test Device Capable of  
Automatically Performing Carpet Static Loading Tests**

Maher Alsayed, Hatice Kübra Kaynak, Halil İbrahim Çelik ..... 126

**Optimizing the Material-Product Transformation Processes  
in the Clothing Manufacturing Line**

Mehmet Küçük, Meral İşler, Mücella Güner ..... 135

**Effects of Different Stitch Types and Stitch Combinations  
on the Seam Bursting Strength and Seam Strength of Workwear**

Sukran Kara ..... 146

**Performance characteristics in textile application of  
photochromic dye capsules**

Seniha Morsümbül, E. Perrin Akçakoca Kumbasar ..... 155

**Investigation of Performance Characteristics of 3D Printing  
Textiles in Terms of Design and Material**

Fatma Bulat, Fatma Nur Başaran ..... 166

**The Usage of Carbon-Based Filament Yarns in Different Forms  
in the Design of Textile Reinforced Concrete Structures**

Mutlu Kurban, Osman Babaarslan, İsmail Hakkı Çağatay ..... 173

## CONTACT


Ege Üniversitesi Tekstil ve Konfeksiyon Araştırma-Uygulama Merkezi  
35100 Bornova – İzmir, TÜRKİYE  
Tel: +90 232 311 38 89-83

www.dergipark.gov.tr/tektstilvekonfeksiyon  
E-mail: tektstilkonfeksiyon@mail.ege.edu.tr



# The Relief Effects of Thermoplastic Structured-Shrunken Yarns on Woven Fabrics

Elif Kurtuldu Dönmez<sup>1</sup>  0000-0001-7118-9574

Nesrin Önlü<sup>1</sup>  0000-0003-4674-3179

<sup>1</sup>Dokuz Eylül University / Faculty of Fine Arts / Textile and Fashion Design Department / Izmir / Türkiye

**Corresponding Author:** Elif Kurtuldu Dönmez, deu.elifkurtuldu@gmail.com

## ABSTRACT

This study aims to investigate the relief effects on woven fabrics by using heat-sensitive thermoplastic-shrink yarns and different yarn types together. The purpose of examining the relief effects is to create innovative surfaces and increase aesthetic value in the design of woven fabrics with yarns that gain permanent shape by shrinking with heat treatments. In line with the purpose, first of all, thermoplastic yarns and the studies carried out in this context, the fabrics produced were examined. The information gained was evaluated within the scope of woven fabric design, and relief effect woven fabrics were designed within the scope of a theme. Before the production process of the main fabric designs, preliminary research fabrics were woven for the selection of the appropriate yarn type, weaving structure, and knitting that will create the relief effects in the designs in the most accurate way. With the data obtained from the preliminary research, yarn, woven, and woven fabric structures were determined for fabrics and main designs and production calculations were made. After weaving production, all fabrics were heat-treated to create permanent relief effects after being removed from the loom. The relief effects seen in all fabrics after heat treatment were evaluated in terms of both structural and theme-related appearance by relating the type of yarn used in the production of fabrics, weaving, and woven structure.

Evaluations were also made according to the numerical and visual data determined during the design and production process. The preliminary research results and the descriptions of the main fabrics are discussed under the relevant sections, and their contributions to the design and production process are stated in the conclusion section. In the production process of the fabrics, dobby weaving techniques were used in the preliminary research fabrics, and jacquard weaving techniques were used in the production of the main fabrics. Single-layer, self-connecting double-layer, and double-layer bag structures were used as woven fabric structures. The yarns used are thermoplastic yarns that are heat sensitive and cotton and polyester yarns that do not heat sensitive. In the design and application works considered as interior textiles; in addition to thermoplastic yarns, the effects of non-thermoplastic yarns in terms of relief were also observed in terms of aesthetic quality and structure. In addition to the use of thermoplastic yarns with non-thermoplastic yarns, the desired aesthetic relief effects have been achieved with the combination of weaving structures, weave, and yarn density selected depending on the designs revealed in line with the themes of the fabrics.

It is thought that the study will contribute to the development of innovative perspectives in terms of function and aesthetics in creating relief effects in woven fabric design with the use of thermoplastic and non-thermoplastic materials, and weaving techniques.

**To cite this article:** Kurtuldu Dönmez E, Önlü N. 2022. The relief effects of thermoplastic structured-shrunken yarns on woven fabrics. *Tekstil ve Konfeksiyon*, 32(2), 87-98.

## ARTICLE HISTORY

Received: 15.12.2020

Accepted: 19.04.2022

## KEYWORDS

Woven fabric, shrinking, thermoplastic, heat treatment, relief

## 1. INTRODUCTION

From past to present, textiles have different usage areas and visuality depending on the changing structures of societies such as belief, ethnicity, geography, socio-economic status. Textiles are produced with three basic techniques: weaving, knitting, and non-woven surfaces. Among these techniques, weaving is the most commonly used production technique in textiles.

In both the functionality and visual appearance of textiles, the elements such as raw materials, color, weave, technique, and finishing processes are the main factors in creating difference and innovation. The physical and chemical properties of the yarns used in woven fabrics have important effects on the usage function and visual appearance. These effects may differ according to the raw material of the yarns. Many properties of the yarns, such as twisting properties, fineness and thickness, color, being transparent and opaque, make significant contributions to the visuality of the fabrics. They can give different visuals of aesthetic quality to fabrics. These different visual effects also contribute to the diversification of usage areas. For example, weaving fabric samples that created relief effects by using twisted yarns in different directions were exemplified in detail by Ann Richards [1]. In the first fabric, Z twisted yarn in the warp and weft, in the second fabric Z twisted yarn in the warp, S twisted yarn in the weft, in the third fabric S twisted yarn in the weft and warp, and the last fabric S twisted yarn in the warp and Z twisted in the weft was used (Figure 1).

Depending on the raw material of the yarns, chemical properties such as felting, shrinking, and dyeing are also effective in the usage function and visual appearance of woven fabrics. "Increasing raw material demand due to industrial development and the industrial revolution brought along the efforts of developing alternative raw materials and thus produced man-made fiber" [2]. The discovery and development of man-made fibers and their reactions as a result of the applied finishing processes have provided functional and visual diversity in the design and production of woven fabrics. For instance, shibori is the most known technique for both dimensional and visual appearance on woven fabrics. In Figure 2, a three-dimensional and colorful shibori-weaving by Brachmann is seen.

One of the important properties of man-made fibers is that they are sensitive to heat. This property of man-made fibers is called thermoplastic property and is also referred to as thermoplastic fibers and yarns in the sources. In other words, these yarns are the yarns that change their shape after heat treatment and have the potential to maintain these forms. Thermoplastic yarns are also called heat-sensitive or shrink-yarns in the textile industry. In this study, this yarn is referred to as a thermoplastic shrink yarn depending on the applications made. The reason for the use of this term is to differentiate "the finishing process, such as the bleaching, felting, or shrinking effect of the fiber depending on the elastane property" [4]. Another reason; it is to describe the relief effect that occurs as a result of 'finishing processes such as bleaching, felting, shrinking applied after weaving, depending on the elastane feature of the yarn' [4].



Figure 1. Different twisted yarns' effects on woven fabrics [1].

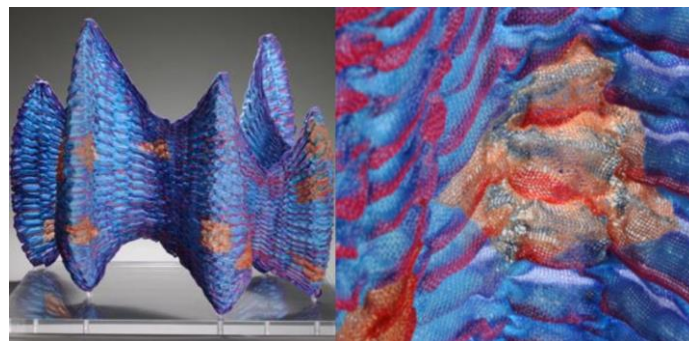


Figure 2. 'Folded Currents', Heat treatment and shibori-woven technique, Holly Brackmann, 2008 [3].



The use of thermoplastic-shrinkable yarns in the design and production of woven fabrics has provided permanent relief effects on the fabrics. Such relief effects have brought woven fabrics to different visual appearances with an innovative perspective. Due to their raw material, the thermoplastic structured- shrunken yarns can be melted at different temperatures and can maintain their permanence when the dry heat is removed. The reasons for the use of thermoplastic yarns in the design and production of woven fabrics; the infinite diversification of the material and technique, the possibility of an unlimited design, is an innovative material, low cost, functionality, and performance can be improved. In the 1960s, textile materials and techniques have become used as an art form. Especially in the 1970s, the Japanese designers reinterpreted fabrics produced from thermoplastic yarns. These fabrics can be considered as the best examples of the combination of traditional techniques and technology in the cooperation of arts and crafts concepts. Reiko Sudo, who has made great efforts in weaving fabrics with relief and volume effects using thermoplastic yarns, has also signed many innovative designs with Nuno Corporations [Figure 3].



**Figure 3.** ‘Jellyfish’ fabric with thermoplastic yarn by Reiko Sudo, 1994 [5].



**Figure 4.** ‘Pleats Please’ pleated fabrics by Issey Miyake, 2012 [6].

Structures with many different relief effects, natural or artificial; take place at every point of life, and with the formation of modern design consciousness, the idea of simple, effective, functional design shapes aesthetics and tastes [7]. The reflections of this situation are also seen in the design and production of woven fabrics in textiles. “Design and manufacture of woven fabrics with relief effects with thermoplastic yarns reached the highest level with the search for alternative surfaces and forms in the 1980s” [5]. In 1981, the Japanese designers provided to highlight man-made fibers by forming thermoplastic fibers with textile techniques and technology. Moreover, they

brought an aesthetic approach with innovative surfaces. “In general, they have concentrated on fabric design rather than form in their collections and integrated the fabrics with minimal garment forms providing to express their high technology and aesthetic properties” [5]. By the end of the 20th Century, “thermoplastic structured fibers such as acetate, triacetate, polyamide, polyester, polypropylene, polyurethane elastomer” [8] brought fabrics to very different dimensions in terms of functionality and visuals combined with technology and art.

In the 21st century, fabrics made from thermoplastic yarns have been redesigned with a creative and innovative perspective. In the production of these new designs, fiber, yarn, weaving techniques, and finishing processes were used together. This different approach brought the industry and art cooperation to the highest point in weaving design. One of these creative and innovative approaches is relief effects. Relief effects also have an outstanding place in the design of woven fabrics in terms of aesthetics and technique. Because relief effects carry woven fabrics to an innovative and distinctive visuality. “Relief is defined as embossing of surface and divided into four groups as low and high relief, either inwards or outwards” [9]. Another definition of relief is as follows, apart from the definition that is identified with the art of sculpture in plastic arts: “Relief is the method of creating figures on the surface by leaving some parts hollow and some parts embossed” [10]. The relief effect is also the effect of light on embossed surfaces. It is the shadow effect that reveals deeply. The higher the voluminous areas on the woven fabric surface, the greater the depth of light and shadow, and the greater the relief effects [2].

Within the scope of art and design, relief is characterized as a form of texture and surface formation, especially in architecture and sculpture. Relief in the design of woven fabrics; is expressed as voluminous and fluffy surfaces created by the combination of yarn, weave, density, and weaving techniques. In relief effect woven fabrics, light is an important factor in the perception of fluffy and voluminous effects. Light-dependent shadow effects can change the perception of relief effects. In this change, the use of yarn type, weave, density and weaving technique parameters is also important depending on the design. Depending on these parameters, the greater the difference between the indentation and protrusion in the created relief, the greater the depth of light and shadow. The smaller the difference between indentation and protrusion, the less depth of light and shadow. These increases and decreases will cause different relief effects on the surface of woven fabrics. On the other hand, depending on the aforementioned parameters, the flexibility and softness of the fabric are of great importance in the formation of the relief effect.

To create a relief effect in woven fabrics, woven structures are the most used among the parameters mentioned above. These woven structures are multi-layered, reinforced, pile, pleated, pique structures. Also the weave in woven fabric structures reveals effects such as relief, contrast, volume,

vibration, opacity, and shine [11]. Structural features of yarns such as twisting direction, short and long fibers are also important in creating a relief effect. At the same time, properties such as heat shrinkage and shrinkage processes, which depend on the chemical properties of the raw material of the yarns, are also effective issues in creating a relief effect in woven fabrics.

In woven fabrics, the heat sensitivity feature of the thread creates the embossed effect with thermoplastic threads. In addition to thermoplastic threads, different types of threads should be used in fabrics. When heat treatment is applied to fabrics in which thermoplastic yarns are used, bulky relief effects occur on the surface depending on the design of the fabric and the production parameters used. These voluminous relief effects create different visual aesthetic qualities on the fabric surface. Elsasser explained the physical and chemical properties of the yarns are affecting the design in terms of relief and volume in her book named 'Textiles: Concepts and Principles' [12].

In the light of all pieces of information, the study aims to examine the relief effects to be obtained by using thermoplastic yarn in the design and production of woven fabrics in terms of aesthetic visual effects that will occur in connection with creativity. The main reason why thermoplastic yarns are preferred to create a relief effect is that they can take permanent shape with heat. During the research phase of the subject, sectoral studies and publications on this subject were examined and read. In all accessible sources, it has been observed that the effects such as volume and relief obtained by applying heat treatment to fabrics woven with thermoplastic yarns are not examined in detail in terms of aesthetic visuality concerning design and creativity. In the available resources, studies on the use of elastane yarn and felt to add volume to the fabric with the use of different materials have been reached. Regarding thermoplastic yarns, it has been seen that fabrics with finishing processes such as pleating and embossing and double-layered woven fabrics are mentioned. A detailed scientific study has not been found about the relief, volume, and sizing that occur depending on the structure and weave of the fabric with the use of heat-sensitive thermoplastic yarns in woven fabrics.

For this reason, it is thought that the study will guide those who will work in the field of aesthetic visual effects created by heat-sensitive thermoplastic yarns in the design of woven fabrics.

## 2. MATERIAL AND METHOD

Within the scope of this study, 7 preliminary research fabrics and 12 main fabrics were designed and produced to investigate the effects of thermoplastic yarns and relief in woven fabrics. Before the main fabric designs and production, seven preliminary research fabrics were designed and produced to observe the different relief effects of the thermoplastic yarn depending on the weave, woven technique, density, and material variables. After the heat

treatment results of the preliminary research fabrics were evaluated, the main fabrics were designed and produced.

Pre-research fabrics were produced on a 55 cm wide, metal, handloom with 24 heald shafts. The main material used in fabrics is threads of thermoplastic structure. The thermoplastic yarn was used only as weft yarn. The yarns used in the weft are 300-denier polyester shrink yarn, Nm 40/2 cotton yarn, Nm 25/2 cotton yarn, Nm 30 polyester boucle yarn, Nm 50/2 polyester yarn. Nm 50/2 polyester yarn, which is not likely to shrink during heat treatment, was used as a warp thread. Plain, 2/2 twill, 2/2 weft ribs were used as the weave. Material and production information of these samples are given in Table 1. In the tabulation of the standard and variable values used in the study, the work of Acar, Meriç and Kurtuldu structurally was taken as a reference. [4]. The comparison of the appearance of these samples before and after heat treatment in terms of relief effect is given under the title of 'Evaluation of Relief Effects of Preliminary Research Fabrics'.

In the face-to-face meeting with Küçüklerler Tekstil Ticaret Sanayi, it was learned that these yarns are heat-treated with dry hot air between 155-165°C. For this reason, all fabrics were kept in 160°C, dry hot air for 3 minutes from a distance of 10 cm, to shrink them and take their permanent shape.

These patterns were prepared in the computer-aided weaving program and woven on 2400 platinum Somet Staubli Jacquard Loom with three weft yarn groups. In the 12 woven fabrics, 300-denier thermoplastic structured-shrunken yarn, 300 denier polyester non-shrunken yarn, Nm 4 micro polyester chenille yarn, and 1800 denier polyester air texturized yarn were used as weft yarns. As the warp yarn, 150-denier polyester non-shrunken yarn was used.

After evaluating the results of the preliminary research fabrics in terms of relief effects, the design and production of the main fabrics were started. 12 main fabrics were designed. In the main fabrics, 150 denier polyester yarn in the warp, 300 denier polyester yarn in the weft, 300 denier polyester thermoplastic yarn, Nm 4 micro polyester chenille yarn, 1800-denier polyester air-textured yarn were used. Thermoplastic structured yarns; It is only used as weft yarn because it has very thin filaments is less twisted, and has low breaking strength. The main fabrics were woven in a double-layer bag structure on a 2400 platinum Somet-Staubli jacquard loom. The weave of the fabrics was fixed as a plain weave.

The reason why thermoplastic structured-shrunken yarns are used only in weft is that they are not suitable for use as a warp yarn due to their very fine structure and low twist due to their rupture quickly [2]. Due to the results of pre-research fabric samples, the weave is fixed as a plain weave in main fabrics which are designed and prepared for production. The production criteria of the main fabrics are given in Table 2. In the tabulation of the standard and variable values used in the study, the work of Acar, Meriç, and Kurtuldu structurally was taken as a reference. [4]. The comparison of the appearance of these fabrics before and after heat treatment in terms of relief effect is given under the title of 'Design and Production Process of Main Fabrics'.

**Table 1.** Technical information of the pre-research fabric samples

STANDARTS	Weaving technique	Dobby weaving
	Warp yarn	Nm 50/2 polyester non-shrunken yarn
	Warp density	16 threads/cm
	Fabric length	10 cm
Heat treatment details		160 <sup>0</sup> C dry heat air, 3' from 10 cm length for each fabric
VARIABLES	Fabric structure	Single-layer (Sample 1,2,3)
		Double-layer (Sample 4,5,6,7)
	Reed number and change	80/2 (Sample 1,2,3)
		100/2 (Sample 4,5,6,7)
	Weft yarns	300-denier polyester shrunken yarn (Sample 1),
		300-denier polyester shrunken yarn, Nm 40/2 cotton yarn (Sample 2)
		300-denier polyester shrunken yarn, Nm 30 polyester bouclé yarn (Sample 3)
	Warp density	300-denier polyester shrunken yarn, Nm 50/2 polyester yarn (Sample 4)
		300-denier polyester shrunken yarn, Nm 25/2 cotton yarn (Sample 5, 6, 7)
		16 threads/cm (Sample 1,2,3)
	Total weft density	20 threads/cm (Sample 4,5,6,7)
		12 threads/cm (Sample 1)
8 threads/cm (Sample 2,3)		
Weaving structure	20 threads/cm (Sample 4,5,6,7)	
	1/1 plain weave (Sample 1,4,5,6,7)	
	2/2 weft ribs (Sample 2)	
Fabric width on the loom	2/2 twill weave (S direction) (Sample 3)	
	20 cm (Sample 1,2,3)	
	18 cm (Sample 4,5,6,7)	
Warp yarn arrangement	Only shrunken yarn (Sample 1)	
	10 cotton yarn, 2x (4 shrunken yarn, 4 cotton yarn) (Sample 2)	
	16 bouclé yarn, 10 shrunken yarn ( Sample 3)	
	10x(1 polyester yarn, 1 shrunken yarn), 8 polyester ( Sample 4)	
	10x(1 cotton yarn, 1 shrunken yarn), 8 polyester ( Sample 5)	
	20x(1 cotton yarn, 1 shrunken yarn), 2 cotton yarn ( Sample 6)	
	20x(1 cotton yarn, 1 shrunken yarn) ( Sample 7)	

**Table 2.** Technical information of the main woven fabrics

STANDARTS	Weaving technique	Jacquard weaving
	Weaving machine	Somet Staubli Jacquard Loom (2400 hooks)
	Warp yarn	150-denier polyester non-shrunken yarn
	Warp density	66 threads/cm
	Reed number and change	11/6
	Weaving structure	Ground: 1/1 plain
		Structure: double-layer bag-structure
Fabric width on the loom	Border weave: 3/3 ribs	
Fabric length on the loom	170 cm	
Heat treatment detail	50 cm	
	Monforts Ram Toptex/ Monfortex 8000, 155 <sup>0</sup> C, 16m/min (Group 1)	
	Monforts Ram Toptex/ Monfortex 8000, 165 <sup>0</sup> C and 14m/min (Group 2)	
VARIABLES	Weft yarn groups	Monforts Ram Toptex/ Monfortex 8000, 155 <sup>0</sup> C, 16m/min (Group 3)
		Group 1 (Bankiz 1, Kanyon 1, Tsunami 1, Mistral 1)
		300-denier polyester shrunken yarn, Nm 4 micro polyester chenille yarn
	Total weft density	Group 2 (Bankiz 2, Kanyon 2, Tsunami 2, Mistral 2) 300-denier polyester shrunken yarn, 300-denier polyester yarn, Nm 4 micro polyester chenille yarn
		Group 3 (Bankiz 3, Kanyon 3, Tsunami 3, Mistral 3)
Fabric quality	300-denier polyester shrunken yarn, 1800-denier polyester air texturized yarn	
	20 threads/cm (Group 1)	
	21 threads/cm (Group 2)	
	20 threads/cm (Group 3)	
	1/1 (Group 1)	
	4/1 (Group 2)	
	1/1 (Group 3)	

### 3. RESULTS AND DISCUSSION

#### 3.1. Evaluation of Relief Effects of Preliminary Research Fabrics

As a first step, the width and length shrinkage of seven fabrics woven for experimental purposes was observed after weaving and heat treatment. After the weaving process was finished and the fabric was taken off from the loom, it was observed that the fabrics had shrinkage only in the width. After heat treatment was applied to the fabrics, it was determined that there was shrinkage in both width and length. Changes in the dimensions of these samples are given in Table 3. The appearances of the pre-research fabrics before and after the heat treatment are given in Figures 5-11.

If we evaluate the changes after heat treatment, it has been observed that the samples woven in double-layer structure shrunk more than the samples woven in a single-layer structure (Figure 5). Added at the end of the paragraph above the table.

Sample 1, which is given before and after the heat treatment appearances in Figure 5, was woven in a single-layer fabric structure with a plain weave. As a weft yarn, only thermoplastic structured-shrunken 300-denier polyester yarn was used.

It was observed that this sample shrank unevenly as a result of the heat treatment and a clear and regular relief effect could not be obtained (Figure 5-B). The first is the one-to-one binding of the weft and warp threads due to the plain weave used. Therefore, weaving has a dense structure. The second is the use of a second non-thermoplastic yarn in the weft.

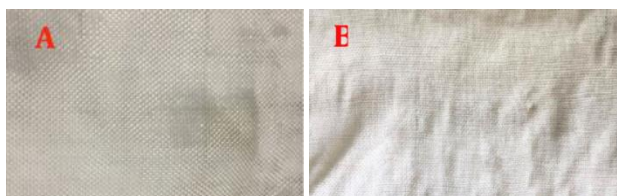


Figure 5. A) Appearance of Sample 1 before heat treatment, B) Appearance of Sample 1 after heat treatment [2].

Sample 2, which is given before and after heat treatment appearances in Figure 6, was woven in a single layer structure with a 2/2 weft ribs. As a weft yarn, thermoplastic structured shrunken 300-denier polyester yarn and Nm 40/2 cotton yarn were used. A high relief effect was observed on the fabric after heat treatment. Despite the single-ply fabric structure, it was concluded that the relief effect on the fabric is due to the use of 2/2 ribs as weave and cotton yarn and thermoplastic polyester yarn as weft yarn.

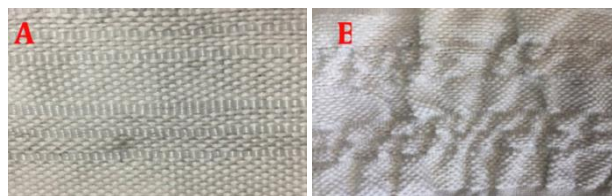


Figure 6. A) Appearance of Sample 2 before heat treatment, B) Appearance of Sample 2 after heat treatment [2].

Sample 3, which is given before and after heat treatment appearances in Figure 7, was woven in a single-layer structure with a 2/2 twill weave. As a weft yarn, thermoplastic structured- shrunken 300-denier polyester and Nm 30 polyester air texturized yarns were used. Despite the single-ply woven structure of the fabric, the use of air-textured and thermoplastic shrinking yarn as weft yarn and 2/2 twill as weave has created high relief effects on the fabric after heat treatment.

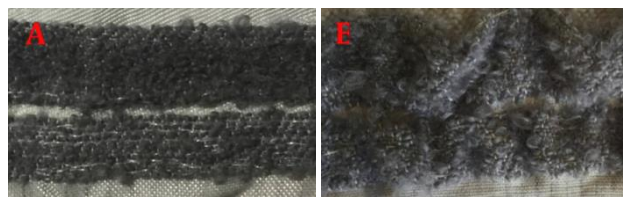


Figure 7. A) Appearance of Sample 3 before heat treatment, B) Appearance of Sample 3 after heat treatment [2].

Sample 4, whose views before and after heat treatment were given in Figure 8, were woven in plain weave. Single and double woven structures were used together in the fabric. The weft yarns used are 300-denier polyester yarn and Nm 50/2 polyester yarn with a thermoplastic structure.

Table 3. Dimensional changes of pre-research fabric samples

Pre-reseach fabric samples' numbers	Fabric width on the loom	Fabric width before heat treatment	Fabric width after heat treatment*
Sample 1	20 cm	19,5 cm	15 cm
Sample 2	20 cm	19,5 cm	16 cm
Sample 3	20 cm	19,5 cm	17 cm
Sample 4	18 cm	17 cm	14,5 cm
Sample 5	18 cm	17 cm	14,5 cm
Sample 6	18 cm	17 cm	14,5 cm
Sample 7	18 cm	17 cm	14,5 cm

\* 160°C heat treatment, 3' from 10 cm length for each fabric



After the fabric is heat-setted, it is seen that the areas where thermoplastic structured-shrunken yarn and polyester yarn are used are straight, but the areas where only polyester yarn is used have a wavy appearance. Another reason for this appearance is the use of single and double-layered structures on the fabric surface with unit repetitions. It is thought that both the fabric structure and the yarn arrangement affect on the formation of high relief effects in the single-ply parts by pulling the thermoplastic shrinking yarn in the double-ply parts by heat treatment.



**Figure 8.** A) Appearance of Sample 4 before heat treatment, B) Appearance of Sample 4 after heat treatment [2].

Sample 5, which is given before and after heat treatment appearances in Figure 9 was woven in both single and double-layer structures with plain weave. Sample 5, whose views before and after heat treatment are given in Figure 9, was also woven as plain weave. Depending on the design of the fabric, single and double woven structures were used together. As a weft yarn, thermoplastic structured- shrunken 300 denier polyester yarn and 25/2 cotton yarn were used. The difference of Sample 5, woven in the same weaving structure with Sample 4, is the use of cotton yarns instead of polyester as weft yarn. When the appearance of the fabric is examined; although the thermoplastic shrink yarn shrunk after the heat treatment and created a relief effect on the fabric, the expected relief effect did not occur due to the thick and hard structure of the cotton yarn. The relief effect is minimal.

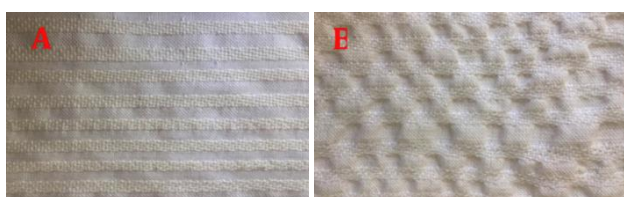


**Figure 9.** A) Appearance of Sample 5 before heat treatment, B) Appearance of Sample 5 after heat treatment [2].

Sample 6, which is given before and after heat treatment appearances in Figure 10, was woven in double-layer and bag structure with plain weave. As a weft yarn, thermoplastic structured- shrunken 300-denier polyester yarn and Nm 25/2 cotton yarn were used. The use of a double-layer bag structure in the fabric gave the fabric a relief effect with a wavy appearance after heat treatment. The combination of double layer and bag structure in the

fabric gave the fabric a wavy appearance and a relief effect after heat treatment. Plain weave has negatively affected the degree of relief despite the double-layered structures. A much lower, irregular relief effect occurred than expected.

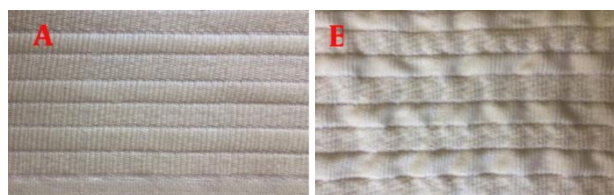


**Figure 10.** A) Appearance of Sample 6 before heat treatment, B) Appearance of Sample 6 after heat treatment [2].

Sample 7, which is given before and after heat treatment appearances in Figure 11, was woven in a double-layer structure with a plain weave. As a weft yarn, thermoplastic-structured shrunken 300-denier polyester yarn and Nm 25/2 cotton yarn were used. The fabric was woven in a double-layered structure by choosing the connection points in diagonal form. Thanks to the regions where the connection points are after heat treatment, wavy relief effects have been formed on the fabric.

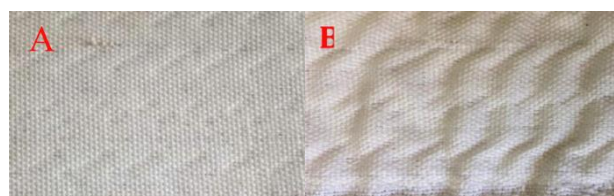


**Figure 11.** A) Appearance of Sample 7 before heat treatment, B) Appearance of Sample 7 after heat treatment [2].

When the relief effects occurred after heat treatment on all fabrics are compared; it has been observed that higher relief effects formed in fabrics woven in a single-layer structure where thermoplastic yarns and non-thermoplastic yarns are used together. With this result, it has been determined that the ratio of thermoplastic shrink yarn used as weft yarn should be at least 50% to obtain a relief effect on woven fabrics. This result also supports the findings in Ann Richards' book "Woven Textiles Shaping Themselves" [1].

When we evaluated the relief effects in terms of weave factor;

- It was determined that the weave factor is also important in the formation of relief.
- It was understood that the use of 2/2 ribs and 2/2 twill weaves caused a higher relief effect than the tightly connected plain weave.
- It was concluded that the lower bonding rates in the weft and warp yarns were effective in the shrinkage rates of the thermoplastic yarn after heat treatment and increased the degree of relief effect.

It is seen that the use of cotton yarn together with thermoplastic yarn in the weft increases the relief effect in plain weave fabrics where single and double layer structures are used together. The use of polyester yarn as the second weft yarn resulted in a low relief effect. It has

been determined that the connection points in double-layer structures are also effective in the degree of relief effect. The effect of the connection points on the relief effect is also valid for the fabrics where double layer and bag structure are used together.

### 3.2. Design and Production Process of Main Fabrics

The first step in the design and production process of main fabrics is the design process. The main fabrics are designed and produced as upholstery or curtains for the interior. During the design process, first of all, current fabric fashion trends were researched. A 'Timeless' collection was created with the idea of a future-oriented approach. The science of biomimetics, which is the science of imitation of nature by human beings, has been integrated with the idea of timelessness, and four themes have been determined under the title of 'Timeless', inspired by the ever-changing but inexhaustible formations of nature. These themes are respectively; it was named Bankiz, Kanyon, Tsunami, and Mistral. Three designs were made for each theme. While determining the inspiration sources of the themes, the relief effects obtained in the preliminary research fabrics were also taken into consideration.

Bankiz-themed designs are based on the view that is formed by the breaking of the 1-2 meter thick ice sheets formed by the freezing of the sea surface in the regions close to the polar points, due to natural or artificial reasons. Kanyon-themed designs are based on the flow of water, which easily passes through layers such as soft soil and limestone, forming a deep, curved valley. In Tsunami-themed designs; Along with the high wave movements on the sea, the environmental changes in the coastal areas as a result of this were also taken into consideration. In Mistral-themed designs; The winds formed by the gradually narrowing movements of the low and high-pressure points have been the source of inspiration.

During the design process, only white and beige colors were used, considering that the color would affect on creating relief. In the designs, relief effects related to light-shadow were aimed to be brought to the fore. Based on the data in the preliminary research fabrics, weave, technique, and material selection were determined with the aim of creating a relief effect depending on light-shadow.

The designs for each theme were produced in four different ways by keeping the density, technique and weave constant, and the yarn factor variable. The yarn properties of the fabrics are given in the method section. The designs were prepared for production in the NedGraphics computer-aided design program. It was sized according to the product type according to material-technical differences.

In the production preparation process; In line with the information obtained from the preliminary research fabrics, the weft and warp densities of the materials to be used were calculated. It was passed through a number 11 comb suitable for a 2400 platinum loom, with 6 warp threads in one heald wire, as 66 threads/cm. Depending on the dimensions of the patterns and the weft insertion order of the yarns used, 2400 platinum numbers were kept constant, but different peak numbers were used. The warp and weft

densities, platinum counts, reed numbers, and reed counts of the 12 fabrics produced are given in Table 2. The reed change count is the count of picks required to complete one repeat of the pattern.

As a result of the design and production of the preliminary research fabrics, it has been observed that the double-ply bag structure is the most effective weaving technique in the formation of relief effects in woven fabrics with the use of thermoplastic yarn. For this reason, a double-layered bag structure was preferred in the main designs. In the areas where these structures are used, plain weave is used and the weave is kept constant. The reason why the weave was chosen as plain is that, based on the data of the preliminary research fabrics, it is desired to obtain a low relief effect on the fabrics with this weave, which has the most frequent connection structure. Weaving structures and weaves used in woven fabrics are given in Table 2.

As a result of the data of the preliminary research fabrics, it was seen that the optimum relief effects were obtained by using a thermoplastic yarn in the weft and different yarn. For this reason, polyester yarn, polyester chenille yarn, polyester air-textured yarn were used together with thermoplastic shrink yarn in the production of main fabrics.

The main fabrics were woven on 2400 platinum Somet Staubli Jacquard Loom. All information of production is given in Table 2, under 'Material and Method'. The heat treatment application was performed on a heat treatment machine named as Monforts Ram Toptex/ Monfortex 8000. A temperature of 155°C at 16m/min was applied to the first and third group fabrics woven with a weft density of 20 threads/cm. The second group of fabrics, woven with a weft density of 21 threads/cm, was heat-treated at 14m/min at 165°C. According to the heat treatment, it was observed that twelve fabrics shrunk by 17,64% and had a permanent shape (Table 4). Since the shrink yarn with thermoplastic structure was used only as weft yarn, shrinkage occurred in the fabrics only in the weft direction. No shrinkage was observed in the warp direction of the fabrics.

Before and after heat treatment appearances of the fabrics produced with three different weft yarn groups are given in Figures 12-23 and relief effects are examined. The first groups of fabrics (Figures 12-15) were woven in double-layer bag fabric structure, 66 threads/cm warp density, 20 threads/cm weft density, 11/6 reed number. As a warp yarn, 150-denier polyester yarn was used. 300 denier polyester shrunken yarn, Nm 4 micro-polyester chenille yarn were used as weft yarns.

After the heat treatment applied to the fabrics in all main fabrics, because of shrinkage of the thermoplastic yarn, the pattern areas in which the double-layered bag structure is used gained volume. In different visuality relief effects have emerged according to their patterns designed depending on the themes of the fabrics. Accordingly, when we examine the visual effects of all fabrics in groups one by one, the results are as described below. Due to the structure of chenille yarn used



as weft yarn, the fabrics have a soft handle. These fabrics are suitable for use as upholstery and curtain fabrics.

Fabrics belonging to the first group are Bankiz 1, Kanyon 1, Tsunami 1, and Mistral 1. The views of the fabric named Bankiz 1 before and after heat treatment are given in Figure 12. The relief effect on the fabric has an amorphous structure depending on the origin of the theme. These amorphous relief views increase or decrease depending on the angle of incidence of light.

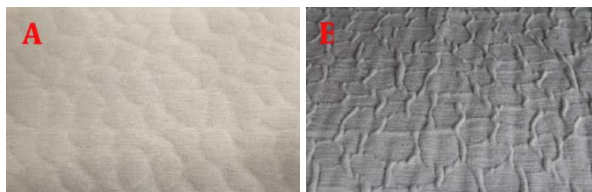


**Figure 12.** A) Appearance of Group 1-Bankiz fabric before heat treatment, B) Appearance of Group 1-Bankiz fabric after heat treatment [2].

The views of Kanyon 1 fabric before and after heat treatment are given in Figure 13. Depending on the theme of the fabric, a relief effect has been achieved giving the appearance of water waves. The wavy relief effect changes shape according to the position of the light.

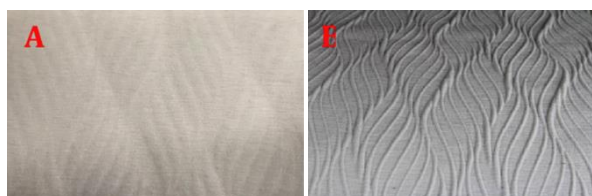


**Figure 13.** A) Appearance of Group 1-Kanyon fabric before heat treatment, B) Appearance of Group 1-Kanyon fabric after heat treatment [2].

The views of Tsunami 1 fabric before and after heat treatment are given in Figure 14. It consists of amorphous triangular patterns with shapes suitable for the relief effect theme of the fabric.

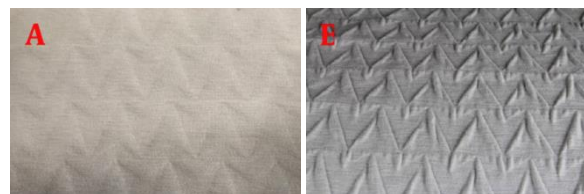


**Figure 14.** A) Appearance of Group 1-Tsunami fabric before heat treatment, B) Appearance of Group 1-Tsunami fabric after heat treatment [2].

The views of Mistral 1 fabric before and after heat treatment are given in Figure 15. The design of the fabric consists of lozenge-shaped patterns in different sizes depending on the theme. The thermoplastic yarn was shrunk after heat treatment, creating a voluminous semi-amorphous relief effect in double-ply bag-structured areas.

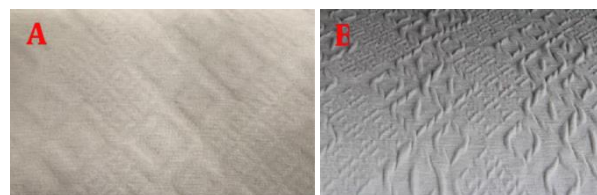


**Figure 15.** A) Appearance of Group 1-Mistral fabric before heat treatment, B) Appearance of Group 1-Mistral fabric after heat treatment [2].

The second group of fabrics (Figures 16-19), were woven in double-layer bag-structured with 66 threads/cm warp density, 21 threads/cm weft density, 11/6 reed number. As a warp yarn, 150-denier polyester yarn was used. 300-denier polyester shrunken yarn, 300-denier polyester yarn, and Nm 4 micro-polyester chenille yarn were used as weft yarns. These fabrics are softer than the first group fabrics due to the 300 denier polyester yarn added as weft yarn. Fabrics belonging to the second group are Bankiz 2, Kanyon 2, Tsunami 2, and Mistral 2.

**Table 4.** Dimensional changes of main fabric designs

Main fabric designs		Fabric width on the loom	Fabric width before heat treatment	Fabric width after heat treatment*
Group 1	Bankiz 1	170 cm	169 cm	140 cm
	Kanyon 1	170 cm	169 cm	140 cm
	Tsunami 1	170 cm	169 cm	140 cm
	Mistral 1	170 cm	169 cm	140 cm
Group 2	Bankiz 2	170 cm	169 cm	140 cm
	Kanyon 2	170 cm	169 cm	140 cm
	Tsunami 2	170 cm	169 cm	140 cm
	Mistral 2	170 cm	169 cm	140 cm
Group 3	Bankiz 3	170 cm	169 cm	140 cm
	Kanyon 3	170 cm	169 cm	140 cm
	Tsunami 3	170 cm	169 cm	140 cm
	Mistral 3	170 cm	169 cm	140 cm

\*155°C, 16m/min for Group 1 and Group 3, 165°C and 14m/min for Group 2.

The views of the fabric named Bankiz 2 before and after heat treatment are given in Figure 16. In the design made depending on the theme of the fabric, the motifs in

amorphous structure have a complex arrangement. The shrinkage of the thermoplastic yarn after the heat treatment

applied to the fabric caused relief effects in the amorphous structure in the double-ply bag structured pattern areas.

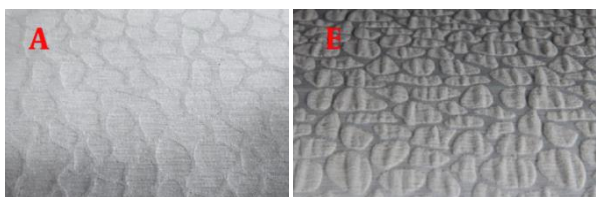


**Figure 16.** A) Appearance of Group 2-Bankiz fabric before heat treatment, B) Appearance of Group 2-Bankiz fabric after heat treatment [2].

The views of the fabric named Kanyon 2 before and after heat treatment are given in Figure 17. In this fabric that has a wavy pattern reminiscent of water waves depending on its theme, double-layered bag areas have gained volume with the shrinkage of the thermoplastic yarn after heat treatment. The fact that the areas in the double-layer bag structure are very dense in the pattern increased the degree of relief effect.

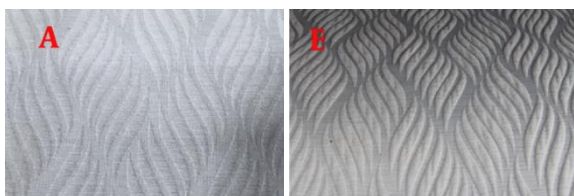


**Figure 17.** A) Appearance of Group 2-Kanyon fabric before heat treatment, B) Appearance of Group 2-Kanyon fabric after heat treatment [2].

The views of the fabric named Tsunami 2 before and after heat treatment are given in Figure 18. After the heat treatment on the fabric with triangular motifs, high relief effects similar to tidal waves were formed in the direction of the fabric's theme.

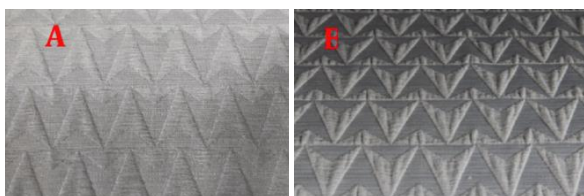


**Figure 18.** A) Appearance of Group 2-Tsunami fabric before heat treatment, B) Appearance of Group 2-Tsunami fabric after heat treatment [2].

The views of the fabric named Mistral 2 before and after heat treatment are given in Figure 19. The design of the fabric consists of lozenge-shaped patterns in different sizes, depending on the theme. The thermoplastic yarn shrank after heat treatment, creating a voluminous semi-amorphous, regular relief effect in the double-ply bag-structured areas.

The third group of fabrics (Figures 20-23), were woven in double-layer bag fabric structure, 66 threads/cm warp density, 20 threads/cm weft density, 11/6 reed number. As a warp yarn, 150-denier polyester yarn was used. 300-denier polyester shrunken yarn and 1800-denier polyester air-texturized yarn were used as weft yarns.

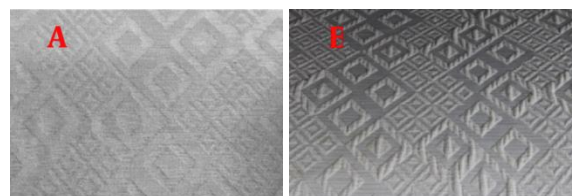


**Figure 19.** A) Appearance of Group 2-Mistral fabric before heat treatment, B) Appearance of Group 2-Mistral fabric after heat treatment [2].

The views of the fabric named Bankiz 3 before and after heat treatment are given in Figure 20. In the design made depending on the theme of the fabric, the motifs in amorphous structure have a complex arrangement. The shrinkage of the thermoplastic yarn after the heat treatment applied to the fabric caused amorphous embossed effects in the double-ply bag structured pattern areas, as in Bankiz 1 and 2 fabrics. After the heat treatment, a very low embossing effect occurred on the fabric as an expected result of the design. This is because the air-textured polyester yarn is used together with thermoplastic yarn in the weft. Air-textured yarn, which is a hard-touched yarn, reduced the shrinkage rate of thermoplastic yarn after heat treatment. The use of plain weave in the areas where air-textured yarn is used has been effective in the degree of low relief effect.

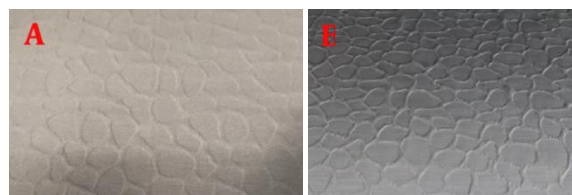


**Figure 20.** A) Appearance of Group 3-Bankiz fabric before heat treatment, B) Appearance of Group 3-Bankiz fabric after heat treatment [2].

The views of the fabric named Kanyon 3 before and after heat treatment are given in Figure 21. The fabric that has a long wavy appearance depending on the design of the fabric has a low relief effect after heat treatment. The fabric that has a long wavy appearance depending on the design of the fabric has a low relief effect after heat treatment. Due to the structure and flatweave of the air-textured yarn used as weft yarn, the fabric has a hard touch and the shrinkage rate of the thermoplastic yarn has decreased.

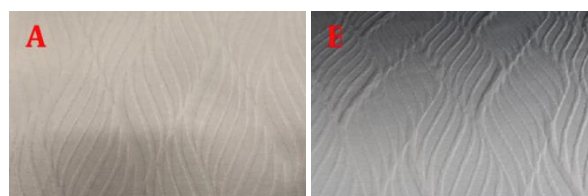


**Figure 21.** A) Appearance of Group 3-Kanyon fabric before heat treatment, B) Appearance of Group 3-Kanyon fabric after heat treatment [2].

The views of the fabric named Tsunami 3 before and after heat treatment are given in Figure 22. After the heat-treatment was applied to the fabric, the relief effect in the double-layered bag structures was very low. The reason for

this is; in addition to the design of the fabric, air textured polyester yarn is used in the weft. Air textured yarn is a tough yarn. Flat weaving is also used in areas where yarn is used. Both factors reduced the shrinkage rate of the thermoplastic yarn and a low relief effect occurred.

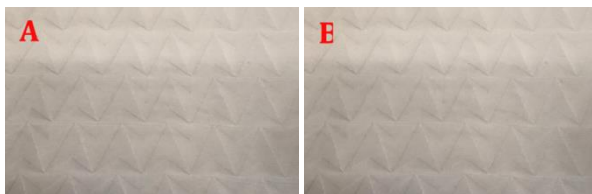


**Figure 22.** A) Appearance of Group 3-Tsunami fabric before heat treatment, B) Appearance of Group 3-Tsunami fabric after heat treatment [2].

The views of the fabric named Mistral 3 before and after heat treatment are given in Figure 23. As with Bankiz 3, Kanyon 3, Tsunami 3 fabrics, the relief effect of Mistral 3 fabric is low relief. In the lozenge-shaped patterns of the fabric, a voluminous, semi-amorphous, irregular relief effect compared to Mistral 2 and 3 was formed in the double-layered bag-shaped areas after heat treatment. The reason for this desired result due to the design of the fabric is that the second yarn used in the weft is air-textured. Another reason is the use of plain knitting in areas where air-textured yarn is used.

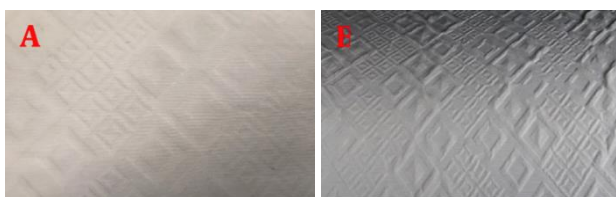


**Figure 23.** A) Appearance of Group 3-Mistral fabric before heat treatment, B) Appearance of Group 3-Mistral fabric after heat treatment [2].

When we evaluate the transition process of fabrics belonging to three groups from design to production, the main aim was to obtain relief effects suitable for the designs made in line with the themes of the fabrics during the transition to production. For this purpose, the yarn type, weaving structure and weave, yarn density, and the degree of heat treatment to be applied were determined by considering the data in the preliminary research fabrics. Production calculations of the main fabrics were made with the determined data.

When we evaluate the fabrics of the three groups in terms of the formation process of the relief effects, it has been observed that the yarns used and the heat treatment applied is of primary importance. Another important factor is the choice of the weave. The selected plain weave, the determined yarn types belonging to each group, gave the right result in obtaining low and high relief effects suitable for the designs depending on the weaving structure.

As a result of these choices, the first layer of the fabric gained volume after the heat-treatment, and relief effects were formed in the pattern areas of the fabrics where thermoplastic yarn is used. No relief effect was observed at

the junction of the 1st and 2nd layers. Bag-structured areas have gained volume thanks to the points where the two layers meet and the shrinking ropes. Depending on the angle of the light, the forms of relief effects are perceived differently. A decrease in the degree of relief effect is observed in the light incident at an angle of 180 degrees.

#### 4. CONCLUSION

With the widespread use of synthetic fibers in the 1940s, heat treatments were applied to create permanent different visual effects on the fabric. Especially Japanese designers played a major role in the 1980s in giving fabrics permanent shapes with different appearances. This movement of Japanese designers has been described as an innovative movement in fabric design. Today, by applying heat treatment to the garment and home textile fabrics in which thermoplastic yarns are used is obtained pleat, relief, volume, etc. texture effects. Designed and produced with the use of thermoplastic yarns with fabrics, especially in fashion; creative solutions are offered to designers in search of innovative materials and forms.

In addition to heat treatment; weaving, fabric structure, raw materials used, density and color are also of great importance in the formation of relief effects in woven fabrics. With the variability of all these factors, an infinite number of fabric types can be provided. In the production of the fabrics designed within the scope of the study, it is aimed that the relief effects created depending on the theme take permanent forms. To achieve this goal, thermoplastic yarns were used in the production of fabrics, and heat treatment was applied after the fabrics were removed from the loom. While creating permanent relief effects, the functionality of the fabrics is also kept in the foreground. In terms of functionality, it is desired that the fabrics can be used for a longer period of time without being deformed during washing and use, depending on the permanent shape they have gained thanks to the use of thermoplastic yarn.

This contributes to the establishment of the concept of slow fashion in home textile fabrics by giving the product a sustainable quality. The aesthetic visual contribution of this function, which enables the use of interior textiles produced with thermoplastic yarns for a longer period; These are the relief effects that change according to the angle of the light, together with the permanent low and high relief effects with an aesthetic texture and voluminous structure. Different appearances due to low and high relief effects together with the angle of the light coming on the surface of the fabric can create more than one aesthetic appearance on the same product. Such appearances will make a difference in terms of visibility in the interior use of fabrics and will be the reason for preference.

In the research phase of the study, first of all, the ability of thermoplastic yarns to take permanent shape with heat treatments in creating relief effects was investigated. Examples from designers working on this subject were examined. The differences in the fabrics of the designers

who produce fabric using thermoplastic yarn have been observed in terms of technical and aesthetic visuality. The information obtained was evaluated together with the factors that were effective in the formation of design and production. With the results of the research, the concepts of design and creativity were evaluated in terms of woven fabrics, and an innovative and aesthetic interpretation that would make a difference was desired to be brought to the designed fabrics.

According to this; for thermoplastic yarns to create aesthetically qualified low and high relief effects on woven fabrics:

- Thermoplastic yarns should be used together with non-thermoplastic yarns,
- The properties of non-thermoplastic yarns such as fineness, thickness, hardness-softness, twist are effective in the permanent shaping of the thermoplastic yarn after heat treatment,
- Fabrics designed with double-layer bag structures have better relief effects than single-layer fabrics,

- It has been concluded that the selected weaves and the determined densities of yarns are the factors that affect the formation of low and high relief effects on the fabric, depending on the fabric structure and yarn type.

In addition to all these results of the study, it is predicted that the effect of colored yarns will create different depth perceptions in these relief-affected weaving fabrics. Thus using the thermoplastic structured-shrunken yarns in woven fabrics and the effect of the color factor in creating these relief effects will carry out the next study.

#### Acknowledgment

The authors wish to thank Pehlivan Mensucat in İzmir and Küçükerler Tekstil in Bursa for their contributions and support about jacquard weaving and heat treatment processes respectively, and Instructor Seyhan Sayar, member of Dokuz Eylül University, Faculty of Fine Arts, Photograph Department for their photograph studio support.


#### REFERENCES


1. Richards, A. 2012. *Weaving textiles that shape themselves*. London: Crowood Press.
2. Kurtuldu, E. 2017. Dokuma kumaş tasarımı ve üretiminde termoplastik yapıli ipliklerle rölyef etkilerinin araştırılması (Master's Thesis). Dokuz Eylül University Institute of Fine Arts, İzmir. Available from [www.tez.yok.gov.tr](http://www.tez.yok.gov.tr) (Thesis Number 469772).
3. Brackmann, H. (2008). <http://www.hollybrackmann.com/2008/Gallery/Details/Folded-CurrentsDetail.html> 19.04.2017
4. Acar, S., Meriç D., Kurtuldu, E. 2019. Pleat effects with alternative material and finishing methods *Journal of Textile and Apparel* 29(1), 41-49.
5. Handley, S. 2000. *Nylon: The story of a fashion revolution*. USA: The Johns Hopkins University Press.
6. Kitamura, M. (ed). 2012. *Pleats Please: Issey Miyake*, Taschen.
7. Yaşar, N. 2008. Kumaş modasında yenilikçi etkiler *Atatürk Üniversitesi Güzel Sanatlar Fakültesi Sanat Dergisi*, 13, 117-127.
8. Özkavruk Adanır, E. 2015. *Tekstil lifleri, özellikleri ve kullanım alanları*. İzmir: Mungan Kavram Press.
9. Huntürk, Ö. 2016. *Heykel ve sanat kuramları*. İstanbul: Hayalperest Press.
10. Sözen, M. Tanyeli, U. 2016. *Sanat kavram ve terimler Sözlüğü*, 16. Press, İstanbul: Remzi Books.
11. Önlü, N., Halaçeli, H. 2005. Dokuma kumaşlarda farklı malzemelerin estetik açıdan oluşturduğu yüzey görünümünün araştırılması, *Tekstil Maraton* 4.
12. Elsasser, V. H. 1997. *Textiles: Concepts and principles*. London: International Thomson Publishing Inc



# ***Bacillus aryabhatai* SMNCH17-07 Strain: First Isolation and Characterization from Textile Wastewater with Evaluation of Its Decolorization Ability against Azo Dyes**

Safiye Elif Korcan<sup>1</sup>  0000-0001-7875-5516

Kübra Çitekeçi<sup>2</sup>  0000-0003-3497-0606

Büşra Aydın<sup>2</sup>  0000-0002-1199-5600.

Ahmed Badri Abed<sup>2</sup>  0000-0002-7803-7917

Gülderen Uysal Akkuş<sup>3</sup>  0000-0002-0790-0170

<sup>1</sup> Uşak Health Training School, Uşak University, 1 Eylül Campus, 64300, Uşak, Türkiye

<sup>2</sup> Department of Molecular Biology and Genetics Department, Faculty of Arts and Sciences, Uşak University, 1 Eylül Campus, 64300, Uşak, Türkiye

<sup>3</sup> Chemistry Department, Faculty of Science and Literatures, Afyon Kocatepe University, 03200, Afyon, Türkiye

**Corresponding Author:** Safiye Elif KORCAN, elif.korcan@usak.edu.tr

## **ABSTRACT**

In this study, SA3 bacterial isolate, has been collected from textile wastewater area in industrial zone located in Uşak province, Turkey. Phenotypic identification and phylogenetic determination on the basis of partial 16S rDNA sequence comparisons indicated that this strain is 100 % *Bacillus aryabhatai* SMNCH17-07. The decolorizing ability of this strain was evaluated against CI Acid Blue 193 CI 15707 and CI Acid Red 88 CI 15620 dyes. The results showed that absorbance rate of Acid Blue 193 by this isolate was (33, 17%) after 216 hours. While Absorbance rate of Acid Red 88 by this isolate was (62,68 %) after 120 hours. According to FTIR spectrometer results of dyes adsorption it was found that bacterial retention sites were possibly aromatic and aliphatic (C = C, C = N, N = N) as well C-O groups. As the first report on the isolation of *Bacillus aryabhatai* SMNCH17-07 strain from textile wastewater with the evaluation of its ability to remove azo dyes, we suggest testing this bacterium as a low cost and ecofriendly bioremediator agent against further harmful dyes and pollutants

## **1. INTRODUCTION**

Dyes are largely entered into various industrial products such as textile, medicinal compounds, body care preparations and etc [1-3]. Usually these dyes have a complex form due to their aromatic nature which increases resistance against biodegradation [4,5]. Around 10,000 diverse dyestuffs are applied in the fabric industry and about 7x10<sup>5</sup> tons per year are manufactured worldwide [6].

Among these dyes, azo dyes are greatly entering into textile manufacturing, and form about 50% of the synthetic dyes used globally [7]. Azo dyes are poisonous, carcinogenic and genetic mutation inducer compounds and found to be harmful to some aquatic life and phototrophs in water due to reduced light penetration which can significantly affect

photosynthetic activity [3,8]. Adsorption, coagulation, flocculation, oxidation and electrochemical methods are usually used for treatment of dyestuffs from wastewater. But several disadvantages are related with these methods such as cost elevation, and the excessive sludge and by-products formation [3,9].

Conversely, biological processes can overcome physical and chemical methods disadvantages and can be more preferable for treating textile effluent due to their low cost, eco-friendly characters, and the low sludge production [10]. Bacterial strains isolated from dye-polluted sites have been demonstrated capability of decolorization and detoxification of azo dyes [11]. Decolorization of indigo carmine, Congo red, Reactive Black5 and reactive blue dyes have been evaluated by using *Streptomyces coelicolor*,

**To cite this article:** Korcan SE, Çitekeçi K, Aydın B, Abed AB, Uysal Akkuş G. 2022. *Bacillus aryabhatai* SMNCH17-07 strain: First isolation and characterization from textile wastewater with evaluation of its decolorization ability against azo dyes. *Tekstil ve Konfeksiyon* 32(2), 99-107.

## **ARTICLE HISTORY**

Received: 05.05.2021

Accepted: 18.07.2021

## **KEYWORDS**

*Bacillus aryabhatai*, azo dyes, decolorization, Acid Blue 193, Acid Red 88

Bacillus sp., *Shewanella oneidensis* WL7 and *Pseudomonas* sp. respectively [9,12-16].

Collecting air from the upper atmosphere by cryotubes was the step that led to the isolation of *Bacillus aryabhatai* for the first time [17]. Since that date few studies have been published on this bacterium and were concentrated in the field of bioremediation, health and the production of biopolymers. [18-22]. Recent published studies pointed that this bacterium can be used as a promise biocontrol source against *Bacillus glumae* [23] as well for producing and identification of biosurfactants associated with the biopharmaceutical products [24]. The attention on *B. aryabhatai* has been increased recently, due to the need of more studies on their genome, characteristics and abilities. Even the classification of this bacterium has been undergone to evaluation. Recent study suggested reclassifying of *B. aryabhatai* Shivaji et al. as a later taxonomic synonym of *Bacillus megaterium* [25].

This study has been notified and published in the list of changes in taxonomic opinion no.32 [26]. Recently Gupta RS et al. depended on the potent phylogenetic and molecular findings, suggested that 17 *Bacillus* species clades should be identified as new genera. This study reclassified *B. aryabhatai* to *Priestia aryabhatai* [27]. Studies about the ability of this bacterium to remove dyes are still very limited. *B. aryabhatai* DC100 ability to decolorize Coomassie Brilliant Blue, Remazol Brilliant Blue R and Brilliant Green was evaluated [28]. *B. aryabhatai* SMNCH17-07 strain was isolated for the first time in 2019 in Peru during the evaluation of the endophytic microbiota of rice cultivation against growth inhibition of *B. glumae* THT strain [29]. This strain was put in NCBI in 2019 under the accession number MK449444 [30]. To our knowledge there's a lack of studies about this strain and we couldn't find a published article pointed to the isolation of this strain from textile wastewater. Hence we are trying in our study to give more information about the characteristics and the abilities of *B. aryabhatai* SMNCH17-07 strain and indicate for the first time to the isolation of this strain from textile wastewater, as well

testing the ability of this strain to remove CI Acid Blue 193 CI 15707 and CI Acid Red 88 CI 15620 azo dyes.

## 2. MATERIAL AND METHOD

### 2.1 Material

Acid Blue 193, Acid Red 88, and Acid Yellow 42 used in the study were obtained from the textile factories of Uşak province (Table 1).

### 2.2 Method

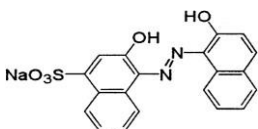
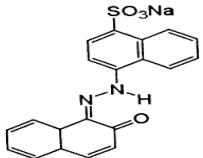
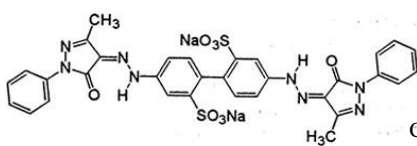
#### 2.2.1. Determination of morphological, physical and biochemical properties of SA3 isolate

Samples of the untreated textile wastewater and activated sludge were collected from textile wastewater sludge area located in Industrial Zone (10 1 10 5) in Uşak province, Turkey. After samples being diluted at 65 ° for 45 minutes in a water bath, the strain has been isolated [31]. Gram staining preparations of the isolated strain have been performed. Their microscopic morphology and whether they formed spores were determined. Growth at different conditions, temperatures (18, 23, 37, 40 °C), pH (4, 7, 10) and 6.5% sodium chloride (NaCl) was evaluated. Also, starch hydrolysis, Voges Proskauer test (VP), catalase and citrate tests have been done.

#### 2.2.2. Molecular identification

High Pure PCR Template Preparation Roche kit was used for DNA Isolation. Purity controls and quantification were performed spectrophotometrically using the Thermo Scientific-Nanodrop 2000c device. As a result, A260 / A280 ratio of 1.5µl DNA sample is aimed. Amplification of the 16S gene fragment was performed using the Taq DNA Polymerase Kit (HelixAmp™). PCR components and quantities of 1 µl primers sequence [11F (5'-GTTTGATCCTGGCTCAG-3') and 1492R (5'-TACGGCTACCTTGTTACGACTT-3')] has been used. The identification of the isolate was processed by analyzing the 16S rRNA gene sequence and comparing it with the existing 16S rRNA sequences present in Genbank and high scoring rRNA sequences in BLAST searches

**Table 1.** Acid Blue 193, Acid Red 88 and Acid Yellow 42 azo dyes used in this study.

Dye name	Open formula	Closed formula	Molecular weight
CI Acid Blue 193, CI15707		C <sub>20</sub> H <sub>13</sub> N <sub>2</sub> NaO <sub>5</sub> S	416.38
CI Acid Red 88, CI15620		C <sub>20</sub> H <sub>13</sub> N <sub>2</sub> NaO <sub>4</sub> S	400.38
CI Acid Yellow 42, CI22910		C <sub>32</sub> H <sub>24</sub> N <sub>8</sub> Na <sub>2</sub> O <sub>8</sub> S <sub>2</sub>	758.69



## 2.2.3. Decolorization experiments

### 2.2.3.1. Detection of decolorization in solid media

After the cultivation of the obtained isolates with coloring medium (starch 10 g/L, nutrient broth 8 g/L, agar 20 g/L, dyestuff 0.15 g/L), decolorization has been evaluated based on the lightening of the color around the colonies after the incubation and the color of the colony that have been taken from the dye [32].

### 2.2.3.2. Decolorization experiment in brouth medium

Bacterial isolates used in the study were inoculated into Luria bertani (LB) brouth medium and incubated at 37 °C. 10 ml of 0.5 McFarland (1.5 10<sup>8</sup> cells/mL) prebacterium culture was inoculated into 90 ml of LB brouth medium containing dye. Incubation was carried out in a shaking at 37 °C and pH7 (optimal conditions for the isolate). Samples taken at regular intervals were centrifuged at 1600 rpm for 25 minutes. The maximum absorbance value of the supernants was read in the spectrophotometer.

The decolorization ability of isolated strain has been tested using 2 different dyes (CI Acid Blue 193, CI15707 and CI Acid Red 88). The peak value of CI Acid Blue 193 dye that we used was determined as 578 nm as a result of UV spectrophotometric measurement and the peak value of CI Acid Red 88 dye was determined as 504 nm. Measurements were made at different dye concentrations to create a standard curve. The decolorization percentage (%) results were calculated using the equations obtained from the standard curve [33]. Decolorization percentage was calculated according to the formula below.

Decolorization percentage (%) = [A0 (initial absorbance) – A (Absorbance after decolorization)] / A0 x 100 [34].

### 2.2.4. FTIR (Fourier Transform Infrared Spectrometer) color removal Analysis

2 mg of sample was weighed with a precision scale and 100 mg of KBr (Potassium Bromide) was added and the mixture was crushed in a mortar and a homogeneous mixture was obtained. This mixture was pressed into thin transparent discs and analyzed by FTIR (SHIMADZU IRAffinity-1S) [35]. Each new section and subsection should have a heading consisting of an arabic numeral followed by a period. Please a single space before and after the section title (see this template).

## 3. RESULTS AND DISCUSSION

### 3.1. Morphological, physiological and biochemical characters of isolate SA3

Isolate SA3 was observed as gram positive (Gr +) central spore forming bacillus. Isolated colony on nutrient agar medium showed a round, straight edges, cream color, shiny-oil and fluff shaped colony (Figure 1). Isolate SA3 used glucose as a carbon source, where it grows very well at temperatures between 18- 40 °C and pH values between

4-10. It has been observed that the isolate can also use fructose, arabinose and sucrose. In this study, it was determined that the optimum development of SA3 isolate was 37 degrees at pH7. Therefore, decolorization studies were carried out under optimum conditions. SA3 strain gave positive results for catalase, NaCl, Voges-Proskauer, starch hydrolysis assays and negative results for the citrate reaction (Table 2).

## 3.2. Molecular identification of SA3 isolate

### 3.2.1. Amplification of 16S rRNA Genes by Polymerase Chain Reaction (PCR)

The SA3 isolate yielded by using primers 11F and 1492R and were clearly determined to have bacteria 16S rRNA

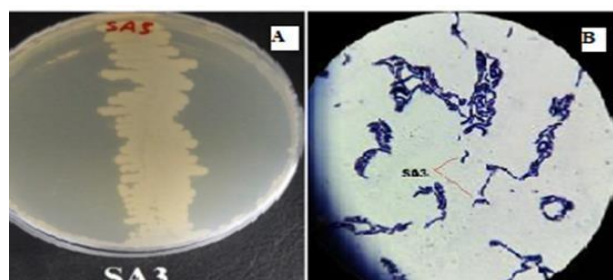


Figure 1. Colony appearance of isolated strain SA3 on nutrient agar (A), and microscopic appearance on 400x (B).

Table 2. Morphological, physiological and biochemical properties of SA3 isolate

Morphological		
Microscopic morphology	Gr (+)	
Spore	Bacil	
Colony color	Central Cream	
Physiological and biochemical properties		
pH	4	+
	7	+++
	10	++
Temperature (°C)	18	+
	23	++
	37	+++
	40	+
Sugar tests	Glucose	+++
	Fructose	++
	Arabinose	++
	Sucrose	++
Biochemical tests	Catalase	+
	Citrate	·
	VP	+
	NaCl	+
	Starch hydrolysis	*

(+) moderate, (++) good, (+++) very good growth

### 3.2.2. Sequence analysis of 16S rRNA genes

BLAST results, similarity ratio of the isolate obtained showed that SA3 isolate belong% 100 to *B. aryabhatai* (Table 3).

**Table 3.** Blast result of isolate SA3

Isolate no.	Length of sequence	Number of matched bases	Nearest in the gene bank	NCBI accession no.
SA3	2134	1155/1155	% 100 <i>Bacillus aryabhatai</i> strain SMNCH17-07	MK449444.1

### 3.3. Decolorization results

#### 3.3.1. Decolorization results in solid media

Growth results of the SA3 isolate in acid yellow, Acid Red 88 and Acid Blue 193 dyes showed a positive result of adsorption for the three dyes (figure 2).

#### 3.3.2. Determination result of the standard curve of Acid Blue 193 and Acid Red 88 Azo dyes

The peak value of CI Acid Blue 193 and CI Acid Red 88 dyes that determined as (578 nm) and (504 nm) as a result of UV spectrophotometric as well the measurements that made at different dye concentrations to create a standard curve are showed in (Figures 3 and 4)

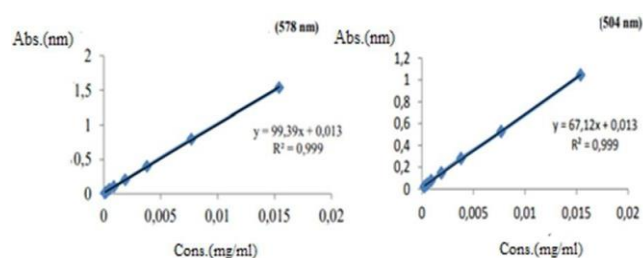
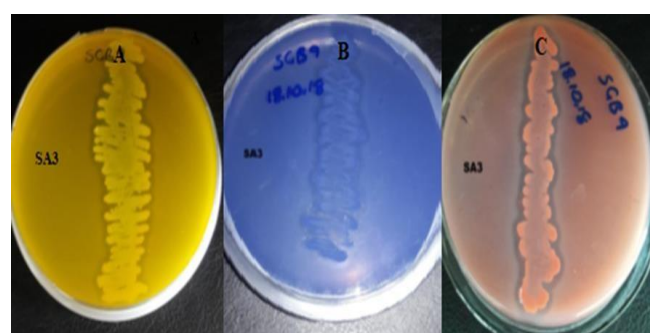


**Figure 3.** Acid Red 88 and Acid Blue 193 dye absorbance-concentration graph



(A) Adsorption on Acid Yellow media (B) Adsorption on Acid Blue 193 media and (C) Adsorption on Acid Red

**Figure 2.** Images of SA3 colonies formed on colored agar

#### 3.3.3. Result of decolorization in LB Medium

The decolorization (%) rate of SA3 isolate used in this study against CI Acid Blue 193 and CI Acid Red 88 at (578 nm) and (504 nm) respectively and at 37 °C depending on time showed that the absorbance value of SA3 isolate against Acid Blue 193 continuously increased in the first 96th hour. It did not increase much later. While the result of the decolorization percentages of Acid Red 88 showed that the absorbance value increased up to (14%) in 24 hours, although the absorbance value increased slightly until the 216th hour (33%) (Table 4). The decolorization rate (%) of SA3 isolate against Acid Red 88 (504 nm) and Acid Blue 193 (578 nm) dyes depending on the time is given in (Figure 5).

**Table 4.** Spectrophotometer readings and decolorization rate (%) by SA3 isolate against Acid Blue 193 and Acid Red 88 dyes

Time (hour)	Acid Blue 193			Acid Red 88		
	Readings on spectrophotometer	Dye concentration	Absorbance (%)	Readings on spectrophotometer	Dye concentration	Absorbance (%)
Control	SA3	SA3	SA3	Control	SA3	SA3
0.80				0.50		
24	0.68	68.10	%14	0.37	25.05	%25
48	0.65	64.92	%17	0.26	17.26	%48
72	0.64	64.02	%18	0.23	15.25	%54
96	0.63	62.83	%20	0.20	13.37	%60
120	0.61	60.94	%22	0.18	12.43	%63
144	0.60	59.65	%24			
168	0.56	56.17	%28			
192	0.54	53.69	%32			
216	0.53	52.49	%33			

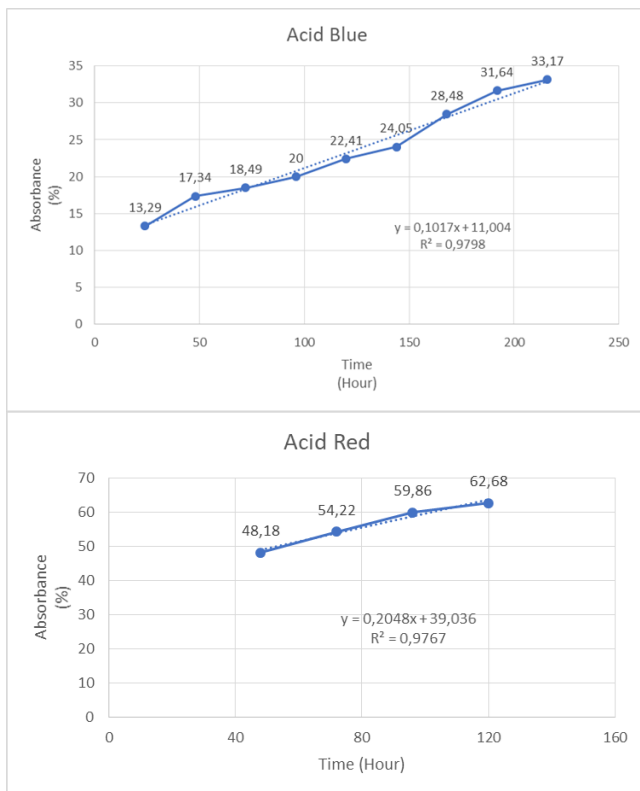


**Figure 6.** Percentage of decolorization of Acid Red 88 and Acid Blue 193 dye at optimum growth conditions

### 3.3.4. Results of color removal analysis with FTIR

FTIR analysis of isolate grown in Acid Red, Acid Blue 193 and Acid Yellow media are shown in (Table 5). Looking at the spectrum of the isolate grown in medium containing Acid Red 88 dye, secondary amine (N-H), (SO<sub>3</sub>Na) and

carbonyl functional group (C=O) at approximately 3400 cm<sup>-1</sup>, 1370 cm<sup>-1</sup>, and 1700 cm<sup>-1</sup> were observed, respectively. Stretching peaks of (-N=N-) belonging to azo groups were seen at approximately 1500 cm<sup>-1</sup>. In addition, stretching vibration peaks were seen for aromatic (C-H) bonds at 1640 cm<sup>-1</sup> and 700 cm<sup>-1</sup> and (C-N) bonds at 1200 cm<sup>-1</sup>.

Growing in medium containing Acid Blue 193 dye showed that the spectrum belongs to the hydroxyl functional group (O-H), sulfonate functional group (S=O) and stretching vibration of azo groups (-N=N-) at approximately 3300 cm<sup>-1</sup>, 1373 cm<sup>-1</sup>, and 1520 cm<sup>-1</sup> respectively. Aromatic (C-H) bonds at 1640 and 700 cm<sup>-1</sup> and stretching vibration of (C-N) bonds at 1200 cm<sup>-1</sup> were observed.

In medium containing acid yellow dye, spectrum was belongs to secondary amine (N-H), carbonyl functional group (C=O), azo groups (-N=N-), sulfonate (SO<sub>3</sub>Na) functional group and aromatic (C-H) bonds at approximately 3520 cm<sup>-1</sup>, 1650 cm<sup>-1</sup>, 1500 cm<sup>-1</sup>, 1372 cm<sup>-1</sup> and 700 cm<sup>-1</sup> respectively. Stretching vibration peaks of (C-N) bonds were seen at 1200 cm<sup>-1</sup>.

When looking at the spectra of the isolates interacted with the Acid Red 88 dye (peak number 2), it was seen that the peak of the secondary amine (N-H) disappeared at 3400 cm<sup>-1</sup>, instead a wide peak of (O-H) stretching was formed. Note that the peak intensity of the carbonyl functional group (C=O) increased at 1700 cm<sup>-1</sup>, and the peak of azo groups (-N=N-) at about 1500 cm<sup>-1</sup> and the peak of (C-N) bonds at 1220 cm<sup>-1</sup> disappeared. When compared to the isolate control spectrum given by the number 3 in the spectrum, it was determined that the isolate adsorbed the Acid Red 88 dye (Figure 6).

**Table 5.** FTIR analysis of SA3 isolate

Acid Red		Acid Blue		Acid Yellow	
Functional group	(cm <sup>-1</sup> )	Functional group	(cm <sup>-1</sup> )	Functional group	(cm <sup>-1</sup> )
Secondary amine (N-H)	3400	Hydroxyl group (OH)	3410	Secondary amine (N-H)	3400
(SO <sub>3</sub> Na) group	1070	Sulfonate group (S=O)	1064	Carbonyl group (C=O)	1650
Carbonyl group (C=O)	1700	(-N=N-) group	1520	Azo group (-N=N-)	1520
Azo group (-N=N-)	1500	Aromatic bonds (C-H)	1649-700	(SO <sub>3</sub> Na) group	1068
Aromatic bonds (C-H)	1640-700	(C-N) stretching	1396	Aromatic bonds (C-H)	1640-700
(C-N) stretching	1220			(C-N) stress vibration	1276

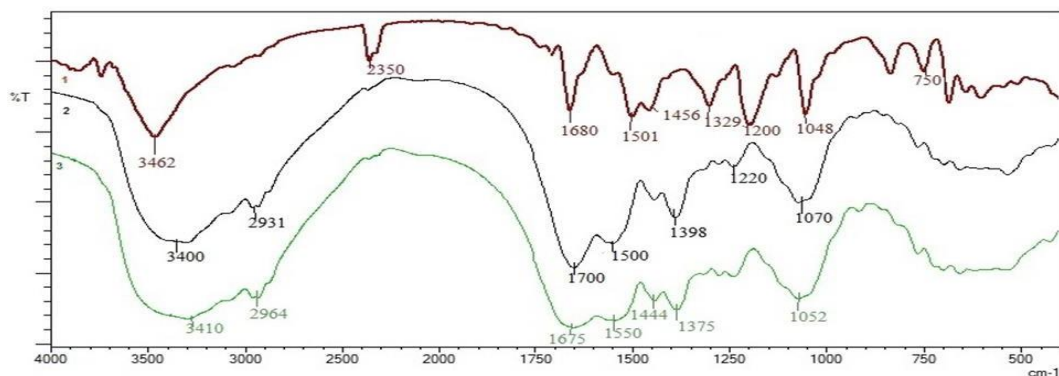


**Figure 6.** FTIR analysis of SA3 isolate Acid Red 88 (product) dye, (1) Acid Red 88, (2) Acid Red 88 dye adsorbed by the isolate (3) isolate itself

When looking at the spectra of the isolates interacted with Acid Blue 193 dye (peak number 2), the increase in the intensity of the peaks of  $3410\text{ cm}^{-1}$  dehydroxyl functional groups (O-H), the formation of new peaks of the carbonyl functional group (C=O) at  $1649\text{ cm}^{-1}$  were observed.

It was also observed that the peak of azo groups ( $-\text{N}=\text{N}-$ ) at approximately  $1520\text{ cm}^{-1}$  and the peak of (C-N) bonds seen at  $1064\text{ cm}^{-1}$  disappeared. When compared to the isolate control spectrum given by number 3 in the spectrum, it was determined that the isolate adsorbed the Acid Blue 193 dye (Figure 7).

When looking at the spectra of the isolates interacted with the Acid Yellow dye (peak number 2), it was seen that the peak of the amine (N-H) at  $3400\text{ cm}^{-1}$  disappeared and instead a wide peak of the hydroxyl functional group (O-H) was formed.

The intensity of the peak of the carbonyl functional group (C=O) increased at  $1650\text{ cm}^{-1}$ , and the disappearance of the peaks of the azo functional groups ( $-\text{N}=\text{N}-$ ) at about  $1520\text{ cm}^{-1}$  indicated that the azo bonds were broken and interacted with the isolate from here. Again, looking at the spectrum, it was noteworthy that the stress vibration band of the C-N bonds seen at approximately  $1068\text{ cm}^{-1}$  disappeared. When compared to the isolate control spectrum given by the number 3 in the spectrum, it was

determined that the isolates adsorbed the Acid Yellow dye (Figure 8).

#### 4. DISCUSSION AND CONCLUSION

Wastewater of textile factories is released to the nature containing many toxic materials and dyestuffs including azo dyes which considered as harmful synthetic compounds [36]. Toxicity of azo dyes is attributed to their chemical composition which contains

$-\text{N}=\text{N}-$  bond besides the presence of aromatic rings which gives these dyes strong persistency in nature particularly in the water ecosystem [37,38].

Due to cost effectiveness and environmentally friendly approaches, microbial processes have been chosen to reduce the damage to humanity. *Bacillus* sp. is a remarkable bacterium with a high potential to produce various metabolites in different uses, it has been investigated whether they can potentially degrade crystal violet dye at different concentrations and time intervals. Fewer studies have reported that *Bacillus* species collected from textile industry wastewater can break down crystal violet dye used in these industries [39].

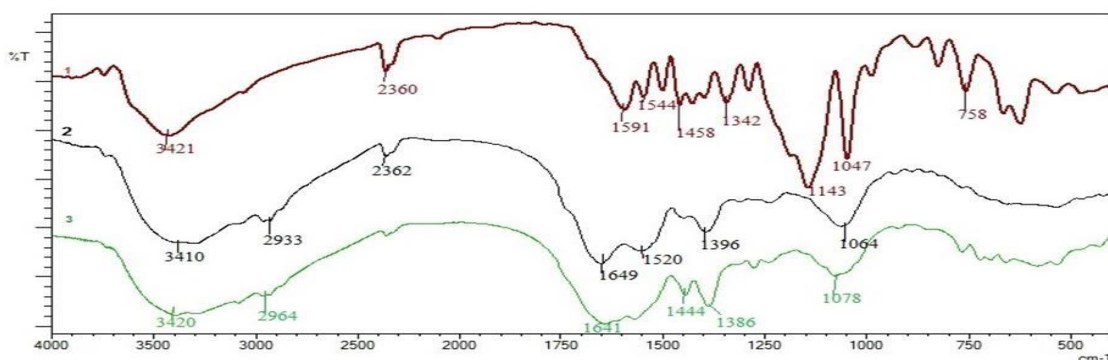


**Figure 7.** FTIR analysis of SA3 isolate and Acid Blue 193 (product) dye, (1) Acid Blue 193, (2) Acid Blue 193 adsorbing by the isolate), (3) isolate itself

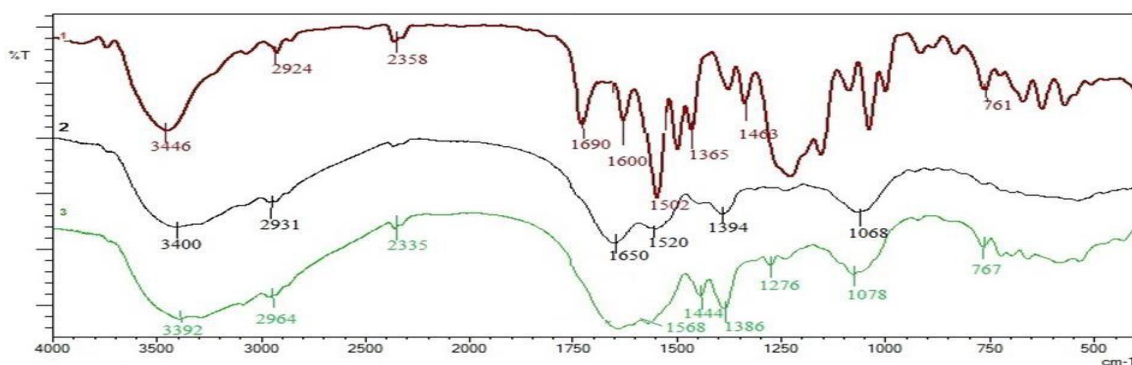


**Figure 8.** FTIR analysis of SA3 isolate and Acid Yellow (product) dye, (1) Acid Yellow, (2) Acid Yellow adsorbed by the isolate, (3) isolate itself



Recently, an interest towards *Bacillus aryabhatai* has been increased noticeably. Recent articles reported to the wide characters and abilities of novel strains belong to this bacterium. In our study SA3 strain which belongs to *B. aryabhatai* found to grow very well at (18-22) °C and the best growth value was in range between 37-40 °C. This result reveals the ability of this bacterium to live under a wide range of temperature. This can go with the findings that indicated to the ability of this bacterium to grow in different environments such as the stratosphere layer at an elevation between 27 and 41 km [17], the soil of Tibet at the elevation of 4123 m [40], the agricultural soil in India [41], and rhizosphere soil in South Korea [42,43].

Varieties in biochemical reactions have been observed also, since in our study SA3 strain revealed + result to Voges–Proskauer which is similar to *B. aryabhatai* EF 114313T, from Shivaji et al. (2009) which isolated from Upper atmosphere [17], but different from *B. aryabhatai* P1 isolated from poultry farm soil and from *Bacillus aryabhatai* FACU isolated from agroindustrial zone which found negative to Voges–Proskauer [44,45]. Evaluation of *B. aryabhatai* in degradation of pollutants including dye stuffs has been reported but in limited studies. This bacterium with its efficient enzymes was described as a multi-functions bacterium. It has been recommended in using for industrial purposes as a converter of lignocellulosic wastes into by products, a biodegrader of textile dyes and also as a biotransformer of effluents phenolics into add-value flavors and aromas [28,46,47]. Recent study proposed the usage of *B. aryabhatai* FACU3 as a bioremediator of glyphosate in pollutant sites [45].

Certain strains of *B. aryabhatai* has been tested against different types of dyes. These dyes included Direct Red-81 (DR-81) and Direct Orange-34 (DO-34) [44], Coomassie Brilliant Blue G-250 (CBB), Indigo Carmine (IC) and Remazol Brilliant Blue R (RBBR) [48], chrysoidine G, acid orange 74, carmine, crystal violet, etythrosine, reactive blue 19 and adizol black B [49]. Some studies reported that certain enzymes of *B. aryabhatai* found to be involvement efficiently in decolorizing of azo dyes [49,50].

The application of live cells is highly advantageous as both biosorption and biodegradation mechanisms may occur, often leading to enhanced dye removal. But the decolorization time will be long. Rapid decolorization of

dead cell lysates has lower saturation points due to the electrostatic interaction of cationic or anionic dye molecules with negatively charged functional groups present on biomass (e.g., amino, carboxyl, hydroxyl, and phosphate) [51]. For this reason, live bacterial isolate was used in our study.

In our study two new azo dyes have been tested which are CI Acid Blue 193 and CI Acid Red 88. Our results showed that the absorbance value of the CI Acid Blue 193 dye by SA3 isolate was 17.34% in the first 48 hours, but it was increasing in a low fixed degree until the 216th hour.

While the absorbance value of CI Acid Red 88 dye reached 48.18%, a very high increase, within 48 hours and the increase rate continued until the 120th hour.

This difference in absorbance values by SA3 isolate towards the two dyes depending on time is close to the findings of Rathod and Pathak (2017) who inferred that the absorbance rate (%) by *B. aryabhatai* P1 towards Direct Red-81 was 11.18% within 48 hours and the increase rate continued until the 120th hour which reached to 40.3%. While the absorbance rate (%) towards Direct Orange was 14.51% within 72 hours and was increasing in a low fixed degree until the 144th hour [44]. This indicates that the type of dye and time are factors that may determine the ability of *Bacillus aryabhatai* to removal dyes.

In conclusion we report in this study the first isolation of *B. aryabhatai* SMNCH17-07 strain from textile wastewater as well the evaluation of the ability of this strain to remove CI Acid Blue 193 and CI Acid Red 88 azo dyes. Showing the ability of this strain to remove azo dyes presents biological, low cost and ecofriendly strategy in treatment of harmful dyes. This can add more information about this bacterium which may permits for further studies to test wide range of dyes and pollutants. Moreover, studying the enzymes which involve in bioremediation processes and factors that enhance the activity of these enzymes are also demanded in future studies. Finally, novel strains belong to *Bacillus aryabhatai* are reporting continually and these strains which found in different habitats showed a wide characteristics and abilities under a different scales of conditions. All these facts about this species make it as a promising bacteria that can be applied alone or in synergism with other bacteria in bioremediation of many pollutants.

## REFERENCES





- Kant R. 2012. Textile dyeing industry an environmental hazard. *Natural Science* 04(01), 22-6. DOI:10.4236/ns.2012.41004
- Hossen MZ, Hussain ME, Hakim A, Islam K, Uddin MN, Azad AK. 2019. Biodegradation of reactive textile dye Novacron Super Black G by free cells of newly isolated *Alcaligenes faecalis* AZ26 and *Bacillus* spp obtained from textile effluents. *Heliyon* 5(7), 02068. <https://doi.org/10.1016/j.heliyon.2019.e02068>
- Aksu Z. 2005. Application of biosorption for the removal of organic pollutants. *Process Biochemistry* 40(3-4), 997-1026. <https://doi.org/10.1016/j.procbio.2004.04.008>
- Dellamatrice PM, Silva-Stenico ME, Moraes LAB, Fiore MF, Monteiro RTR. 2017. Degradation of textile dyes by cyanobacteria. *Brazilian Journal of Microbiology* 48(1), 25-31. <https://doi.org/10.1016/j.bjm.2016.09.012>
- Celia MP, Suruthi S. 2016. Textile dye degradation using bacterial strains isolated from textile mill effluent. *Int J Appl Res* 2, 337-41.
- Sathishkumar K, AlSalhi MS, Sanganyado E, Devanesan S, Arulprakash A, Rajasekar A. 2019. Sequential electrochemical oxidation and bio-treatment of the azo dye congo red and textile effluent. *Journal of Photochemistry and Photobiology B: Biology* 200, 111655. <https://doi.org/10.1016/j.jphotobiol.2019.111655>
- Venkata MS, Chandrasekhar RN, Krishna PK, Karthikeyan J. 2002. Treatment of simulated Reactive Yellow 22 (Azo) dye effluents using *Spirogyra species*. *Waste Management* 22(6), 575-82.
- Kurade MB, Waghmode TR, Patil SM, Jeon B, Govindwar SP. 2017. Monitoring the gradual biodegradation of dyes in a simulated textile

- effluent and development of a novel triple layered fixed bed reactor using a bacterium-yeast consortium. *Chemical Engineering Journal* 307, 1026-36. <https://doi.org/10.1016/j.cej.2016.09.028>
9. Guo G, Li X, Tian F, Tian F, Liu T, Yang F, Ding K, Liu C, Chen J, Wang C. 2020. Azo dye decolorization by a halotolerant consortium under microaerophilic conditions. *Chemosphere* 244, 125510. <https://doi.org/10.1016/j.chemosphere.2019.125510>
  10. Cao J, Sanganyado E, Liu W, Zhang W, Liu Y. 2019. Decolorization and detoxification of Direct Blue 2B by indigenous bacterial consortium. *Journal of Environmental Management* 242, 229-37. DOI:10.1016/j.jenvman.2019.04.067
  11. Dubé E, Shareck F, Hurtubise Y, Daneault C, Beauregard M. 2008. Homologous cloning, expression, and characterisation of a laccase from *Streptomyces coelicolor* and enzymatic decolourisation of an indigo dye. *Appl Microbiol Biotechnol* 79(4), 597-603. <https://doi.org/10.1007/s00253-008-1475-5>
  12. Park J., Kim W., Lee Y., Kim J., 2019, "Decolorization of Acid Green 25 by Surface Display of CotA laccase on *Bacillus subtilis* spores", *Journal of Microbiology and Biotechnology*, Vol:29(9), pp:1383-90. <https://doi.org/10.4014/jmb.1907.07019>
  13. Gopinath KP, Murugesan S, Abraham J, Muthukumar K. 2009. *Bacillus* sp. mutant for improved biodegradation of Congo red: Random mutagenesis approach. *Bioresource Technology* 100(24), 6295-300. <https://doi.org/10.1016/j.biortech.2009.07.043>
  14. Wu J, Kim K, Sung N, Kim C, Lee Y. 2009. Isolation and characterization of *Shewanella oneidensis* WL-7 capable of decolorizing azo dye Reactive Black 5. *J Gen Appl Microbiol* 55(1), 51-5. <https://doi.org/10.2323/jgam.55.51>
  15. Kalyani DC, Telke AA, Govindwar SP, Jadhav JP. 2009. Biodegradation and Detoxification of Reactive Textile Dye by Isolated *Pseudomonas* sp. SUK1", *Water Environment Research*, Vol:81(3), pp:298-307. <https://doi.org/10.2175/106143008X357147>
  16. Shivaji S, Chaturvedi P, Begum Z, Pindi PK, Manorama R, Padmanaban DA, Shouche YS, Pawar S, Vaishampayan P, Dutt CBS, Datta GN, Manchanda RK, Rao UR, Bhargava PM and Narlikar JV. 2009. Janibacter hoylei sp. nov., *Bacillus isronensis* sp. nov. and *Bacillus aryabhatai* sp. nov., isolated from cryotubes used for collecting air from the upper atmosphere. *International Journal of Systematic and Evolutionary Microbiology* 59(12), 2977-86. <https://doi.org/10.1099/ijs.0.002527-0>
  17. Ramesh A, Sharma S.K, Sharma MP, Yadav N, Joshi OP. 2014. Inoculation of zinc solubilizing *Bacillus aryabhatai* strains for improved growth, mobilization and biofortification of zinc in soybean and wheat cultivated in Vertisols of central India. *Applied Soil Ecology* 73, 87-96. <https://doi.org/10.1016/j.apsoil.2013.08.009>
  18. Verma DK, Hasan SH, Singh DK, Singh S, Singh Y. 2014. Enhanced Biosorptive remediation of hexavalent chromium using chemotailored biomass of a novel soil isolate *Bacillus aryabhatai* ITBHU02: Process Variables Optimization through Artificial Neural Network Linked Genetic Algorithm. *Ind Eng Chem Res* 53(9), 3669-81. <https://doi.org/10.1021/ie404266k>
  19. Singh Y, Srivastava SK. 2013. "Performance improvement of *Bacillus aryabhatai* ITBHU02 for high-throughput production of a tumor-inhibitory L-asparaginase using a kinetic model based approach. *J Chem Technol Biotechnol* 89(1), 117-27. <https://doi.org/10.1002/jctb.4121>
  20. Singh Y, Gundampati RK, Jagannadham MV, Srivastava SK. 2013. Extracellular L-Asparaginase from a Protease-Deficient *Bacillus aryabhatai* ITBHU02: Purification, Biochemical Characterization, and Evaluation of Antineoplastic Activity In Vitro. *Appl Biochem Biotechnol* 171(7), 1759-74. DOI: 10.1007/s12010-013-0455-0
  21. Tanamool V, Imai T, Danvirutai P, Kaewkannetra P. 2013. An alternative approach to the fermentation of sweet sorghum juice into biopolymer of poly-β- hydroxyalkanoates (PHAs) by newly isolated, *Bacillus aryabhatai* PKV01. *Biotechnology and Bioprocess Engineering* 18(1), 65-74. DOI:10.1007/s12257-012-0315-8
  22. Valdez-Núñez RA, Ríos-Ruiz WF, Ormeño-Orrillo E, Torres-Chávez EE, Torres-Delgado J. 2020. Caracterización genética de bacterias endofíticas de arroz (*Oryza sativa* L.) con actividad antimicrobiana contra *Burkholderia glumae*. *Revista Argentina de Microbiología* 52(4), 315-27. <https://doi.org/10.1016/j.ram.2019.12.002>
  23. Yaranguppi DA, Deshpande SH, Bagewadi ZK, Kumar S, Muddapur UM. 2021. Genome Analysis of *Bacillus aryabhatai* to Identify Biosynthetic Gene Clusters and In Silico Methods to Elucidate its Antimicrobial Nature. *Int J Pept Res Ther* 27, 1331-1342. <https://doi.org/10.1007/s10989-021-10171-6>
  24. Narsing RMP, Dong Z, Liu G, Li L, Xiao M, Li W. 2020. Reclassification of *Bacillus aryabhatai* Shivaji et al. 2009 as a later heterotypic synonym of *Bacillus megaterium* de Bary 1884 (Approved Lists 1980), *FEMS Microbiology Letters* 366(22), fnz258. <https://doi.org/10.1093/femsle/fnz258>
  25. Oren A, Garrity G, 2022. Notification of changes in taxonomic opinion previously published outside the IJSEM. List of changes in taxonomic opinion no. 35 *International Journal of Systematic and Evolutionary Microbiology* 72(1), 1-3. <https://doi.org/10.1099/ijsem.0.005164>
  26. Gupta RS, Patel S, Saini N, Chen S. 2020. Robust demarcation of 17 distinct *Bacillus* species clades, proposed as novel Bacillaceae genera, by phylogenomics and comparative genomic analyses: description of *Robertmurraya kyonggiensis* sp. nov. and proposal for an emended genus *Bacillus* limiting it only to the members of the *Subtilis* and *Cereus* clades of species. *International Journal of Systematic and Evolutionary Microbiology* 70(11), 5753-98. DOI:10.1099/ijsem.0.004475
  27. Paz A, Carballo J, Pérez MJ, Domínguez JM. 2016. *Bacillus aryabhatai* BA03: a novel approach to the production of natural value-added compounds. *World J Microbiol Biotechnol* 32(10), 159. DOI:10.1007/s11274-016-2113-5
  28. Ríos Ruiz WF, Torres Delgado J, Valdez Nuñez RA. 2020. Selección de microorganismos endofíticos de arroz (*Oryza sativa* L.) con actividad inhibitoria "in vitro" frente a *Burkholderia glumae* en la zona norte del Perú. Universidad Nacional de San Martín – Tarapoto. <http://hdl.handle.net/11458/3677>
  29. National Center for Biotechnology Information, U.S. National Library of Medicine. <https://www.ncbi.nlm.nih.gov>
  30. Katı H, Karaca B, Gülşen ŞH. 2016. Topraktan izole edilen *Bacillus* türlerinin tanımlanması ve biyolojik özelliklerinin araştırılması. *SAÜ Fen Bil Der* 20, 281-90. DOI:10.16984/saufenbilder.04840
  31. Fidan S, Korcan SE, Çiğerci İH, Erdoğan F. 2010. Effects of Some Metals on Laccase, MnP Enzym Activities and Dye Decolorization of *Pleurotus* species. *Electronic Journal of BioTechnology* 1(1), 1-6
  32. El Nembr A, El Sadaawy MM, Khaled A, El Sikaily A. 2014. Adsorption of the anionic dye Direct Red 23 onto new activated carbons developed from *Cynara cardunculus*: Kinetics, equilibrium and thermodynamics. *Blue Biotechnology Journal* 3(1), 121.
  33. Asad S, Amoozegar M, Pourbabae A, Sarbolouki M, Dastgheib S, 2007. Decolorization of textile azo dyes by newly isolated halophilic and halotolerant bacteria. *Bioresource Technology*, 98(11), 2082-2088. <https://doi.org/10.1016/j.biortech.2006.08.020>
  34. Nair RL, Begum D, Ragunathan D. 2017. Biodegradation of Azo Dyes Using *Bacillus megaterium* and Its Phytotoxicity Study. *IOSR Journal of Environmental Science, Toxicology and Food Technology* 11(07), 12-20. DOI:10.9790/2402-1107011220
  35. Pandey A, Singh P, Iyengar L, 2007. Bacterial decolorization and degradation of azo dyes", *International Biodeterioration & Biodegradation* 59(2), 73-84. DOI:10.9790/2402-1107011220
  36. Saratale R, Saratale G, Chang J, Govindwar S. 2011. Bacterial decolorization and degradation of azo dyes: A review. *Journal of the Taiwan Institute of Chemical Engineers* 42(1), 138-57. <https://doi.org/10.1016/j.jtice.2010.06.006>
  37. Lade H, Kadam A, Paul D, Govindwar S. 2015. Biodegradation and detoxification of textile azo dyes by bacterial consortium under sequential microaerophilic/aerobic processes. *EXCLI J* 14, 158-74. DOI: 10.17179/excli2014-642



38. Eva MA, Zerín T, Shomi F.Y. 2020. Microbiological Decolorization of Crystal Violet Dye by Indigenous *Bacillus* spp. Isolated from Garden Soil. *IOSR Journal of Environmental Science, Toxicology and Food Technology* 14(2), 29-34.
39. Yan Y, Zhang L, Yu M, et al, 2016. The genome of *Bacillus aryabhatai* T61 reveals its adaptation to Tibetan Plateau environment. *Genes Genom* 38(3), 293-301. <https://doi.org/10.1007/s13258-015-0366-2>
40. Pailan S, Gupta D, Apte S, Krishnamurthi S, Saha P, 2015. Degradation of organophosphate insecticide by a novel *Bacillus aryabhatai* strain SanPS1, isolated from soil of agricultural field in Burdwan, West Bengal, India. *International Biodeterioration & Biodegradation* 103, 191-5. <https://doi.org/10.1016/j.ibiod.2015.05.006>
41. Park Y, Mun B, Kang S, et al. 2017. *Bacillus aryabhatai* SRB02 tolerates oxidative and nitrosative stress and promotes the growth of soybean by modulating the production of phytohormones. *PLoS ONE* 12(3), 0173203. <https://doi.org/10.1371/journal.pone.0173203>
42. Lee S, Ka J, Song H. 2012. Growth promotion of *Xanthium italicum* by application of rhizobacterial isolates of *Bacillus aryabhatai* in microcosm soil. *J Microbiol* 50(1), 45-9. <https://doi.org/10.1007/s12275-012-1415-z>
43. Rathod MG, Pathak AP. 2017. Efficient decolorization of textile dyes by alkaline protease producing bacterial consortia. *Indian Journal of Geo Marine Science* 47(07), 1468-1477.
44. Nagwa IE, Abdelhadi AA, Rasha HA, Ibrahim S, Ibrahim AA, Gamal O Dalia SA. 2020. *Bacillus aryabhatai* FACU: A promising bacterial strain capable of manipulate the glyphosate herbicide residues. *Saudi Journal of Biological Sciences* 27(9), 2207-14. <https://doi.org/10.1016/j.sjbs.2020.06.050>
45. Paz A, Outeiriño D, Pinheiro de Souza Oliveira R, Domínguez JM. 2018. Fed-batch production of vanillin by *Bacillus aryabhatai* BA03. *New Biotechnology* 40, 186-91. <https://doi.org/10.1016/j.nbt.2017.07.012>
46. Paz A, Costa-Trigo I, Tugores F, Míguez M, de la Montaña J, Domínguez JM. 2019. Biotransformation of phenolic compounds by *Bacillus aryabhatai*. *Bioprocess Biosyst Eng* 42(10), 1671-9. <https://doi.org/10.1007/s00449-019-02163-0>
47. Paz A, Carballo J, Pérez MJ, Domínguez JM. 2017. Biological treatment of model dyes and textile wastewaters. *Chemosphere* 181, 168-77. <https://doi.org/10.1016/j.chemosphere.2017.04.046>
48. Wang F, Xu Z, Wang C, et al. 2021. Biochemical characterization of a tyrosinase from *Bacillus aryabhatai* and its application. *International Journal of Biological Macromolecules* 176, 37-46. <https://doi.org/10.1016/j.chemosphere.2017.04.046>
49. Paz A, Costa-Trigo I, Oliveira RPDS, Domínguez JM. 2020. Ligninolytic Enzymes of Endospore- Forming *Bacillus aryabhatai* BA03. *Curr Microbiol* 77(5), 702-9. <https://doi.org/10.1007/s00284-019-01856-9>
50. Adenan NH, Lim YY, TingY. 2020. Discovering Decolorization Potential of Triphenylmethane Dyes by Actinobacteria from Soil. *Water, Air, & Soil Pollution* 231, 56. <https://doi.org/10.1007/s11270-020-04928-w>

# Effects of Age, Body Region and Mineral Contents on the Fleece Characteristics of Central Anatolian Merino Sheep

Sedat Behrem<sup>1</sup>  0000-0002-7351-1229  
Mahmut Keskin<sup>2</sup>  0000-0002-8147-2477  
Sabri Gül<sup>2</sup>  0000-0001-6787-8190  
Engin Ünay<sup>3</sup>  0000-0002-2648-2250  
Abdülkadir Erişek<sup>3</sup>  0000-0002-4724-0031

<sup>1</sup> Aksaray University, Faculty of Veterinary Medicine, Department of Genetic, Aksaray/Türkiye

<sup>2</sup> Hatay Mustafa Kemal University Agriculture Faculty Department of Animal Sciences, Hatay/Türkiye

<sup>3</sup> International Center for Livestock Research and Training, 06852, Lalahan, Ankara/Türkiye

**Corresponding Author:** Sedat Behrem, sedatbehrem1071@gmail.com / sedatbehrem@aksaray.edu.tr

## ABSTRACT

The fibre characteristics of fleece determine its fate through the textile industry. Parameters such as diameter, length, elasticity and strength define the functional quality of fleece. Therefore, the aim of the present study was to investigate effects of different environmental factors as well as wool mineral contents on fleece fibre quality traits in Central Anatolian Merino sheep (CAM). Additionally, the mineral contents of CAM fleece were investigated. For this purpose, 300 samples were equally collected from 3 different body regions (shoulder, rib and rump) of 100 animals from five different age groups. Samples were analysed for fibre quality (diameter, length, elasticity and strength) traits and mineral contents (calcium, iron, potassium, magnesium, copper, manganese and zinc). A wide range of statistical relationships were found among the focused traits and those factors. The findings of this study highlight the importance of minerals as well as environmental factors on fleece quality parameters.

## 1. INTRODUCTION

Historical use of natural fibres in textile, with the purpose of clothing and protection from severe natural conditions, was recently found to be dating approximately 170.000 years ago and the fibre from the various breeds of sheep (wool) is by far the most commonly-used animal fibre [1, 2]. However, recent sustainability concerns rendered yield and quality to be the two major components of the fibre production for textile purposes. Furthermore, organic fibre production, as a recently focused concept, promotes the use of natural fibres in clothing sector [3]. When the countries producing fleece that is suitable for textile industry are examined, Australia appears to be the major fleece producing country with 24 % of the global fleece production, while China, New Zealand and South Africa follows with 15 %, 10 % and 2.6 %, respectively [4].

As it is widely known, most of the global wool production is sourced from Merino sheep and its crossbreds [5]. Additionally, Merino is considered among the primary sheep breeds that is meeting the fibre quality demands of the textile industry [6]. Merino, with a population size of approximately 3 million of animals and 9453 tonnes of wool produced, is among the major sheep breeds of Turkey that extensively contributes overall meat and fleece production [7]. Crossbreeding Merino with an indigenous sheep breed is currently a popular approach to utilize its productivity as well as fibre quality while increasing the adaptive capacity of the crossbred [5, 8, 9]. It is also expected that the fleece to demonstrate uniformity among different body parts. However, several studies focused on various species previously showed that body parts have significant differences regarding fibre characteristics [10-12].

**To cite this article:** Behrem S, Keskin M, Gül S, Ünay E, Erişek A. 2022. Effects of age, body region and mineral contents on the fleece characteristics of Central Anatolian Merino sheep. *Tekstil ve Konfeksiyon* 32(2), 108-114.

The fibre characteristics of fleece determine its fate through textile industry. Parameters such as diameter, length, elasticity and strength define the functional quality of fleece. Particularly, fibre diameter and length are important factors affecting industrial processing of fleece for textile usage [13]. On the other hand, elasticity and strength are the other factors which alter the efficiency of production as well as the lifespan of the final product [14, 15].

There are several factors contributing fleece yield, quality and uniformity in sheep such as genetic, age, breed, body parts and content of feed [10, 16, 17]. For example, the lack of zinc, copper and amount of mineral matter negatively affects the length and fineness of the fleece. [18-20].

Therefore, the aim of the present study was to investigate the effects of different environmental factors as well as wool mineral contents on fleece fibre quality traits in Central Anatolian Merino sheep. Additionally, the descriptive characteristics of mineral contents of Central Anatolian Merino fleece were determined.

## 2. MATERIAL AND METHOD

### 2.1 Material

Animal procedures were approved by the International Centre for Livestock Research and Training Research Animal Care and Use Committee (29.11.2016/2787-131). The study was carried out on 100 Central Anatolian Merino sheep. It is a crossbred of German Mutton Merino and Akkaraman (White Karaman) sheep, owned by the farmer under the National Community-Based Small Ruminant Breeding Programme in Ankara, Turkey. In total, 300 samples were equally collected from 3 different body regions (shoulder, rib and rump) of 100 animals which belong to five different age groups. 25-50 gr fleece samples were collected from each body region (shoulder, rib and rump) of animals by shearing machine. As routine management practice, the animals used in the study and all other animals in herds are sheared once a year in June. Further details on the study population were given by [21].

### 2.2 Method

The fleece samples were analysed for fibre quality traits and mineral contents in the laboratories of the International Center for Livestock Research and Training. The fibre diameter and length measurements were implemented on OFDA 100 [22]. The analysis of fibre length; the fibres were first aligned and straightened from the one end and placed into the OFDA 2000 device and automatically measured by the optical measuring tool of the instrument in millimetres (mm) [23, 24]. The fibre elasticity and strength were measured on the FAFEGRAPH METM (Textechno, Moenchengladbach, Germany) instrument. Finally, calcium (Ca), iron (Fe), potassium (K), magnesium (Mg), copper (Cu), manganese (Mn) and zinc (Zn) contents were determined using atomic absorption spectroscopy. Additionally, the information on body regions (shoulder, rib and rump) and age were recorded as categorical

variables. Animals were categorized by age in five groups as 1 (<6-month), 2 (12-18-month), 3 (18-30-month), 4 (30-42-month) and 5 (>42-month).

### Statistical Analyses

The descriptive statistics were obtained and presented in Table 1. To estimate the effect sizes of different environmental factors, multiple univariate linear regression analyses were performed for each trait. Subsequently, Duncan's Test were implemented to those significant categorical variables to obtain multiple comparisons among groups [25]. Lastly, Pearson's correlations were obtained between the traits. All statistical analyses were performed using the base packages of R statistical environment [26].

The outliers of the variables (i.e. values exceeding mean  $\pm$  3 x standard deviation) were checked. Primarily, the effects of different environmental factors and covariates were tested to build final linear model with all significant effects for each trait. Subsequently, the linear regression models were fitted with relevant significant factors and covariates to estimate the effect size of body region, age groups, Ca, Fe, K, Mg, Cu, Mn and Zn on diameter, length, elasticity and strength. Normality of the traits were tested with Shapiro-Wilk test. Furthermore, homogeneity of variance was visually inspected by plotting residual vs fitted values of the traits. The linear regression model descriptions for responses are given below:

Model;  $y_{ijk} = \mu + a_i + c_j + b_{ijk} X + e_{ijk}$

Where  $y_{ijk}$  are the observations of the dependent variables (i.e., fibre diameter, length, elasticity and strength);  $\mu$  is the intercept;  $a_i$  is the effect of age groups (5 levels);  $c_j$  is the effect of body regions (3 levels);  $b_{ijk}$  is the regression coefficient of independent variables (mineral contents);  $X$  is the incidence matrix of fixed effects; and  $e_{ijk}$  is the residual error of observations in the models.

## 3. RESULTS AND DISCUSSION

In this study, the characteristics of fleece minerals and the effects of age, body region and fleece mineral contents were investigated on the fibre quality traits of Central Anatolian Merino sheep. With this purpose, regression based statistical analyses were conducted. The responses were checked for the outliers which were removed from further analyses. Descriptive statistics for fibre diameter, length, elasticity, strength and the mineral contents are presented in Table 1. The responses were normally distributed and showed homogenous variance. During the models building stage, all interactions between independent variables were checked and no interaction was found. After the preliminary significance testing, those significant effects suggested in Table 2 were used to build final models for each trait. Accordingly, full models explained 0.21, 0.60, 0.11 and 0.16 of the total variances presents in the fibre diameter, length, elasticity and strength respectively.

The difference between each group for each dependent variable was determined by regression analysis and this

difference was given as effect size in Table 2. The effect sizes obtained in the regression analysis define the difference between groups when all other fix factors in the model are zero. Studies regarding estimation of the effect sizes for age, body region and mineral contents on fibre quality parameters were extremely scarce in the literature, which nominates our study among the very first studies regarding the topics. Therefore, the effect sizes found in our study were evaluated against various correlations and least square estimates of comparable studies where appropriate.

### 3.1 Fleece Mineral Contents

The relevant descriptive statistics were presented in Table 1. The mean Ca content of fleece in the study was found to be 550.40 mg/kg. It Fe content of fibre varies from 13.60 mg/kg to 52.8 mg/kg [30, 31]. The mean Fe content of fleece in this study was found to be 29.34 mg / kg. This falls within the range provided by previous studies. On the other hand, K contents from previous studies were found between 204 and 2499.2 mg/kg [19, 32, 33]. Similarly, the mean K content of fleece in our study drop within this range with 392.16 mg / kg on average. The reports show that Mg content of fleece in sheep has a wide range of 47.8-590.8 mg / kg [19, 32, 33]. In our study, the mean of Mg content was 221.16 mg/kg. The content of Cu and Zn were 3.79 mg/kg and 82.90 mg/kg, respectively. Various studies reported Cu and Zn contents ranging between 1.70 - 25 mg/kg and 18.3 - 336.9 mg/kg respectively, which are consistent with this study [30, 34–36]. Lastly, the content of Mn was found to be 27.61 mg/kg. Previously, studies reported Mn contents higher than [27] and slightly lower than [19] our findings.

The reference range of the mentioned minerals were observed to be extremely varying among different studies. Possible reasons for these discrepancies were suggested to be the condition of pasture (i.e., soil, plant) and the feed type which are known as significantly effective on the mineral content of fleece [16]. Accordingly, the mineral content of fleece is observed in a wide spectrum as seen in our study and previous studies.

### 3.2 Fibre Diameter

In the study, the mean fibre diameter was found as 24.18  $\mu\text{m}$ , which is well suited for textile industry since it is

slightly below than the commonly accepted threshold of 24.6  $\mu\text{m}$  [3]. In Karacabey Merino sheep, Atav et al. [9] reported that the mean of wool diameter as

28.67  $\mu\text{m}$  which is higher than our result. However, the study conducted on Saxon Merino sheep and Anatolian Merino sheep (i.e., Central Anatolian Merino), the fibre diameters were found respectively, as 18.8  $\mu\text{m}$  and 20.08  $\mu\text{m}$  which is significantly lower than our study [37, 38].

The linear regression model was fitted for fibre diameter and the effect of age, body region, Zn content were found to be significant (p- value <0.05). The effect size of age groups was presented on Table 2. According to the results, the intercept for the model was estimated as  $23.26 \pm 0.33 \mu\text{m}$  and the effect sizes of 2., 3., 4. and 5. age groups were  $0.96 \pm 0.41$ ,  $0.47 \pm 0.37$ ,  $0.94 \pm 0.38$  and  $1.31 \pm 0.40 \mu\text{m}$  respectively. The differences between 1-4 and 1-5 groups were found statistically significant (p-value<0.05). The detailed information of multiple comparisons was presented in Table 3. The study conducted by Atav et al. [9] reported that the fibre diameter of younger (0-2 ages) animals is coarser than the elders (above 2 ages). The results of this study correspond to the results of our study. Generally, studies suggest that age significantly affects fibre diameter and increasing age leads to the increased fibre diameter [39].

The effect size of the body regions was estimated and according to the results, the diameter of samples taken from rump was  $1.97 \pm 0.30$

$\mu\text{m}$  higher than the samples taken from shoulder and rib (See Table 2). As shown in the Table 3, while the differences between shoulder- rump and rib-rump were significant (p-value<0.05), the difference between shoulder and rib was not significant. The study conducted on Karacabey Merino sheep found shoulder, rib and rump fibre diameters of 28.46, 28.19 and 29.33  $\mu\text{m}$  respectively [10]. Similar with the current study, the coarser fibre diameter was found for rump and the thinner were found for shoulder and rib. Additionally, a previous study implemented on Anatolian Merino sheep found that the fibre diameter of rump to be coarser the other regions [40].

**Table 1.** Descriptive statistics of the variables.

Variables	N	Mean	sd	Minimum	Maximum
Diameter ( $\mu\text{m}$ )	295	24.18	2.29	19.21	31.01
Length (cm)	299	6.04	1.67	2.50	10
Elasticity (%)	292	24.52	6.44	6.28	42.12
Strength (cN)	286	16.48	4.77	8.17	31.77
Ca (mg/kg)	300	550.40	204.22	122.16	1067
Fe (mg/kg)	196	29.34	25.95	3.40	271.60
K (mg/kg)	299	392.15	4.29	6.93	2945
Mg (mg/kg)	300	221.16	91.27	70.32	476.80
Cu (mg/kg)	288	3.79	3.03	0.60	25.70
Mn (mg/kg)	299	27.61	17.43	0.38	52.93
Zn (mg/kg)	294	82.90	68.80	9.80	383.60

Notes: N=number of observations; SD=standard deviation.

Of the minerals, only Zn was found to be effective on the diameter (p-value<0.05). Results suggests that an increase of one mg Zn in fleece was estimated to decrease 0.005 µm of fibre diameter. The thinner fibre is more demanded for the textile sector and a higher quality woven product is obtained with thinner fleece. In this context, the increase in the Zn content in the fleece reduces the thinness of the fleece and provides a positive effect on the fleece quality. Conversely, the study conducted on Merino sheep the correlation between amount of zinc in fleece and the fibre diameter was 0.68. Furthermore, Zn supplementation to feed was also found to be effective on fibre diameter in the same study. The finding of the study showed that the sheep with additional Zn had higher than control groups [41].

The correlations between the fibre diameter and other quality parameters are presented in Table 4. The correlation between the fibre diameter-length and the fibre diameter-strength were found to be significant (p-value<0.05). Moreover, the correlation values were 0.09 and 0.41, respectively. The correlation between fibre diameter and elasticity was not statistically significant. In a previous study, the correlation between the fibre diameter-length, diameter-elasticity and diameter-strength were found to be 0.54, -0.55 and -0.50, respectively in Merino sheep [40]. However, it is important note that the sample size of that study was significantly lower than our study.

### 3.3 Fibre Length

Descriptive statistics for the fibre length are presented in Table 1. The findings showed that the effects of age, body region, Fe, Mg and Zn on the fibre length were significant (p-value <0.05). The mean of the regression model fitted for length was calculated as 4.18 ± 0.30 cm. Further, the effect sizes of the 2., 3., 4., and 5. age groups were 3.92 ± 0.25, 2.41 ± 0.24, 2.97 ± 0.24 and 2.60 ± 0.24 cm,

respectively. The multiple comparisons among the groups were presented in Table 4. The difference between group 1 and the other groups were found to be significant (p-value <0.05). Similarly, the difference between group 2 and the other age groups are significant (p-value <0.05). However, the difference between the age group 3, 4 and 5 were observed to be statistically insignificant. The group 1 had shorter length and group 2 had longer fibre length. This is probably due to the fact that while shearing is done every 12 months in adult animals (group 3, 4 and 5), this period is limited to a maximum of 6 months in group 1 (lambs) and prolonged to 18 months in group 2 (yearling). In the study of Atav et al. [9], the fiber lengths were longer than the current study, but the differences between the age groups were significant as similar to our study. Likewise, they found that the younger animals had longer fiber than the elders. The possible reason of the different fiber length between the study of Atav and our study may be different genotype and environment.

The effect sizes of the body regions on length were found as 0.23 ± 0.17 and 0.49 ± 0.19 cm for rib and rump, respectively, while the intercept was 4.18 ± 0.29 cm. On the other hand, the difference between shoulder and rump was significant (p-value<0.05), whereas, the difference between shoulder-rib and rib-rump was not significant. The length of fibres was found to be 9.10, 8.92 and 8.67 cm for shoulder, rib and rump, respectively. Similar with our study, the differences between shoulder and rump was found to be significant whereas, the differences of shoulder-rib and rib-rump were not found to be significant in a recent study [10]. In another study implemented on 18 months-old female sheep, the fibre length were 4.77, 4.83 and 4.72 cm for shoulder, rib and rump, respectively and the differences among groups were not significant [40].

**Table 2.** The summary of the sample size, effect sizes and relevant p-values for the analysed traits

Fixed Effects	Diameter (µm)			Length (cm)			Elasticity (%)			Strength (cN)		
	N	Effect size ± SE	P	N	Effect size ± SE	P	N	Effect size ± SE	P	N	Effect size ± SE	P
Age (year)	299		**	299		***	292		***	292		NS
1 (0-6 month)	60	---		60	---		58	---		58	---	
2 (12-18 month)	60	0.96±0.41		60	3.92±0.25		59	2.28±1.15		59	NG	
3 (18-30 month)	60	0.47±0.37		60	2.41±0.24		59	4.80±1.12		59	NG	
4 (30-42 month)	59	0.94±0.38		59	2.97±0.24		57	3.20±1.16		55	NG	
5 (>42 month)	60	1.31±0.40		60	2.60±0.24		59	4.55±1.17		59	NG	
<b>Body regions</b>												
Shoulder	100	---	***		---	***		--	NS		---	***
Rib	100	0.005±0.29			0.23±0.17			2.03±0.89			0.65±0.65	
Rump	100	1.97±0.30			0.49±0.19			-1.04±0.90			3.39±0.70	
<b>Minerals</b>												
Ca (mg/kg)	300	NG	NS	300	NG	NS	300	NG	NS	300	NG	NS
Fe (mg/kg)	196	NG	NS	196	0.013±0.004	**	196	NG	NS	196	0.04±0.01	**
K (mg/kg)	299	NG	NS	299	NG	NS	299	NG	NS	299	NG	NS
Mg (mg/kg)	300	NG	NS	300	-0.003±0.001	*	300	NG	NS	300	-0.01±0.004	***
Cu (mg/kg)	288	NG	NS	288	NG	NS	288	0.29±0.12	*	288	NG	NS
Mn (mg/kg)	299	NG	NS	299	NG	NS	299	NG	NS	299	NG	NS
Zn (mg/kg)	294	-0.005±0.001	**	294	-0.003±0.001	**	294	NG	NS	294	NG	NS
Intercept		23.26±0.33	***		4.18±0.29	***		20.07±1.06	***		17.27±0.96	***
Adj. R-squared		0.18	***		0.59	***		0.11	***		0.16	***

Notes: SE = standard error; N=number of observations; \*\*\*p <0.001; \*\*= p < 0.01; \*= p < 0.05 NS= not significant, NG=not given.

**Table 3.** Multiple comparison of age and body region groups (LSM ± SE)

Groups	Diameter (µm)	Age (months)	Length (cm)	Strength (cN)
		Elasticity (%)		
1 (0-6 month)	23.60 ± 0.29 <sup>b</sup>	3.73 ± 0.09 <sup>c</sup>	21.47 ± 0.86 <sup>b</sup>	16.04 ± 0.60
2 (12-18 months)	24.27 ± 0.27 <sup>ab</sup>	7.25 ± 0.16 <sup>a</sup>	23.97 ± 0.74 <sup>a</sup>	14.59 ± 0.49
3 (18-30 months)	23.98 ± 0.27 <sup>ab</sup>	6.04 ± 0.13 <sup>b</sup>	26.30 ± 0.91 <sup>a</sup>	15.73 ± 0.53
4 (30-42 months)	24.41 ± 0.32 <sup>ab</sup>	6.50 ± 0.18 <sup>b</sup>	24.66 ± 0.81 <sup>a</sup>	16.51 ± 0.59
5 (>42 months)	24.61 ± 0.32 <sup>a</sup>	6.09 ± 0.14 <sup>b</sup>	26.04 ± 0.74 <sup>a</sup>	15.90 ± 0.65
<b>Body Regions</b>				
Shoulder Rib	23.56 ± 0.22 <sup>a</sup>	5.69 ± 0.16 <sup>b</sup>	24.17 ± 0.65 <sup>b</sup>	14.34 ± 0.38 <sup>b</sup>
Rump	23.51 ± 0.22 <sup>b</sup>	5.93 ± 0.16 <sup>ab</sup>	26.33 ± 0.68 <sup>a</sup>	15.21 ± 0.38 <sup>b</sup>
	25.81 ± 0.24 <sup>b</sup>	6.16 ± 0.17 <sup>b</sup>	22.95 ± 0.58 <sup>b</sup>	17.50 ± 0.43 <sup>a</sup>

Notes: SE = standard error.

On the other hand, the regression coefficients of Fe, Mg and Zn contents on the fibre length were found as  $0.013 \pm 0.004$ ,  $-0.037 \pm 0.001$  and  $-0.003 \pm 0.001$  cm, respectively. In other words, one-unit increase in Fe content in fleece provides 0.013 cm increase in fibre length, while one-unit increase in Mg and Zn provides a decrease of 0.037 and 0.003 cm, respectively. In brief, the effect of Fe on the fibre length was favourable, however, the effect of Mg and Zn were negative. The correlation between fleece Zn content and the fibre length was to be 0.60 in Merino sheep [41]. The correlation between fibre length-diameter and the fibre length-elasticity was found to be significant ( $p$ -value<0.05) and was 0.12 and 0.22, respectively. The correlation between fibre length and strength was not found to be significant. On the other hand, they were found as 0.54, -0.11 and -0.30 for length-diameter, length-elasticity and length-strength, respectively in the study of [41]. Unfortunately, no study has been encountered for the effect of Fe and Mg on fibre quality.

### 3.4 Fibre Elasticity

Descriptive statistics of the fibre elasticity is presented in Table 1. In the fitted linear model, age, body regions and Cu were found to be significant ( $p$ -value<0.05). According to the results illustrated in Table 2, the intercept of the model for elasticity was  $20.07 \pm 1.06\%$ . The effect sizes of age groups were found to be 2.28 ± 1.15, 4.80 ± 1.12, 3.20 ± 1.16 and 4.55 ± 1.17% for 2., 3., 4., and 5. age groups respectively. The comparative results of the difference between groups are shown in Table 3. According to these results, the difference between the group 1 and the others were found to be significant ( $p$ -value <0.05). However, no statistically significant difference was found among the other groups. The mean of fibre elasticity according to age group were found to be 19.42, 20.78 and 21.11% for 0-2, 2- 4 and 4-6 years, respectively in the Karacabey Merino sheep and the differences among the groups were not to be significant [10]. Another study conducted on Karakul sheep, the fibre elasticity was found to be 36.67, 37.68 and 37.62% for male lambs, yearling and ewes, respectively [42]. These finding were significantly higher than our study.

On the other hand, the effects of different body parts were  $2.03 \pm 0.89$  and  $-1.04 \pm 0.90\%$  for rib and rump.

Surprisingly, there was no difference between shoulder and rump in body regions, while the difference between shoulder-rib and rib-rump was significant ( $p$ -values

<0.05). [10] reported that the fibre elasticity for shoulder, rib and rump were 20.30, 18.78 and 22.22%, respectively. They found that shoulder-rib and shoulder-rump was not significant, while rib-rump was significant. Besides, [40] showed that shoulder, rib and rump were 28.72, 26.90 and 26.43%, respectively. In the study, only the significances between shoulder and other region were significant.

Among the minerals used in the study, only Cu was found to be statistically effective ( $p$ <0.005) and was added to the fitted model as covariate variable. The regression coefficient of Cu content of fleece was found as  $0.29 \pm 0.12$ . The amount of one-unit increase of the Cu element in the fleece results in 0.29 % of increases on the elasticity of the fleece. In other words, the increase in Cu level in the fleece provides a positive effect on the elasticity characteristic. The correlation between elasticity and other quality features are seen in Table 4. Previous research has illustrated the significant effect of Cu on the hair growth in sheep [18]. As expected, a negative relationship was found between fibre diameter and elasticity (-0.08), but this relationship was not statistically significant. On the other hand, a positive direction (0.23, 0.22), respectively and a statistically significant relationship was found between fibre elasticity-length and fibre elasticity-strength ( $p$ -value <0.05). Moreover, in a previous study the correlation between elasticity-diameter, elasticity-length and elasticity-strength were reported as -0.11, -0.55 and 0.44, respectively [42].

### 3.5 Fibre Strength

The body region, Fe and Mg were found to be effective on the strength where no significant effect was detected for age. The mean of the model is  $17.27 \pm 0.96$  and the effect sizes of the body regions are  $0.65 \pm 0.65$  and  $3.39 \pm 0.70$ , respectively (Table 2). In the multiple comparison of the groups, there was no significant difference between shoulder and rib, but the difference between shoulder-rump and rib-rump were significant ( $p$ -value <0.05).



**Table 4.** Below the diagonal shows the correlations of the traits and above the diagonal shows p-values

Correlations/ Traits	Diameter ( $\mu\text{m}$ )	Length (cm)	Elasticity (%)	Strength (cN)
Diameter ( $\mu\text{m}$ )	---	**	NS	***
Length (cm)	0.09		***	
Elasticity (%)	-0.08	0.23		***
Strength (cN)	0.41	-0.001	0.22	

NS, not significant; \*\*\*= $p < 0.001$ ; \*\*= $p < 0.01$ ; \*= $p < 0.05$

The regression coefficients of Fe and Mg in fleece were found to be  $0.04 \pm 0.01$  and  $-0.01 \pm 0.004$ , respectively, which means that an increase of one-unit in the amount of Fe in the fleece resulted in 0.05 cN increase in fibre strength. However, the same is not true for Mg, one-unit increase in the amount of Mg resulted in -0.01 cN a decrease in fibre strength. The correlations for fibre strength-diameter, strength-length and strength-elasticity were found to be 0.41, -0.001 and 0.22, respectively. While the correlation between fibre strength- diameter and fibre strength-elasticity were found significant ( $p$ -values  $< 0.05$ ), the relationship between strength and length was found insignificant. The study of [40], the correlation was found to be -0.50, -0.30 and 0.44 for strength-diameter, strength-length and strength- elasticity respectively.

#### 4. CONCLUSION

In this study, the relationship between environmental factors such as age, body region and fleece mineral contents and the fleece characteristics were investigated in Central Anatolian Merino sheep. Furthermore, amount of various macro- and microelements in fleece were characterized. A wide range of statistical relationships were found among the focused traits and those factors. Finding of this study highlights the importance of minerals as well as environmental factors on fleece quality parameters. Therefore, the results of our study have a wide range of implications regarding various disciplines such as herd management and textile industry.


#### REFERENCES

1. Toups MA, Kitchen A, Light JE, Reed DL. 2011. Origin of clothing lice indicates early clothing use by anatomically modern humans in Africa. *Molecular Biology and Evolution* 28(1), 29–32.
2. Bahtiyari M, Akça C, Duran K. 2008. Novel Usage of Wool. *Tekstil ve Konfeksiyon* 18(1), 4-8.
3. Van Dam JEG. Environmental benefits of natural fibre production and use. Proceedings of the Symposium on Natural Fibres 3–17. <http://www.fao.org/3/i0709e/i0709e03.pdf>.
4. IWTO. 2020. IWTO's Specifications for Wool Sheep Welfare. <https://iwto.org/wp-content/uploads/2020/05/IWTO-Wool-Sheep-Welfare.pdf>.
5. Ingham VM, Fogarty NM, Gilmour AR, Afolayan RA, Cummins LJ, Gaunt GM, Stafford J, Hocking Edwards E. Genetic evaluation of crossbred lamb production. 4. Genetic parameters for first-cross animal performance. *Australian Journal of Agricultural Research* 58(8), 839–846.
6. Cilek S. 2015. Determination of Fleece Qualities of Malya Sheep (11/16 Akkaraman X 5/16 Deutsches Merinofleischschaf) and Effect of Age and Sex on These Qualities. *Pakistan Journal of Agricultural Sciences* 52(2).
7. TUIK. 2021. Livestock Production, Number of Sheep and Goat. <https://data.tuik.gov.tr/Kategori/GetKategori?p=tarim-111%7B%5C&%7Ddil=1>.
8. Ciani E, Lasagna E, D'andrea M, Alloggio I, Marroni F, Ceccobelli S, Pilla F. 2015. Merino and Merino-derived sheep breeds: a genome-wide intercontinental study. *Genetics Selection Evolution* 47(1), 1-12.
9. Dellal G, Söylemezoglu F. 2000. Anadolu Merinosu Koyunlarının Bazı Yapağı Özellikleri Üzerine Bir Araştırma. *Tarım Bilimleri Dergisi* 6(2), 48–53.
10. Atav R, Gürkan Ünal P, Soysal Mİ. 2020. Investigation of the Quality Characteristics of Wool Obtained from Karacabey Merino Sheep Grown in Thrace Region-Turkey. *Journal of Natural Fibers*. doi: 10.1080/15440478.2020.1795777.
11. Behrem S, Keskin M, Gul S, Unay E, Satilmis M, Unal M, Sacli Y, Erisek A. 2021. Investigation on the Hair Characteristics of Damascus and Kilis Goats. *Journal of Natural Fibers*. doi: 10.1080/15440478.2021.1990173.
12. Olivier JJ, Cloete SWP, Bezuidenhout AG. 1993. Differences in mean fibre diameter and fibre diameter variance in fine wool, strong wool, and fine x strong wool Merino sheep sampled at five body locations. *South Africa Journal of Animal Science* 23(5), 201–203.

13. Botha AF, Hunter L. 2010. The measurement of wool fibre properties and their effect on worsted processing performance and product quality. Part 1: The objective measurement of wool fibre properties. *Textile Progress* 42(4), 227-339.
14. Kaynak HK, Babaarslan O. 2015. Breaking strength and elongation properties of polyester woven fabrics on the basis of filament fineness. *Journal of Engineered Fibers and Fabrics* 10(4).
15. Uyanik S. 2019. A Research on Determining Optimum Splicing Method in Terms of Fiber Types and Yam Count. *Tekstil ve Konfeksiyon* 29(1), 22-29.
16. Sahoo A, Soren NM. 2011. Nutrition for wool production. *Webmed Cent NUTR.* 2(10), 1–11.
17. Hatcher S, Atkins KD, Thornberry KJ. 2005. Age changes in wool traits of Merino sheep in western NSW. In Association for the Advancement of Animal Breeding and Genetics 16, 314-317.
18. Khan MJ, Abbas A, Ayaz M, Naeem M, Akhter MS, Soomro MH. 2012. Factors affecting wool quality and quantity in sheep. *African Journal of Biotechnology* 11(73), 13761-13766.
19. Patkowska-Sokoła B, Dobrzański Z, Osman K, Bodkowski R, Zygadlik K. 2009. The content of chosen chemical elements in wool of sheep of different origins and breeds. *Archives Animal Breeding* 52(4), 410-418.
20. Szigeti E, Kátai J, Komlósi I, Oláh J, Szabó C. 2020. Newly Grown Wool Mineral Content Response to Dietary Supplementation in Sheep. *Animals* 10(8), 1390.
21. Behrem S. 2021. Estimation of genetic parameters for pre-weaning growth traits in Central Anatolian Merino sheep. *Small Ruminant Research* 197. doi: <https://doi.org/10.1016/j.smallrumres.2021.106319>.
22. Baxter BP, Brims MA, Taylor TB. 1992. Description and performance of the optical fibre diameter analyser (OFDA). *Journal of the Textile Institute* 83(4), 507-526.
23. Walker JW, Stewart WC, Pope R, Spear SL, Ebert M, Murphy TW. 2018. Evaluation of mean fiber diameter measurements by FibreLux micron meter and OFDA2000 in Texas and Intermountain west wool. *Small Ruminant Research* 159, 31-37.
24. Behrendt R, Gloag C, Konstantinov K. 2004. Estimates of repeatability for wool traits measured by OFDA2000. *Science Access* 1(1), 216-216.
25. Steel RG, Torrie JH. 1997. Principles and procedures of statistics a biometrical approach. McGraw-Hill:New York.
26. R Core Team. 2020. R: A language and environment for statistical computing. R Foundation for Statistical Computing, Vienna, Austria.
27. Altıntaş A. 1990. Mineral madde metabolizmasına bir bakış. Tarımda kaynak (TAKVA). Tarımsal Kalkınma Vakfı Yayın Organı 1(2), 19-21.
28. Aitken FJ, Cottle DJ, Reid TC, Wilkinson BR. 1994. Mineral and amino acid composition of wool from New Zealand Merino sheep differing in susceptibility to yellowing. *Australian Journal of Agricultural Research* 45(2), 391-401.
29. Kumaresan A, Kapiroh MA. 1984. Hair as indicator of mineral status in Yankassa sheep. *Revue d'élevage et de médecine vétérinaire des pays tropicaux* 37(1), 61-64.
30. Georgievskii VI, Annenkov BN, Samokhin VT. 2013. Studies in the agricultural and food sciences. Mineral nutrition of animals, Elsevier. pp. 321–346.
31. Wojcikowska-Soroczynska M, Sztych D. 1994. Selected microelements in wool of Polish sheep. *Annals of Warsaw Agricultural University. Animal Science* 30, 59-68.
32. Gabryszuk M, Klewec J, Czauderna R, Baranowski A, Kowalczyk J. 2000. The content of mineral compounds in sheep wool depending on the breed and physiological state. *Rocz Nauk Zoot Supplemented* 5, 147–151.
33. Krośnicka-Bombała R. 1996. Influence of a season of the year and a colour on pigment and microelements content in a coat of differently coloured sheep and goats. *Zesz Nauk Przeg Hod PTZ* 23, 117-32.
34. Szigeti E, Kátai J, Komlósi I, Oláh J, Szabó C. 2020. Newly Grown Wool Mineral Content Response to Dietary Supplementation in Sheep. *Animals* 10(8), 1390.
35. Baranowski PIOTR. 2002. Genetic and environmental factors of macroelements concentration in blood serum and osseous tissue of lambs in north-west Poland. *Archives Animal Breeding* 45(6), 565-574.
36. Patkowska-Sokoła B, Dobrzański Z, Bodak E, Panyiotu P, Kołacz R. 2003. Comparative study on the concentration of elements in the wool of sheep of Cyprus and Poland origin. *Chem Agric* 4, 182–189.
37. McGregor BA, Butler KL. 2016. Coarser wool is not a necessary consequence of sheep aging: allometric relationship between fibre diameter and fleece-free liveweight of Saxon Merino sheep. *Animal* 10(12), 2051-2060.
38. Koyuncu M, Tuncel E, Ferik A. 1996. Anadolu Merinosu, Kıvrıkcık, Türkgeldi koyunlarının yapağı verim ve özellikleri üzerine bir araştırma. Uludağ of University. *Journal of Agricultural Science* 12, 101-108.
39. Scobie DR, Grosvenor AJ, Bray AR, Tandon SK, Meade WJ, Cooper AMB. 2015. A review of wool fibre variation across the body of sheep and the effects on wool processing. *Small Ruminant Research* 133, 43-53.
40. Arık İZ, Dellal G, Cengiz F. 2003. Anadolu merinosu, Akkaraman, Ile de France X Anadolu merinosu (F1) ve Ile de France X Akkaraman (F1) Melezi koyunlarda bazı yapağı fiziksel özellikleri. *Turkish Journal of Veterinary and Animal Sciences* 27(3), 651-656.
41. Wyrostek A, Kinal S, Patkowska-Sokoła B, Bodkowski R, Cholewińska P, Czyż K. 2019. The influence of zinc-methionine bioplex supplementation to pregnant and lactating sheep on selected wool parameters. *Archives Animal Breeding* 62(1), 99–105.
42. Erol H, Akçadağ Hİ. 2009. Some production characteristics of Karagül sheep on insitu conditions. *Lalahan Hayvancılık Araştırma Enstitüsü Dergisi* 49(2), 91-104.

# Flame Retardant and Antibacterial Coating on Cotton Fabric by Layer-by-Layer Assembly With Huntite-Hydromagnesite, Ammonium Polyphosphate, Chitosan and Aptes

Nurhan Onar Çamlıbel<sup>1</sup>  0000-0002-2647-4728

Emre Koç<sup>2</sup>  0000-0001-5909-9592

<sup>1</sup> Pamukkale University, Engineering Faculty, Textile Engineering Department, Kinikli Campus, Kinikli, Denizli, Türkiye

<sup>2</sup> Gamateks A.Ş., Denizli, Türkiye

**Corresponding Author:** Nurhan Onar Camlibel, nonar@pau.edu.tr

## ABSTRACT

In this study, it was investigated the coating of cotton fabric with huntite-hydromagnesite (HH) or ammonium polyphosphate (APP) solutions as anionic layer and chitosan solutions and nanosols as cationic layer by layer-by-layer (LBL) assembly to gain flame retardancy and antibacterial properties. Growth bilayer number, drying conditions and anionic layer type (HH or APP) affected the flame retardancy and antibacterial properties of coating with LBL assembly. 17% and 22% reduction in the peak heat release rate and 69% and 87% reduction in total smoke release and 26% and 14% reduction in mass loss rate were observed for fabric samples coated with AP solutions for 15 layers with drying after every dipping process (AP15DE) and fabric samples coated with HH solutions for 15 layers with drying after every dipping process, (H15DE) respectively. Thermogravimetric analysis revealed that the residual chars at 600 °C in air increased. The AP15DE exhibited the antibacterial activity against *E. coli* and *S. aureus* while H15DE displayed the antibacterial activity against only *S. aureus*.

## ARTICLE HISTORY

Received: 01.07.2021

Accepted: 06.12.2021

## KEYWORDS

Huntite-hydromagnesite;  
ammonium polyphosphate;  
flame retardancy; antibacterial;  
layer-by-layer

## 1. INTRODUCTION

Cotton fabric as a type of the most popular natural fibers have been widely used applications in apparel, home textiles, medical textiles, military textiles and industrial textiles due to their excellent properties such as dyeability, hydrophilicity, hygroscopicity, biocompatibility, breathability, comfortableness, warmth retention. However, they suffer from their flammable nature with low oxygen index and ignition temperature, which restricts their application. Meanwhile they ensure living condition for the growth of bacteria due to their hydrophilic and porous surface and affects the health of wearers [1]. Therefore, the manufacture of multifunctional cotton fabrics with antibacterial and flame retardant properties recently attracts great interest.

Huntite ( $Mg_3Ca(CO_3)_4$ ) and hydromagnesite ( $Mg_5(CO_3)_4(OH)_2 \cdot 4H_2O$ ) mixture as flame retardant agent exhibit the endothermic decomposition between 200 and 400 °C and releases water vapor and/or carbon dioxide, which gives rise to fall down of temperature, the dilution of flammable gases and isolation of flame [2-5]. APP as an acid source would collaborate with fabric with necessity additional carbon source such as chitosan to improve the efficiency. Cationic chitosan in acid solution could be paired with anionic APP solution by LBL assembly. Chitosan with nitrogen content and APP with intumescent nature improve the flame retardancy properties of treated materials [6]. Coatings with silica based nanosols could ensure fire protection by forming inorganic barrier. Silica together with nitrogen-based compounds could catalyze the dehydration and carbonization of substrate and decrease the amount of

**To cite this article:** Onar Çamlıbel N, Koç E. 2022. Flame retardant and antibacterial coating on cotton fabric by layer-by-layer assembly with huntite-hydromagnesite, ammonium polyphosphate, chitosan and aptes. *Tekstil ve Konfeksiyon*, 32(2), 115-125.

combustible gases [7, 8]. HH, APP, chitosan and silica instead of halogenous flame retardants with harmful and toxic effects could be proposed as alternative, sustainable flame retardant agents for cotton fabrics.

Various processes such as plasma, microcapsule and UV-curable flame retardant coatings have been improved and studied by most researchers to decrease the combustibility of cotton and/or to achieve its antibacterial activity. But the physical or chemical processes have caused to more difficulties in their industrial applications and/or environmental pollutions. Recently, LBL assembly technique as environmental friendly, simple and low cost due to being water-based technique were investigated to develop multifunctional cotton fabric in academic area and industrial application. The technique is regularly alternating physical deposition of negatively and positively charged nanoparticles or polyelectrolytes on various substrates such as textile fabric. Various flame retardant and antibacterial coatings were applied to textiles with LBL assembly by means of its multiple performances by combining different molecules.

Nonhalogenated flame retardants containing nitrogen, phosphorus and silicon compounds have been researched widely to develop the flame cotton fabrics [9, 10]. Huntite-hydromagnesite [11], APP [6,12-17], chitosan [6,12-15,20,18-26], silica based materials [12,13,25,27-31] were researched to gain flame retardant or antibacterial properties for various textiles by LBL assembly. There are some reports on multifunctional assembly coatings on textiles with flame retardancy and antimicrobial property [1,30,32-37]. The introducing of huntite-hydromagnesite together with APP, APTES and chitosan as antibacterial and flame retardant agent by LBL assembly has not been reported.

In our study, it was recently investigated characterization and manufacturing of flame retardant and antibacterial cotton fabric via layer-by-layer assembly. Anionic charged huntite-hydromagnesite or ammonium polyphosphate solutions and cationic charged chitosan and silica based nanosols has been prepared and coated with 5, 10 and 15 bilayers, substantially. Phosphorous (APP) or CaO and MgO (HH) and silica (GPTMS and APTES), nitrogen (APP, APTES and chitosan) synergism was researched and compared. The cotton fabrics by LBL assembly were structurally characterized by SEM, elemental analysis and FTIR-ATR. Textile characteristics were determined by add-on value, whiteness, tensile strength, elongation. The flame retardancy and thermal behavior of the cotton fabric treated by LBL were studied by limit oxygen index, vertical flame retardancy, cone calorimetry and thermogravimetric analysis (DTA-TG). The antibacterial activity of the fabrics by treated by LBL were measured by bacterial reduction against *E. coli* as gram-positive bacteria and *S.aureus* as gram-negative bacteria.

## MATERIAL AND METHOD

### 2.1 Material

Scoured and bleached cotton fabric (plain weave, 118 g/m<sup>2</sup>, 32 ends/cm, and 22 picks/cm) was used in this research. All chemicals used were of reagent grade. Huntite-hydromagnesite powder (HH, Ultracarb 1250) was supplied from Setas Company, Turkey. Ammonium polyphosphate (APP) were provided by Tecnosintesi SPA, Italy. (3-Amino propyl) triethoxy silane (APTES, Sigma-Aldrich, Germany), (3-Glycidyloxy propyl) trimethoxy silane (GPTMS, Merck KGaA, Germany), chitosan (Mw:50000 Da, the degree of deacetylation: 93.2%, Merck KGaA, Germany), sulphuric acid, glacial acetic acid and sodium hydroxide were used for preparation of solutions in layer by layer coating. GPTMS precursor due to high crosslinking effect to improve coating durability and silica content to develop their flame retardancy and APTES due to silica and ammonium content were utilized to enhance their flame retardancy and antibacterial properties. Tecnosintesi APP is an effective flame retardant with 72.5% of phosphorus content (as P<sub>2</sub>O<sub>5</sub>), low water solubility and 15 µm of average particle size. The APP is proper for solvent and water based intumescent coatings.

### 2.2 Method

Nanosol (CA) containing APTES (aq. 5 w/v%) and GPTMS (aq. 1 v/v%), chitosan aq. solution (CC), huntite-hydromagnesite (aq. 1 w/v%) (AH) and ammonium polyphosphate (aq. 0.2 w/v%) (AA) solutions were prepared and their pH values respectively adjusted to 3.4, 3.5 and 11 with sulphuric acid, glacial acetic acid and sodium hydroxide. AH and AA solutions stirred for 1 hour on magnetic stirrer. The fabric samples were first dipped into cationic solution called CA code containing APTES and GPTMS aqueous solutions for 30 min, rinsed (30 sec) and dried an oven at 100 °C for 15 min. Then the treated fabrics were dipped into anionic solutions called AH or AA codes containing HH or APP aqueous solutions. The fabric was dipped to each solution during 5 min for first layer and 1 min for later layers, rinsed and dried at 100 °C for 15 min. One bilayer (BL) including one cationic and one anionic layer on cotton fabrics was gain in the all assembly cycle process. The first BL was composed of cationic solution containing nanosol (CA code) and anionic solution (AH or AA codes) and the second BL was formed from cationic solution containing chitosan (CC code) and anionic solution (AH or AA codes). The fabric was alternately dipped into anionic and cationic solution until the planned number of bilayers on fabrics was reached [25]. The interactions of cationic and anionic charged chemicals with cellulose were schematically illustrated in Figure 1. Firstly, APTES and GPTMS were reacted with hydroxyl groups on cellulose by hydrolysis and condensation reaction. Then APP, HH and chitosan could be bonded by electrostatical interactions to fabric.

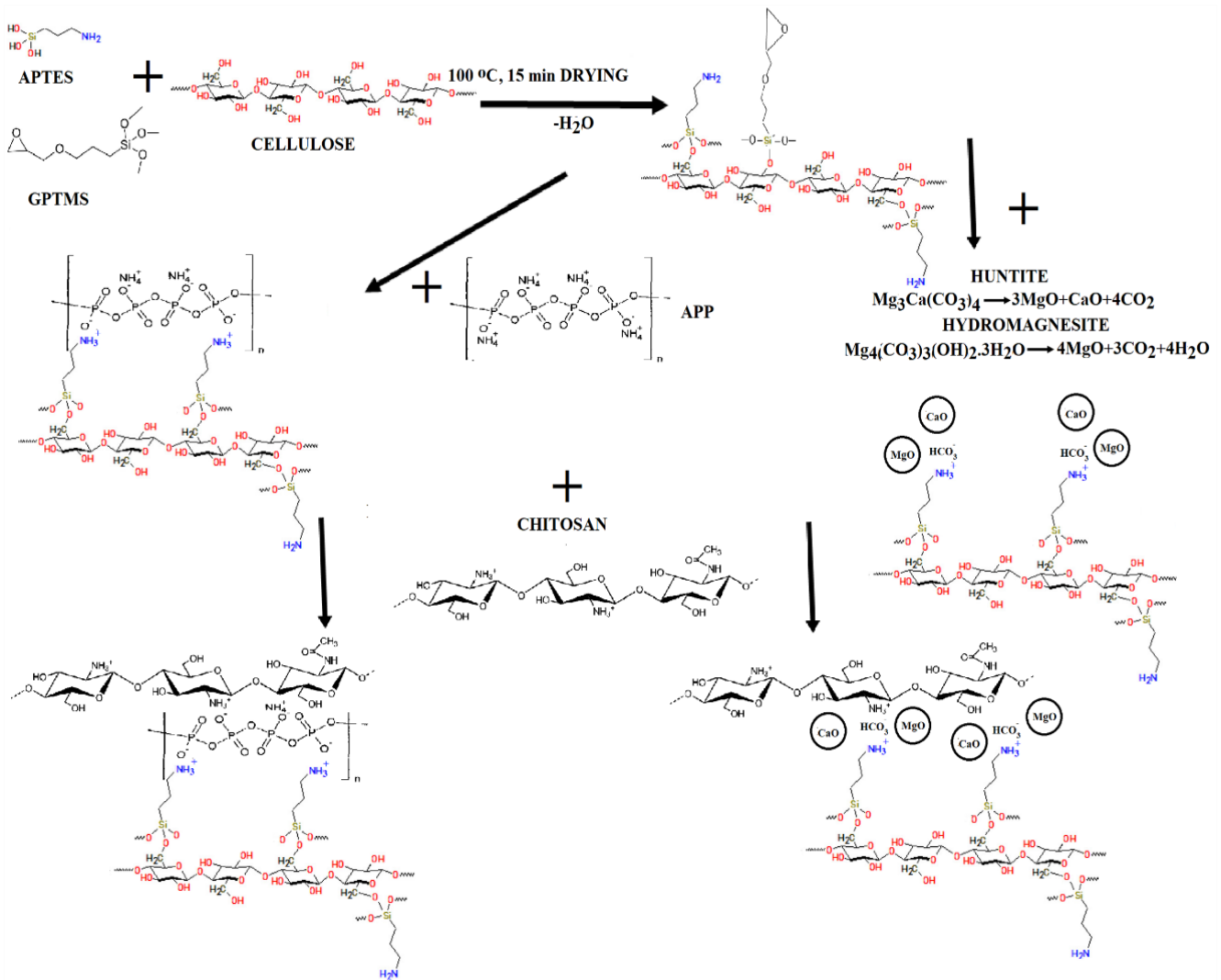


**Figure 1.** Schematic presentation of interaction of anionic and cationic charged chemicals with cellulose

In the study, experimental parameters were the type of anionic solution, the presence of drying step after every coating and the number of bilayers. The fabrics were dried at 100 °C for 15 min after every dipping process (DE) or only last dipping process (DL). The codes were given as HxDE, HxDL and APxDE, APxDL for coating with HH and APP as anionic layer with x=5, 10 and 15 bilayers and drying (DE code) after every dipping process or drying (DL) only last dipping, respectively.

### 2.3 Measurement and Characterization

Mineral contents and mean particle size values of HH powders were given in our previous paper [11]. The weight gain of cotton fabrics was designated by measuring the fabric weights before and after LBL assembly. Tensile strength values of fabric samples were measured by tensile testing machine (Tinius Olsen Ltd.) according to ASTM D5035-95 standard (strip method). The yellowness index (E313) and whiteness index (Stensby) were determined by DataColor SpectraFlash 600 spectrophotometer (D65 day light, 10° standard observer). The limited oxygen indexes

(LOI) of samples were analyzed by LOI measurement device (Qualitest Inc., Canada) in accordance with the ASTM D2863 standard. Vertical flame spreading tests (VFT) were applied with face ignition on rectangular samples (50x150 mm<sup>2</sup>). The short side of the samples was exposed to the flame (20 mm length) for 5 secs. Afterflame time and afterglow time values were determined as explained in ISO 13943 [38]. The images of fabric samples after vertical flame spreading tests were taken. Cone calorimetry test was carried out to characterize the combustion properties of fabric samples (100mm x 100mm x 0.3mm) under 35 kW/m<sup>2</sup> of irradiative heat flux according to ISO 5660 in horizontal configuration by cone calorimeter (Fire Testing Technology, UK) [39]. Samples were held with a frame and metallic grid in right position. The total heat release (THR), heat release rate and peak heat release rate (HRR, pkHRR), total smoke release (TSR), CO<sub>2</sub>/CO yield, specific extinction area (SEA), time to ignition (TTI), residues at the end of test (wt.%) and mass loss rate (MLR) were evaluated [40]. Thermal analysis of fabric samples was carried out at a heating rate of 20 °C/min in the temperature range of 30-600 °C under



air atmosphere by using DTA-TG machine (Setaram Setsys 1750). The antibacterial activity of the fabric samples was tested as ASTM 2149 standard for *S. aureus* as Gram-positive organism and *E. coli* as Gram-negative organism. Bacterial reduction (%) were calculated as Durán et al. 2007 [41]. The surface morphologies of the fabric samples were observed in 1000x and 2000x magnification by using scanning electron microscopy (FESEM, Zeiss Supra 40VP) at acceleration voltage of 20 kV. SEM images of fabric samples were taken before and after vertical flame test (VFT). Their elemental compositions of fabric samples exposed VFT were determined with energy-dispersive X-ray spectroscopy (EDX) before and after 5 washing cycles at 40 °C with ECE reference detergent (non-phosphate) as ISO 105 C06. FTIR-ATR spectra of fabric samples were recorded using a Bruker Hyperion 1000 IFS-66/s Infrared Spectrometer with diamond universal ATR accessory and with a resolution of 4 cm<sup>-1</sup> over a range of 400 to 4000 cm<sup>-1</sup>.

## 2. RESULTS AND DISCUSSION

The add-on values, tensile strength, elongation, whiteness and yellowness index values, vertical flame test results (residue amount, after-flame time, after-glow time) and LOI values of the fabric samples are given in Table 1.

### 3.1 Fabric Characterization

Mass of coating added on the fabrics increased while whiteness of fabric samples was decreasing with the growth of bilayer number, as shown in Table 1 and Figure 2. APP led to further decrease in whiteness and further increase in the mass of coating added on the fabrics compared to HH. Moreover, DE samples possessed lower whiteness and higher add-on values than DL samples. Higher tensile strength of DE samples and lower tensile strength of DL samples in comparison with untreated fabric were illustrated in Figure 3 and Table 1. The tensile strength of all fabric samples increased with the growth of bilayer number. Especially HHxDE samples have the highest tensile strength. Lower elongation of DE samples and

higher elongation of DL samples were observed in comparison with untreated fabric.

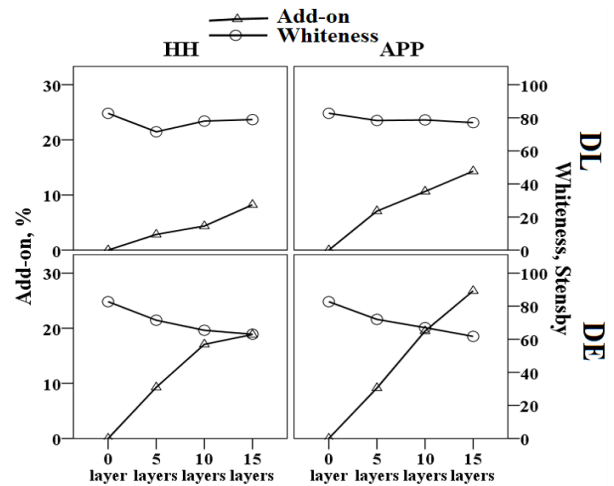


**Figure 2.** Add-on and whiteness values of fabric samples with respect to anionic layer type (HH or APP), bilayer numbers and drying conditions (DL or DE)

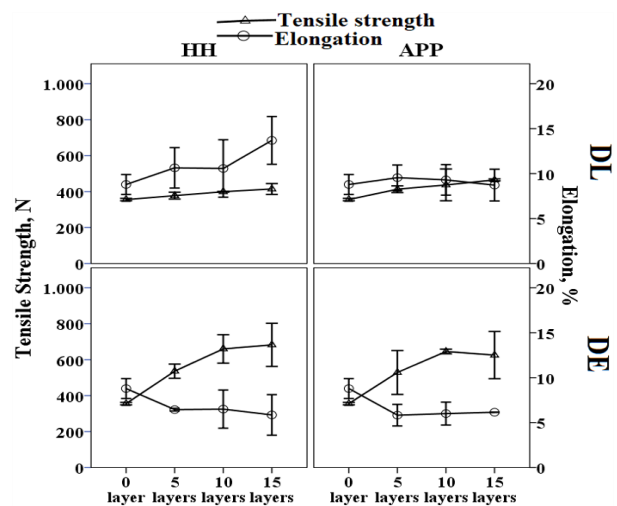


**Figure 3.** Tensile strength and elongation values with respect to anionic layer type (HH or APP), bilayer numbers and drying conditions (DL or DE)

**Table 1.** The add on values, tensile strength, elongation, whiteness and yellowness index values, vertical flame test results (residue amount, after-flame time, after-glow time) and LOI values of the fabric samples. \*UT-Untreated

Code	Add-on, %	Yellowness index, E313	Whiteness index, Stensby	Tensile Strength, N	Elongation, %	Vertical flame test			LOI, %
						Damaged length, mm	After-flame time, s	After-glow time, s	
UT*	-	6.49	82.72	355.60	8.79	120	16	23	17
H5DE	9.9	12.50	71.52	536.00	6.45	120	22	-	18
H10DE	16.3	15.74	65.44	660.00	6.50	120	24	-	19
H15DE	20.4	16.75	63.05	682.50	5.85	120	25	-	19
AP5DE	10.0	11.85	72.02	528.75	5.83	86	18	-	19
AP10DE	20.9	14.35	67.02	645.50	6.00	86	19	-	20
AP15DE	24.6	17.25	61.72	625.50	6.15	90	15	-	22
H5DL	2.4	8.50	78.03	377.60	10.65	120	19	-	18
H10DL	4.1	8.72	78.92	399.20	10.57	120	19	-	18
H15DL	7.9	8.87	78.36	414.75	13.70	120	20	-	18
AP5DL	5.2	8.25	79.54	413.25	9.55	120	24	-	19
AP10DL	9.7	8.59	78.72	437.25	9.30	120	19	-	19
AP15DL	13	9.26	77.09	465.00	8.73	88	13	-	20

### 3.2 Flame retardancy properties of fabrics

The after-glow time (23s) could be determined for only untreated fabric while all coated fabric samples did not exhibit glow burning behavior, which proved their flame retardant properties. After-flame time of AP code samples decreased from 16s to 15s in comparison with untreated fabric while their damaged length with integrity of char residues have been reducing from 120 mm to 90 mm (Figure 4 h,i,j,m). After-flame time of H code samples increased from 16s to 25 s in comparison with untreated fabric, which ascribed slowing of flame spreading on the samples. LOI values of all treated fabrics were increased compared with untreated fabric (17%). LOI values of H code samples (19%) were lower than AP code samples. AP15DE were exerted the highest LOI value (22%) (Figure 5). The results demonstrated their flame retardancy due to high amount of char residue of APP coating and long flame spreading time of HH coating.

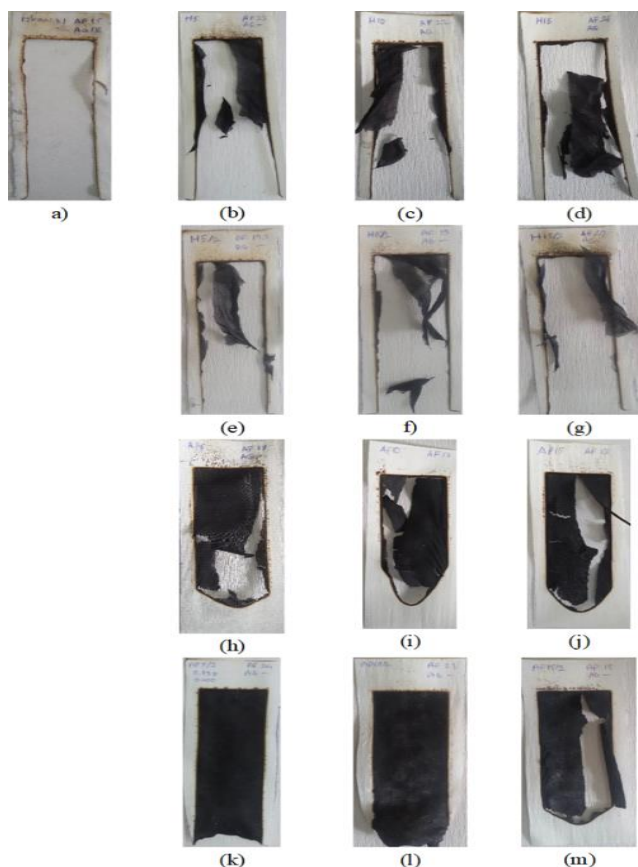


**Figure 4.** The images of fabric samples exposed to vertical flame test a) UT, b), c), d) HxDE samples with 5, 10 and 15 bilayers, respectively, e), f), g) HxDL samples with 5, 10 and 15 bilayers, respectively, h), i), j) APxDE samples with 5, 10 and 15 bilayers, respectively, k), l), m) APxDL samples with 5, 10 and 15 bilayers, respectively.

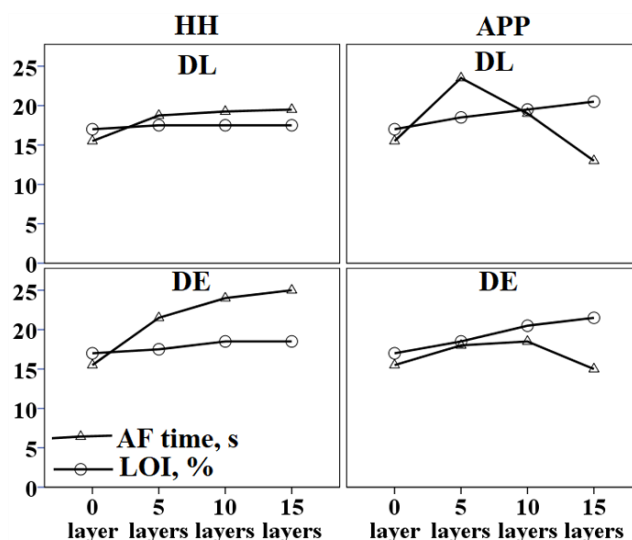


**Figure 5.** After-flame times and LOI values of samples with respect to anionic layer type (HH or APP), bilayer numbers and drying conditions (DL or DE)

### 3.3 Cone calorimeter test

Flame retardancy properties of fabric samples were explored by cone calorimeter test. Heat release rate (HRR) and total smoke release (TSR) curves of fabric samples were shown in Figure 6 a) and b). Cone calorimeter test results were depicted in Table 2. It can be observed that the deposition of chitosan, APTES and GPTMS, APP or HH by LBL assembly reduced TTI, pkHRR, pkMLR and TSR values of fabric samples in comparison with untreated fabric. pHRR and MLR values of H15DE and AP15DE samples exhibited further decrease in comparison with H15DL and AP15DL samples. The lowest pHRR (194 kW/m<sup>2</sup>) and TSR (18.5 m<sup>2</sup>/m<sup>2</sup>) values were achieved in H15DE samples while the lowest MLR (11.27 g/(s.m<sup>2</sup>)) and residues at the end of test (50%) were succeeded in AP15DE samples. In Figure 7, the images of cone calorimetry test depicted that more residual char amount of AP15DE samples in comparison with untreated fabric and H15DE samples. The samples applied APP in anionic layer acquired lower CO<sub>2</sub>/CO yield in comparison with untreated fabric and samples applied HH in anionic layer. Low CO<sub>2</sub>/CO yield could be attributed to unyield combustion due to limited diffusion of oxygen to pyrolysis area [13,42]. Hence fabric samples used APP or HH in anionic layer exhibited different flame retardancy mechanisms. Reduction on heat release and smoke release attributed flame retardancy (FR) mechanism of samples applied HH in anionic layer. The FR mechanism of the fabric samples used APP as intumescent flame retardant agent was based on high residual char amount, forming a barrier for flame, reducing oxygen diffusion from residual barrier and decelerating of flame progressing. The results were supported by the other flame retardancy test results.

**Table 2.** The cone calorimetry test results

Code	pkHRR [kW/m <sup>2</sup> ]	THR [MJ/m <sup>2</sup> ]	pkMLR [g/(s.m <sup>2</sup> )]	TSR [m <sup>2</sup> /m <sup>2</sup> ]	CO <sub>2</sub> /CO yield	TTI [s]	pkSEA (m <sup>2</sup> /kg)	Residues [%]
UT	248	4.2	15.26	146.4	54	11	2407	2
H15DE	194	3.3	13.07	18.5	27	9	2033	3
H15DL	249	2.5	15.00	25.4	20	8	605	1

AP15DE	206	2.1	11.27	45.6	2.64	8	1318	50.19
AP15DL	212	1.8	14.43	23.8	2.45	7	615	16.53

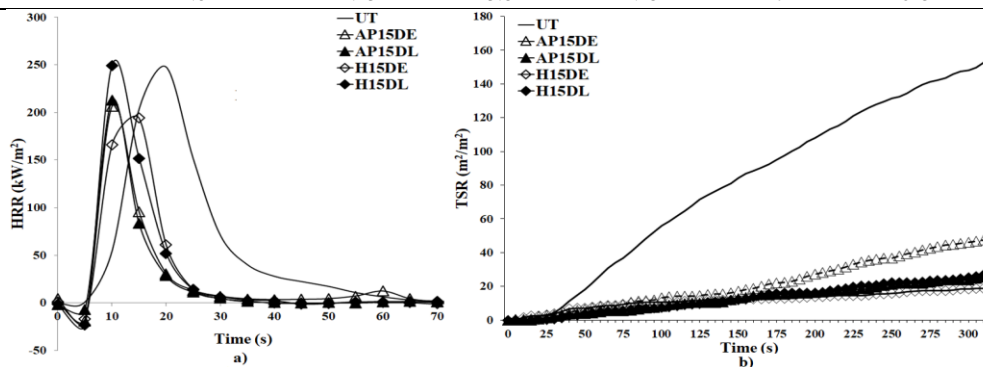


Figure 6. a) HRR and b) TSR curves of fabric samples

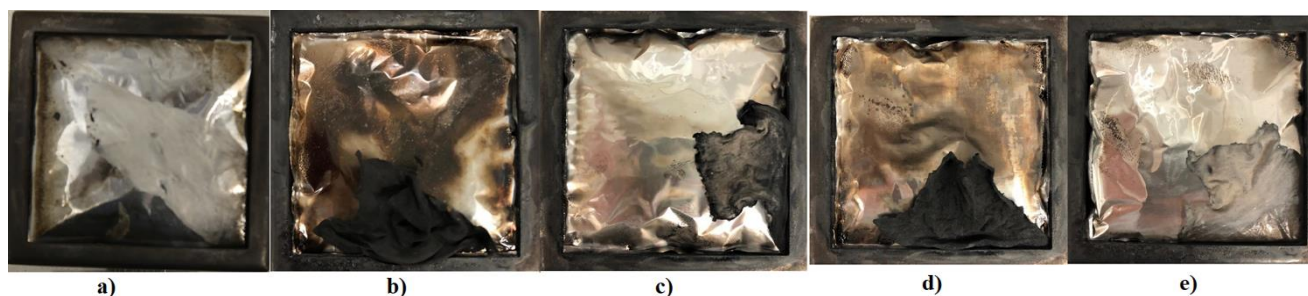


Figure 7. The fabric images after cone calorimetry test a) UT, b) AP15DE, c) H15DE, d) AP15DL, e) H15DL

### 3.4 Thermogravimetric analysis of fabric samples

The thermal stability of the fabric samples has been investigated by thermogravimetric analysis in air atmosphere. DTG and TG curves of the fabric samples were illustrated in Figure 8 a) and b), respectively and the corresponding datas were summarised in Table 3. Silica was bonded to cellulose by hydrolysis and condensation reactions and then exploited electrostatically interaction with phosphoric acid formed by APP or bicarbonate anions generated by HH. Substantially chitosan as additional carbon source electrostatically collaborated with Cellulose-Silica-APP or Cellulose-Silica-HH to improve FR efficiency of samples (Figure 1). Cationic chitosan in acid solution could be paired with anionic APP solution or HH solution by LBL assembly. Chitosan with nitrogen content and APP with intumescent nature improve the flame retardancy properties of treated materials [6]. Coatings with silica based nanosols could ensure fire protection by forming inorganic barrier. Silica together with nitrogen-based compounds could catalyze the dehydration and carbonization of substrate and decrease the amount of combustible gases.

All samples exhibited two-step thermal degradation processes, where the first step temperature decreased and the second step temperature increased for HxDE, APxDE and APxDL samples in comparison with UT samples. Cotton begins to decompose at 220 °C ( $T_{\text{onset}5\%}$ ) and showed the maximum weight loss rate at 360 °C ( $T_{\text{max}1}$ ) in the first step, which may be attributed to depolymerization and dehydration of cellulose, formation of aliphatic char. During the second step, the aliphatic char carbonizes into aromatic char and then oxidizes into  $\text{CO}_2$  and CO with the

maximum weight loss rate at 495 °C ( $T_{\text{max}2}$ ) [6]. Lower pyrolysis temperature ( $T_{\text{max}1}$ ) and higher  $T_{\text{max}2}$  are evident that fabric samples treated LBL show good thermal stability. Especially APxDE samples have lower  $T_{\text{max}1}$  and higher  $T_{\text{max}2}$  in comparison with HxDE samples. It was indicated that APP samples had higher thermal stability and higher char residues than HH samples because of the synergistic interaction between phosphorus, nitrogen and silicon atoms in its molecular structure [43]. By introducing the CH-APTES-APP (AP15DE) assembly coating, the fabrics (152 °C) showed reduced decomposition temperature ( $T_{\text{onset}5\%}$ ) compared with untreated fabric (220 °C). Lower  $T_{\text{onset}5\%}$  temperature generally could be attributed to thermal degradation of cotton which catalyzed by hydroxyl groups of chitosan and silica [13,44]. APxDE and HxDE exhibited lower pyrolysis temperatures ( $T_{\text{max}1}$ ) in the first step, which is attributable to the catalyzed thermal degradation of cotton in the presence of Si, nitrogen, APP or HH [6]. The growth of bilayer number resulted in a lower pyrolysis temperature and thus higher thermal stability of cotton in the whole degradation process. Because char forming at lower temperatures and volatile species releasing inhibited the further degradation and combustion of cotton at higher temperature [6,13,45]. Hence the second degradation step of AP15DE and H15DE fabric samples ( $T_{\text{max}2}$ ) was postponed to 527 and 516 °C respectively, dedicating more stable char at higher temperatures in comparison with the uncoated cotton (495 °C). Final residue amounts of the fabric samples at 600 °C increased in comparison with UT samples (0.06%). According to char residue datas, the char residue of AP15DE and H15DE were 6.73 and 0.60%, respectively. The char residues of APP and HH samples may be

attributed to the presence of amino and silane groups, benzene rings and phosphate groups or calcium and magnesium oxides. All these results indicated that thermal stability of LBL treated fabric samples improved the by

supporting the char formation and preventing the production of volatile species.

**Table 3.** DTA-TG datas for untreated and treated fabric samples.  $T_{\text{onset}5\%}$ : Initial decomposition temperature (for 5% weight loss) [40].  $T_{\text{max}}$ : Maximum weight loss temperature (from DTG curves)

Code	$T_{\text{onset}5\%}, ^\circ\text{C}$	$T_{\text{max}1}, ^\circ\text{C}$	$T_{\text{max}2}, ^\circ\text{C}$	Residue at $T_{\text{max}1}, \%$	Residue at $T_{\text{max}2}, \%$	Residue at $600^\circ\text{C}, \%$
UT	220	360	495	48	5	0.06
AP5DE	261	335	521	55	9	1.25
AP10DE	249	330	536	61	14	6.00
AP15DE	152	314	527	61	16	6.73
H5DE	276	358	520	50	6	0.25
H10DE	281	346	508	55	8	0.32
H15DE	232	340	516	52	7	0.60

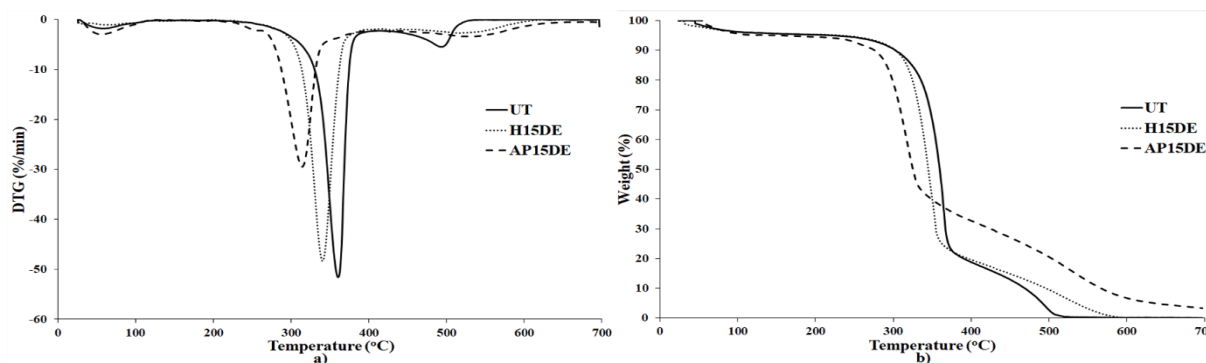


**Figure 8.** a) DTG and b) TG graphs of fabric samples

### 3.5 Antibacterial properties of fabric samples

The bacterial reduction for *E. coli* and *S. aureus* was examined in H15DE and AP15DE samples. It was found from Figure 9 and 10 that AP15DE samples had high bacterial reduction, 100% and 98% against *E.coli* and *S. aureus*, respectively. The antibacterial activity of APP did not previously study in the literature. Nitrogen and phosphate contents of APP attributed to their antibacterial activity. An effective bacteriostatic effect stem from cationic ammonium and polyphosphates in its structure [46, 47]. Amino groups through ionic interaction could absorbed on the anionic cell walls of bacteria [48]. The bacterial reduction of H15DE sample against to *S. aureus* reached to 93% due to the presence of CaO and MgO ensuring superoxide forming in HH powder while the bacterial reduction against to *E.coli* was 61%. Rough coating with HH powder observed SEM images could provide higher specific area and thus efficient contact and interaction between HH powder and *S. aureus* (Figure 11). Antibacterial activity of MgO and CaO could be ascribed to form of superoxide on material surface [11,49]. APP or HH in outer layer of fabric samples was in charge of bacteriostatic activity [50].

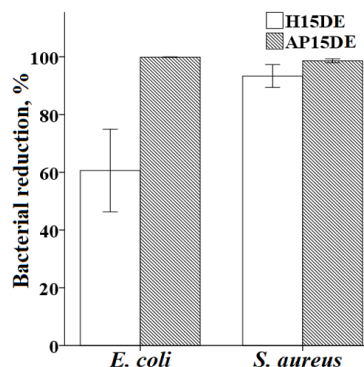


**Figure 9.** Bacterial reduction of fabric samples againsts *E. coli* and *S. aureus*

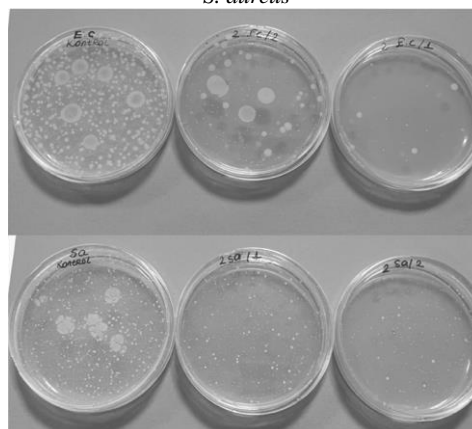


**Figure 10.** Images of bacterial reduction test a) UT, b) H15DE, c) AP15DE against to *E.coli* and d) UT, e) H15DE, f) AP15DE against to *S.aureus*

### 3.6 SEM-EDS and FTIR Analyses



The SEM images in Figure 11 showed the surface structure of the fabric samples. These micrographs reveal that all fibers treated LBL with HH in anionic layer exhibited superficial and rough coating and no bridging between fibers while HxDL samples displayed the presence of particulate matters on the surface with the growth of bilayer numbers. Aggregation of HH powder was observed in HxDL samples while regular film form was exhibited in HxDE samples with attribution based on drying processes. The coating on APxDE samples was filling between fiber with continuous and denser layer while some cracks were observed on the coating on APxDL samples. Figure 12 illustrated the SEM images of UT, AP15DE and H15DE samples after VFT and washing cycles+VFT. The treated samples protected integrity after VFT and washing cycles+VFT. Especially AP15DE sample exhibited better continuity after VFT, which supported by photos and residual amounts in VFT and cone calorimetry analysis.

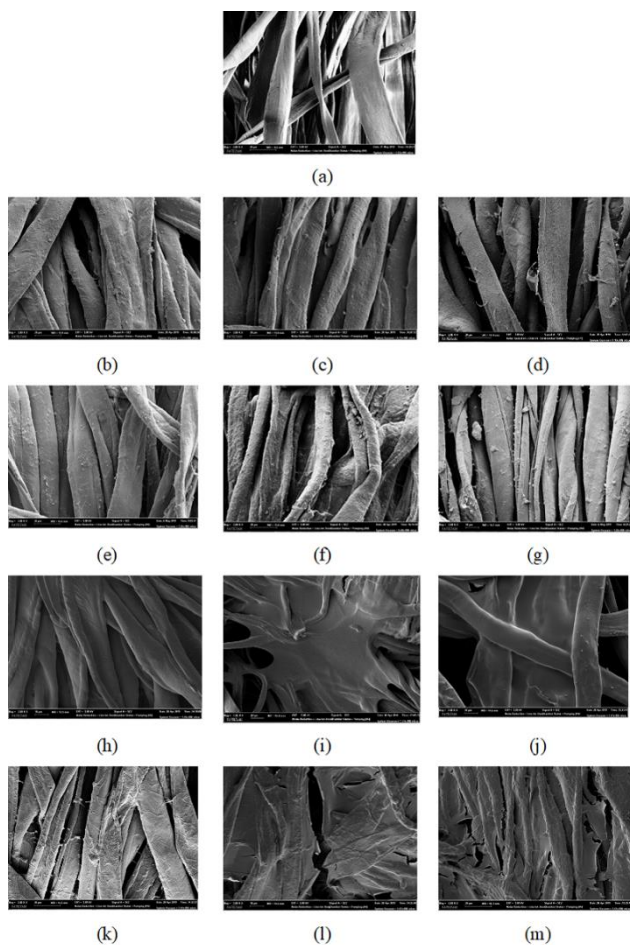


**Figure 11.** SEM images of fabric samples a) UT, b)H5DE, c)H10DE, d)H15DE, e)H5DL, f)H10DL, g)H15DL, h)AP5DE, i)AP10DE, j)AP15DE, k)AP5DL, l)AP10DL, m)AP15DL

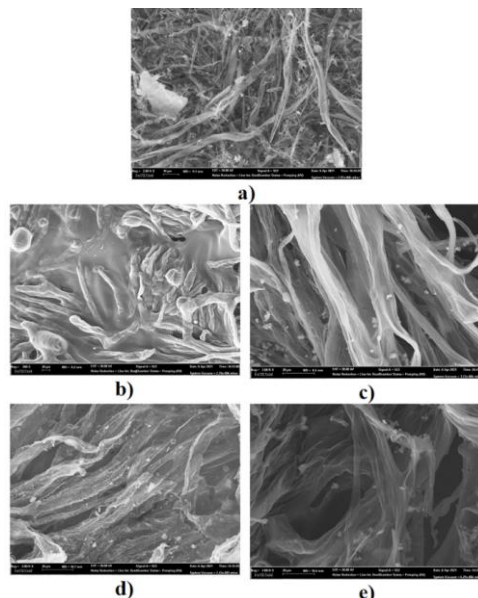


**Figure 12.** SEM images After washing cycles and vertical flame test a) UT after VFT b) AP15DE after VFT c) AP15DE after washing cycles and VFT d) H15DE after VFT e) H15DE after washing cycles and VFT

To confirm the flame-retardant composition on fabric samples, the presence and durability of the elements on treated fabric samples were analyzed by SEM-EDS techniques. Elemental analysis results of AP15DE and H15DE samples after VFT and washing cycles+VFT were given in Figure 13. The result showed that the samples contained silicium element from APTES and GPTMS and nitrogen element from APTES, chitosan and APP. It was also confirmed the presence of Ca and Mg elements in H code samples and the presence of phosphate in AP code samples. The flame retardant efficiency of especially APxDE samples could be attributed to high content of P, N, and Si. The results proved the durability of coated samples to washing.

The chemical structures of untreated and LBL treated fabrics have been evaluated by FTIR-ATR spectra. As shown in Figure 14, all fabric samples showed wide peak between 3000 and 3600  $\text{cm}^{-1}$ , characteristic signals between 1035 and 1160  $\text{cm}^{-1}$ , peaks about 2900  $\text{cm}^{-1}$ , 1635  $\text{cm}^{-1}$ , 1428  $\text{cm}^{-1}$ , 1361  $\text{cm}^{-1}$  and 1053  $\text{cm}^{-1}$  ascribed to the stretching at OH groups, the C-O-C of cellulose backbone, stretching vibration at C-H groups in alkyl chains, bending at O-H groups of adsorbed water, deformation vibration at -CH<sub>2</sub>-, bending vibration of C-H groups and stretching vibration of C-O-C groups which these peaks were stems from cellulose nature [6,13,25]. The signals between 1000 and 1100  $\text{cm}^{-1}$  in all fabrics were ascribed to Si-O-Si bond asymmetric stretching vibration, which indicated the presence of silica network, and overlapped with inherent peaks of cellulose [51,52]. Chitosan depicted similar peaks to cellulose and also wide peak at 3333  $\text{cm}^{-1}$  attributed to stretching vibration of N-H groups. The peak at 1740  $\text{cm}^{-1}$  contributed by stretching vibration of carbonyl group (C=O) [53]. Furthermore, APP, HH and APTES in coating layer demonstrated characteristic peaks on spectras of fabric samples in Figure 14. The band at 1440  $\text{cm}^{-1}$  corresponds to the bending vibration of CH<sub>2</sub> groups next to the nitrogen atom [54]. Meanwhile a peak at 1532  $\text{cm}^{-1}$



contributed by bending vibration of  $-NH_2$  groups from APTES and chitosan appeared in LBL treated fabrics. The peak at  $1232\text{ cm}^{-1}$  ascribed to stretching vibration of P-O-aryl proved the presence of phosphate on AP code samples, which overlapped Si-C band at  $1200\text{ cm}^{-1}$  for all LBL treated fabric samples [6,25,55]. It was determined that a peak at  $1040\text{ cm}^{-1}$  ascribed to stretching vibration of P-O-C from AP15DE overlapped with peak at  $1052\text{ cm}^{-1}$  ascribed to stretching vibration of C-O-C from cellulose, which was supported by Pan et al. 2015 [30]. Two peaks for H15DE at

$1538\text{ cm}^{-1}$  and  $1508\text{ cm}^{-1}$  were ascribed to asymmetric bands of  $CO_3^{2-}$  groups of HH. The peak at  $1538\text{ cm}^{-1}$  overlapped with bending vibration of  $-NH_2$  groups at  $1532\text{ cm}^{-1}$  from APTES and chitosan. Furthermore, two peaks at  $870$  ve  $891\text{ cm}^{-1}$  were ascribed to carbonate ligand from HH [11,16,56]. Overall, the FTIR-ATR spectra confirmed that chitosan, APTES and APP or HH were successfully applied to fabric samples.

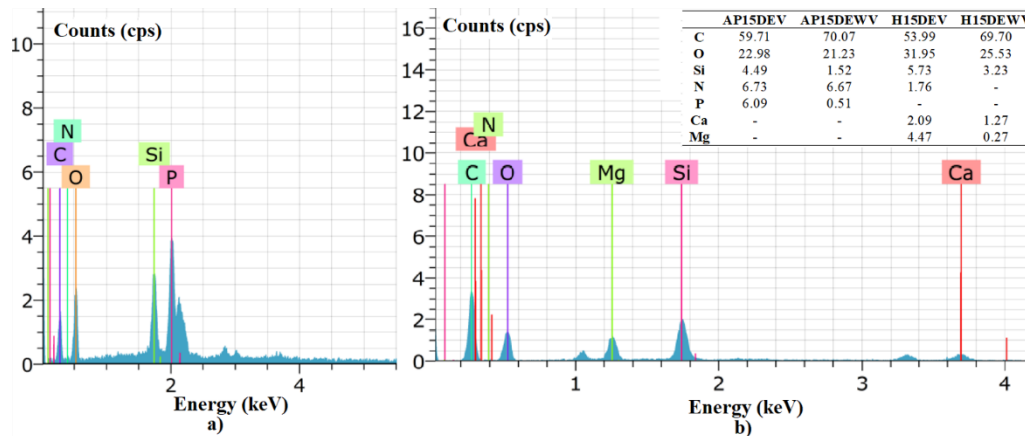


**Figure 13.** The elemental composition of the fabric samples by EDS analysis (gravimetric, %) after vertical flame test (V) and washing cycles (W) a)AP15DEV and b) H15DEV samples

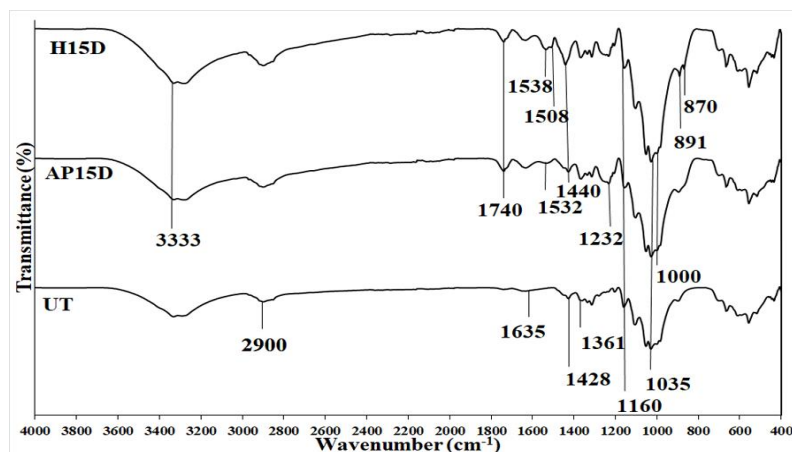


**Figure 14.** FTIR spectrum for UT, AP15DE and H15DE samples.

### 3. CONCLUSION

In this article, we have demonstrated that successful fabrication of flame retardant, smoke suppressed and antibacterial cotton fabric with application of chitosan, and APTES as cationic layer and APP or HH as anionic layer by LBL assembly. It was investigated the effect of bilayer numbers (5, 10 and 15 bilayers), anionic layer type (APP or HH) and drying conditions (DE or DL) on multifunctionality of cotton fabrics. LBL treated fabrics displayed different behaviors in terms of fabric characteristics and hence, reflected on their flame retardant and antibacterial properties. LBL treated fabric samples revealed some increase in LOI values (i.e., from 17% to 22% for AP15DE and 19% for

H15DE), get longer AF time (from 16s to 25s for H15DE) and shorter damaged length (from 12 cm to 9 cm for AP15DE) in vertical flame test, significant decrease in pHRR and TSR value (from 248 to 194  $\text{kW/m}^2$  and from 146 to 18.5  $\text{m}^2/\text{m}^2$  for H15D) in cone calorimetry test and significant increase residue at  $600\text{ }^\circ\text{C}$  (6.73% residue for AP15DE) in DTA-TG analysis in comparison with untreated fabric. It was concluded that the flame retardancy mechanism of AP15DE samples as intumescent flame retardant agent was based on increasing char amount, which formed a barrier for flame, decreased oxygen transfer, and decelerating of flame progressing while the mechanism of H15DE samples was resulted from long afterflame time and decreasing smoke density and heat release. AP15DE imparted high

bacteriostatic reduction against two bacteria while H15DE exhibited high bacterial reduction against only *S. aureus*. In conclusion, it was proved the antibacterial and flame retardancy properties of the coated fabrics with HH or APP as anionic layer and chitosan and silane based nanosols as cationic layer by LBL assembly. There was some researches on the using of APP for LBL assembly on cotton fabric while the using of HH solution as anionic layer for LBL assembly on cotton fabric were firstly studied in literature. Their antibacterial and flame retardancy performance was compared and they were proposed their usage for medical, industrial, home and military textiles.

## REFERENCES


- Li, S., Lin, X., Liu, Y., Li, R., Ren, X., & Huang, T. S. 2019. Phosphorus-nitrogen-silicon-based assembly multilayer coating for the preparation of flame retardant and antimicrobial cotton fabric. *Cellulose*, 26(6), 4213-4223.
- Onar Camlibel N, Topcu H. 2021. Flame retardant cotton fabric modified with silica nanosols containing huntite-hydromagnesite grafted with GPTMS and VTES. *The Journal of The Textile Institute*, 112(7), 1129-1143.
- Atay, H. Y., & Engin, B. 2019. Use of glass fibers and glass spheres to improve mechanical properties of huntite and hydromagnesite reinforced flame retardant composites. *Revista Română de Materiale/Romanian Journal of Materials*, 49(4), 468-474.
- Hollingbery, L. A., & Hull, T. R. 2010. The thermal decomposition of huntite and hydromagnesite—a review. *Thermochimica Acta*, 509(1-2), 1-11.
- Kangal, O., Kökkılıç, O., & Burat, F. 2009. Production of huntite and hydromagnesite with flame retardant featured by flotation. *Mining, Metallurgy & Exploration*, 26(2), 109-113.
- Fang, F., Zhang, X., Meng, Y., Gu, Z., Bao, C., Ding, X., ... & Tian, X. 2015. Intumescent flame retardant coatings on cotton fabric of chitosan and ammonium polyphosphate via layer-by-layer assembly. *Surface and Coatings Technology*, 262, 9-14.
- Wang, X., Romero, M. Q., Zhang, X. Q., Wang, R., & Wang, D. Y. 2015. Intumescent multilayer hybrid coating for flame retardant cotton fabrics based on layer-by-layer assembly and sol-gel process. *RSC advances*, 5(14), 10647-10655.
- Devaux, E., Rochery, M., & Bourbigot, S. 2002. Polyurethane/clay and polyurethane/POSS nanocomposites as flame retarded coating for polyester and cotton fabrics. *Fire and Materials*, 26(4-5), 149-154.
- Grancaric, A. M., Colleoni, C., Guido, E., Botteri, L., & Rosace, G. 2017. Thermal behaviour and flame retardancy of monoethanolamine-doped sol-gel coatings of cotton fabric. *Progress in Organic Coatings*, 103, 174-181.
- Spontón, M., Ronda, J. C., Galià, M., & Cádiz, V. 2009. Development of flame retardant phosphorus-and silicon-containing polybenzoxazines. *Polymer degradation and stability*, 94(2), 145-150.
- Camlibel, N. O., Avinc, O., Arik, B., Yavas, A., & Yakin, I. 2019. The effects of huntite-hydromagnesite inclusion in acrylate-based polymer paste coating process on some textile functional performance properties of cotton fabric. *Cellulose*, 26(2), 1367-1381.
- Alongi, J., Carosio, F., & Malucelli, G. 2012. Influence of ammonium polyphosphate-/poly (acrylic acid)-based layer by layer architectures on the char formation in cotton, polyester and their blends. *Polymer Degradation and Stability*, 97(9), 1644-1653.
- Carosio, F., Alongi, J., & Malucelli, G. 2012. Layer by layer ammonium polyphosphate-based coatings for flame retardancy of polyester-cotton blends. *Carbohydrate Polymers*, 88(4), 1460-1469.
- Mateos, A. J., Cain, A. A., & Grunlan, J. C. 2014. Large-scale continuous immersion system for layer-by-layer deposition of flame retardant and conductive nanocoatings on fabric. *Industrial & Engineering Chemistry Research*, 53(15), 6409-6416.
- Jimenez, M., Guin, T., Bellayer, S., Dupretz, R., Bourbigot, S., & Grunlan, J. C. 2016. Microintumescent mechanism of flame-retardant water-based chitosan-ammonium polyphosphate multilayer nanocoating on cotton fabric. *Journal of Applied Polymer Science*, 133(32).
- Zhang, T., Yan, H., Peng, M., Wang, L., Ding, H., & Fang, Z. 2013. Construction of flame retardant nanocoating on ramie fabric via layer-by-layer assembly of carbon nanotube and ammonium polyphosphate. *Nanoscale*, 5(7), 3013-3021.
- Wattanatanom, W., Churuchinda, S., & Potiyaraj, P. 2017. Intumescent flame retardant finishing of polyester fabrics via the layer-by-layer assembly technique. *International Journal of Clothing Science and Technology*, 29(1), 96-105.
- Li, H., & Peng, L. 2015. Antimicrobial and antioxidant surface modification of cellulose fibers using layer-by-layer deposition of chitosan and lignosulfonates. *Carbohydrate polymers*, 124, 35-42.
- Shirvan, A. R., Nejad, N. H., & Bashari, A. 2014. Antibacterial finishing of cotton fabric via the chitosan/TPP self-assembled nano layers. *Fibers and Polymers*, 15(9), 1908-1914.
- Joshi, M., Khanna, R., Shekhar, R., & Jha, K. 2011. Chitosan nanocoating on cotton textile substrate using layer-by-layer self-assembly technique. *Journal of Applied Polymer Science*, 119(5), 2793-2799.
- Ali, S. W., Joshi, M., & Rajendran, S. 2011. Novel, Self-Assembled Antimicrobial Textile Coating Containing Chitosan Nanoparticles. *Aatcc Review*, 11(5).
- Gadkari, R. R., Ali, S. W., Joshi, M., Rajendran, S., Das, A., & Alagirusamy, R. 2020. Leveraging antibacterial efficacy of silver loaded chitosan nanoparticles on layer-by-layer self-assembled coated cotton fabric. *International Journal of Biological Macromolecules*, 162, 548-560.
- Saini S, Gupta A, Singh N, Sheikh J. Functionalization of linen fabric using layer by layer treatment with chitosan and green tea extract. *J. Ind. Eng. Chem.* 2020; 82: 138-143.
- Leistner, M., Abu-Odeh, A. A., Rohmer, S. C., & Grunlan, J. C. 2015. Water-based chitosan/melamine polyphosphate multilayer nanocoating that extinguishes fire on polyester-cotton fabric. *Carbohydrate polymers*, 130, 227-232.
- Liu, Y., Wang, Q. Q., Jiang, Z. M., Zhang, C. J., Li, Z. F., Chen, H. Q., & Zhu, P. 2018. Effect of chitosan on the fire retardancy and thermal degradation properties of coated cotton fabrics with sodium phytate and APTES by LBL assembly. *Journal of analytical and applied pyrolysis*, 135, 289-298.
- Yu, X., Pan, Y., Wang, D., Yuan, B., Song, L., & Hu, Y. 2017. Fabrication and properties of bio-based layer-by-layer coated ramie fabric-reinforced unsaturated polyester resin composites. *Industrial & Engineering Chemistry Research*, 56(16), 4758-4767.
- Carosio, F., Laufer, G., Alongi, J., Camino, G., & Grunlan, J. C. 2011. Layer-by-layer assembly of silica-based flame retardant thin

## Acknowledgement

The study was funded by Pamukkale University Scientific Research Project under Grant 2019FEBE014. The authors wish to thank Tecnosintesi SPA and Setas Company for supplying of ammonium polyphosphate and huntite-hydromagnesite powder, respectively Authors greatly acknowledge ODTU for supporting the FTIR-ATR and DTA-TG analysis, ILTAM for supporting SEM-EDS analysis.

- film on PET fabric. *Polymer Degradation and Stability*, 96(5), 745-750.
28. Laufer, G., Carosio, F., Martinez, R., Camino, G., & Grunlan, J. C. 2011. Growth and fire resistance of colloidal silica-polyelectrolyte thin film assemblies. *Journal of colloid and interface science*, 356(1), 69-77.
  29. Pan, H., Song, L., Ma, L., Pan, Y., Liew, K. M., & Hu, Y. 2014. Layer-by-layer assembled thin films based on fully biobased polysaccharides: chitosan and phosphorylated cellulose for flame-retardant cotton fabric. *Cellulose*, 21(4), 2995-3006.
  30. Pan, H., Wang, W., Pan, Y., Song, L., Hu, Y., & Liew, K. M. 2015. Formation of self-extinguishing flame retardant biobased coating on cotton fabrics via Layer-by-Layer assembly of chitin derivatives. *Carbohydrate polymers*, 115, 516-524.
  31. Pan, Y., Wang, W., Pan, H., Zhan, J., & Hu, Y. 2016. Fabrication of montmorillonite and titanate nanotube based coatings via layer-by-layer self-assembly method to enhance the thermal stability, flame retardancy and ultraviolet protection of polyethylene terephthalate (PET) fabric. *RSC advances*, 6(59), 53625-53634.
  32. Li, Y., Wang, B., Sui, X., Xie, R., Xu, H., Zhang, L., ... & Mao, Z. 2018. Durable flame retardant and antibacterial finishing on cotton fabrics with cyclotriphosphazene/polydopamine/silver nanoparticles hybrid coatings. *Applied Surface Science*, 435, 1337-1343.
  33. Li, P., Wang, B., Liu, Y. Y., Xu, Y. J., Jiang, Z. M., Dong, C. H., ... & Zhu, P. 2020. Fully bio-based coating from chitosan and phytate for fire-safety and antibacterial cotton fabrics. *Carbohydrate Polymers*, 237, 116173.
  34. Nine, M. J., Tran, D. N., ElMekawy, A., & Losic, D. 2017. Interlayer growth of borates for highly adhesive graphene coatings with enhanced abrasion resistance, fire-retardant and antibacterial ability. *Carbon*, 117, 252-262.
  35. Safi, K., Kant, K., Bramhecha, I., Mathur, P., & Sheikh, J. 2020. Multifunctional modification of cotton using layer-by-layer finishing with chitosan, sodium lignin sulphonate and boric acid. *International Journal of Biological Macromolecules*, 158, 903-910.
  36. Fang, F., Xiao, D., Zhang, X., Meng, Y., Cheng, C., Bao, C., ... & Tian, X. 2015. Construction of intumescent flame retardant and antimicrobial coating on cotton fabric via layer-by-layer assembly technology. *Surface and Coatings Technology*, 276, 726-734.
  37. Fang, F., Chen, X., Zhang, X., Cheng, C., Xiao, D., Meng, Y., ... & Tian, X. 2016. Environmentally friendly assembly multilayer coating for flame retardant and antimicrobial cotton fabric. *Progress in Organic Coatings*, 90, 258-266.
  38. Alongi, J., Cuttica, F., Carosio, F., & Bourbigot, S. 2015. How much the fabric grammage may affect cotton combustion?. *Cellulose*, 22(5), 3477-3489.
  39. Tata, J., Alongi, J., Carosio, F., & Frache, A. 2011. Optimization of the procedure to burn textile fabrics by cone calorimeter: Part I. Combustion behavior of polyester. *Fire and materials*, 35(6), 397-409.
  40. Alongi, J., Ciobanu, M., Tata, J., Carosio, F., & Malucelli, G. 2011. Thermal stability and flame retardancy of polyester, cotton, and relative blend textile fabrics subjected to sol-gel treatments. *Journal of Applied Polymer Science*, 119(4), 1961-1969.
  41. Durán, N., Marcató, P. D., De Souza, G. I., Alves, O. L., & Esposito, E. 2007. Antibacterial effect of silver nanoparticles produced by fungal process on textile fabrics and their effluent treatment. *Journal of biomedical nanotechnology*, 3(2), 203-208.
  42. Kandare, E., Kandola, B. K., Price, D., Nazare, S., & Horrocks, R. A. 2008. Study of the thermal decomposition of flame-retarded unsaturated polyester resins by thermogravimetric analysis and Py-GC/MS. *Polymer Degradation and Stability*, 93(11), 1996-2006.
  43. Zhao, P., Li, X., Zhang, M., Liu, S., Liang, W., & Liu, Y. 2014. Highly flame-retarding cotton fabrics with a novel phosphorus/nitrogen intumescent flame retardant. *Korean Journal of Chemical Engineering*, 31(9), 1592-1597.
  44. Xie, W., Gao, Z., Pan, W. P., Hunter, D., Singh, A., & Vaia, R. 2001. Thermal degradation chemistry of alkyl quaternary ammonium montmorillonite. *Chemistry of materials*, 13(9), 2979-2990.
  45. Horrocks, A. R. 2011. Flame retardant challenges for textiles and fibres: New chemistry versus innovative solutions. *Polymer Degradation and Stability*, 96(3), 377-392.
  46. Wang, L., Wen, X., Zhang, X., Yuan, S., Xu, Q., Fu, F., ... & Liu, X. 2021. Durable antimicrobial cotton fabric fabricated by carboxymethyl chitosan and quaternary ammonium salts. *Cellulose*, 28(9), 5867-5879.
  47. Lee TS, Kim SJ, Chang DS. 1988. Bacteriostatic effect of condensed phosphate on the growth of bacteria. *Korean Journal of Fisheries and Aquatic Sciences*, 21(2), 97-104.
  48. Liu, J., Dong, C., Wei, D., Zhang, Z., Xie, W., Li, Q., & Lu, Z. 2019. Multifunctional antibacterial and hydrophobic cotton fabrics treated with cyclic polysiloxane quaternary ammonium salt. *Fibers and Polymers*, 20(7), 1368-1374.
  49. Yamamoto, O., Ohira, T., Alvarez, K., & Fukuda, M. 2010. Antibacterial characteristics of CaCO<sub>3</sub>-MgO composites. *Materials Science and Engineering: B*, 173(1-3), 208-212.
  50. Pérez, O. P., & Matte, Y. C. 2017. Synthesis, characterization, and assessment of the antimicrobial activity of MgO-calcium alginate porous beads. *Tecnia*, 26(2), 7-13.
  51. Cireli, A., Onar, N., Ebeoglugil, M. F., Kayatekin, I., Kutlu, B., Culha, O., & Celik, E. 2007. Development of flame retardancy properties of new halogen-free phosphorus doped SiO<sub>2</sub> thin films on fabrics. *Journal of Applied Polymer Science*, 105(6), 3748-3756.
  52. Onar Ni, Mete G. 2016. Development of water repellent cotton fabric with application of ZnO, Al<sub>2</sub>O<sub>3</sub>, TiO<sub>2</sub> and ZrO<sub>2</sub> nanoparticles modified with ormosils. *Textile and Apparel*, 26(3), 295-302.
  53. Jiang, C., Liu, W., Sun, Y., Liu, C., Yang, M., & Wang, Z. 2019. Fabrication of durable superhydrophobic and superoleophilic cotton fabric with fluorinated silica sol via sol-gel process. *Journal of Applied Polymer Science*, 136(4), 47005.
  54. Mosnáčková, K., Chehimi, M. M., Fedorko, P., & Omastová, M. 2013. Polyamide grafted with polypyrrole: formation, properties, and stability. *Chemical Papers*, 67(8), 979-994.
  55. Škoc, M. S., Macan, J., & Pezelj, E. 2014. Modification of polyurethane-coated fabrics by sol-gel thin films. *Journal of Applied Polymer Science*, 131(4).
  56. Şen, F., Madakbaş, S., & Kahraman, M. V. 2014. Preparation and characterization of polyaniline/Turkish Huntite-hydromagnesite composites. *Polymer composites*, 35(3), 456-460.

# Design and Development of an Innovative Test Device Capable of Automatically Performing Carpet Static Loading Tests

Maher Alsayed  0000-0001-6619-3907

Hatice Kübra Kaynak  0000-0001-6548-3398

Halil İbrahim Çelik  0000-0002-1145-6471

Gaziantep University / Textile Engineering Department / 27310 Gaziantep, Türkiye

**Corresponding Author:** Maher Alsayed, ma00111@mail2.gantep.edu.tr

## ABSTRACT

The resistance of carpets to texture deformation is considered one of the most important properties that affects the quality of carpet. Static load is an essential factor that has a profound impact on carpets causing compression of carpet pile yarns. Mainly, two tests are available to test the performance of carpets in terms of compressibility and resilience, including thickness loss after brief moderate static loading and thickness loss after prolonged heavy static loading. Currently, the commercially available test devices have drawbacks, including a requirement for an additional apparatus to test performance, conducting tests manually which leads to personal faults, and inability of storing test data. In this study, a newly developed test device for measuring compressibility and resilience performance of carpet was designed and manufactured. The newly designed test device is statistically verified and capable of performing carpet thickness measurement, brief moderate static loading and prolonged heavy static loading tests automatically.

## 1. INTRODUCTION

Indeed, carpets are frequently utilized by human in different aspects of life. Carpets are used in order to obtain sound and heat insulation, in addition to provide an aesthetic appearance that is favourable by end-users. [1]. During usage, carpets are prone to many stresses resulting in negative effects on their surface texture. To be more specific, static and dynamic loads are significant applied stresses on carpets, which leads to deformation of the surface texture. There are different tests used to assess the performance of carpets in terms of compressibility and resilience, the most important of which are thickness loss after brief moderate and heavy static loading tests [1-3].

Several studies and researches were accomplished regarding carpet performance measurement and the effects of manufacturing parameters. For instance, some researchers investigated the thickness loss under dynamic

and static loading [4-7] while others studied the carpet performance under short and long term static loading [8-11]. Additionally, in the literature there are many studies on mechanical, physical and appearance properties of carpet [12-18].

Besides, in the literature, there are several studies which deal with the designs of different textile performance measurement systems. For instance, a measuring approach to examine the compression behavior of spacer fabrics was proposed by Mecit and Roye [19]. An instrument was developed by Fujimoto et al. to test and determine the surface friction of carpets and fabrics readily which enables to design pile products with high quality [20]. A new testing approach and a testing mechanism were proposed by Yao and Li through integrated assessment of fabric handle utilizing a virtual tool [21]. Li et al. proposed a testing approach to measure fabric touch feels [22]. Joshua et al.

**To cite this article:** Alsayed M, Kaynak HK, Çelik Hİ. 2022 Design and development of an innovative test device capable of automatically performing carpet static loading tests, *Tekstil ve Konfeksiyon*, 32(2), 126-134.

proposed a developed testing tool that is used for different lunar wheel tread material to test wear viability [23]. A measuring tool was proposed by Sengupta et al. to measure technical textiles in terms of bending behavior [24]. Alsayed et al. proposed a design of a test device to measure the performance of carpets in terms of resilience and compressibility [25, 26].

As it can be seen from the literature survey, the researchers are quite interested in static loading tests to evaluate the carpet performance. It is a fact that brief, moderate and prolonged heavy static loading tests are commonly preferred test methods. However, an automatic device that has the ability to measure the thickness and applies static loads on carpets has not been investigated yet. In this research, it is planned to create and manufacture a new and multipurpose test device in order to test thickness loss of carpet after the application of static loading and to store test data in a digital environment. The test device is fully automatic in terms of loading and unloading specimens, changing the loads, and recording test results as well without the intervention of an operator. Additionally, the developed test device is also capable of testing specimens that have a thicker structure, such as 3D fabrics.

## MATERIAL AND METHOD

### 2.1 Definition of Need and Statement of Problem

The application of static loading tests requires a thickness measurement tool, in addition to the existence of a loading mechanism in order to determine the thickness loss caused by the loading process before and after recovery periods. Regarding the static loading test, firstly, by using the thickness measurement device, the thickness of the specimen is tested under 2 kPa pressure. Following that, according to the related standard, the specimen is exposed to a specific value of pressure for a specific period of time. Then, as soon as the loading period is completed, the load is removed and the specimen is kept without loading for a

duration of time determined according to the standard. After that, the thickness is measured again. Eventually, the deformation that occurs due to the application of loads expresses the thickness loss of specimen. Determination of thickness loss can be obtained by two types of tests; prolonged heavy static loading and brief moderate static loading. For prolonged heavy static loading test, after the thickness is measured, 700 kPa load is applied for a time period of 24 hours on the specimen. Following that, the applied load is removed, and the specimen's thickness is measured after 2 minutes, 1 hour and 24 hours recovery periods [27, 28].

With respect to brief moderate static loading test, after the thickness of the carpet specimen is determined, an application of 220 kPa load for 2 hours takes place. Following the load application process, the carpet specimen left unloaded and thickness is determined in three intervals of time: after 15, 30, and 60 min. As a test requirement, five specimens must be tested for both static loading tests (heavy and brief moderate static loading) [29-31]. There are many difficulties to perform these tests. Several loading tools, and an additional carpet thickness measurement tool must be available in order to perform the previously mentioned tests. In fact, this will result in an important level of investment costs for users, such as research center, universities, and production plants as well. Additionally, both test processes are too complicated that cause personal faults due to manual equipments. Also, for the available manual test procedure it is not possible to securely record the test data in digital environment. There are several commercial brands which provide this type of manual carpet test devices [32, 35]. Today, it is a need to provide these time consuming and high labor tests automatically with a solo test device.

Table 1 provides a comparison between the commercially available test devices (A, B, C, D) and the newly developed test device (E) in terms of the capability of testing, drawbacks, and the control system.

**Table 1.** Comparison between the commercially available test devices (A, B, C, D) and the newly developed test device (E)

Test device	Capable of	Control system	Drawbacks
A	Applying static loads and testing thickness of carpet	Manual	Manual control Test results are not stored
B	Measuring carpet thickness, and underlay compression, and recovery	Manual	Manual control Test results are not stored automatically
C	Applying static loads	Manual	Additional tool is required to measure thickness Manual control Test results are not stored automatically
D	Testing recovery after applying a load for specific time	Manual	Additional tool is required to measure thickness Manual control Test results are not stored automatically
E	Measuring carpet thickness, application of brief and moderate and prolonged loading test	Automatic	None



---

The newly designed test device is superior to the commercially available test devices because of lower investment cost, decreasing the place requirement and automatically performing the test and storing the data. Additionally, accurate and precise thickness measurements can be obtained since the tests are implemented automatically without intervention of an operator for loading and unloading samples and writing down the measurements of thickness, thereby the possibility of faults from the operator side can be decreased. Moreover, test results can be stored in a digital environment. Another advantage is that thicker textile material, such as 3D fabrics can be tested using the newly developed test device.

## 2.2. Design Requirement and Constraints

Several and essential issues of design requirements were studied and taken into consideration while designing the test device in order to have a reliable test device that is capable of providing accurate and precise measurement and following the related standards. The design requirements and constraints are:

- i. The test device must have a presser foot with an area between 300 mm<sup>2</sup> and 1000 mm<sup>2</sup>.
- ii. The applied pressure must not have high fluctuation among the application duration.
- iii. It must be ensured that the force on the specimen is identical at every part of specimen.
- iv. The presser foot must move perpendicularly on the specimen and must run smoothly.
- v. The component of the test device must be easy to manufacture (less number of moving components) and not expensive.
- vi. The test device must be able to be controlled automatically.
- vii. The structure of the test device must handle the forces which is identified in standards that are going to be applied during the static loading tests, such as 700 kPa.
- viii. The usage of the test device must be easy and does not require skilled operator.
- ix. The components of the test device must not make annoying sounds while working.
- x. The test device must be equipped with a tool to ensure its balance before testing due to the importance of performing tests on a flat surface to achieve regular pressure on specimens.
- xi. Test results should be able to be stored in a digital environment.
- xii. The test device must be able to provide a low pressure on specimen such as 2 kPa for thickness measurements and a high pressure such as 220 kPa and 700 kPa for the static loading tests.
- xiii. The test device must be equipped with a reliable load cell to measure the applied forces and ensure that the applied pressures are within the standards.
- xiv. The test device must be adequate cost and affordable.
- xv. The test device must be safe for users. Indeed, pneumatic systems have astounding advantages in terms of safety [36].

## 2.3. Design of Prototype Test Device

The working principle of the test device is based on receiving instructions from an interface of Arduino. A USB connection between Arduino and the laptop is used to control each component of the test device.

In terms of the synchronization of components, the test initializes when the solenoid receives a command to be opened, from the main controller, then the piston moves down due to the provided air from the air pressure regulator and the piston presses on the sample through its presser foot. The piston applies the required loads on the sample. The value of the applied load is detected previously using the load cell which is equipped to the test device.

The position sensor, which is attached to the piston, plays an essential role in determining the stroke of the piston continually. With the help of the position sensor, the thickness of the sample is measured. All the obtained measurements are stored and displayed in the interface of Arduino software. The scenarios of the tests that the newly developed test device is capable of implementing are shown in Figure 1.

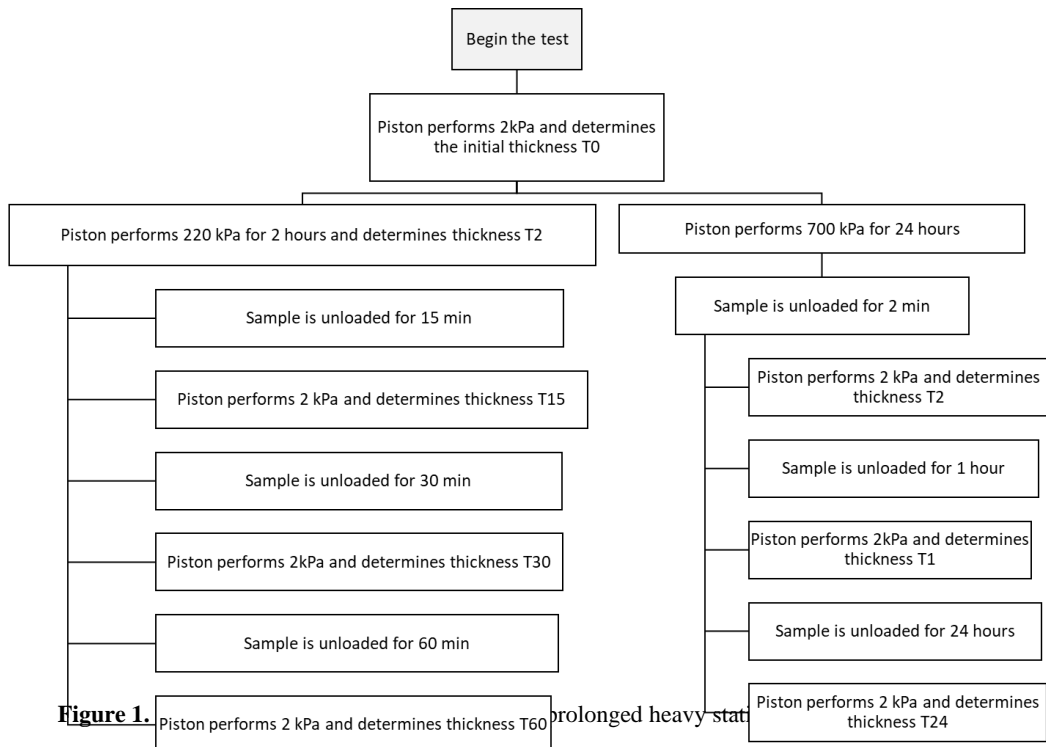


**Figure 1.** Prolonged heavy stat

The diagram in Figure 2, represents the control block diagram of the newly developed test device.

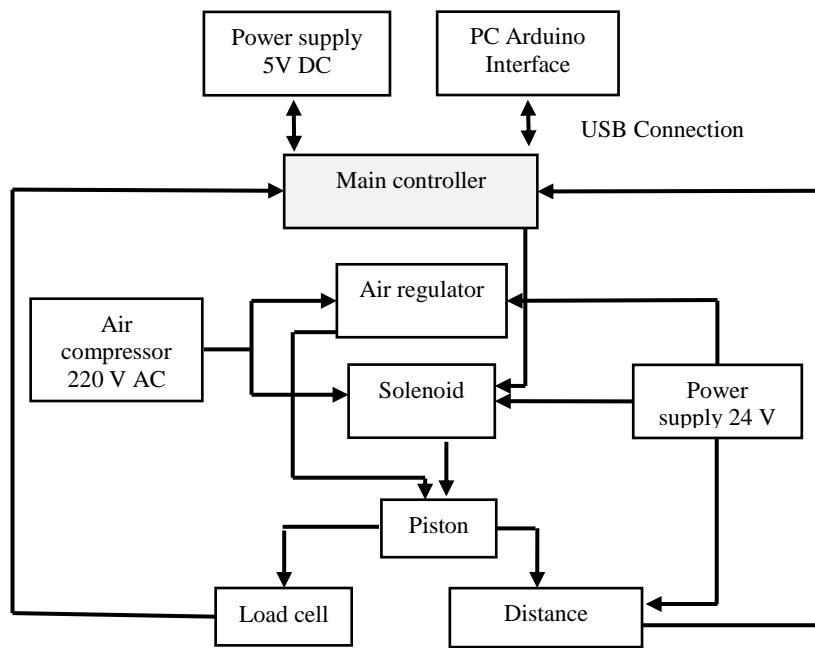


**Figure 2.** Block diagram of the communication in the testing process.

The main controller is the center of the control circuit. By the cooperation between the main controller and the position sensor, the thickness of carpet samples is measured.

As it is explained in Figure 2, the main controller sends orders to the pressure regulator and solenoid to control the movement of the piston and the amount of the pressure that will be applied. At the same time, the main controller

receives data from the position sensor and the load cell and shows them in the interface of Arduino. The circuit is equipped with two power supplies; 5V DC for the microcontroller and 220V DC for the pressure regulator, position sensor, and solenoid.

Regarding the movement system of the piston, it moves linearly and perpendicularly on to the device base. The piston has 9 cm stroke and makes this stroke in 1 second.

The moving component of the mechanism is the piston, and its degree of freedom is 1 since the piston is able to move linearly in one direction (up and down).

The two-position and three-way 3/2 pneumatic solenoid valve is the in charge of determining the movement direction. 3/2 means two working positions and three ports in the piston body, namely 1 the inlet port, 2 and 3 are the outlet ports. The inlet port 1 is where the air is supplied to the valve, port 2 is where the supplied air pushes the piston, and port 3 is where the exhausted air goes outside the circuit. When the circuit is closed, the solenoid allows the air to go to the upper part of the piston, thereby the pressure of air P1 becomes bigger than the pressure of air in the lower part of the piston P2, thereby the piston goes down, and vice versa.

#### 2.4. Construction of Prototype Test Device

The external body holds the components of the test device and maintains the conditions of the experiment balance. The body was made of durable metal to handle the loads that the test device applies. The process of manufacturing was accomplished using laser cutting technique to obtain clean edges. Basically, the external body has four screws and hex nuts that ensure and guarantee the balance of the test device by calibrating them before conducting tests. The dimension of the base of the external body is 29.5 cm × 40.7 cm × 5.0 cm. Figure 3 shows the photographic view of the newly designed test device and its components.

## 2. RESULTS AND DISCUSSION

### 3.1. Verification of the Test Device

As the newly developed test device applies static tests according to standards published by International Standardization Organizations, thereby, there is no change planned to the applied method. Only the principle of application of static loading with previously accepted devices is changed, which means that a new method is not implemented by the developed test device. Therefore, there is no need for a validation procedure. However, the verification procedure is necessary. The verification procedure is a procedure that does not contain as many details as the validation procedure, but it makes significant determinations. For the verification procedure, the accuracy criterion of the thickness measurement is taken into consideration. The accuracy criterion is determined by identifying trueness and precision. In order to verify the newly developed test device regarding trueness, the thickness measurements of the newly designed test device and a reference test device are compared and the difference between them is measured. While precision is measured by testing samples under repeatable and reproducible conditions [37, 38]. Two different samples; a cut-pile carpet and a loop-pile carpet were used as samples for the

verification procedure. Table 2 exhibits the applied tests for the verification process of the newly test device

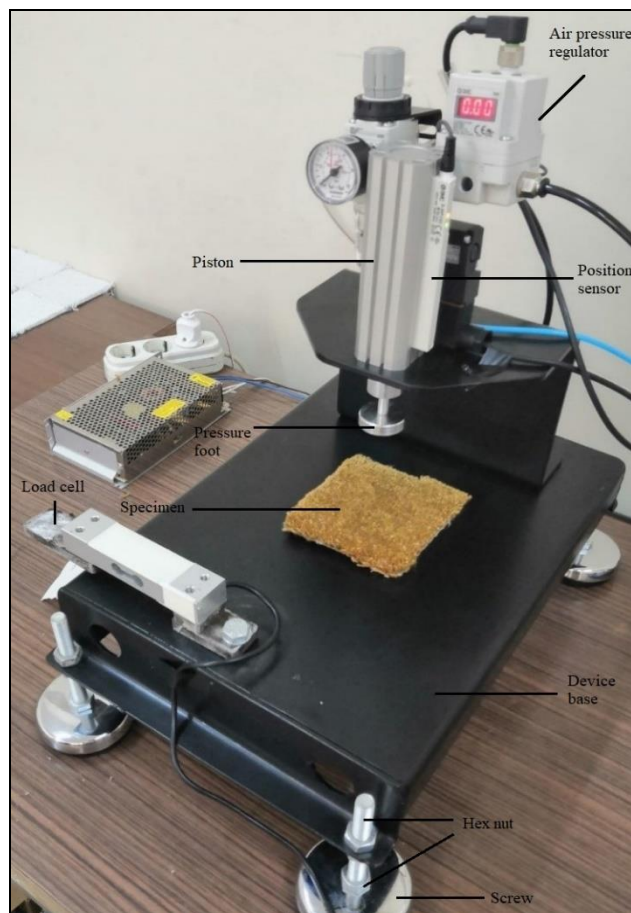


Figure 3. Photographic view of the newly designed test device

#### 3.1.1 Determination of Trueness by Using Reference Method

To prepare the samples for testing, 15 specimens 10\*10 cm from each sample were cut and conditioned in the laboratory for 24 h. The measurements of thickness were made utilizing the newly developed test device and the carpet thickness tester (as a reference). The test results are presented in Table 3.

To analyze the obtained data using SPSS, firstly, normality test was carried out, it was revealed that the findings are normally distributed. Accordingly, paired-Sample t-test was conducted. The results of the data analysis of test are shown in Table 4. The findings of the data analysis prove that statistically there is no significant difference between the thickness measurements of carpet thickness tester and the newly designed test device since Sig. (2. Tailed) = 0.728 > 0.05.

#### 3.1.2. Determination of Repeatability

In order to determine the repeatability of the test device, the thickness of the same sample was measured three times in one-day duration. The test results are shown in Table 5. Following that, statistical analyses were carried out to

determine the statistical significance between groups. accomplished for both cut-pile and loop-pile sample. Thickness measurements and statistical analyses were

**Table 2.** Verification procedure of the newly developed test device

	Test done by	Number of samples	Number of measurements	Purpose of procedure
1	Newly developed test device + carpet thickness tester	2	30	Determination of trueness by using reference method
2	Newly developed test device	2	30	Determination of repeatability
3	Newly developed test device	2	30	Determination of reproducibility over a long time period
4	Newly developed test device	2	30	Determination of reproducibility by different analysts

**Table 3.** Thickness measurement results of samples for determination of trueness

Specimen	Cut-pile sample		Loop-pile sample	
	Carpet thickness tester	Newly developed test device	Carpet thickness tester	Newly developed test device
1	14.28	14.50	7.04	7.16
2	14.23	14.36	7.06	7.43
3	14.61	14.55	7.23	7.42
4	14.55	14.51	6.81	7.1
5	14.56	14.85	7.2	7.16
6	14.25	14.03	7.25	7.23
7	14.76	14.91	7.5	7.24
8	14.67	14.70	6.86	6.81
9	14.54	14.35	6.85	7.27
10	14.67	14.40	6.82	7.34
11	14.47	14.40	7.25	7.41
12	14.74	14.71	7.12	7.06
13	14.88	14.92	6.98	7.13
14	14.40	14.16	7.4	6.84
15	14.76	14.66	7.14	7.13
Average	14.56	14.53	7.10	7.18
Standard deviation	0.20	0.26	0.21	0.19

**Table 4.** The results of Paired-Samples Test

	Paired Differences							
	Mean	Std. Deviation	Std. Error	95% Confidence Interval of the Difference		t	df	Sig. (2-tailed)
				Lower	Upper			
SDL Atlas-Prototype	-0.025	0.078	0.055	-0.723	0.678	-0.455	1	0.728

**Table 5.** Thickness measurement results of cut-pile and loop-pile samples for determination of repeatability

Sample	Specimen	Measurement 1	Measurement 2	Measurement 3
Cut-pile	1	14.38	14.14	14.53
	2	14.39	14.73	14.59
	3	14.47	14.63	14.75
	4	14.58	14.52	14.31
	5	14.57	14.59	14.54
Loop-pile	1	7.10	6.96	7.11
	2	6.83	7.02	6.51
	3	7.46	7.21	7.54
	4	7.21	6.98	7.10
	5	7.18	7.35	7.39

In order to analyze repeatability of the newly developed test device, ANOVA was conducted for thickness measurements of each sample separately. The results of statistical analyses of cut-pile and loop-pile sample thickness measurements are provided in Table 6. The values of cut-pile and loop-pile thickness measurements are normally distributed. The results of the ANOVA show that

statistically there is no difference in thickness measurement between the groups of the two samples at the three rounds of testing as the significance level of cut-pile and loop-pile sample 0.823 and 0.958 > 0.05, respectively.

### 3.1.3. Determination of Reproducibility over Long Time Period

Determination of reproducibility over long time period was done utilizing 15 specimens from each sample. The test was held for 3 days. Each day, 15 specimens from each sample were tested. The test results are given below in the Table 7.

Following thickness measurements, ANOVA was carried out to analyze the obtained test results. The results of statistical analysis of cut-pile and loop-pile carpet thickness measurements are presented in Table 8. It was found that the values of thickness measurement are normally distributed and statistically there is no significant difference between thickness measurement of the cut-pile and loop-pile samples over three days of testing as the significance

level of cut-pile and loop-pile sample is 0.888 and 0.624 > 0.05, respectively.

### 3.1.4. Determination of Reproducibility by Different Analysts

In order to determine the reproducibility of the test device by different analysts, thickness measurements of fifteen specimens from each sample were tested by different analysts. For this aim, three technologists participated in this test. Each technologist tested 15 specimens from each sample using the newly developed test device. Table 9 represents the test results of test.

**Table 6.** ANOVA results for cut-pile and loop-pile samples

Sample		ANOVA				
		Sum of Squares	df	Mean Square	F	Sig.
Cut-pile	Between Groups	0.011	2	0.006	0.199	0.823
	Within Groups	0.341	12	0.028		
	Total	0.353	14			
Loop-pile	Between Groups	0.007	2	0.003	0.043	0.958
	Within Groups	0.942	12	0.078		
	Total	0.948	14			

**Table 7** Thickness measurements of samples for reproducibility over long time period

Specimen	Cut-pile sample			Loop-pile sample		
	Day 1	Day 2	Day 3	Day 1	Day 2	Day 3
1	14.32	14.34	14.76	7.77	6.98	7.20
2	14.38	14.45	14.55	6.78	7.00	6.96
3	14.39	14.24	14.67	7.13	7.43	7.37
4	14.47	14.43	15.12	7.15	7.46	7.43
5	14.51	14.68	14.61	6.94	7.27	7.43
6	14.59	14.16	14.45	7.06	7.57	7.50
7	14.70	14.86	14.14	7.64	7.84	6.99
8	14.55	14.22	14.20	7.66	6.97	6.98
9	14.53	14.63	14.51	7.39	7.30	7.10
10	14.66	14.63	14.81	6.73	7.22	7.20
11	14.50	14.62	14.82	6.82	6.95	6.98
12	14.78	14.56	14.65	7.37	7.37	7.55
13	14.42	14.77	13.97	7.20	6.96	7.14
14	14.73	14.49	14.78	6.82	6.99	7.19
15	14.67	14.75	14.39	6.95	7.60	7.04
Average	14.55	14.52	14.56	7.16	7.26	7.20

**Table 8.** ANOVA results for cut-pile and loop-pile samples

Sample		ANOVA				
		Sum of Squares	df	Mean Square	F	Sig.
Cut-pile	Between Groups	0.012	2	0.006	0.119	0.888
	Within Groups	2.160	42	0.051		
	Total	2.172	44			
Loop-pile	Between Groups	0.075	2	0.038	0.477	0.624
	Within Groups	3.321	42	0.079		
	Total	3.397	44			



**Table 9.** Thickness measurement results of cut-pile and loop-pile samples for determination of reproducibility by different analyst

Sample	Specimen	Thickness measurements		
		Analyst 1	Analyst 2	Analyst 3
Cut-pile	1	14.45	14.50	14.38
	2	14.60	14.45	14.13
	3	14.24	14.17	14.83
	4	14.52	14.39	14.63
	5	14.57	14.72	14.81
	6	14.14	14.77	14.83
	7	14.87	14.67	14.79
	8	14.55	14.17	14.43
	9	14.49	14.83	14.38
	10	14.59	14.9	14.73
	11	14.47	14.89	14.67
	12	14.50	14.63	14.75
	13	14.89	14.73	14.73
	14	14.29	14.63	14.29
	15	14.54	14.40	14.34
Loop-pile	1	7.25	7.40	7.72
	2	7.07	7.09	7.22
	3	7.25	7.28	7.20
	4	7.94	7.07	6.66
	5	7.17	7.56	7.79
	6	6.92	7.16	6.86
	7	7.02	7.67	7.04
	8	6.98	7.17	7.50
	9	7.10	6.99	7.43
	10	7.43	7.26	7.06
	11	7.32	7.21	7.21
	12	7.47	7.50	7.08
	13	7.00	7.33	7.55
	14	6.97	7.34	6.91
	15	6.83	7.20	7.46

ANOVA was carried out to analyze the obtained data. The statistical analysis of the thickness measurements of the cut-pile and the loop-pile carpet samples was accomplished separately. The results of the data analysis are exhibited in Table 10. The data is distributing normally. As the findings of ANOVA show that, statistically, there is no significant difference between the thickness measurement of the technicians as the significance level is found to be  $0.597 > 0.05$  and  $0.591 > 0.05$  for cut-pile and loop-pile, respectively.

**Table 10.** ANOVA results for cut-pile and loop-pile samples

Sample		ANOVA				
		Sum of Squares	df	Mean Square	F	Sig.
Cut-pile	Between Groups	0.052	2	0.026	0.52	0.597
	Within Groups	2.090	42	0.050	2	
	Total	2.142	44			
Loop-pile	Between Groups	0.078	2	0.039	0.53	0.591
	Within Groups	3.077	42	0.073	3	
	Total	3.155	44			

### 3. CONCLUSION

The purpose of this study is designing and manufacturing a multifunctional, innovative, automatic, and solo test device that has the ability of measuring thickness loss after static

loading and storing test result in a digital environment. Following the design process, the newly test device was manufactured and a verification process was carried out to know whether the test device is able to accurately measure the thickness of samples. In the precision measurement, repeatability and reproducibility were applied. Regarding repeatability, thickness of the carpet samples was measured under repeatability conditions while thickness measurement of the carpet samples for reproducibility procedure was carried out under two conditions as; a long period of time and by different analysts, and by one analyst at different time intervals. This research concentrated on thickness measurements, and the applied load, 2kPa, was determined using a load cell. For future work, the code for both brief moderate loading test and prolonged loading test should be written and identified for system. Following that, brief moderate loading test and prolonged loading test should be implemented utilizing the newly developed test device and a reference test device for verification.

By using the SPSS software, the ANOVA was conducted. It was found that for the cut-pile sample, statistically, there is no significant difference between the thickness measurement of the technicians as the Sig. is found to be  $0.597 > 0.05$ . In regard to the loop-pile sample, the Sig. was found to be  $0.591 > 0.05$ , which means that the newly developed test device meets the reproducibility conditions. The statistical results revealed that the new test device has repeatability and reproducibility conditions.

As a conclusion the newly developed test device provides true and precise thickness measurements and is capable of applying all the required loads for thickness measurement test, brief, moderate static loading test, and prolonged heavy static loading test. Moreover, the repeatability and reproducibility conditions are met using the test device. Therefore, the newly designed test device is considered an effective, accurate, precise and verified test device that can be used for its advantage which can be concluded as; accurately measuring the thickness of carpets, a solo test device that can apply the static loading tests, all the test are automatically conducted without an intervention from the side of operator. Additionally, test results can be stored automatically.

In the scope of this study, the used samples for testing are two different types of carpets. For future work, other type of textile materials can be tested, such us nonwoven fabrics, 3D fabrics, etc.

### Acknowledgement

This work was supported by the Scientific Research Projects Governing Unit of Gaziantep University, under Grant [MF.YLT.18.26]. Authors would like to thank Dr. Burak Şahin for production the frame of the prototype test device.


## REFERENCES

1. Gupta S. K., Goswami, K. K. 2018. Floor Covering Wear Performance. The Textile Institute Book Series, Second Edition. Elsevier Ltd., 443-466.
2. Dayiary, M., Najar, S. S., Shamsi, M. 2009. A New Theoretical Approach to Cut-Pile Floor Covering Compression based on Elastic-Stored Bending Energy. *J. Text. Inst.*, 100(8), 688-694.
3. Carnaby, G. A. Wood, E. J. 1989. The Physics of Floor Coverings. *The Journal of The Textile Institute*, 71-90.
4. Celik, N., Koc, E. 2010. Study on the Thickness Loss of Wilton-Type Carpets under Dynamic Loading. *Fibres and Textiles in Eastern Europe*, 18(1), 54-59.
5. Javidpanah, M., Shaikhzadeh Najar, S., Dayiary, M. 2014. Study on Thickness Loss of Cut-pile Carpet Produced with Heat Process-modified Polyester Pile Yarn. Part I: Static Loading. *The Journal of The Textile Institute*, 105(12), 1265-1271.
6. M. Javidpanah, Shaikhzadeh Najar, S., Dayiary M. 2015. Study on Thickness Loss of Cut-Pile Carpet Produced with Heat Process Modified Polyester Pile Yarn. Part II: Dynamic Loading. *The Journal of The Textile Institute*, 106(3), 236-241.
7. Celik, N., Koc, E. 2007. An Experimental Study on Thickness Loss of Wilton Type Carpets Produced with Different Pile Materials after Prolonged Heavy Static Loading. Part 2: Energy Absorption and Hysteresis Effect. *Fibres and Textiles in Eastern Europe*, 15, 87-92.
8. Korkmaz, Y., Dalcı Kocer, S. 2010. Resilience Behaviors of Woven Acrylic Carpets under Short- and Long-Term Static Loading. *The Journal of The Textile Institute*, 101(3), 236-241.
9. Çelik, H. İ. 2017. Effects of Fiber Linear Density on Acrylic Carpet Performance. *Journal of Engineered Fibers and Fabrics*, 12(1), 1-11.
10. Çelik, N., Kaynak, H. K., Degırmenci, Z. 2009. Performance Properties of Wilton-Type Carpets with Relief Texture Effect Produced Using Shrinkable, High-Bulk and Relaxed Acrylic Pile Yarns. *AATCC Review*, 43-47.
11. Özdil, N., Bozdoğan, F., Kayseri, G.Ö., Mengüç, G.S. 2012. Compressibility and Thickness Recovery Characteristics of Carpets. *Tekstil ve Konfeksiyon*, 22(3), 203-211.
12. Mirjalili, S. A., Sharzehee, M. 2005. An Investigation on The Effect of Static and Dynamic Loading on The Physical Characteristics of Handmade Persian Carpets: Part I – The Effect of Static Loading. *The Journal of The Textile Institute*. 96(5), 287-293.
13. Moghassem, A. R., Gharehaghaji, A. A., Shaikhzadeh Najar, S. 2012. Analysis of Two Soft Computing Modeling Methodologies for Predicting Thickness Loss of Persian Hand-Knotted Carpets. *Fibers Polym*, 675-683.
14. Watson, S. A., Warnock, M. M. 2003. Comparative Analysis between Recycled and Newly Manufactured Carpets. *Family and Consumer Sciences Research Journal*, 31(4), 425-441.
15. Babaarslan, O., Sarioglu, E., Sıdka Ziba, O. 2017. Compressibility and Resiliency Properties of Wilton Type Woven Carpets Produced with Different Fiber Blend Ratio. *IOP Conference Series: Materials Science and Engineering*, 254(8), 1-6.
16. Radhakrishnaiah, P. 2005. Comparison of The Performance Properties of Carpets Containing Nylon 6 and Nylon 66 Face Yarns. *Textile Research Journal*, 75(2), 157-164.
17. Vuruşkan, D., Saroğlu, E., Çelik, H. İ., Kaynak, H. K. 2017. Compression Properties of Woven Carpet Performance under Dynamic Loading. *Periodicals of Engineering and Natural Sciences (PEN)*, 5, 279-283.
18. Hearle, J. W. S., Liu, H. Tandon, S. K., Wood, E. J. 2005. Computational Model of Wool Carpet Wear. *The Journal of The Textile Institute*, 96(3), 137-142.
19. Mecit, D., Roye, A. 2009. Investigation of a Testing Method for Compression Behavior of Spacer Fabrics Designed for Concrete Applications. *Textile Research Journal*, 79(10), 867-875.
20. Fujimoto, T., Sunderland, M., Tandon, S., Asano, C., Asano, A., Murata, C., Fukuyama, H. 2008. Measurement of Surface Property Using a Special Sensor Developed of Pile Materials. *Indian Journal of Fibre & Textile Research*, 33, 253-257.
21. Yi, L., Yao, B. 2011. Virtual Instrument Based Measurement System for Handle Properties Evaluation of Textile Materials. *Third International Conference on Measuring Technology and Mechatronics Automation, IEEE, Shanghai, China*, 3, 1120-1223.
22. Liao, X., Li, Y., Hu, J. et al. 2014. A Simultaneous Measurement Method to Characterize Touch Properties of Textile Materials, *Fibers Polym*, 15, 1548-1559.
23. Orr, M., Stowe, D., Thoe, S, Northup, K., Torok, M., ODell, A., Summers, J., Blouin, V., Joseph, P. 2013. Design of a Scaled Off-Vehicle Wheel Testing Device for Textile Tread Wear, *Conference: SAE World Congress, SAE Technical Paper. Detroit, Michigan, United States*. 1-6.
24. Sengupta, S., Debnath, S., and Sengupta, A. 2016. Fabric Bending Behavior Testing Instrument for Technical Textiles. *measurement*, 87, 205-215.
25. Alsayed, M., Kaynak, H. K., and Çelik, İ., H. 2020. Design of a Test System for Compressibility and Resilience Performance Measurement of Floor Coverings. *Çukurova University Journal of the Faculty of Engineering and Architecture*, 35(2), 469-475.
26. Alsayed, M., 2020. Development of a Functional Test Device Capable of Automatically Performing Main Carpet Performance Tests. MSc, Gaziantep University, Gaziantep, Turkey. 1-80.
27. British standard. 1987. Method for Determination of Thickness Loss of Carpets after Prolonged Heavy Static Loading, BS 4939.
28. American Society for Testing and Materials (ASTM). 2017. Standard Test Method for Measuring Recovery Properties of Floor Coverings after Static Loading, ASTM F970.
29. British standard. 1975. Determination of Thickness, Compression, and Recovery Characteristics of Textile Floor, C: BS 4098.
30. Turkish standard. 1991. Carpets-Determination of Thickness Loss After Brief, Moderate Static Loading, TS 3378.
31. British standard. 1987. Method for Determination of Thickness of Carpets, BS 4051.
32. WIRA Instrumentation, 01.05.2020, WIRA Floor Covering Static Loading Tester. Retrieve from: <http://aygenteks.com/media/dosyalar/2017/09/statik-y%C3%BCKleme.pdf>
33. WIRA Instrumentation, 01.05.2020, WIRA Digital Thickness Gauge Floor Coverings. Retrieve from: <https://aygenteks.com/media/dosyalar/2017/09/kal%C4%B1n%C4%B1k-%C3%B6l%C3%A7me.pdf>
34. IDM instrument, 01.05.2020, Static Load Tester for Carpet. Retrieve from: <https://idminstruments.com.au/testing-instruments/products/static-load-tester-for-carpet.html>
35. WIRA Instrumentation, 05.01.2020, WIRA Dynamic Load Machine. Retrieve from: <http://www.wira.com/media/other/37656/WiraDynamicLoading.pdf>
36. Hussain, M. K. G., Babu, T. J., Hussain, S. A. 2016. Fabrication Of Pneumatic Water Pumping System. *International Research Journal of Engineering and Technology (IRJET)*, 3(7), 2032- 2041.
37. Magnusson, B. Örnemark, U. 2018. Eurachem Guide: The Fitness for Purpose of Analytical Methods – A Laboratory Guide to Method Validation and Related Topics, 1-62.
38. Yılmaz, A. 2010. Turklab Kimyasal Analizlerde Metot Validasyonu Ve Verifikasyonu.

# Optimizing the Material-Product Transformation Processes in the Clothing Manufacturing Line

Mehmet Küçük<sup>1</sup>  0000-0002-0017-5762

Meral İşler<sup>2</sup>  0000-0002-9654-4664

Mücella Güner<sup>1</sup>  0000-0001-8910-7338

<sup>1</sup>Ege University, Engineering Faculty, Textile Engineering Department, İzmir, Türkiye

<sup>2</sup>Selçuk University, Faculty of Architecture and Design, Fashion Design Department, Konya, Türkiye

**Corresponding Author:** Mehmet Küçük, mehmet.kucuk@ege.edu.tr

## ABSTRACT

In current economic conditions, one of the major problems in the textile and apparel industry is unable to determine the unnecessary movements of resources (operators, machines, materials). Especially during the production processes, to adjust and decrease the movements of the resources are more difficult, because the focus is mostly on the workers and materials. “Method Study” has developed for resolving these challenges. The string diagram which is one of the techniques of the method study, helps to provide minimum movements of the resources during manufacturing activities. In this study, the production activities of a clothing company were examined with the help of the string diagram to achieve the objectives of eliminating unnecessary movements of the resources, increasing the working speed, providing better working conditions, balancing the production lines. So in the study, the current status of the production system and the parts to be improved were determined. In this direction, the string diagram and line balancing methods were applied for improvements and generation of a new layout plan. As a result of the research, the journal distance of the pieces before sewing together for obtaining the end product was shortened by 39% and the number of operators working in the line was reduced from 32 to 26.

## 1. INTRODUCTION

In a production environment, resources (operators and/or materials and/or machines) have to move between the predetermined stations necessarily or unnecessarily. These unnecessary displacements cause mess, chaos, loss of time and efficiency in the workplace. For this reason, it has always been extremely important for companies to arrange the workplace and the workflow by following the shortest path from the entrance to the exit. A string diagram is a scaled plan or a model to follow and measure the paths of resources along a specific sequence of events. A resource to be evaluated in the string diagram method is monitored as the work moves from one station to another. Each station where the resource moves, and if these movements are long, the arrival and departure times need methodically to

be recorded and evaluated. Then, according to these evaluations, the flow and the working areas need to be corrected in order to minimize the movement distance. Since the clothing industry is a labor-intensive sector, the number of employees is relatively high. In addition to this, the materials used in production consist of many large and small parts (for instance, the pieces of a shirt), and the variety of machines used also prevents unnecessary movements in production from being easily seen.

The string diagram is frequently used alone or in combination with other method study applications to detect and eliminate unnecessary movements in many manufacturing and service industries. As a result of the literature reviews on the subject, the following studies were obtained.

**To cite this article:** Küçük M, İşler M, Güner M. 2022. Optimizing the material-product transformation processes in the clothing manufacturing line. *Tekstil ve Konfeksiyon*, 32(2), 135-145.

## ARTICLE HISTORY

Received: 28.08.2021

Accepted: 18.04.2022

## KEYWORDS

Clothing industry, method study, workflow, string diagram, sweatshirt production, line balancing

---

C. R. Duguay, S. Landry and F. Pasin compared the mass production system with the agile production system in a study they conducted in 1997. In this direction, the main differences between the two systems were stated. So, at the end of this study, the importance of the agile system and agile operators were mentioned [1]. In a study conducted by R. Quintana in 1998, they examined the suitability of American companies to lean and agile production systems in order to maintain their competitive advantage [2]. Liu G and Fu Y. investigated the motion of satellites in space using the string diagram in a study that they conducted in 2001. By analyzing these movements in the light of the data obtained, it was proven that the string diagram could be used effectively in different disciplines as well [3]. In a study conducted by Lozier and Gawarkiewicz in 2001, the string diagram was used to examine the movements of boats of different sizes along the bay [4]. Donahue used a string diagram to observe nurses working in a hospital in 2009. The study aimed to reduce the lost time of nurses by detecting and eliminating unnecessary movements. Accordingly, thanks to the method, the way nurses traveled during the day was modeled. This time saved has been allocated to patient care [5]. In 2009, Aakre et al. used the string diagram to determine a flow chart of patients who came to a hospital for bone densitometer measurement. As a result of preparing the hospital's current and improved situation with the help of the string diagram, they enabled patients to complete their treatment with covering less distance [6]. In a study conducted by Bevilacqua et al. in 2015, a lean applications study was carried out on the packaging line of a pharmaceutical company. In this direction, they managed to reduce the total process time by 50% and increase the overall equipment efficiency by 25% using the string diagram [7]. In a study conducted by Ferreira et al. in 2015, new tools have been developed to apply lean manufacturing practices in different sectors over the years. In the research, a roadmap for the application of lean manufacturing methods in industrial settings was proposed [8]. In a study by Gebrehiwet and Odhuno in 2017, various improvement scenarios related to the way of doing business and layout were presented. First of all, an enterprise's current status was examined, and then the current situations were rearranged with line balancing methods. In the new case created due to the study, productivity by 25.74%, performance by 35.5% was increased, and the production per hour was increased from 49 to 68 pieces [9]. In a 2018 study by Chan and Tay, they tried to combine lean manufacturing techniques to increase productivity and achieve defined goals in a printing company. In this direction, between 10-30% productivity raise was achieved in the assembly line of the printing company. As a result of the study, it was suggested to use lean production techniques by combining them [10].

Güngör and Ağaç in 2014 were analysed the small scale companies' assembly lines with line balancing technique. They used COMSOAL which is meta-intuitive algorithm to evaluate the data from the assembly line [20]. Manaye in 2019 aimed on increasing the accuracy of process times and

work rearrangements among the operators and work stations line balancing techniques. At the end of the study, the production capacity was increased from 850 t-shirts to 1768 daily and the line efficiency was improved from 69,8% to 76,4% with the help of the line balancing methods [21]. In 2021, Paredes et al. made an application of the line balancing method in a clothing company. At the end of this study, they proposed a solution model optimize the production process. Results reveal the usefulness of the optimization tools for improving both efficiency and revenue at the company level [22]. Amira and Nejb in 2021 were analysed the parameters that influence the decline in production. After the line balancing implementations, the results showed that, the parameter "Machine failures" had a 34.6% effect on production, and "lack of versatility" 19.7%, while the parameter "heavy launch" had an effect of 17.1%, "lack of supplies" 9%, touch-ups 3%, and "lack of cut parts" 2% [23].

Within the scope of this study, firstly a garment was selected for following each manufacturing step in a clothing company that produces mostly knitted garments. The workflow that the materials went through during the transformation into the final product was determined. Accordingly, shortening the workflow path, rising efficiency, and accelerating the flow as much as possible were aimed.

## 2. MATERIAL AND METHOD

### a. Material

This study was carried out in a clothing company. The product features whose production process was examined in the company are as follows (Table 1).

The model examined has embroidery on the front body and a zipper on the collar. Each product has 1 ornament tag, 1 washing instruction, 1 size tag, and 1 belt tag. The production stages of the model and the machines used are shown in Table 2.

The company where the study was conducted consists of 2 floors. The characteristics of the floors and the number of machines on these floors are shown in the tables below (Table 3).

While the basement was organized in accordance with fabric spreading and cutting processes, the first floor was for sewing, ironing, packaging, and quality control processes. Accordingly, there were 1 foreman and 13 laying and cutting operators in the basement, and 2 foremen and 51 sewing operators on the first floor.

### b. Method

The method to be used in examining the selected product was the string diagram. The string diagram is one of the most useful techniques of method study. It is a scaled plan or model made by entangling a thread to track and measure the movement paths of resources along a specific sequence of events [11].

**Table 1.** Examined product



Product Group: Male Top Group  
 Product Type: Fleece Sweatshirt  
 Fabric: 100% PES  
 Color: Turquoise  
 Daily Production: 1250 pieces

**Table 2.** Operation sequence and machines

Operation	Machine
1-Attaching Ornament Tag	Lockstitch Machine
2- Attaching Washing Instructions	Lockstitch Machine
3- Preparation of Fly Tip	Lockstitch Machine
4- Fly Overcast	Overlock Machine
5- Fly and Zipper Seam	Lockstitch Machine
6- Fly Place Marking	Handwork
7- Attaching Fly to the Body Pieces	Lockstitch Machine
8- Shoulders Combining (front-back)	Overlock Machine
9- Shoulder Flatlock	Coverstitch Machine
10- Collar Preparation	Overlock Machine
11- Collar Attaching	Overlock Machine
12- Zipper Attaching	Lockstitch Machine
13- Facing	Lockstitch Machine
14- Collar Foot Stitch	Lockstitch Machine
15- Collar End Stitch	Lockstitch Machine
16- Front Foot Stitch	Lockstitch Machine
17- Sleeves Setting	Overlock Machine
18- Side Seam	Overlock Machine
19- Hemline Flatlock	Coverstitch Machine
20- Sleeve Flatlock	Coverstitch Machine
21- Attaching a Folding Tag	Lockstitch Machine

**Table 3.** Floors and machines

Floor	Area	Equipment	Personnel
Basement	250 m <sup>2</sup>	Warehouses	1 foreman - 13 operators
		Sorting area	
		1 roll fabric opening machine	
		1 fabric spreading table	
		1 cutting table (cutter)	
		1 fabric control table	
		3 wheeled shelf system	
		1 transport trolley	
		Placing baskets	
		Transfer baskets	
First floor	420 m <sup>2</sup>	Sorting shelf	2 foreman - 51 operators
		15 lockstitch machines	
		8 overlock machines	
		5 coverstitch machines	
		4 sorting table	
		1 handwork table	
		2 meto label table	
		2 thread cleaning table	
		4 precontrol table	
		2 final control table	
		1 packaging table	
		Transfer baskets	

The string diagram is a scaled diagram that provides to show the movement paths of the resources in their own manufacturing processes. Like the method study schemes, the string diagram is prepared on the basis of the process, showing the entire process without going into details. On a scaled sketch of the workplace, the method tries to determine between which stations and how often the source travels, by counting the threads that a source passed through the stations [12].

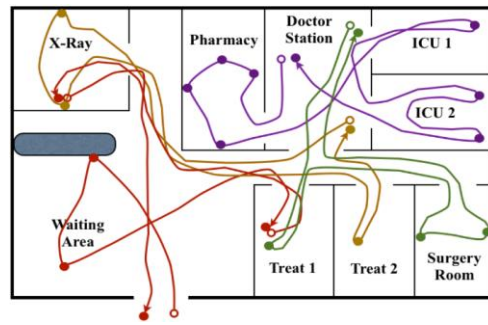


**Figure 1.** A string diagram example

Preparation of the string diagram starts like other method studies; Firstly, all events related to direct observation are recorded. The work-study expert watches the resource of interest during it moves from one point to another as the work is performed. If the expert gives a sign such as numbers, letters to various machines, warehouses, and other points during the examination, the work will be followed in a simpler way [13].

This recording process continues until the work-study expert is sure about having enough information to show the resource's movements. This period can be a few hours, a day, or longer. Thus, the expert can obtain all the information about all the movements made by the source and how often these movements are repeated relatively. If the expert observes only a part of the sequence of movements made by the source, the study will be insufficient and cause to reach wrong conclusions. Also, during such a study, the source may have used a different path than the standard route. A string diagram can be created, only when the expert believes that he/she has obtained the necessary and enough information and be sure that there is no unobserved movement. Additionally, he/she should check all the gathered information together with someone who observes the manufacturing activities continuously, such as a foreman, to avoid missing something out [13].

Machinery, equipment, warehouses, and all points should be drawn to scale. In addition to these, doors, pillars and partitions that have effects on movement paths should be shown. In the conventional technique, the completed plan should be placed on a soft board and pinned with pins to be put on the "stop" points shown in the plan. The remaining part of the needle should not be less than 1 cm. At the same time, pins should be placed at turning points on the path. Then a measured piece of thread is taken and wrapped around the needle located at the starting point of the movements. The thread is then wrapped around the needles at the other points in the order shown on the study until all the movements are completed. As a result, a complete string diagram can be obtained that shows the resource's all motion paths [14]. Today, some computer software can be used in the drawings to be made in this direction.

In order to eliminate unnecessary movements in the study, the line balancing method was also applied to the production line with the string diagram. The traditional assembly line balancing problem considers the production



process in which products are created by assigning tasks sequentially to different workstations. The distribution of tasks among stations depends on the time unit required to complete each task as well as the existing priority constraints between tasks. The product is allowed to stay in each station for a maximum of the cycle time. [15]

There are 2 options in the traditional line balancing problem scenario. One of them is to minimize the required number of stations by fixing the cycle time. The other is the minimization of cycle time in a fixed number of stations [16]. To achieve these objectives, assigning tasks to sequential workstations is called line balancing, with providing the priority relationships are not violated and cycle time is not exceeded. In this study, the required number of stations is minimized by taking the cycle into account.

### 3. FINDINGS

Following the examinations and follow-up procedures for the production of the selected product, first of all, the current situation of the company was prepared by the string diagram method. With the studies on the current situation and the calculations of the distance traveled by the product, some implementations were made to shorten this distance.

In the basement of the company, the spreading and cutting processes of the fabrics were completed. Afterward, the cut pieces were carried to the 1st floor by elevators after going through the meto labeling processes. On the 1st floor, the cut pieces were shipped to the production line. After

sewing, the products were transferred to yarn cleaning, ironing, and packaging processes. Findings of the whole process were given below (Figure 2-3).

As a result of the examinations and studies carried out in the company, no reorganization was required due to the volumetric size of the tables and other immovable materials used in the basement. Also, improvements were made only on the 1st floor. The current and improved situation of the floors were drawn with Microsoft Visio Standard 2019 software. Drawings were created in a 1/100 ratio.

#### a. The Current Flow

##### *Basement*

The way the raw material is spread and cut in the company is as shown below (Figure 2).

##### *The 1<sup>st</sup> Floor*

Similarly, the flow on the 1st floor of the company is as follows. The arrow colors and names used in displaying the flow are also shown in Figure 3.

In the Figure 3, the numbers refer the operation numbers and the letters refer the operators in Table 5. According to this configuration, the operators, operation numbers, processes and machines were indicated in Table 5.

The processes applied to the product at each station on the 1st floor are shown in the table below (Table 6).

**Table 5.** Current 1<sup>st</sup> floor – operators, operations and machines

OPERATOR	OPERATION NO	PROCESS	MACHINES
A	16	Attaching Ornament Tag	Lockstitch Machine
B	17	Attaching Washing Instructions	Lockstitch Machine
C	18	Preparation of Fly Tip	Lockstitch Machine
D	19	Fly Overcast	Overlock Machine
E	20	Fly and Zipper Seam	Lockstitch Machine
F	21	Fly Place Marking	Handwork
G	22	Attaching Fly to the Body Pieces	Lockstitch Machine
H	23	Shoulders Combining (front-back)	Overlock Machine
I	24	Shoulder Flatlock	Coverstitch Machine
J	25	Collar Preparation	Overlock Machine
K	26	Collar Attaching	Overlock Machine
L	27	Zipper Attaching	Lockstitch Machine
M	27	Zipper Attaching	Lockstitch Machine
N	28	Facing	Lockstitch Machine
O	29	Sorting	Sorting Table
P	30	Collar Foot Stitch	Lockstitch Machine
R	30	Collar Foot Stitch	Lockstitch Machine
S	31	Collar End Stitch	Lockstitch Machine
T	32	Front Foot Stitch	Lockstitch Machine
U	31	Collar End Stitch	Lockstitch Machine
V	32	Front Foot Stitch	Lockstitch Machine
Y	33	Sorting	Sorting Table
Z	34	Sleeves Setting	Overlock Machine
AA	34	Sleeves Setting	Overlock Machine
AB	35	Sorting	Sorting Table
AC	36	Side Seam	Overlock Machine
AD	36	Side Seam	Overlock Machine
AE	37	Hemline Flatlock	Coverstitch Machine
AF	37	Hemline Flatlock	Coverstitch Machine
AG	38	Sleeves Flatlock	Coverstitch Machine
AH	38	Sleeves Flatlock	Coverstitch Machine
AI	42	Attaching a Folding Tag	Lockstitch Machine

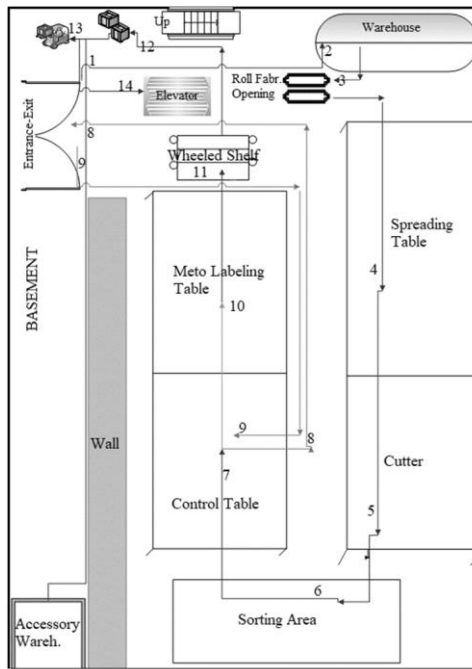


Figure 2. Basement

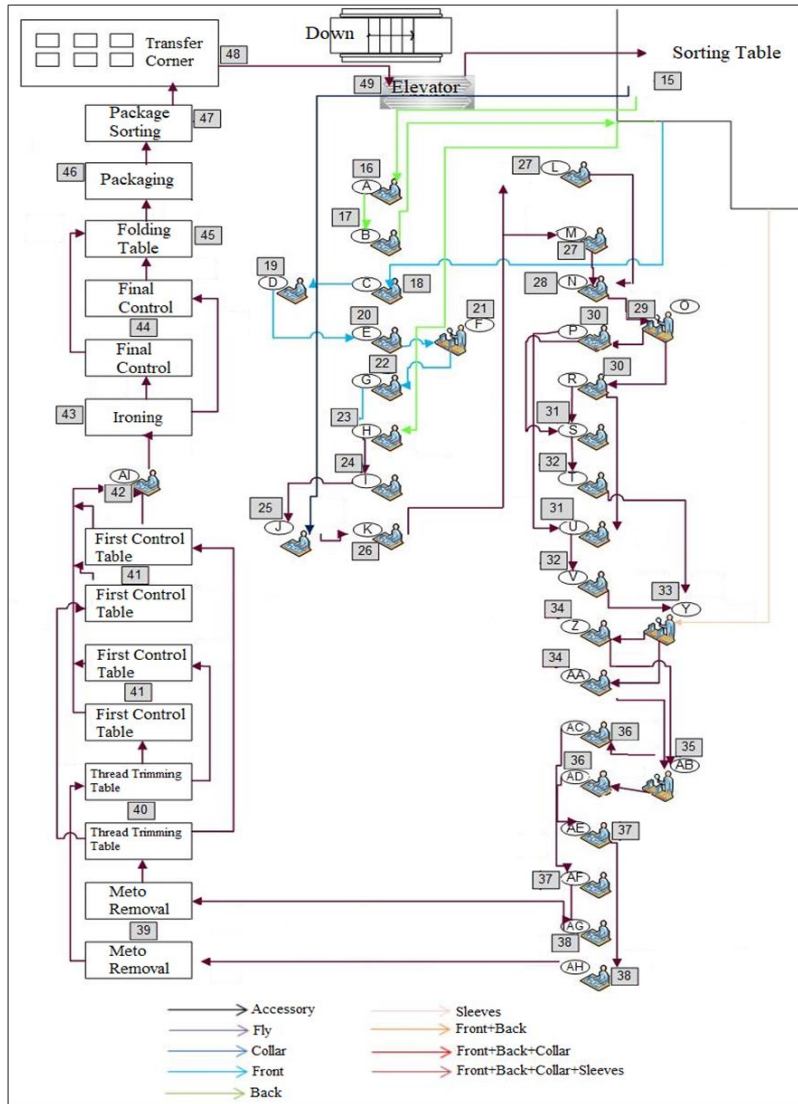


Figure 3. Current 1<sup>st</sup> floor scheme

**Table 4.** Basement workflow

Process Numbers	Processes
	The company supplies the fabrics required for production.
(1-2)	Purchased fabrics are transported from the entrance door to the warehouse.
(2-3)	Fabrics are transferred from the warehouse to the roll fabric opening machine.
(3-4)	The rolls are transferred to the spreading table.
(4-5)	After the spreading processes, fabrics are brought to the cutter for cutting.
(5-6)	The cut pieces are kept in the sorting area.
(6-7)	The parts are brought to the control table for checking the cutting process.
(7-8)	The front pieces are sent to the exit for the embroidery process.
(8-9)	Pieces coming from embroidery are brought to the control table.
(9-10)	After the control process is completed, all pieces are transferred to the meto labeling table.
(10-11)	The pieces are placed in a wheeled rack system.
(11-12)	Baskets are placed on the trolley.
(13)	Meanwhile, accessories are brought from the warehouse and placed in the trolley.
(13-14)	In order for the pieces to enter production line, the transport car is brought to the elevator and raised to the 1st floor.

**Table 6.** The 1<sup>st</sup> floor - current workflow

OPERATION NO	PROCESSES
(15)	Pieces come from basement are placed to the sorting table
(15-16)	From sorting table to the Operator-A for attaching the ornament tag
(16-17)	Then pieces come to the Operator-B for attaching the washing instructions and send to sorting table back
(15-18)	Front pieces come from the sorting table to Operator-C for preparation of fly tips
(18-19)	The pieces are brought to the Operator-D for fly overcast
(19-20)	The Operator-C gets pieces for the fly and zipper seam
(20-21)	The pieces are brought to the Operator-F for fly place marking (handwork)
(21-22)	After the marking processes, pieces are sent to the Operator-G for attaching fly to the body pieces
(22-23)	Front pieces are brought to the Operator-H for shoulders combining process. At the same time, the back pieces that are waiting on the sorting table are brought to the Operator-H as well for the same process
(15-23)	
(23-24)	The pieces are sent to the Operator-I for shoulder flatlock stitches
(24-25)	
(15-25)	Pieces then comes to the Operator-J and at the same time the collar pieces are brought for collar preparation process
(25-26)	After the preparation process, pieces are brought to the Operator-K for collar attaching
(26-27)	The pieces coming out of the Operator-K are divided into two and brought to the Operator-L and Operator-M for zipper attaching
(27-28)	After the zipper attaching processes, the pieces are brought to the Operator-N for facing
(28-29)	Then the pieces come to Operator-O for sorting (handwork)
(29-30)	The pieces are brought to Operator-P and Operator-R from the sorting table for collar foot stitch
(30-31)	The pieces are sent to Operator-S and Operator-U for collar end stitches
(31-32)	The pieces are brought to the Operator-T and Operator-V for front foot stitches
(32-33)	
(15-33)	The pieces are brought to the Operator-Y for sorting process. At the same time, sleeves also are brought to this sorting table
(33-34)	The pieces after this matching process are brought to the Operator-Z and Operator-AA for sleeves setting processes
(34-35)	Then the pieces come to the Operator-AB for sorting
(35-36)	The pieces are sent to the Operator-AC and Operator-AD for side seam
(36-37)	The pieces are brought to the Operator-AE and Operator-AF for hemline flatlock
(37-38)	The pieces are then brought to the Operator-AG and Operator-AH for sleeves flatlock
(38-39)	After that the pieces are brought to the meto label removing table
(39-40)	Then they are sent to the thread trimming table
(40-41)	The pieces are brought to the first control table for controlling in detail
(41-42)	Then the pieces are sent to Operator-AI for attaching a folding tag process
(42-43)	Then the products are brought to the ironing processes
(43-44)	The products then sent to the final control table
(44-45)	The products are brought to the folding table
(45-46)	The products are brought to the packaging table
(46-47)	The products are brought to the package sorting table
(47-48-49)	The packages are brought to the transfer corner
	The shipping processes.

As a result of the analysis, in the current situation of the 1st floor of the company, a total of 32 operators and 28 machines were employed only on the sewing line (excluding control and packaging processes). It has been observed that the pieces traveled 51m 5cm in the 250 m2 area on the basement and 108m 9cm in the 420 m2 space on the 1<sup>st</sup> floor until turning into the final product form, starting from the first station of raw material warehouse.

### b. 1st Floor New Layout

Within the scope of the study, in order to minimize the distance that materials traveled in the sewing line and to re-establish the band with the optimum number of machines and operators, the line balancing application was also carried out on the line with the string diagram. Firstly, the number of machines allocated for the order in question, the number of operators, the daily working time, and the standard times of each operation were recorded.

Standard times calculation procedures were carried out on each production activity according to the time study

method. After that, during the line balancing implementations, the standard times and the daily production numbers were taken into account. Subsequently, the reorganization processes were carried out with the string diagram. As a result of these method implementations and practices, the sewing line's new improved layout was generated. In this direction, the distance traveled by the materials while transforming into the sweatshirt was measured in the latest status of the sewing line, as well.

The new layout obtained as a result of the string diagram and line balancing applications performed for eliminating the unnecessary movements of the materials on the 1st floor current form is as follows (Figure 4).

The operations performed at each station on the new 1st floor were shown in the table below (Table 8). In addition, unlike the current situation, the decisions taken to make the flow more regular were specified in each operation step.

**Table 7.** New layout 1<sup>st</sup> floor – operators, operations, machines and times

Operator	Operation No	Process	Machine	Std Time (Sec)	Output (Pcs)	Time Needed (Min)	Time Remaining (Min)
A	16	Attaching Ornament Tag	Lockstitch Machine	9.00	1250	188	
A	17	Attaching Washing Instructions	Lockstitch Machine	13.00	1250	271	22
B	18	Preparation of Fly Tip	Lockstitch Machine	22.40	1250	467	13
C	19	Fly Overcast	Overlock Machine	20.80	1250	433	47
D	20	Fly and Zipper Seam	Lockstitch Machine	35.70	1250	744	
E	20	Fly and Zipper Seam	Lockstitch Machine	35.70	1250	744	
E	21	Fly Place Marking	Handwork	9.00	1250	188	29
F	22	Attaching Fly to the Body Pieces	Lockstitch Machine	21.00	1250	438	43
G	23	Shoulders Combining (front-back)	Overlock Machine	31.20	1250	650	
H	24	Shoulder Flatlock	Coverstitch Machine	22.90	1250	477	3
I	23	Shoulders Combining (front-back)	Overlock Machine	31.20	1250	650	-3
I	25	Collar Preparation	Overlock Machine	15.00	1250	313	
J	26	Collar Attaching	Overlock Machine	44.20	1250	921	
K	26	Collar Attaching	Overlock Machine	44.20	1250	921	39
L	27	Zipper Attaching	Lockstitch Machine	46.20	1250	963	
M	27	Zipper Attaching	Lockstitch Machine	46.20	1250	963	-3
N	28	Facing	Lockstitch Machine	22.00	1250	458	22
O	29	Collar Foot Stitch	Lockstitch Machine	23.40	1250	488	-8
P	30	Collar End Stitch	Lockstitch Machine	45.00	1250	938	
R	30	Collar End Stitch	Lockstitch Machine	45.00	1250	938	
R	31	Front Foot Stitch	Lockstitch Machine	47.10	1250	981	1
S	31	Front Foot Stitch	Lockstitch Machine	47.10	1250	981	
T	31	Front Foot Stitch	Lockstitch Machine	47.10	1250	981	
U	32	Sleeves Setting	Overlock Machine	49.40	1250	1029	
V	32	Sleeves Setting	Overlock Machine	49.40	1250	1029	
Y	33	Side Seam	Overlock Machine	42.40	1250	883	
Z	33	Side Seam	Overlock Machine	42.40	1250	883	77
Z	32	Sleeves Setting	Overlock Machine	49.40	1250	1029	7
AA	34	Hemline Flatlock	Coverstitch Machine	23.20	1250	483	-3
AB	35	Sleeve Flatlock	Coverstitch Machine	23.00	1250	479	1
AC	36	Attaching a Folding Tag	Lockstitch Machine	20.00	1250	417	63
<b>Total</b>				<b>668.60 sec</b>			

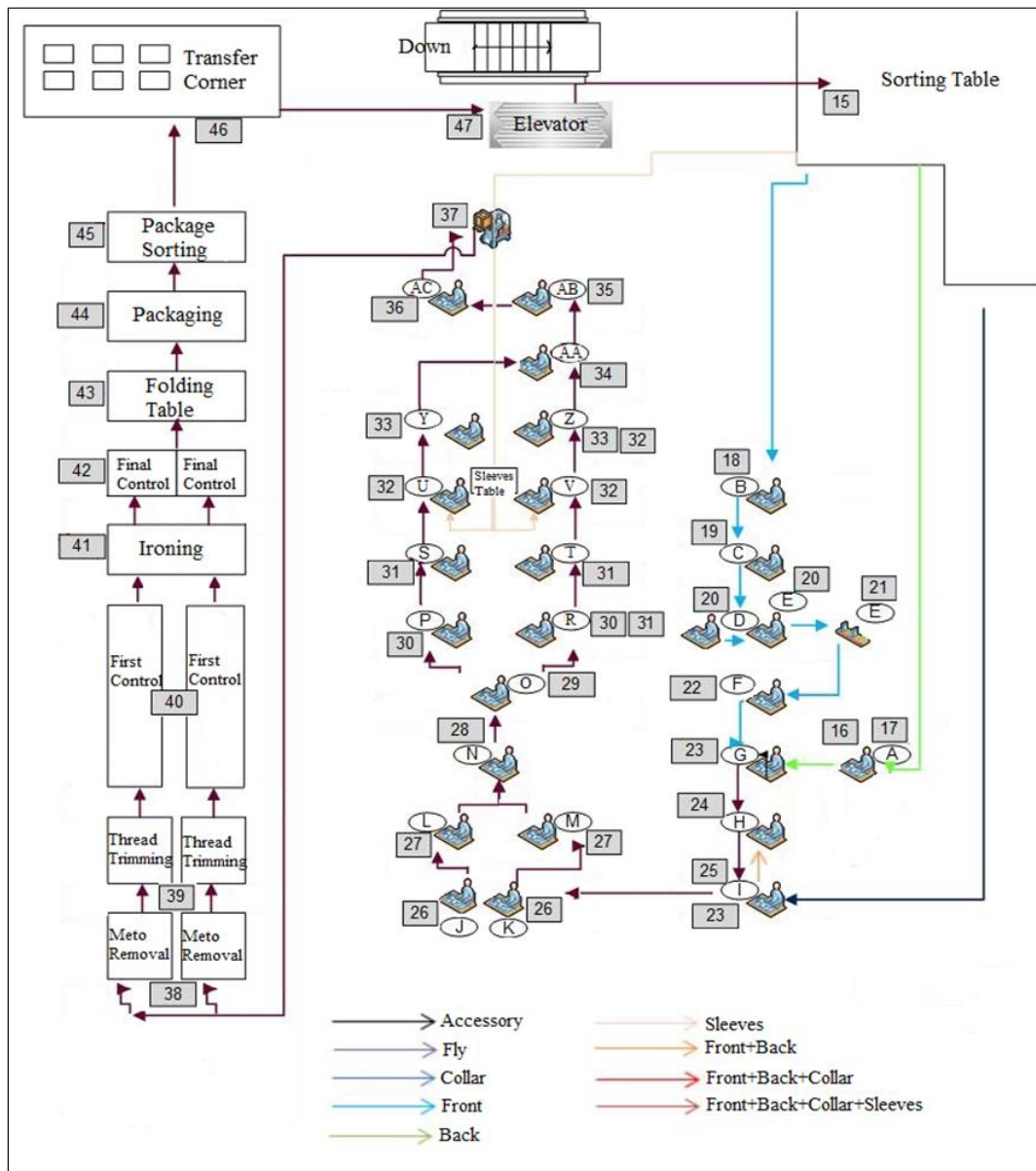


Figure 4. The 1<sup>st</sup> floor new layout

In the quality-control, ironing and packaging area, the positions of the tables were changed to make the operators move less with the material. In this direction, the tables were mostly placed parallel to each other. Thus, it is thought that this area was relieved by a path between the tables.

As a result of the improvements applied with the string diagram and line balancing technique, 26 operators and 26 machines in total were employed in the production of the sweatshirt only in the sewing line (excluding control and packaging processes) in the new situation of the 1st floor of the company.

Accordingly, while this transformation to the sweatshirt, the pieces took 108m and 9cm in current situation. This distance was reduced to 66m and 3cm in the new layout. Thus, improvements were made to complete manufacturing steps of the sweatshirt with around 39% less traveling of the pieces in the sewing room.

#### 4. RESULTS AND DISCUSSIONS

Method study implementations are among the most frequently used methods to solve problems such as blockages in the work flow, delays, waiting for pieces, idle times or overloading of machines, not being able to use the factory area efficiently and delaying delivery times to the customer and so on, encountered in manufacturing industry. Finding solutions to this kind of problems has become even more important in dynamic sectors such as the clothing sector, where a large number of people work and orders are made with short deadlines. In this study, minimizing the biggest problems experienced in clothing industry, such as excessive accumulation of end products or pieces of them in unnecessary places, ergonomic complaints of the employee in the workplace, unnecessary extension of production time, unnecessary transportations, were aimed to minimize and/or eliminate.



**Table 8.** The 1<sup>st</sup> floor – new workflow

<b>OPERATION NO</b>	<b>PROCESSES</b>
(15)	Pieces come from basement are placed to the sorting table
(15-16-17)	The pieces are sent to the Operator-A for the processes of attaching ornament tag and attaching washing instructions <i>(Operator-A does these both processes)</i>
(15-18)	Front pieces come from the sorting table to Operator-B for preparation of fly tips
(18-19)	The pieces are brought to the Operator-C for fly overcast
(19-20)	The pieces are sent to Operator-D and Operator-E for the fly and zipper seam <i>(The fly and zipper seam processes are done by 2 different operators to provide a more optimum flow)</i>
(20-21)	Operator-E does the fly place marking process his/her own remaining time <i>(Operator-E moves to the table for the process number-21 in the remaining time.)</i>
(21-22)	After the marking processes, pieces are sent to the Operator-F for attaching fly to the body pieces
(22-23)	The pieces after the fly processes from Operator-F and washing instruction processes from Operator-A are brought to the Operator-G and Operator-I for the shoulders combining (front and back) processes <i>(Operator-I also does the shoulders combining process with the collar preparation process due to available time remaining)</i>
(23-24)	The pieces are sent to the Operator-H for shoulder flatlock stitches
(24-25)	The pieces then comes to the Operator-I and at the same time the collar pieces are brought for collar preparation process
(25-26)	After the preparation process, the pieces are brought to the Operator-J and the Operator-K for collar attaching <i>(As a result of the line balancing processes, collar attaching process is done by 2 operators)</i>
(26-27)	The pieces coming out of the Operator-J and Operator-K are brought to the Operator-L and Operator-M for zipper attaching
(27-28)	After the zipper attaching processes, the pieces are brought to the Operator-N for facing
(28-29)	The pieces are brought to Operator-O for collar foot stitch
(29-30)	The pieces are sent to Operator-P and Operator-R for collar end stitches
(30-31)	The pieces are brought to the Operator-S and Operator-T for front foot stitches <i>(This process is also done by the Operator-R that has enough remaining time, in order to provide a better flow)</i>
(31-32)	The pieces are brought to the Operator-U, Operator-V and Operator-Z for sleeves setting processes <i>(Sleeves pieces wait on the middle table)</i>
(32-33)	The pieces are sent to the Operator-Y and Operator-Z for side seam <i>(The Operator-Z also does the sleeves setting process and side seam process due to available time remaining)</i>
(33-34)	The pieces are brought to the Operator-AA for hemline flatlock <i>(As a result of the line balancing processes, hemline flatlock process is done by just 1 operator)</i>
(34-35)	The pieces are then brought to the Operator-AB for sleeves flatlock <i>(As a result of the line balancing processes, sleeves flatlock process is done by just 1 operator)</i>
(35-36)	Then the pieces are sent to Operator-AC for attaching a folding tag process <i>(It has been decided that there is no need to perform a first control just before attaching a folding tag, for that reason this process is placed at the end of the sewing line)</i>
(36-37)	The products are brought to vehicle
(37-38)	After that the products are brought to the meto label removing table
(38-39)	Then they are sent to the thread trimming table
(39-40)	The pieces are brought to the first control table for controlling in detail
(40-41)	Then the products are brought to the ironing processes
(41-42)	The products then sent to the final control table
(42-43)	The products are brought to the folding table
(43-44)	The products are brought to the packaging table
(44-45)	The products are brought to the package sorting table
(45-46-47)	The packages are brought to the transfer corner The shipping processes.

Sewing department is one of the most important departments in textile and apparel industry and an efficient line balancing improves motivation of the workers and benefit of the establishment. The line balancing method is of great importance in apparel manufacturing processes having a large number of employees. As one of the method study techniques, the string diagram provides to measure all the faults in their current situation in the most effective way and allow the numerical values of the improvements to be made as a result of observations [17]. Also in the study, the string diagram was contributed with the line balancing method.

In this study, the whole production process of a sweatshirt was examined. After all the examinations were carried out in the production, the sewing line needed to be reorganised mode urgently throughout the production process. In this direction, it is thought that all unnecessary activities were eliminated, and the most appropriate layout was generated. To obtain a more effective and permanent layout plan, while the string diagram was applied on the sewing line, the standard times of each operation were also calculated for supporting the diagram with line balancing method. Production line balancing is of great importance in apparel manufacturing processes which works a large number of employees [18].

Unnecessary movements in the production line were eliminated owing to the method. In parallel with this, it is thought that by shortening the work flow path, the time of transformation of materials to end product was reduced. In addition, it is thought that the delivery time and the new product processes into production were accelerated, and thus the factory area was used more efficiently.

Since the tables, devices, and shelves on the basement were large in volume, it was caused restrictions in terms of changes in replacement. However, this area was dealt with other lean production techniques such as 5S, Muda-murimura and general arrangements were made accordingly. On the 1st floor where mostly sewing machines were located, while 32 operators and 28 sewing machines were used in total in current flow, these numbers were reduced to 26 operators and 26 sewing machines in the new layout plan. Besides, in the new layout plan, the same operation was assigned to more than one operator as well as more than one operation to one operator considering the standard times. Simultaneously, unnecessary processes in the sewing line were also eliminated and the machine layout was changed, allowing the pieces to travel less. Thanks to the string diagram and line balancing techniques, while a product was ready after traveling 108m 9cm in the current situation, this distance was reduced to 66m 3cm in the new layout plan.


By improving the production processes in the sectors like clothing, the lean tools have enough importance on this goal. Analysing the the current situation requires some observation methods. To carry out this analysis an observation plan was used, having the Spaghetti diagram as a reference as well as the line balancing method [19]. It is thought that supporting the string diagram with some other method study techniques like line balancing is a must in today's competitive environment for manufacturing companies. Thus, by eliminating the problems experienced by these companies in the assembly lines, production activities will be completed in the shortest time and in the most efficient way. In this context, this study is intended to be a useful roadmap, especially for the clothing industry, in theoretical and practical ways.

## REFERENCES

1. Duguay, C.D., Landry, S. and Pasin, F. (1997), "From mass production to flexible/agile production", *International Journal of Operations & Production Management*, Vol. 17 No. 12, pp. 1183-1195.
2. Quintana, R. (1998), "A production methodology for agile manufacturing in a high turnover environment", *Int. J. Oper. Prod. Manag.*, Vol.21 No. 5/6, pp. 630-644.
3. Liu, G. and Fu, Y. (2001), "The characteristics of tropical precipitation profiles as inferred from satellite radar measurements", *Journal of the Meteorological Society of Japan*, Vol. 79 No. 1, pp. 131-143.
4. Lozier, S. and Gawarkiewicz, G. (2001), "Cross-frontal exchange in the middle atlantic bight as evidenced by surface drifters", *Journal of Physical Oceanography*, Vol. 31, pp. 2498-2510.
5. Donahue, L. (2009), "A pod design for nursing assignments", *AJN*, Vol. 109 No. 11.
6. Aakre, K.T., Valley, T.B. and O'Connor, M.K. (2010), "Quality initiatives: improving patient flow for a bone densitometry practice: results from a mayo clinic radiology quality initiative", *RadioGraphics*, Vol. 30 No. 2, pp. 309-315.
7. Bevilacqua, M., Ciarapica, F.E., De Sanctis, I., Mazzuto, G. and Paciarotti, C. (2015), "A changeover time reduction through an integration of lean practices: a case study from pharmaceutical sector", *Assembly Automation*, Vol. 35 No. 1, pp. 22 - 34. doi: 10.1108/AA-05-2014-035
8. Ferreira, T., Baptista, A.A., Azevedo, S. and Charrua-Santos T. (2015), "Tool development for support lean manufacturing implementation in intermittent production environment", *Proceedings of the World Congress on Engineering*, July 1 - 3, 2015, London, U.K, pp. 972-977.
9. Gebrehiweta, T.B. and Adhiambo, M. (2017), "Improving the productivity of the sewing section through line balancing techniques: a case study of almeda garment factory", *International Journal of Sciences: Basic and Applied Research (IJSBAR)*, Vol. 34 No. 1, pp.318-328.
10. Chan, C.O. and Tay, H.L. (2018) "Combining lean tools application in kaizen: a field study on the printing industry", *International Journal of Productivity and Performance Management*, Vol. 67 No. 1, pp. 45-65. doi:10.1108/IJPPM-09-2016-0197
11. Senderská, K., Mareš, A. and Václav, Š. (2017), "Spaghetti diagram application for workers' movement analysis", *U.P.B. Sci. Bull., Series D*, Vol. 79, No. 1, pp. 139-150.

- 
12. Mahajan, M., Christopher, K.B., Shiva, H. and Prasad, H.C. (2019), "Implementation of lean techniques for sustainable workflow process in Indian motor manufacturing unit", 2nd International Conference on Sustainable Materials Processing and Manufacturing (SMPM 2019), *Procedia Manufacturing* 35, pp. 1196–1204.
  13. Yalçın, M., Elyas, C., Yıldız, S., Alpşen, C. and Yalçın, G. (2018), "The improvement of hospital laboratory processes using the principles of lean methodology (toyota production system-spaghetti diagram)", *Konuralp Medical Journal*, Vol. 10 No. 1, pp. 99-104.
  14. Cohen, B.A. and Decker, M.C. (2017), "Implementation of lean methodology in a free clinic", *Free Clin Res Collect*, Vol. 3.
  15. Delice, Y., Aydoğan, E.K., Özcan, U. and İlkay, M.S. (2017), "A modified particle swarm optimization algorithm to mixed-model two-sided assembly line balancing", *J Intell Manuf*, Vol.28 pp. 23–36, doi: 10.1007/s10845-014-0959-7.
  16. Ajenblit, D.A. and Wainwright, R.L. (1998) "Applying genetic algorithms to the u-shaped assembly line balancing problem", *IEEE*, pp. 96-101.
  17. Gürsor, A. and Kırçalı Gürsoy, N. (2015), "On the flexibility constrained line balancing problem in lean manufacturing", *Tekstil ve Konfeksiyon*, Vol. 25 (4), pp.345-351.
  18. Güner, M., Yücel, Ö. and Ünal, C. (2013), "Applicability of different line balancing methods in the production of apparel", *Tekstil ve Konfeksiyon*, Vol. 23 (1), pp.77-84.
  19. J C Sá et al. (2021), "Lean Safety - assessment of the impact of 5S and visual management on safety", *IOP Conf. Ser.: Mater. Sci. Eng.* 1193 012049.
  20. Güngör, M. and Ağaç, S. (2014), "Resource-constrained mixed model assembly line balancing in an apparel company", *Tekstil ve Konfeksiyon*, Vol. 24 (4), pp. 405-412.
  21. Manaye, M. (2019), "Line balancing techniques for productivity improvement", *International Journal of Mechanical and Industrial Technology*, Vol. 7, Issue 1, pp: 89-104.
  22. Paredes et al. (2021), "Efficiency improvement in a clothing manufacturing company: a peruvian case study", 10th International Conference on Industrial Technology and Management, DOI 10.1109/ICITM52822.2021.00037.
  23. Amira, L. and Nejib, S. (2021), "Study of Parameters Influencing the Production and Improvement of the Launch System in a Production Department: Case Study in the Clothing Industry in Tunisia", *Fibres & Textiles in Eastern Europe*, 29, 6(150): 4-10. DOI: 10.5604/01.3001.0015.2715.

# Effects of Different Stitch Types and Stitch Combinations on the Seam Bursting Strength and Seam Strength of Workwear

Şükran Kara  0000-0001-8866-2129

Dokuz Eylül University / Engineering Faculty / Textile Engineering Department / Tınaztepe Campus, Buca, İzmir, Türkiye

**Corresponding Author:** Şükran Kara, sukran.kara@deu.edu.tr

## ABSTRACT

Workweares are produced to protect the wearer against occupational or environmental hazards. One of the shared properties of several workwear types is resisting external forces during occupation. As for workwear fabrics, the seams of the workwear should be strong enough to resist uniaxial or multiaxial forces to maintain the properties in the cut and sewn parts of the garment. Therefore, in this study, effects of different stitch types and their combinations on the workwear seam strength and bursting strength were evaluated. According to results, a 2-step failure was observed at the seam strength tests of samples those contained stitch combinations. Here, the main function of the second stitch row was to form a safety stitch rather than increasing the overall performance. Contrarily, usage of stitch combinations obviously contributed to the seam bursting strengths. In this case, the stitch rows responded to the bursting forces together therefore the bursting failures occurred in 1-step.

## 1. INTRODUCTION

Fabrics can be gathered together via different assembling methods in order to form 3-dimensional garments and other textile end-products. Stitching is the most common assembling method, as it is easy to apply, cheap and suitable for most of the applications [1, 2]. In textile industry, six standard classes of stitches are used as chain stitch, hand stitch, lock stitch, overlock stitch, multi-yarn chain stitch and cover stitch [3, 4]. These stitch types provide advantages in different applications. For example, lock stitch is a universal stitch type that can be applied to both woven and knitted fabrics. It has low yarn consumption and it is very secure. In contrast, single yarn chain stitch is preferred for temporary seams as it is easy to unstitch [1, 2].

For workwear, thicker and heavier fabrics are preferred in order to resist external forces during occupation and to provide protection to the wearer. Specialty fibers or traditional synthetic/natural fibers can be utilized for these fabrics in order to balance the performance and the cost of the end-product [5-7]. As for workwear fabrics, seams of

the workwear should be strong enough to resist the forces. Therefore, seam properties of workwear should be investigated properly in order to maintain the unsewn fabric properties.

In the literature, there are many research studies that subjected the seam strength of different classical fabrics for various end-products [8-21]. Lock stitch was used in most of these studies, as the lock stitch machine is the most available sewing machine. Also, in recent years, effects of other stitch types on the seam strength and other seam properties were evaluated [22-26]. On the other hand, there is a very limited number of research studies on the bursting strength of sewn fabrics. In one of the related studies, effects of different seam types (sewn with stitch type ISO 401) on the multiaxial strength of selected woven and knitted fabrics were determined [27]. In another study, the multiaxial seam strength of sewn automobile seat covers (sewn with lock stitch) was determined by a self- developed bursting apparatus [28]. Rajput et al studied the effects of 3 stitch types, 3 fabric types and sewing yarn fineness on the hydraulic bursting strength of knitted fabrics [29]. Yesilpinar investigated the effect of different sewing

**To cite this article:** Kara S. 2022. Effects of different stitch types and stitch combinations on the seam bursting strength and seam strength of workwear. *Tekstil ve Konfeksiyon* 32(2), 146-154.

techniques (lock stitch techniques) on the bursting strength of apparel fabric [30].

As seen from the literature search, seam properties of workwear are very important as they ensure the continuity of the fabric properties in the joint areas. Although the uniaxial seam strengths of different fabrics were determined in several studies, seam efficiency of different stitch types and multi-axial strength (bursting strength) of workwear fabrics have not been studied in details, yet. Therefore, the main goal of this study was to evaluate the effects of different stitch types and stitch combinations on the uniaxial seam strength and bursting strength (multi-axial seam strength) of sewn workwear fabrics. This study differs from the literature as it determines the bursting strength of seams and as it compares 7 types of different stitch types/combinations for workwear.

## 2. MATERIALS AND METHODS

### 2.1 Materials

A cotton/polyester blend fabric was used as it was suitable to be used for workwear [6, 7, 31]. Properties of the fabric are given in Table 1. Sewing yarn was a 2 ply, 60 tex polyester corespun yarn that was also suitable for workwear (Coats Epic). Breaking strength of the sewing yarn was 34.5 N and breaking strain was 29 % (tested according to TS EN ISO 2062 [32]).

### 2.2 Methods

#### 2.2.1 Sample preparation

For this study, both reference (non-sewn) samples and sewn samples were prepared in order to make comparisons. Overall, 7 types of seams were produced by using different stitch types and their combinations as shown in Table 2. As the basic stitch types; lock stitch, 2-yarn chain stitch and 3-yarn overlock stitch were used. Stitch combinations were also formed by using “2-row lock stitch”, “2-row-2-yarn

chain stitch”, “3-yarn overlock + lock stitch” and “3-yarn overlock + 2-yarn chain stitch”. The sample codes, stitch schematics and important stitch dimensions such as seam allowance and distances between stitch rows are given in Table 2. Stitch densities for all types of stitches were 3 stitches/cm. Seam allowances were folded in the back side of fabric and ironed before conditioning the test samples.

For all samples, seams were formed both in warp direction and weft direction as shown in Figure 1. Seam strength and bursting strength tests of samples were performed for warp and weft samples. All the samples were conditioned under standard atmosphere conditions ( $20\pm 2^\circ\text{C}$ ,  $65\pm 4\%$  relative humidity) for 24 h before the tests.

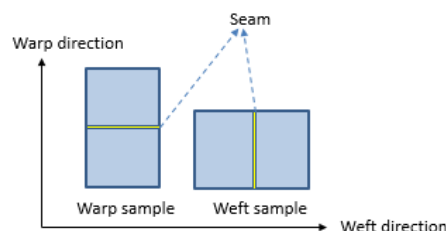


Figure 1. Seam placements and sample definition [33]

#### 2.2.2 Seam strength

Seam strength of samples were determined according to TS EN ISO 13935-2: 2014 standard [34], utilizing Instron 4411 Tensile Tester. Seam strength, strain and failure type of samples were recorded. Also, non-sewn samples were exposed to the same test as reference fabric. Tests were repeated 5 times for each sample type. Representation of seam strength test can be seen in Figure 2.

#### 2.2.3 Seam efficiency calculation

Seam efficiency of samples were calculated by using reference sample strength and seam strengths of sewn samples, by using Equation 1 (ASTM D1683/D1683M – 17 [35]).

Table 1. Fabric properties

Raw material	Weave	Unit mass (g/m <sup>2</sup> )	Thickness (mm)	Warp density (yarns/cm)	Weft density (yarns/cm)
35% cotton 65% polyester	2/2 warp rib	280	0.46	55.1	19.1

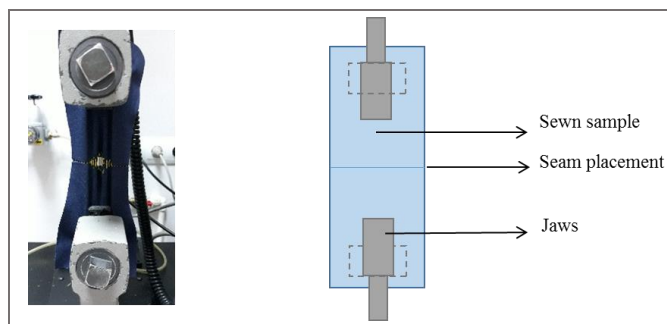
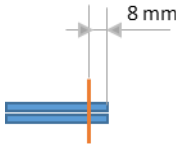
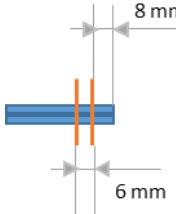
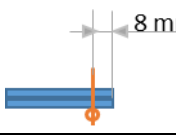
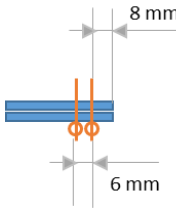
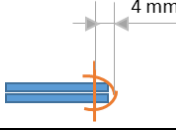
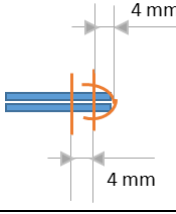
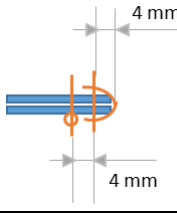


Figure 2. Real image and pictorial representation of uniaxial seam strength test



**Table 2.** Sample codes and seam/stitch information of sewn samples

Main stitch type	Sub stitch type	Stitch schematics and dimensions	Sample code
Non-sewn reference sample	-	-	No seam
Lock stitch (301)	1-row		Lock1
	2-rows		Lock2
Chain stitch (401)	1-row		Chain1
	2-rows		Chain2
Overlock stitch	3-yarn 1-row		Ov3
	5-yarns 2-rows (3-yarn ov.+ 301)		Ov3Lock
	5-yarn 2-rows (3-yarn ov.+ 401)		Ov3Chain

$$\text{Seam efficiency (\%)} = E(\%) = \frac{\text{Seam strength}}{\text{Fabric strength}} * 100 \quad (1)$$

#### 2.2.4 Bursting strength

Bursting strength of samples were determined according to ASTM D6797 – 15 standard [36], utilizing Instron 4411 Tensile Tester with a ball-burst attachment. Sample size was kept as 14 cm x 14 cm and the test speed was 300

mm/min. Tests were repeated 5 times for each sample type. Bursting strength, movement distance of the ball apparatus when the sample bursted, and the failure type of specimens were recorded as the test outputs. Representation of seam bursting strength test can be seen in Figure 3.

### 2.2.5 Seam bursting efficiency calculation

Seam bursting efficiency of samples were calculated as given in Equation 2, similar to the standard seam efficiency equation given in Equation 1. "Seam bursting efficiency" was derived by the author in order reveal how the seams were durable against bursting when compared to non-sewn reference samples.

### 2.2.6 Statistical analysis

SPSS Package Program version 22 was utilized to compare the seam strength, strain, bursting strength and bursting height results of different sample types, statistically. In the first step, normality of data was examined by considering Shapiro-Wilk test, histograms, variation coefficients (%), Skewness/Kurtosis values and Q-Q plots. For normally distributed data, One-way ANOVA analysis were performed. For pairwise comparisons, Tukey and Games-Howell tests were used, for homogeneous and non-homogeneous variance, respectively.

For data, which were not-normally distributed, Kruskal-Wallis analysis were performed. Pairwise comparisons of not-normally distributed data was made by using Mann Whitney U test.

## 3. RESULTS AND DISCUSSION

### 3.1 Seam Strength and Seam Efficiency Results

Seam strength results of samples are given in Table 3, with standard deviation values. The samples which were sewn with stitch combinations (Lock2, Chain2, Ov3Lock and Ov3Chain) failed at 2 steps. At the first step, the inner stitch row broke and the second stitch row that was near to the seam allowance edge, remained safe. These samples were clamped to the machine and a second test cycle was applied in order to break the second row of stitches. Therefore, seam strength results are given for first breaking cycle and second breaking cycle for these samples. Also, seam efficiency results of the samples are given in Table 4. The strain, seam strength and seam efficiency values given for second cycle were directly obtained from the second cycle breaks, so that they were not cumulative data. As the seam break downs were independent in the test cycles, the first cycle and second cycle seam properties are evaluated separately, rather than computing overall seam strength, strain or seam efficiency values.

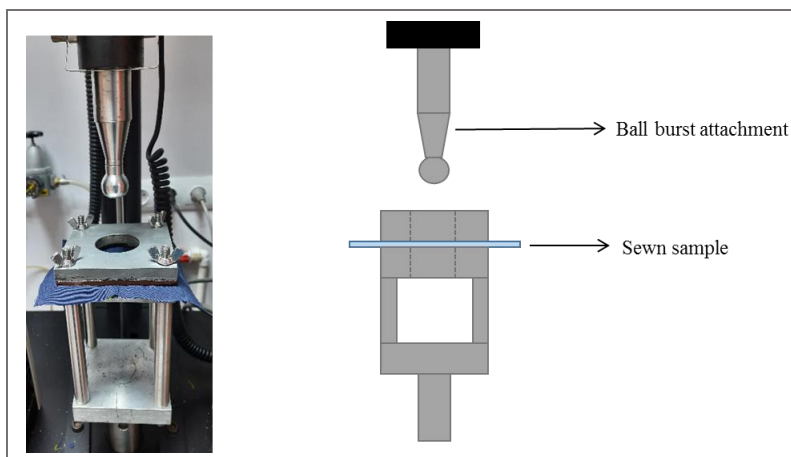


Figure 3. Real image and pictorial representation of bursting (multiaxial seam strength) test

$$\text{Seam bursting efficiency (\%)} = \text{BE (\%)} = \frac{\text{Seam bursting strength}}{\text{Fabric bursting strength}} * 100 \quad (2)$$

Table 3. Seam strength results of samples

Sample code	Seam strength- First cycle				Seam strength - Second cycle			
	Warp		Weft		Warp		Weft	
	Mean (N)	St. Dev. (N)	Mean (N)	St. Dev. (N)	Mean (N)	St. Dev. (N)	Mean (N)	St. Dev. (N)
No seam	1107.00	32.24	855.52	15.76	/	/	/	/
Lock1	404.98	33.46	389.30	23.06	/	/	/	/
Lock2	466.28	17.85	392.76	31.36	522.52	29.76	348.76	155.55
Chain1	486.02	39.04	437.80	43.99	/	/	/	/
Chain2	479.78	34.82	384.62	20.41	560.48	72.03	481.02	25.95
Ov3	490.80	85.32	383.88	22.27	/	/	/	/
Ov3Lock	419.08	19.21	381.96	16.48	490.04	43.49	435.52	35.14
Ov3Chain	494.04	31.36	464.54	15.08	555.73	37.07	442.80	39.68

**Table 4.** Seam efficiency results of samples

Sample code	Seam efficiency- First cycle		Seam efficiency- Second cycle	
	Warp (%)	Weft (%)	Warp (%)	Weft (%)
No seam	/	/	/	/
Lock1	36.58	45.50	/	/
Lock2	42.12	45.91	47.20	40.77
Chain1	43.90	51.17	/	/
Chain2	43.34	44.96	50.63	56.23
Ov3	44.34	44.87	/	/
Ov3Lock	37.86	44.65	44.27	50.91
Ov3Chain	44.63	54.30	50.20	51.76

Seam strength results of samples are visualized for first breaking cycle, in Figure 4.a. According to results, strength of non-sewn samples was 1107 N in warp direction and 856 N in weft direction and they were significantly higher when compared to sewn samples' results (Sig. values < 0.05). Seam strength of sewn samples were lower than 555 N in both warp and weft directions (Table 3) and the highest seam efficiency was calculated around 55% (Table 4). The highest seam strength and seam efficiency values were obtained for Ov3Chain samples in first cycle of tests. The seam strength increment of Ov3Chain sample was statistically significant when compared to non-sewn, Lock1 and Ov3Lock samples (Sig. < 0.05). Ov3Chain sample contained the stitch combinations of 3-yarn overlock stitch and 2-yarn chain stitch. In the literature, it is generally called as safety stitch [37]. The 2-yarn chain stitch is known to provide strength, elasticity and durability for this stitch combination [2]. Our results are partly supported by the studies in the literature. In the study of Ates et al, seam strength of denim fabrics sewn with "chain stitch + overlock stitch" was found higher when compared to its counterpart with "lock stitch + overlock stitch" [24]. Similarly, in our study, when the overlock stitch was combined with lock stitch and chain stitch (Ov3Lock and Ov3Chain, respectively), higher strength of chain stitch contributed to the overall seam strength of samples and

seam strength differences were statistically significant (Sig. values < 0.05).

In general, usage of 2-row lock stitch and 2-row-2-yarn chain stitch did not cause any statistically significant increment in seam strengths when compared to 1 row stitched counterparts (Lock1 and Chain1) (Sig. values > 0.05).

When the 3 basic stitch types (Lock1, Chain1 and Ov3) were compared, the queue was generally Ov3>Chain1>Lock1. Similar to our study, seam strength of sewn fabrics with chain stitch were found higher when compared to that of sewn fabric with lock stitch [25]. However, in our study, after considering standard deviation values and statistical analysis, it was resulted that the effects of basic stitch types were not statistically significant on the seam strengths of samples, in general (Most sig. values > 0.05).

For all samples, seam strengths of warp samples were higher than weft samples. In addition, for all samples, stitches were broken during the sample failure.

Strain results of samples are given in Figure 4.b and Table 5. As for seam strength results, strain results for 2-row stitch combinations (Lock2, Chain2, Ov3Lock and Ov3Chain) were obtained for 2 cycles of tests (Table 5).

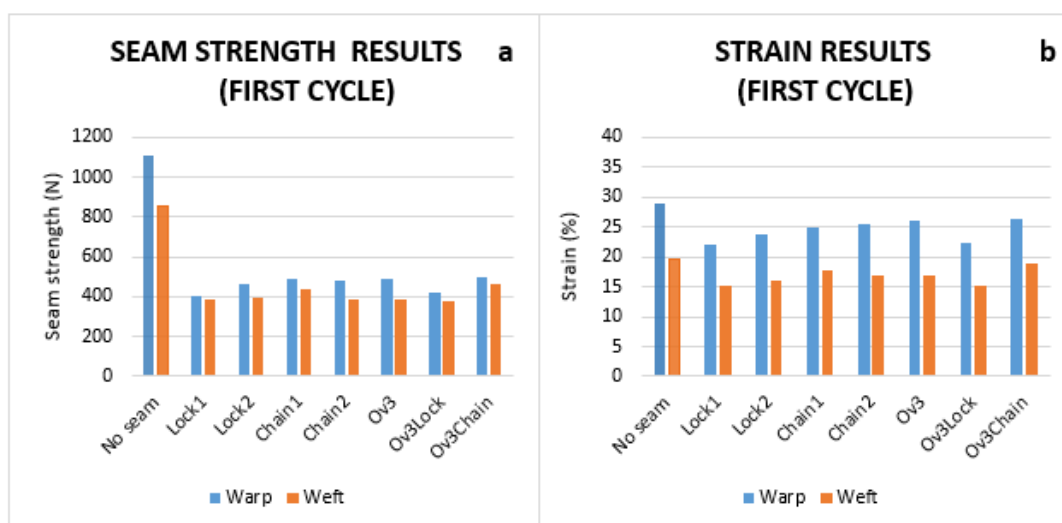


**Figure 4.** Seam strength results of samples for first breaking cycle

**Table 5.** Strain results of samples

Sample code	Strain - First cycle				Strain - Second cycle			
	Warp		Weft		Warp		Weft	
	Mean (%)	St. Dev. (%)	Mean (%)	St. Dev. (%)	Mean (%)	St. Dev. (%)	Mean (%)	St. Dev. (%)
No seam	29.02	5.56	19.50	0.38	/	/	/	/
Lock1	22.02	1.07	15.05	0.56	/	/	/	/
Lock2	23.83	0.89	15.89	0.72	35.15	2.05	22.67	6.3
Chain1	24.83	2.44	17.85	0.68	/	/	/	/
Chain2	25.51	1.43	17.00	0.92	34.76	3.34	27.35	1.01
Ov3	26.04	2.12	16.97	1.10	/	/	/	/
Ov3Lock	22.42	0.57	15.22	0.49	28.20	1.55	21.86	1.46
Ov3Chain	26.32	3.67	18.79	4.01	29.97	1.09	22.50	0.81

Strain of non-sewn samples were around 29 % and 20 % in warp and weft directions, respectively. For sewn samples, strain values decreased to some extent in the first cycle. The lowest strain values were obtained from Lock1 and Ov3Lock samples, as for seam strength values. In parallel, the highest strain values were obtained for Ov3Chain samples that also exhibited the highest seam strength. In general, strain results of samples in warp direction were similar to each other (Sig. values > 0.05) whereas strain of non-sewn sample was higher than sewn samples in weft direction (Sig. values < 0.05).

Strain values of samples sewn with stitch combinations, increased in the second cycle. A similar trend was also observed for seam strength results. It can be due to the supporting effect of remaining stitches of first row that were not broken in the first test cycle. At the first breaking cycle, all of the stitches of first row were not broken during seam failure. In order to simulate the real repetitive usage conditions, samples were clamped to the machine and tested in the second cycle, without removing the remaining stitches of first row. When the second breaking cycle was carried out for these samples, the load was beared by mainly the second stitch row. Nevertheless, the remaining stitches from the first breaking cycle is thought to bear some load during the second cycle, too. This is thought to be the reason of higher seam strengths and strains for the second test cycle of stitch combinations.

### 3.2 Bursting Strength and Seam Bursting Efficiency Results

Normally, bursting strength test examines the strength of samples in all directions so that the test is not repeated for warp and weft directions. However, in this study, the bursting test samples were prepared to have seams in warp and weft directions, as shown in Figure 1. Therefore, the bursting strength and bursting height of sewn samples are given for warp and weft samples, in Table 6. As there were no warp-weft samples in non-sewn sample, its result is given in black colour (Figure 5). Also, the data is visualized in Figure 5. The seam efficiencies of samples against bursting are also calculated and given in Table 7.

Different than seam strength tests, all the samples including 1-row basic stitches (Lock1, Chain1 and Ov3) and 2-rows stitch combinations (Lock2, Chain2, Ov3Lock, Ov3Chain) bursted in only one step.

Bursting strength of non-sewn reference fabric was 1898.75 N (Table 6). For the 3 basic stitch types (Lock1, Chain1 and Ov3), bursting strength in warp and weft directions were lower than that of non-sewn samples. Ov3 sample exhibited the lowest bursting strength among these 3 stitch types (Figure 5.a) and the bursting strength differences of Ov3 sample with the other sample types were statistically significant for both warp and weft samples (Sig. values < 0.05). On the other hand, bursting strength of

**Table 6.** Bursting strength and bursting height results of samples

Sample code	Bursting strength				Bursting height			
	Warp		Weft		Warp		Weft	
	Mean (N)	St. Dev. (N)	Mean (N)	St. Dev. (N)	Mean (mm)	St. Dev. (mm)	Mean (mm)	St. Dev. (mm)
No seam	1898.75	114.39	1898.75	114.39	39.07	13.55	39.07	13.55
Lock1	1751.60	252.34	1447.80	157.84	33.44	2.13	32.42	1.05
Lock2	2529.00	230.19	2367.80	342.34	35.87	3.11	39.75	2.64
Chain1	1771.80	208.62	1527.80	84.14	31.41	2.52	32.55	0.86
Chain2	2462.40	218.50	2319.40	287.31	38.04	1.66	41.01	3.96
Ov3	1309.20	109.62	1075.40	102.40	31.49	1.17	29.32	1.19
Ov3Lock	2368.00	212.00	1675.20	138.89	35.82	1.09	34.62	1.89
Ov3Chain	2398.60	114.72	1770.20	15.00	37.10	1.55	35.11	1.90

samples sewn with stitch combinations (Lock2, Chain2, Ov3Lock and Ov3Chain) exhibited higher bursting strength when compared to non-sewn samples, especially for the warp samples (Sig. values < 0.05). A similar result was obtained by Yesilpinar, when she compared the bursting strength of 1-row lock stitched samples with 2-rows lock stitched counterparts [30]. In contrast with the seam strength tests, the second row of stitches in the combinations supported the seam line against bursting, importantly. As for seam strength results, chain stitch containing samples (Chain1, Chain2, Ov3Chain) exhibited higher bursting strength when compared to lock stitch containing counterparts (Lock1, Lock2, Ov3Lock), but this time the differences were less and not statistically significant (Sig. values between Lock1/Chain1, Lock2/Chain2 and Ov3Lock/Ov3Chain were higher than 0.05). In the literature, the bursting strength of lock stitched samples were found slightly higher than chain stitched samples, but this study was made on knitted fabrics and bursting test procedure was different [29].

For stitch combinations, seam efficiencies against bursting were higher than 100% (Table 7). For all samples, bursting strength of warp samples were higher than weft samples.

Also, when compared to seam efficiencies given in Table 4 (36-55%), seam bursting efficiencies were clearly higher (56-133%) (Table 7).

During bursting tests, generally stitches were broken for 1 row stitch types (Lock1, Chain1, Ov3). Different than the seam strength tests, fabric tear near the seamline accompanied the stitch breakages or only the fabric tear near the seamline was observed in the bursting failure of combination stitches (Lock2, Chain2, Ov3Lock, Ov3Chain).

On the other hand, bursting height of non-sewn reference sample was 39 mm. Only Lock2 and Chain2 samples exhibited higher bursting height for weft samples when compared to non-sewn samples but the differences were not statistically significant (Sig. values > 0.05). It could be advantageous for workwear as the seam line could resist to bursting in higher elongations. For all sewn samples, the bursting heights for warp and weft samples were close to each other.

**Table 7.** Seam bursting efficiency

Sample code	Seam bursting efficiency	
	Warp (%)	Weft (%)
No seam	/	/
Lock1	92.25	76.25
Lock2	133.19	124.70
Chain1	93.31	80.46
Chain2	129.69	122.15
Ov3	68.95	56.64
Ov3Lock	124.71	88.23
Ov3Chain	126.33	93.23

#### 4. CONCLUSIONS

In this study, the effects of different stitch types and their combinations were determined on the seam strength and seam bursting strength of workwear fabric.

In seam strength test, a two-step failure was observed for samples that contained stitch combinations. In the available experimental studies in literature, this phenomenon was not mentioned for stitch combinations. It is an important feature for workwear, because the garment can still provide protection to the wearer after the first row of stitches broke, until the seam is repaired. In addition, it is beneficial to highlight that, the main function of the second row of stitch was to form a safety stitch rather than increasing the overall seam performance. In warp and weft directions, the maximum seam efficiency difference for different stitch types/combinations was around 12%. Seam efficiency values of all samples were around 36.6-44.6 % in warp direction and 44.6-54.3 % in weft direction, for the first breaking cycle. For the stitch combinations, seam efficiency values increased in the second cycle for some amounts. According to the literature, seam efficiency values are dependent on a variety of factors such as fabric structure, seam type, stitch type, stitch density, sewing yarn properties, sewing needle properties etc. and seam efficiency values around 60-80 % are common [3, 38]. Seam efficiency result of the samples prepared in this study are close to the 60% boundary. As the fabric strengths in warp and weft directions were quite high, seam strengths obtained in this study would be acceptable for many uses. Nevertheless, to increase the seam efficiency values, some seam parameters can be differed in the further studies.

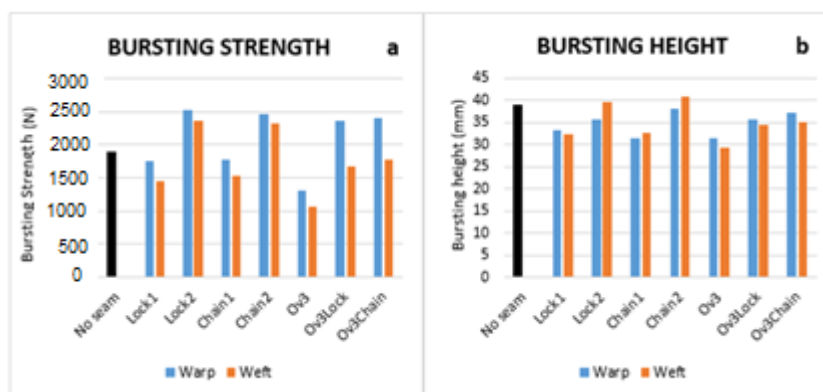


**Figure 5.** Bursting strength and bursting height results of samples



Different than uniaxial seam strength tests, all the sewn samples bursted in only one step independent of including 1-row stitches or 2-rows stitch combinations. Also, the contribution of the second stitch row was clearly observed for the samples containing stitch combinations. For these samples, seam bursting efficiency was higher than 100%, because of the supporting effect of second row of stitches and the seam allowances, in the bursting area. As for seam strength efficiencies, in general, chain stitch containing samples exhibited slightly higher seam bursting efficiencies and bursting heights.

In both seam strength and bursting strength tests, some amounts of higher results were obtained for warp samples. It was a reflection of higher fabric strength in warp direction [39]. It is known that, warp yarns are selected as higher strength yarns in order to bear the loads during warping and weaving processes. Also, higher yarn densities are used in warp direction. As a result, both fabric strength and seam properties are affected from the yarn properties and fabric structural parameters in warp and weft directions.

The information obtained from this study is beneficial for the seam selection of the workwear to obtain more resistant

seams by forming seam combinations. Also, the information inferred from this study can be used for other garment types where the seams are exposed to high uniaxial or multiaxial forces such as in crotch zone.

In the further studies, lock stitch or chain stitch can be selected and, the seam strength and seam bursting properties of workwear with lapped seam types of selected stitches can be studied. Different than this study, the seam rows in the stitch combinations can act together to result with a higher seam strength/efficiency for the lapped seams.

### Acknowledgement

A preliminary version of this study was presented in “International Conferences on Science and Technology-Engineering Science and Technology (ICONST-EST)” on September, 2021, with the caption of “Effects of different stitch combinations on the seam bursting characteristics of PET/Co workwear”. This current study is improved by adding uniaxial seam strength tests and combined evaluations of the test results.


### REFERENCES

1. Kurumer G. 2012. *Konfeksiyon üretimi ve teknolojisi (2nd Press)*. İzmir: Printer Ofset Matbaacılık.
2. Jones I, Stylios GK. 2013. *Joining textiles: Principles and applications*. Cambridge: Woodhead Publishing Limited.
3. Gurarda A. 2019. Seam performance of garments. In: F. Uddin (Ed.), *Textile Manufacturing Processes*. UK: Intechopen.
4. ASTM D6193 – 16. 2020. *Standard practice for stitches and seams*. West Conshohocken: ASTM International.
5. Paul R. (Ed.). 2019. *High performance technical textiles*. USA: John Wiley & Sons.
6. Midha VK, Kothari VK, Chattopadhyay R, Mukhopadhyay A. 2010. Effect of workwear fabric characteristics on the changes in tensile properties of sewing threads after sewing. *Journal of Engineered Fibers and Fabrics* 5(1), 31-38.
7. Haifa IH. 2013. Seam properties of workwear. *Pakistan Textile Journal* 62(1), 42-46.
8. Unal BZ, Baykal PD. 2018. Determining the effects of different sewing threads and different washing types on fabric tensile and sewing strength properties. *Tekstil ve Konfeksiyon* 28(1), 34-42.
9. Choudhary AK, Goel A. 2013. Effect of some fabric and sewing conditions on apparel seam characteristics. *Journal of Textiles* 2013, 1-7.
10. Vijay Kirubakar Raj D, Renuka Devi M. 2017. Performance analysis of the mechanical behaviour of seams with various sewing parameters for cotton canopy fabrics. *Fibres and Textiles in Eastern Europe* 25, 4(124), 129-134.
11. Frydrych I, Greszta A. 2016. Analysis of lockstitch seam strength and its efficiency. *International Journal of Clothing Science and Technology* 28(4), 480-491.
12. Sular V, Mesegul C, Kefsiz H, Seki Y. 2015. A comparative study on seam performance of cotton and polyester woven fabrics. *The Journal of the Textile Institute* 106(1), 19-30.
13. Farhana K, Syduzzaman M, Yeasmin D. 2015. Effect of sewing thread linear density on apparel seam strength: A research on lapped and superimposed seam. *Journal of Advancements and Engineering and Technology* 3(3), 1-7.
14. Namiranian R, Shaikhzadeh Najar S, Etrati SM, Manich AM. 2014. Seam slippage and seam strength behavior of elastic woven fabrics under static loading. *Indian Journal of Fibre and Textile Research* 39(3), 221-229.
15. Bharani M., Shiyamaladevi PSS, Mahendra Gowda RV. 2012. Characterization of seam strength and seam slippage on cotton fabric with woven structures and finish. *Research Journal of Engineering Sciences* 1(2), 41-50.
16. Gurarda A. 2008. Investigation of the seam performance of PET/nylon-elastane woven fabrics. *Textile Research Journal* 78(1), 21-27.
17. Yeşilpınar S, Bahar S. 2007. The effect of sewing and washing processes on the seam strength of denim trousers. *AATCC Review* 7(10), 27-31.
18. Tarafder N, Karmakar R, Mondal M. 2007. The effect of stitch density on seam performance of garments stitched from plain and twill fabrics. *Man-Made Textiles in India* 50(8), 298-302.
19. Gribaa S, Amar SB, Dogui A. 2006. Influence of sewing parameters upon the tensile behavior of textile assembly. *International Journal of Clothing Science and Technology* 18(4), 235-246.
20. Mukhopadhyay A, Sikka M, Karmakar AK. 2004. Impact of laundering on the seam tensile properties of suiting fabric. *International Journal of Clothing Science and Technology* 16(4), 394-403.
21. Chowdhary U, Poyner D. 2006. Impact of stitch density on seam strength, seam elongation, and seam efficiency. *International Journal of Consumer Studies* 30(6), 561-568.
22. Kara S. 2020. Comparison of sewn fabric bending rigidities obtained by heart loop method: Effects of different stitching types and seam directions. *Industria Textila* 71(2), 105-111.

- 
23. Islam MR, Asif AAH, Razzaque A, Al Mamun A, Maniruzzaman M. 2020. Analysis of seam strength and efficiency for 100% cotton plain woven fabric. *International Journal of Textile Science* 9(1), 21-24.
  24. Ates M, Gurarda A, Ceven EK. 2019. Investigation of seam performance of chain stitch and lockstitch used in denim trousers. *Tekstil ve Mühendis* 26(115), 263-270.
  25. Akter M, Khan MR. 2015. The effect of stitch types and sewing thread types on seam strength for cotton apparel. *International Journal of Scientific and Engineering Research* 6(7), 198-205.
  26. Dal V, Yıldız Z. 2014. Investigation of the effects of sewing threads on the sewing performance (Investigarea efectului atei de cusut asupra performantei de coasere). *Industria Textila* 65(2), 85-89.
  27. Yusof NA. 2013. Effect of seam type on selected seam tensile behaviour under multi-axial forces (Doctoral dissertation). University of Otago, New Zealand.
  28. Kovalova N, Kulhavy P, Vosahlo J, Havelka A. 2019. Experimental and numerical study of sewing seams of automobile seat covers under unidirectional and multiaxial loading. *Tekstil ve Konfeksiyon* 29(4), 322-335.
  29. Rajput B, Kakde M, Gulhane S, Mohite S, Raichurkar PP. 2018. Effect of sewing parameters on seam strength and seam efficiency. *Trends in Textile Engineering and Fashion Technology* 4(1), 4-5.
  30. Yesilpınar S. 1997. Kullanım sırasında giysilerde oluşan dikiş patlamaları üzerine bir araştırma. *Tekstil ve Mühendis* 11(56), 30-41.
  31. Verdu P, Rego JM, Nieto J, Blanes M. 2009. Comfort analysis of woven cotton/polyester fabrics modified with a new elastic fiber, Part 1: Preliminary analysis of comfort and mechanical properties. *Textile Research Journal* 79(1), 14-23.
  32. TS EN ISO 2062. 2009. *Textiles - Yarns from packages - Determination of single-end breaking force and elongation at break using constant rate of extension (CRE) tester*. Ankara: Turk Standartlar Enstitüsü.
  33. Kara S, Yesilpınar S. 2021. Comparative study on the properties of taped seams with different constructions. *Fibres & Textiles in Eastern Europe* 29, 2(146), 54-60.
  34. TS EN ISO 13935-2. 2014. *Textiles - Seam tensile properties of fabrics and made-up textile articles - Part 2: Determination of maximum force to seam rupture using the grab method*. Ankara: Turk Standartlar Enstitüsü.
  35. ASTM D1683/D1683M – 17. 2018. *Standard test method for failure in sewn seams of woven fabrics*. West Conshohocken: ASTM International.
  36. ASTM D6797 – 15. 2015. *Standard test method for bursting strength of fabrics constant-rate-of-extension (CRE) ball burst test*. West Conshohocken: ASTM International.
  37. Nayak R, Padhye R. (Eds). 2015. *Garment manufacturing technology*. UK: Elsevier.
  38. Mukhopadhyay A, Midha VK. 2013. The quality and performance of sewn seams. In: I Jones, GK Stylios (Eds.), *Joining textiles*. Cambridge: Woodhead Publishing Limited.
  39. Barbulov–Popov D, Cirkovic N, Stepanovic J. 2012. The influence of stitch density and of the type of sewing thread on seam strength. *TEM Journal* 1(2), 104-110.

# Performance Characteristics in Textile Application of Photochromic Dye Capsules

Seniha Morsümbül  0000-0002-4929-0681

E. Perrin Akçakoca Kumbasar  0000-0001-5295-9131

Department of Textile Engineering, Faculty of Engineering, Ege University, 35100 Bornova, İzmir, Türkiye

**Corresponding Author:** E. Perrin Akçakoca Kumbasar, perrin.akcakoca@ege.edu.tr

## ABSTRACT

Photochromic dyes which change their color with UV light, are water insoluble and sensitive to the environmental conditions. In order to be able to use these dyes in textile industry, the dyes are encapsulated with a polymer, and then the encapsulated photochromic dyes are applied onto the textile materials. The encapsulated photochromic dyes can show different properties according to the photochromic dye and polymer type, capsule size and the encapsulation method applied. In this study, the performance characteristics of different commercial photochromic dye capsules were investigated after the application onto cotton fabrics by pad-cure process. It was observed that the fabrics still provide UV protection at 50 + UPF level even after 20 washing cycles. The photochromic fabrics lost their color and UV protective properties at most 16% and 4%, respectively after 20 UV on-off cycles.

## 1. INTRODUCTION

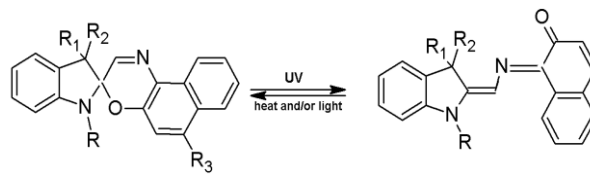
People's expectations from textile materials have changed with the rise of living standards and the developments in technology. The demands for textiles are not only style and durability, but also functional properties. Textile materials, which have functionality in different fields such as medical, protective, sports etc. are getting more interesting and these textiles bring competitive power to the textile companies with their value-added. Photochromic textile materials, which are one of the functional textiles, can be used for both fashion effect and smart textiles such as UV sensors [1].

Photochromic dyes are colorless without UV light and they become colorful by changing their molecular structure under UV irradiation. This color changing is reversible thermally (T-type) or photochemically (P-type), thus the color disappears when the UV light source is removed [2]. Photochromic dyes are divided in many different classes while the photochromic dyes, which change their color based on pericyclic reactions, are more common to use in various industries such as glasses, cosmetics, plastics, textiles etc [1,3]. These photochromic dyes, which are spiropyran, spirooxazines, naphthopyrans (chromenes), diarylethenes and fulgides, show photochromism effect by ring opening/closing reactions (Figure 1) [2,4,5]. These

dyes differ in terms of photochromic properties, resistance to photodegradation (fatigue resistance), etc., depending on their structures [6]. For example, diarylethenes and fulgides show P-type photochromism, while the other dyes show T-type photochromism [7]. Spirooxazines have higher fatigue resistance than spiropyran [6]. Naphthopyran is less sensitive to temperature than spirooxazines [8,9]. In this context, it should also be evaluated whether the photochromic dye has suitable properties for the usage area where it will be applied.

Photochromic dyes also provide UV protection property due to their color changes by absorbing UV light and can be used in the UV protective textile production [10]. UV rays above a certain rate is harmful to human health and precautions such as using sunscreen, dressing, etc. can be taken to protect against UV rays. Although textile materials provide UV protection by absorbing or reflecting UV rays, not all textile materials provide the same protection level. In order to evaluate the UV protection property provided by textile materials, the UV protection factor (UPF) value should be analyzed. UPF is the ratio of the average effective UV rays in the environment ( $ED$ ) to the average of the UV rays passing through the textile material ( $ED_t$ ) [11]:

**To cite this article:** Morsümbül S, Akçakoca Kumbasar EP. 2022. Performance characteristics in textile application of photochromic dye capsules. *Tekstil ve Konfeksiyon*, 32(2), 155-161.



(R: alkyl; R<sub>1</sub>, R<sub>2</sub>:alkyl (usually both methyl); R<sub>3</sub>: H, halogen, etc.)

**Figure 1.** Reversible color change of photochromic dye (spirooxazine) with UV light [2]

$$UPF = \frac{ED}{ED_f} = \frac{\sum_{\lambda=290}^{\lambda=400} E(\lambda)S(\lambda)\Delta\lambda}{\sum_{\lambda=290}^{\lambda=400} E(\lambda)T(\lambda)S(\lambda)\Delta\lambda}$$

where  $E(\lambda)$  is the relative erythemal spectral effectiveness,  $S(\lambda)$  is the solar spectral irradiance in  $Wm^{-2}nm^{-1}$ ,  $\Delta\lambda$  is measured wavelength interval in nm,  $T(\lambda)$  is average spectral transmittance of the fabric specimen, and  $\lambda$  is the wavelength in nm.

In the UV transmittance measurements, four data about UV protection properties of the fabric are obtained. These are the mean UPF, rated UPF, UVA and UVB transmittance values. Mean UPF is the UPF value obtained as a result of averaging the UV transmittance measurements made from 4 different points of a fabric. Mean UPF can be measured up to 2000 UPF, depending on the capacity of the measuring device.

The rated UPF value is the average UPF value of four testing fabrics reduced for the standard error in the average UPF, calculated for the 99% confidence level, and finally rounded down to the nearest multiple of five. If the rated UPF is less than the lowest individual UPF fabric measurement, the rated UPF is the lowest value of measured UPF rounded to the nearest multiple of five [12,13]. UVA and UVB transmittance values are the values that show how much percent the fabric transmits UVA and UVB rays, respectively.

Although many different standards are applied in the UPF analysis of textile materials, the most widely used standard is the Australian / New Zealand standard (AS / NZS 4399: 1996). According to this standard, which classifies the UPF values as in Table 1, textile materials with 40 UPF and above provide excellent protection against UV rays [10–12].

**Table 1.** Classification of UPF values according to AS / NZS 4399: 1996 standard [10–12]

UPF Range	Protection category	Effective UV Transmission (%)	UPF Rating
40 – 50, 50+	Excellent	≤ 2,5	40, 45, 50, 50+
25 – 39	Very good	4,1 – 2,6	25, 30, 35
15 – 24	Good	6,7 – 4,2	15,20

UV protection properties of textile materials depends on many parameters such as fiber type, fabric construction, additives (e.g. UV absorber) in the material etc. Color is also one of the most important properties that affect UPF of textiles. A number of authors has studied UV protection properties of textile dyes [14–21]. However, UV protection properties of photochromic dyes, which change their color

by absorbing UV light, on textile materials have not been studied sufficiently. Thus, in this study, the photochromic textiles were also evaluated from the point of UV protection.

Various application methods have been used to apply the photochromic dyes to textile materials such as embedding the dye in the polymer matrix during the spinning (photochromic yarn) [22–24] or screen-printing process (photochromic T-shirts) [1,25]. In addition to this, several researchers have studied on the application of spirooxazine or naphthopyran dyes onto polyamide, polyester, polyacrylonitrile and cotton fabrics by different methods such as exhaustion, padding or printing [26,27,36–38,28–35].

Although the first photochromic t-shirt was put on the market in 1989 [1], photochromic dyes could not attract the expected attention from the textile industry sufficiently due to their disadvantages such as low water solubility, sensitive structure to high temperature, low affinity to the textile materials and low diffusion ability to high crystalline structures such as synthetic fibers [28,30,33,36]. Thus, textile-dyeing yield of the photochromic dyes are low due to these properties. Microencapsulation can be applied as an alternative method to improve the application of photochromic dyes onto textile materials.

Microencapsulation is a process in which very small particles of liquid or solid material (core material) are coated with a continuous film of polymeric material (shell material) [39]. Capsule shell materials protect the core materials from external factors by wrapping the core material with one or more layers and improve the applicability of the core material by increasing its stability [40,41].

In this study, it was aimed to apply two different commercial photochromic dye microcapsules on cotton fabrics and evaluate the color build-up by UV irradiation, fatigue resistance and UV protective properties of the fabrics after the microcapsule application and consecutive laundering. It was observed that UV protective properties of cotton fabrics can be improved with the application of photochromic dye microcapsules and the photochromic fabrics can retain their properties even after 20 repeated washing and UV on-off cycles.

## 2. MATERIAL AND METHOD

The scoured and bleached interlock knitted 100% cotton fabric was obtained from a textile factory and was used as received (without any further treatment prior to the experimental part). Construction properties of the fabric were shown at Table 2. Thickness of the fabrics was measured on SDL ATLAS Digital Thickness Gauge according to ASTM D 1777-96 standard. Total porosity of the fabric was calculated by using Equation 1 [42,43].

$$\varepsilon = 1 - \frac{\rho_a}{\rho_b} \quad (1)$$

where  $\rho_a$  is the fabric density ( $\text{g/cm}^3$ ),  $\rho_b$  is the fiber density ( $\text{g/cm}^3$ ) and  $\varepsilon$  is the porosity. Fabric density is calculated by dividing the fabric mass per unit area, by fabric thickness. The mean density of cotton fibres is accepted as  $1.52 \text{ g/cm}^3$  [42].

The binder (Itobinder AG - anionic acrylic copolymer) was supplied by LJ Specialities Ltd. Two different types of commercial photochromic dye microcapsules (Violet-powder and Blue-liquid) were used in powder and liquid form. Trade names and structures of the capsules are not revealed for proprietary reasons.

The photochromic dye capsules (50, 75 and 100 g/l) were applied to the fabric by pad-cure process. Wet pick up ratio was set to be 100%. The binder concentration was 50 g/l. After padding, the samples were dried at  $100^\circ\text{C}$  for 3 minutes and cured at  $150^\circ\text{C}$  for 4 minutes in a laboratory scale tenter (Ataç, GK 40, Turkey).

The morphology of the fabrics was investigated by scanning electron microscopy (SEM, Thermo Scientific Apreo S). Each sample was coated with a 1 nm thick Au layer using sputter coater (Leica EM ACE600) prior to SEM observations.

Color measurements were carried out using a Colorlite SPH 870 spectrophotometer (with LED light source), processed using the ColorLite ColorDaTra Professional software, 400-700 nm, under D65 illumination and an observer angle of  $10^\circ$  with a  $45^\circ/0^\circ$  geometry. The samples were placed on the plate kept at constant temperature ( $20^\circ\text{C}$ ) by a peltier system and then the samples were irradiated by solar simulator (ABET Sunlite Solar Simulator) for 3 minutes (Figure 2). After that, the solar light switched off and color measurements were carried out as immediate as possible (within 3 seconds). The color value of unirradiated sample was regarded as the standard. Color build-up on irradiation of the samples was discussed by the difference between the standard and UV irradiated colored samples by using  $\Delta E^*$  (color difference) values.

The solar simulator has a Class A spectral match for the International Electrotechnical Commission (IEC) and the Japanese Industrial Standards (JIS) Committee standards and has an irradiance of AM 1.5G,  $100 \text{ mW/cm}^2$  (1 Sun).

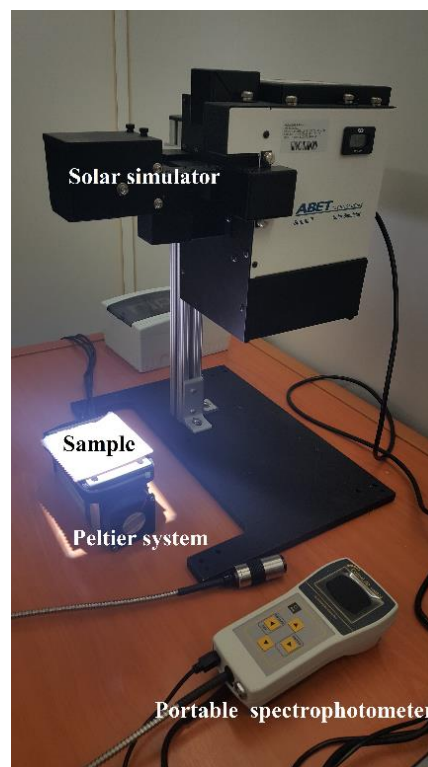


Figure 2. The color measurement setup

Mean UV protection factor (UPF) values of the fabrics were measured with Labsphere UV 2000F device according to standard AS/NZ 4399:1996.

Consecutive laundry washings were applied by ISO 105-C06:2010 (test method A2S) standard for testing the washing durability of the applications. The fastness assessment method with grey-scale is not a suitable for photochromic materials due to the dynamic color changes of photochromic dyes [34]. Therefore, the  $\Delta E^*$  and the mean UPF values of the samples were compared to evaluate the washing durability.

The fatigue resistance tests were carried out based on the literature [36,38]. The samples were irradiated by solar simulator for 2 min and then left in the dark for 5 min to fade back to their original unexposed states. This UV on-off cycle was repeated 20 times for each sample. Color and UV transmittance measurements were carried out after every 5 irradiation cycles.

Table 2. Construction properties of the fabric used in the application studies

Yarn count	Course per cm	Wales per cm	Stitch density	Thickness	Mass per unit area	Total porosity
12 tex	20	40	800 stitch/cm <sup>2</sup>	0,085 cm	0,023 g/cm <sup>2</sup>	83%



### 3. RESULTS AND DISCUSSION

The photochromic capsule applied samples were in a colorless state (white) in the absence of UV light. Reversible violet and blue colors were developed after UV irradiation (Figure 3) and the samples reverted to the colorless state when the UV irradiation source is removed.

SEM images of the fabrics (Figure 4), recorded at three different magnifications (x1000, x5000 x20000), clearly showed that the microcapsules adhered on cotton fibers without obvious breakage during the pad-cure process. The particle size of the photochromic microcapsules ranged from 2 to 5  $\mu\text{m}$  (Figure 4).

As stated by Little and Christie [34], the washing fastness evaluation by comparing with grey scales used for classical textile materials is not suitable for photochromic textile materials that change their color with UV irradiation. In this

context, considering the studies in the literature, the difference between the color values of the fabrics before and after UV irradiation was evaluated after repeated washings in order to examine the washing durability of the microcapsules [34]. Figure 5 illustrates  $\Delta E^*$  values of the samples after padding and consecutive laundering tests. It was observed that the color build-up on UV irradiation of the samples increased with capsule concentration. The level of photocoloration developed by UV irradiation of the samples was observed to decrease at most by 11% after 20 washings. However, some samples have also showed an increase in color values after repeated washing cycles. An explanation for this result may be proposed based on the loosening of the binder structure on the fabric after washings. It provides a more favorable environment for the color change of the photochromic dye by disappearing the film effect of the binder on the microcapsule surface and also increasing the deaggregation of the microcapsules [34].

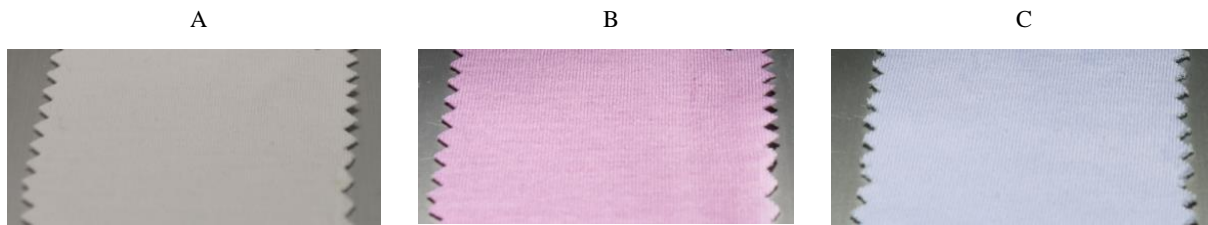


**Figure 3.** Images of the photochromic microcapsules applied samples before (A) and after UV irradiation (B: violet powder and C: blue liquid)

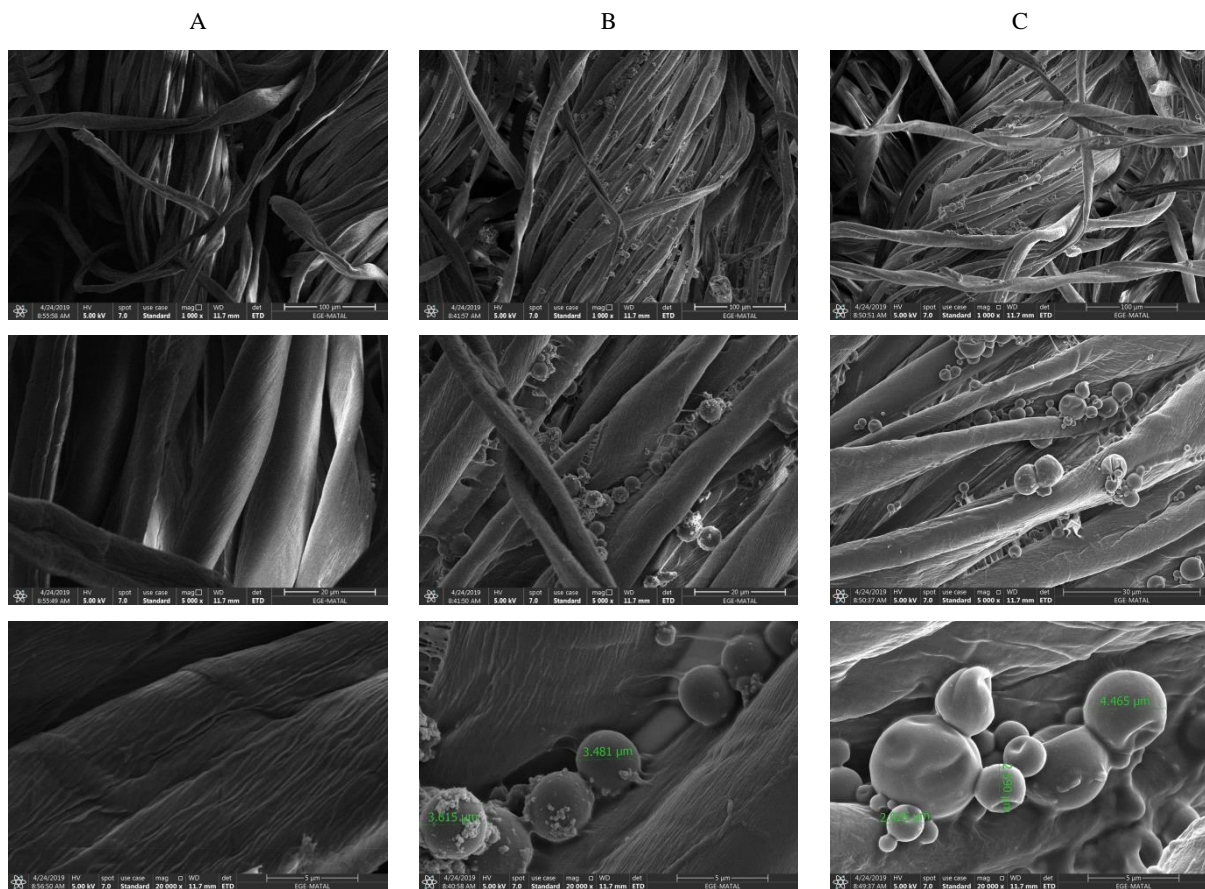


**Figure 4.** SEM images of the untreated fabric (A) and the photochromic microcapsules applied samples (B: violet powder and C: blue liquid) with different magnifications (x1000, x5000 x20000)

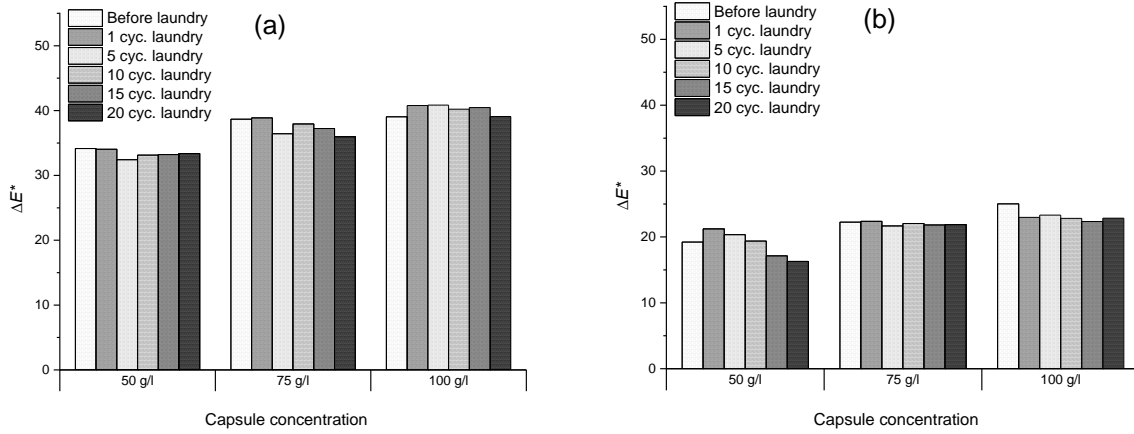


Figure 5.  $\Delta E^*$  values of the samples (a: for violet-powder, b: for blue-liquid) after padding and consecutive laundering tests.

One of the aims of this study is to evaluate the UV protection performance of photochromic textile materials. 50+ mean UPF values were obtained as a result of the photochromic capsule applications as seen in Figure 6, while the mean UPF value of the untreated fabric was 29 (before laundry tests). The mean UPF values also increased with the increasing capsule concentration. In addition, 50+ UPF values were again observed in all photochromic fabric samples even after 20 laundering cycles, while the mean

UPF value of the untreated fabric was about 25-30 UPF after the consecutive laundry tests.

$\Delta E^*$  and UPF values of the samples for every 5 UV on-off cycles were given in Figure 7. Based on the  $\Delta E^*$  values, the samples applied violet-powder and blue-liquid capsules (100 g/l) showed high fatigue resistance after 20 UV on-off cycles, retaining 97% and 84% of their photochromic response, respectively. The samples also showed approximately 4% loss for violet-powder and 0.5% loss for blue liquid in UPF values after 20 UV exposure cycles.

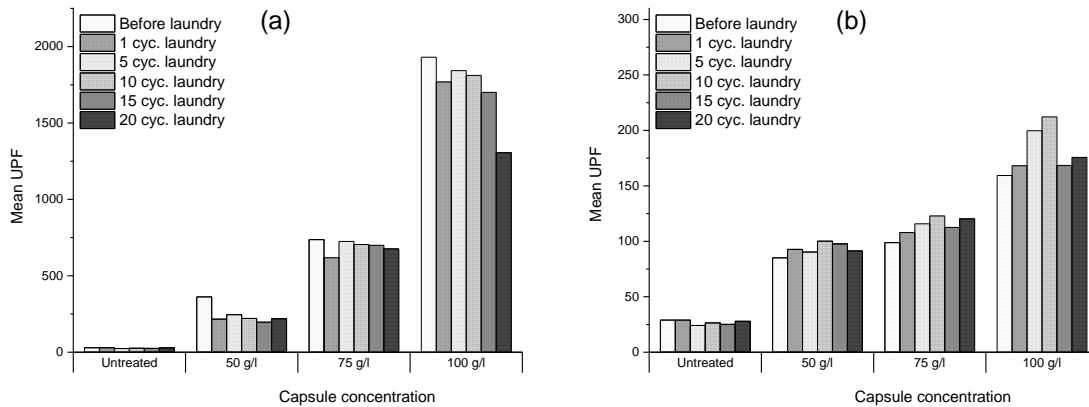


Figure 6. Mean UPF values of the samples (a: for violet-powder, b: for blue-liquid) after padding and consecutive laundering tests.

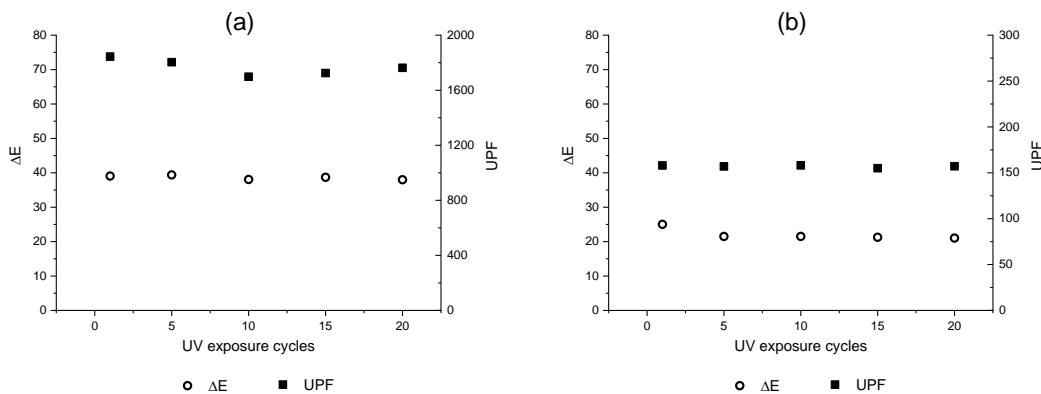


Figure 7. Fatigue resistance of the samples (a: for violet-powder, b: for blue-liquid).

#### 4. CONCLUSION

Application of two different microcapsules on cotton fabrics and evaluation the performance properties of the fabrics were presented in this study. Photocoloration degree of the samples decreased at most by 11% after the washings however, the color values of some samples increased after repeated washing cycles. An explanation proposed is that the binder structure on the samples loosens around the microcapsules with washings, and thereby the conversion between close and open ring forms of the dyes facilitates. The capsule concentration affected the color and UV protection properties of the fabrics positively and this effect is more pronounced for UPF values. Application of the photochromic dye microcapsules was found to improve UV protective properties of cotton fabric.

In general, the advantages of this study are as follows:

- Application conditions of the photochromic microcapsules on cotton fabric are presented.
- The performance properties of the photochromic microcapsules on cotton fabric were evaluated.
- It has been revealed that photochromic textile materials can be applied not only in creating a fashion effect, but also in the production of UV protective clothing as a functional textile material.
- It has been shown that the photochromic fabrics maintained their color and excellent UV protection (50+ UPF) properties after repeated washing and UV on-off cycles.

#### ACKNOWLEDGEMENT

The authors would like to gratefully acknowledge Ege University, scientific research projects through the project no. 18-TKUAM-003 for financial support to this research project.


#### REFERENCES

1. Ferrara M., Bengisu M. 2013. *Materials that Change Color: Smart Materials, Intelligent Design*. London: Springer Briefs in Applied Sciences and Technology.
2. Akçakoca Kumbasar E. P. A., Morsunbul S., Alır, S. 2018. Photochromic Nanofibers. In T. Lin (Ed.), *Novel Aspects of Nanofibers*. London: IntechOpen, 69–85.
3. Akçakoca Kumbasar E. P., Morsunbul S. 2017. Photochromic Textiles. In B. Mahltig (Ed.), *Textiles: Advances in Research and Applications*. New York: Nova Science, 359–380.
4. Bouas-Laurent H., Dürr H. 2001. Organic photochromism. *Pure Appl. Chem.* 73, 639–665.
5. Nigel Corns S., Partington S. M., Towns A. D. 2009. Industrial organic photochromic dyes. *Color. Technol.* 125, 249–261.
6. Crano J. C., Gugliemetti R. J. 2002. *Organic Photochromic and Thermochromic Compounds. Volume 1: Main Photochromic Families*. New York: Kluwer Academic Publishers.
7. Parhizkar M., Zhao Y., Lin T. 2015. Photochromic Fibers and Fabrics. In X. Tao (Ed.), *Handbook of Smart Textiles*. Singapore: Springer, 155–182.
8. Chowdhury M. A., Joshi M., Butola B. S. 2014. Photochromic and thermochromic colorants in textile applications. *J. Eng. Fiber. Fabr.* 9, 107–123.
9. Abate M. T., Seipel S., Vikova M., Vik M., Ferri A., Jinping G., Chen G., Nierstrasz V.A. 2018. Comparison of the photochromic behaviour of dyes in solution and on polyester fabric applied by supercritical carbon dioxide. *IOP Conf. Ser. Mater. Sci. Eng.* 459, 1-8.
10. Akçakoca Kumbasar E. P. A., Çay A., Morsunbul S., Voncina B. 2016. Color Build-Up and UV-protection Performance of Encapsulated Photochromic Dye-Treated Cotton Fabrics. *AATCC J. Res.* 3, 1–7.
11. Hoffmann K., Laperre J., Avermaete A., Altmeyer P., Gambichler T. 2001. Defined UV protection by apparel textiles. *Arch. Dermatol.* 137, 1089–1094.
12. Dubrovski P. D. 2010. Woven Fabrics and Ultraviolet Protection. In P. D. Dubrovski (Ed.), *Woven Fabr. Eng.* London: IntechOpen, 247–296.
13. Australia S, LTD. I. Australian/New Zealand Standard (ASNZS) 4399. Sydney, New South Wales, Australia: 1996.
14. Dubrovski, P. D., Golob D. 2009. Effects of Woven Fabric Construction and Color on Ultraviolet Protection. *Text. Res. J.* 79, 351–359.
15. Dubrovski P. D., Miran B. 2009. Prediction of the ultraviolet protection of cotton woven fabrics dyed with reactive dyes. *Fibres Text. East. Eur.* 17, 55–59.
16. Krzysztof K., Barbara L. S. 2014. Effect of selected metrological parameters of dyed polyester textiles on their UV-barrier properties. *Fibers Polym.* 15, 2077–2085.
17. Wong W., Lam J. K., Kan C., Postle R. 2016. Influence of reactive dyes on ultraviolet protection of cotton knitted fabrics with different fabric constructions. *Text. Res. J.* 86, 512–532.
18. Ibrahim N. A., E-Zairy W. R., Eid B. M. 2010. Novel approach for improving disperse dyeing and UV-protective function of cotton-containing fabrics using MCT- $\beta$ -CD. *Carbohydr. Polym.* 79, 839–846.
19. Paluszkiwicz J., Czajkowski W., Kaźmierska M., Stolarski R. 2005. Reactive dyes for cellulose fibres including UV absorbers. *Fibres Text. East. Eur.* 13, 76–80.
20. Sarkar A. K. 2004. An evaluation of UV protection imparted by cotton fabrics dyed with natural colorants. *BMC Dermatol.* 4(15), 1-8.
21. Wang S. Q., Kopf A. W., Marx J., Bogdan A., Polsky D., Bart, R. S. 2001. Reduction of ultraviolet transmission through cotton T-shirt fabrics with low ultraviolet protection by various laundering methods and dyeing: Clinical implications. *J. Am. Acad. Dermatol.* 44, 767–774.
22. Wuxi City Greg Technology Co. 2021, April 21. China Photochromic Pigment for Yarn Making Ultraviolet UV Photosensitive Color Yarn. Retrieved from <https://photoluminescent.en.made-in-china.com/product/LNKEOsqISBVp/China-Photochromic-Pigment-for-Yarn-Making-Ultraviolet-UV-Photosensitive-Color-Yarn.html>.
23. SolarActive. 2021, April 21. Recent Projects, Color Changing Products, Color Change, Buttons, Beads & Lace Change Color in the Sun. Retrieved from <https://www.solaractive.com/recent-projects-solar-active-uv-color-change-products-ezp-4.html>.
24. Talvenmaa, P. 2006. Introduction to chromic materials. In H. Mattila, *Intelligent Textiles and Clothing*. Woodhead Publishing in Textiles, 193–205.
25. DeFacto. 2021, April 21. Turuncu Erkek Çocuk - Genç Erkek Erkek Çocuk Şekil Değiştiren Baskılı Tişört. Retrieved from <https://www.defacto.com.tr/erkek-cocuk-sekil-degistiren-baskili-kisa-kollu-tshirt-1224518>.
26. Wang P. Y., Wu C. J. 1997. Photochromic behavior of some phenoxanthraquinone dyes in solution and on polyester substrate. *Dye. Pigment.* 35, 279–288.

- 
27. Víková M., Vík, M. 2005. Colour shift photochromic pigments in colour space CIE L\*a\*b\*. *Mol. Cryst. Liq. Cryst.* 431, 403–415.
  28. Lee S. J., Son Y. A., Suh H. J., Lee D. N., Kim S. H. 2006. Preliminary exhaustion studies of spiroxazine dyes on polyamide fibers and their photochromic properties. *Dye. Pigment.* 69, 18–21.
  29. Son Y. A., Park Y. M., Park S. Y., Shin C. J., Kim, S. H. 2007. Exhaustion studies of spiroxazine dye having reactive anchor on polyamide fibers and its photochromic properties. *Dye. Pigment.* 73, 76–80.
  30. Billah S. M. R., Christie R. M., Shamey, R. 2008. Direct coloration of textiles with photochromic dyes. Part 1: Application of spiroindolinonaphthoxazines as disperse dyes to polyester, nylon and acrylic fabrics. *Color. Technol.* 124, 223–228.
  31. Billah S. M. R., Christie R. M., Morgan, K. M., 2008. Direct coloration of textiles with photochromic dyes. Part 2: The effect of solvents on the colour change of photochromic textiles. *Color. Technol.* 124, 229–233.
  32. Little A. F., Christie R. M. 2010. Textile applications of photochromic dyes. Part 1: Establishment of a methodology for evaluation of photochromic textiles using traditional colour measurement instrumentation. *Color. Technol.* 126, 157–163.
  33. Little A. F., Christie R. M. 2010. Textile applications of photochromic dyes. Part 2: Factors affecting the photocolouration of textiles screen-printed with commercial photochromic dyes. *Color. Technol.* 126, 164–170.
  34. Little A. F., Christie R. M. 2011. Textile applications of photochromic dyes. Part 3: Factors affecting the technical performance of textiles screen-printed with commercial photochromic dyes. *Color. Technol.* 127, 275–281.
  35. Durasevic V., Parac D., Sutlovic A. 2011. From Murex Purpura to Sensory Photochromic Textiles. In P. Hauser (Ed.) *Text. Dye.* London: IntechOpen, 57-76.
  36. Aldib M., Christie R. M. 2011. Textile applications of photochromic dyes. Part 4: application of commercial photochromic dyes as disperse dyes to polyester by exhaust dyeing. *Color. Technol.* 127, 282–287.
  37. Billah S. M. R., Christie R. M., Shamey, R. Direct coloration of textiles with photochromic dyes. Part3: Dyeing of wool with photochromic acid dyes. *Color. Technol.* 128, 488–492.
  38. Aldib M., Christie R. M. 2013. Textile applications of photochromic dyes. Part 5: Application of commercial photochromic dyes to polyester fabric by a solvent-based dyeing method. *Color. Technol.* 129, 131–143.
  39. Benita, S. 2006. *Microencapsulation: Methods and Industrial Applications.* New York: Taylor & Francis.
  40. Salaün, F. 2016. Microencapsulation technology for smart textile coatings. In J. Hu (Ed.) *Active Coatings for Smart Textiles.* Woodhead Publishing Series in Textiles, 179-220.
  41. Cheng S. Y., Yuen C. W. M., Kan C. W., Cheuk K. K. L. 2008. Development of Cosmetic Textiles Using Microencapsulation Technology. *RJTA* 12(4), 41-51.
  42. Çay A, Atav R, Duran K. 2007. Effects of warp-weft density variation and fabric porosity of the cotton fabrics on their colour in reactive dyeing. *Fibres Text East Eur* 15, 91–94.
  43. Çay A, Tarakçıoğlu I. 2008. Relation between fabric porosity and vacuum extraction efficiency: Energy issues. *The Journal of The Textile Institute* 99(6), 499-504.



# Investigation of Performance Characteristics of 3D Printing Textiles in Terms of Design and Material

Fatma Bulat<sup>1</sup>  0000-0002-6367-4243

Fatma Nur Başaran<sup>2</sup>  0000-0002-6024-1709

<sup>1</sup> Kırıkkale University / Keskin Vocational High School, 71800, Kırıkkale.

<sup>2</sup> AHBV University / Faculty of Art and Design, Textile Design Department, 06830, Ankara.

**Corresponding Author:** Fatma Bulat, f.bulat@kku.edu.tr

## ABSTRACT

New technologies that are used in the producing and processing of textile surfaces provide significant advantages for the designer. One of the important technologies that offer today's design advantage is three-dimensional "3D" printers. This study attempted to determine the effect of design features used on textile surfaces produced with different 3D printers and materials on performance characteristics. This research aimed to examine and compare the performance characteristics of 3D printers, the relationships between 3D printers and the different materials required by these printers, and one-piece and multi-pieces designs. Accordingly, textile surfaces were produced with 3D printers and the performance properties of these surfaces were determined. Significant differences were observed in the performance of textiles based on the breaking, bursting and weight determination tests. These differences were discussed in terms of the design's structural characteristics, material and the ways of 3D printing to stacking material. Consequently, although the performances of 3D textiles get the better of one another, their breaking and bursting strengths are found to be lower than the conventional fabrics.

## ARTICLE HISTORY

Received: 06.05.2021

Accepted: 07.10.2021

## KEYWORDS

3D printing, Textile Design, Fashion Design, 3D Textile, Performance

## 1. INTRODUCTION

During thousands of years of textile production, there have been many changes in textile machines and processes, however, the approaches to fabric design to attain the desired properties has remained empirical. It is the skill and experience of textile technologists, backed when necessary by trial and error that dominates the production of fabrics [1]. After World War II, tremendous fiber innovation in both North America and Europe continents gave the push for product development towards man-made fibers in the 1950s. In the 1960s, the mills adapted the new fibers to their systems, providing innovative yarns and fabrics [2]. Meanwhile, innovative designs with effective technological developments have been regarded as a driving force in the marketing process and the work of textile designers has taken on a new significance in regard

to bear features, such as authenticity, innovation, compliance with customer expectations, and functionality [3]. In this industry, where personal tastes stand out and tailor-made designs gain importance, the creative process becomes even more significant in regard to, particularly aesthetics elements [4]. Therefore, the designers have obtained the new forms they need by benefiting from science and technology and using new materials and production methods [5,6].

Against the background, three-dimensional (3D) printers are one of the most important technological advances of today, offering new opportunities to designers. Devices that are capable of 3D printing are called 3D printers [7]. 3D printers are one of the primary shaping technologies that enable objects to be generated in various ways with appropriate materials [8]. These printers are machines that

**To cite this article:** Bulat F, Başaran F. 2022. Investigation of Performance Characteristics of 3D Printing Textiles in Terms of Design and Material, *Tekstil ve Konfeksiyon*, 32(2), 162-172.

convert digital data (three-dimensional CAD drawing) into real objects [9]. The basic principle of this technology is the generation of 3D designs by printing them layer by layer [10]. However, formations of the designs by the layers can considerably differ. Therefore, printers that can use different materials have been developed. Accordingly, the materials used in these devices are classified under three main headings. These include; liquid-based materials, solid-based materials and powder materials [11]. 3D production with liquid-based materials is made by exposing the photopolymer material to radiation and solidifying and the printing technologies that commonly use these materials are Stereo Lithography Apparatus and Polyjet [12]. Moreover, solid-based materials are available in filament form or in layers, and such materials are often used in the “Fused Deposition Modeling (FDM)” method [13]. Powder-based materials, on the other hand, are available in granular form, and the most well-known method among others, using these materials, is “Selective Laser Sintering (SLS)” [14].

Three-dimensional printers are also being used in textile production since 2010. The output of these printers differs from conventional textiles for connection types, consist of production form, material and textile. So, they need to develop different parameters to attain different attitudes, such as stretching, flexural, bending and drapability in textiles that are produced with 3D printers. Thus, the designers mostly create different connections to attain these attitudes. The studies have brought up the potentials of this new form of production and the materials used in production in terms of design processes. The designer’s knowledge of the performance characteristics of the emerging new product is an important part of the product design scenario.

This research aimed to identify the effects of connection forms, material and printers’ stacking/combining ways on the performance characteristics of textile surfaces that are produced through 3D printers. In the study that was conducted in three stages through experimental processes,

two different textile surfaces that can be produced with 3D printers were designed and the designs were generated by using Fused Deposition Modeling, Selective Laser Sintering and Polyjet printing. Performance characteristics were identified by doing bursting and breaking strength tests to the 3D textiles produced. The obtained results have been discussed in the context of design, printing process and material.

### 1.1. The Production of Textile Surface with Three-Dimensional Printers

Three-dimensional printers are used in many fields of industrial production as well as in the textile sector. In the meantime, these methods can be used to produce all kinds of work that can be modelled in three dimensions in the computer and this enables the designers to develop innovative designs [15]. Furthermore, textile and fashion designers have been using this technology in many fields, such as in various fashion shows, conceptual artworks, or wearable art objects.

The design and production process with three-dimensional printers begin with determining the intended purpose of textile and modelling studies. In the second stage, three-dimensional drawings of textile design are being prepared in the features and sizes set by the appropriate CAD programs. Then, the created designs are converted into the STL file format. The STL file format is “an unsorted triangle surface list that represents the outer surface of the design” [16]. The data contained in this file is subjected to some pre-processing, such as error checking and building direction, creating support structures if necessary [17]. Finally, geometric textile data is printed by being sliced and sent to the printing machine, which is considered suitable for production (Figure 1). Textiles produced with a three-dimensional printer may be dimensionally incorrect when compared to conventional technologies. Therefore, “the surfaces of critical objects are finally cleaned, cured and brought to final size” [18].

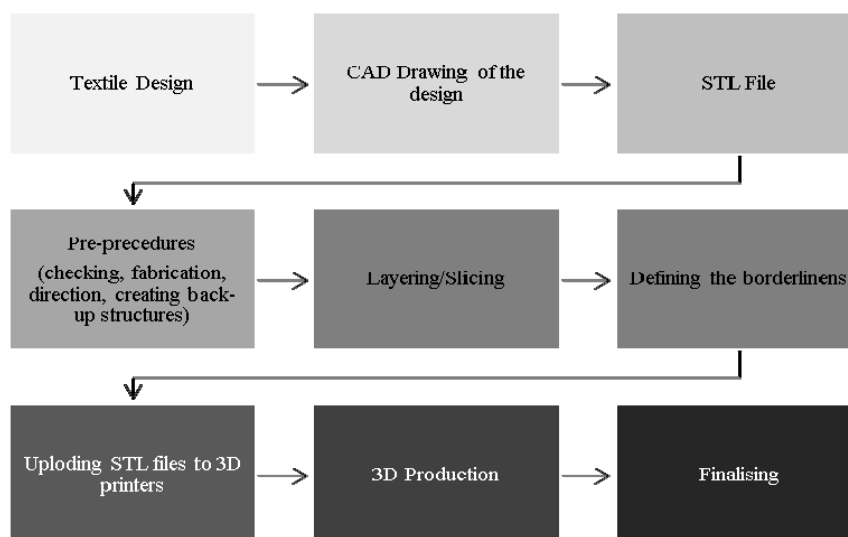


Figure 1. 3D Textile production stages [19].



This research, 3D textiles have been classified from various aspects to clarify the subject (Figure 2). Textiles in literature can be classified in various ways by the structural characteristics of the surface, material, technique, etc. [20,21]. A similar classification is possible within 3D textiles (Figure 3).

Textiles with 3D printers are produced as single-piece or multi-piece (modular). Besides, they can also be used to obtain patterns on conventional textiles or in the brand logo printing process. R&D and Product Development studies related to 3D print textile surfaces continue.

### 1.2. Related Works

Works on three-dimensional printers in the textile and fashion industry have begun in the 2000s and 234 patent had been obtained in this field by 2014. The next generation of designers, such as the Belgian Materialise firm, the American Nervous System, Iris Van Harpen, Michael Schmidt and American costume designer Ruth E. Carter, who won the Oscar for Best Costume Design in 2019 for her works in Black Panther, are among those using with this technology [22,23,24]. The works that are salient include those projects that relate the tradition of textile construction to code or parametric software to create a 3D printed textile

structure. More specifically, the focus is on work that looks at the material behaviour in relationship to that structure rather than focusing on generating the form of the 3D print [25].

In his study, Davis (2012) modelled 3 conventional textile structures with Fused Deposition Modeling (FDM) 3D printers by using Rubber and Acrylonitrile Butadiene Styrene (ABS). He examined the behaviour of 3D textiles from the point of textile unit geometry and material relationship and suggested this as a method that can be used by the textile and fashion designers [25]. Palz, & Thompsen (2009) expand the concept of traditional crafting of textiles by their use of digital modelling and digital 3D printing techniques. In this article Palz and Thompsen explicitly discuss the possible motions that a knit knot unit has as a 3D print [26]. In another study, Melnikova, & colleagues (2014) tried to model the conventional weaving method by using polylactic acid (PLA) and Acrylonitrile Butadiene Styling (ABS) materials through the Selective Laser Sintering method for 3D printers [27]. By the way, Lussenburg and colleagues (2014) indicated that the stretching feature of textiles that are produced with 3D printers can be attained depending on the structure and material (Figure 3).

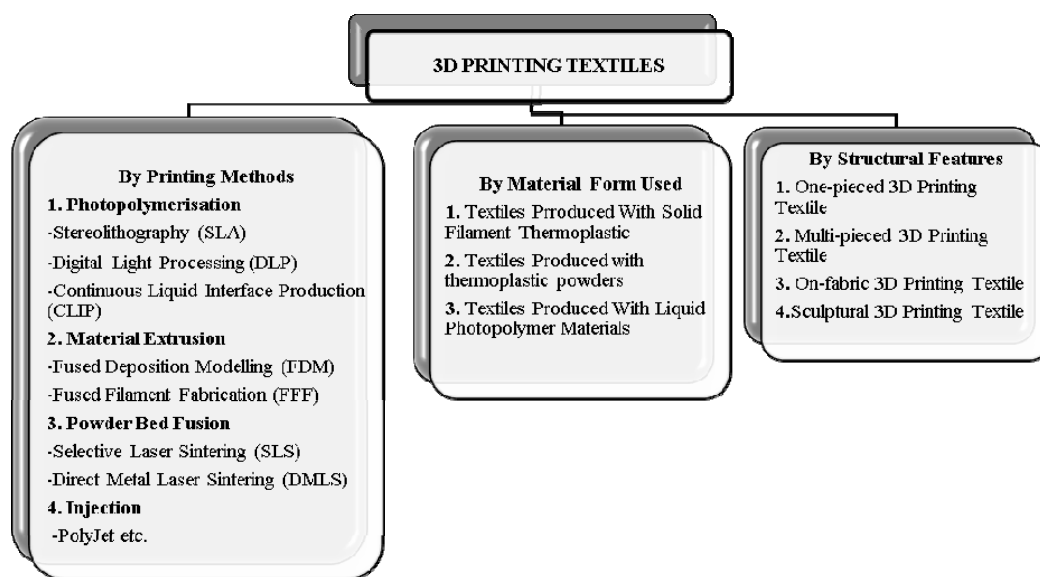


Figure 2. Classification of 3D Textiles [19].

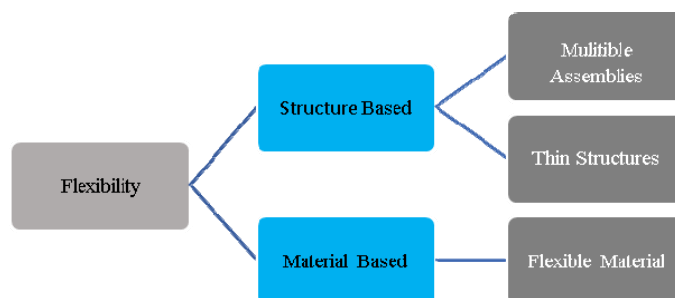


Figure 3. Flexural properties of 3D textiles [28].

Partsch and colleagues (2015) worked to form flexible textile structures with proper tensile, cutting, bending, etc. features by using additive manufacturing (AM) method and they produced three different plain weaving specimens with printers by 3D modelling and evaluate them [29]. Spahiu et al (2016) experienced tailor-made shoe production by using the 3D measurement system with FDM printers and identified the advantages and disadvantages of 3D printing in this field [30]. On the other hand, Safka and colleagues (2016) worked the mechanical testing of polymeric materials (ABSlike, VeroBlack, VeroWhite, VeroClear, Durus) processed using 3D printing and exposed to different chemical compounds [31]. Rivera and colleagues (2017) worked in the printing field on fabric, tried to print conventional textiles by using the 3D method [32].

### 1.3. Performance Characteristics of Textiles Produced with 3D Printers

Since the beginning of textile crafts, the fabrics with different methods and materials are produced by creating various patterns and connections and these fabrics are analyzed for their performances to determine their compliances with the required standards [33]. Fabric performance is affected by the fibers and thread properties, the structure of the fabric and the treatment of the fabric. The performance of any textile structure highly depends on its resistance to the forces it is exposed to. These forces can include tensile, squeezing, bending, flexural and shearing. Such tests enable us to predict the behaviour of textile materials against resistance.

Several types of research in different disciplines have shown that 3D printers affect product quality and researches are available on examining the effects, such as tensile, twisting and impact resistance [34]. According to these researches, parameters that affect the quality of products produced by printers are filling rate, layer thickness, extruder temperature, printing speed, printing style and material [35]. In 3D textiles, as with each textile structure, the geometry and layout of fibers to each other highly establishes the behaviour of that fabric [25]. However, mechanical properties also depend on the 3D printing procedure's own process and material parameters [8]. The use of these printers in almost all fields of industrial production and differentiation of expectations in each industry makes it difficult to generalize over the outcomes. Therefore, it is important that each industry studies evaluate product quality.

## 2. MATERIAL AND METHOD

### 2.1. Material

Two textile surfaces with different structural characteristics in the research were designed in 3D by using Solid Works program.

*The Design I*, was planned as a one piece and prepared for production in 234.474 x 234.474 x 1 mm by evaluating the preliminary design and prototype productions with the latest arrangements. Figure 4a shows three-dimensional Design I.

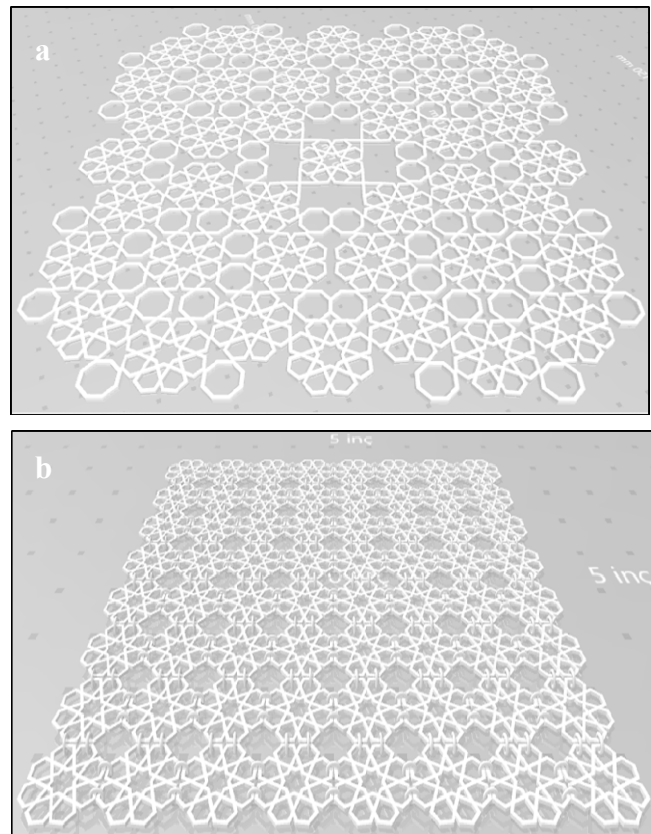


**Figure 4 a.** Design I STL file view **b.** Design II STL file view

*Design II*, was planned as a multi-piece, the final design was attained by making arrangements according to the results obtained from the prototype studies. The dimensions of the surface that were formed by connecting the motifs to one another with rings were set as 202.572 x 202.622 x 1 mm. While setting the production dimensions, it is based on the largest production measure that can be done with 3D printers at once. Figure 4b shows three-dimensional Design II.

The Design I and Design II were converted to the Standard Triangle Language (STL) format after the 3D design processes were completed. The designs were prepared for production after setting the boundary lines, layering and pre-processing (process direction, error checking, construction of supporting structures) and both designs were produced by using Fused Deposition Modeling (FDM), Selective Laser Sintering (SLS) and Polyjet printing. Materials may also differ structurally depending on the printing method used in production. In this research, the polylactic acid (PLA) filament material (Figure 8) in Fused Deposition Modeling (FDM) print, the polyamide (PA) powder material (Figure 9) in Selective Laser Sintering (SLS) print and the opaque photopolymer resin (VeroWhite) material in Polyjet print was used (Figure 10).

### 2.2. Method

The Research model aimed to identify 3D print textiles and performance characteristics and determined three factors that may affect the mechanical performance of 3D textiles. These three factors were used to determine whether there is

a relationship between three variables that are thought to affect the performance characteristics of 3D textiles. Hypotheses were also been created to test the authenticity of these recommendations. Accordingly:

**H<sub>1</sub>**: “the connection forms of 3D printing textiles affect the performance of textiles”

**H<sub>2</sub>**: “the materials used in 3D printing affect the performance of textile surfaces”

**H<sub>3</sub>**: “the way of 3D printing machines to stack and combine materials affects the performance of textile surfaces”

Three-dimensional textile surfaces are generated by considering the three-dimensional printing types and the materials used. The research was done in 3 stages: the design, production and execution of performance tests. The textile surfaces that are produced visually and physically with 3D printers compose the population of the research. Sampling consists of 78 3D textiles produced by 3D printing methods with (FDM, SLS, Polyjet) and solid thermoplastic (PLA), powder thermoplastic (PA), solid opaque photopolymer resin (VeroWhite Plus) materials and Stratasys 450 MC, EOS P 396, Stratasys object 500 connex and Zortrax FDM printers.

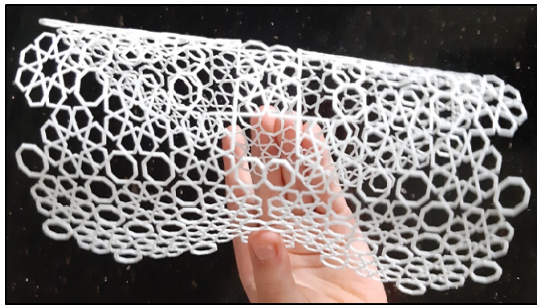


**Figure 5 a.** Design I, SLS Production

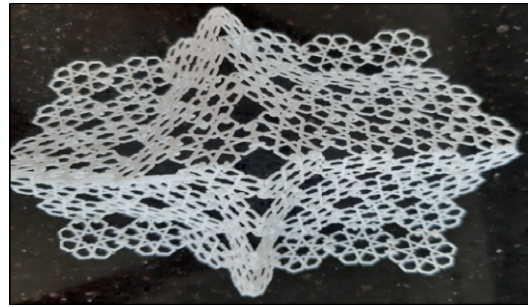


**Figure 5 b.** Design II, SLS Production

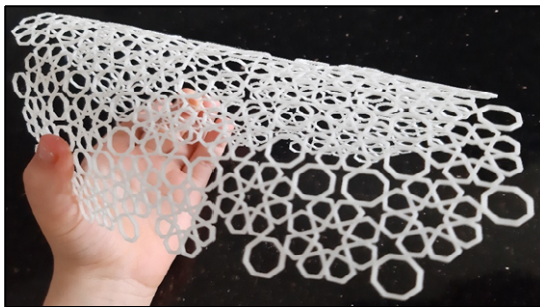


**Figure 6 a.** Design I, Polyjet Production



**Figure 6 b.** Design II, Polyjet Production

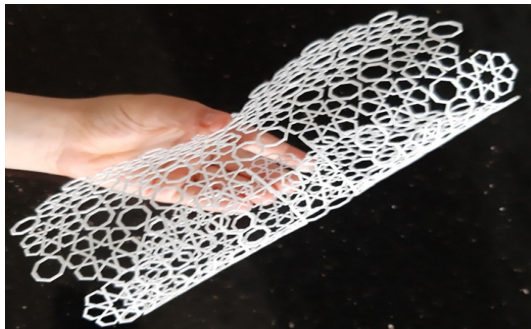


**Figure 7 a.** Design I, FDM Production

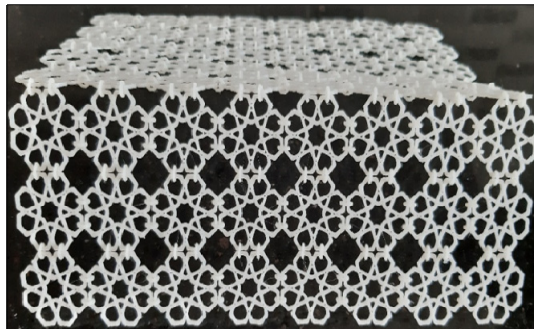


**Figure 7 b.** Design II, FDM Production



**Figure 8.** PLA cartridge filament material [36].



**Figure 9.** PA 2200 powder material [37].



**Figure 10.** VeroWhite plus resin material [38].



There is no standard test method available for the identification of performance characteristics of 3D textiles. These surfaces are recognized as web-like structures for design and thus, TÜBİTAK<sup>2</sup> BUTAL conducted breaking resistance, bursting strength and weight determination tests. Pre-conditioning and test ambient atmospheric conditions of test samples are set according to ISO 139 (20±2°C, 65±4%).

SDL Testometric M350 measuring device was used to determine the breaking and bursting strength of 3D textiles. 5 samples of 15x15cm average were taken from the samples of each production type of the three designs to be used in tests. The breaking test that was applied in weft and warp direction in standard textiles was done according to the size and width of the sample although 3D textiles do not have these systems. The samples were stretched starting from 20 mm, the breaking force at the time of breakage was stated as Newton, and the elongation of breakage as a percentage.

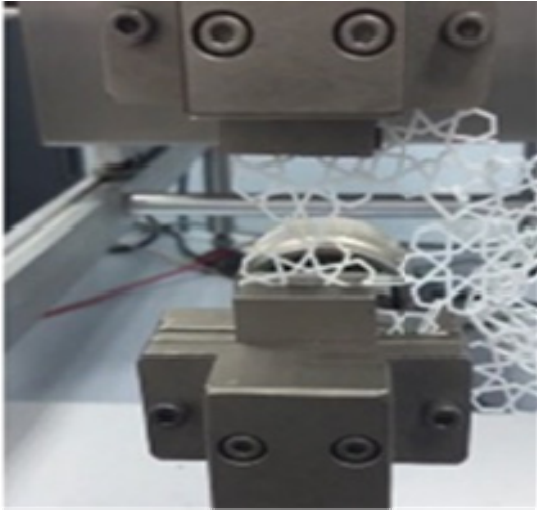


Figure 11. SDL Testometric M350, Breaking Resistance Test

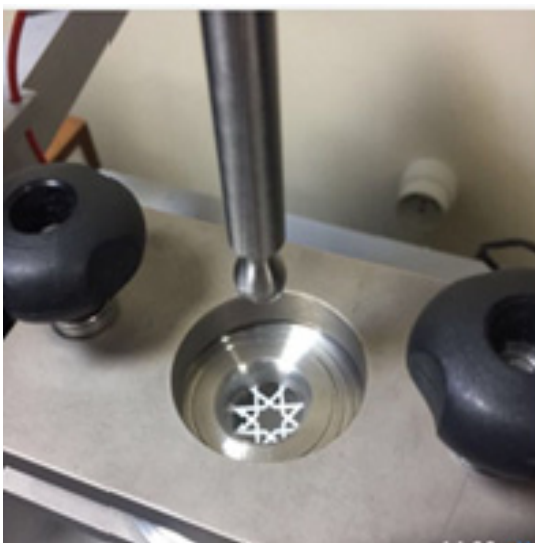


Figure 12. SDL Testometric M350, Bursting Test (Ball)

### Breaking Resistance Tests Experiment Conditions

Test device: SDL Testometric M350-5kN, Load cell: 5000N (Constant elongation rate), Distance between claws: 20 mm, Claw speed: 20mm/min., Pre-Voltage: 0.01 N, Claw type: 1-inch claw.

### Bursting Test (Ball) Experiment Conditions

Test device: SDL Testometric M350-5kN, Load cell: 5000N (Constant elongation rate), Claw speed: 300mm/min., Ball diameter: 25mm (sphere-shaped), Ring Claw Inner Diameter: 44.5 mm., Bursting strength pressure values are given as N/mm<sup>2</sup>.

Precision scales were used for weight determination test. 3 samples of 20 x 20cm average were taken from the samples of each production type in maximum sizes, 18 separate samples in total, were measured and their weights were determined. To verify the hypotheses, non-parametric Kruskal Wallis test was used instead of One-Way Anova test, which is a parametric difference test for variables with more than two groups, since the test results did not provide a parametric distribution in the group for which the results were examined. This test is used to compare three or more samples in non-parametric groups. Result of the test showed a significant difference between the groups and the groups that caused the significant difference were tested with Tamhane T2, one of the non-parametric post-hoc tests.

## 3. RESULTS AND DISCUSSION

The fabric is expected to resist the tests done according to the established standards in the textile industry. It is important that 3D textiles have the flexural and stretching feature that the human body needs, and also resist the tensile during movement. *The Design I* and *Design II* produced with 3D printers were tested for breaking resistance, bursting strength and weight determination and the data from the measurements with the test devices are interpreted as a part of the printing method, material and design.

As depicted in the table, Design 1, which is one-piece, could be produced in the shortest time possible with the SLS method and the lightest product is obtained in this way. The same results apply for multi-piece Design 2. The longest production process in all studies is for Design 2, which is produced with the Polyjet method. The attachment parts used in Design 2 were observed to increase the weight.

### 3.1. Performance Test Results of 3D Textiles

Breaking, bursting and weight values of Design 1 and Design 2 of FDM, SLS and Polyjet production methods are explained with graphics.

As shown in the graphs, the tensile strength of Design I, produced with the Polyjet method and VeroWhite material, is higher than the others. The Polyjet method is followed by

<sup>2</sup> Scientific and Technological Research Council of Turkey

the surfaces produced by the FDM and SLS method, respectively. The breaking force of the surfaces produced by the SLS method is almost half of the Polyjet method. However, the greatest elongation at breaking ratio is seen in the SLS method and the sample produced with PA.

The graphs for Design II shows that the breaking strength of the surface produced with the FDM method and PLA is higher than the others. This method is followed by SLS and Polyjet productions, respectively. The strength of the surface produced by the polyjet method is much less than those produced by the other two methods. Examination of the elongation at breaking indicates that the performance of the surface produced by the SLS method was higher than the others. This method is followed by surfaces produced by Polyjet and FDM method, respectively.

Tensile strength is one of the most important mechanical features for fabrics. Tensile strength is the ability of a material to withstand tensile force [39]. Among these

parameters, the filling rate, material type and design properties were identified as the most important factors for the experiment in this article. The different connection properties of Design I and Design II have significantly affected their breaking strength. In breaking tests, while the seams of Design II were immediately broken, Design I has exerted relatively greater strength. The differences in production methods and materials are also important, but the fact that the breaking is always at the same points, that is, in rings that combine motifs, has drawn more attention to the structural and design characteristics of the surfaces. The fact that the Design I is in one piece has relatively brought out positive effects on breaking resistance. Tensile strength of designs produced with 3D printers was found to be lower than conventional textiles. Generally, the designs with a 100% filling rate, designs acted fragiley during tests. Strenght lack of designs attributed to the rigid structure and thinness parameters of the materials used.

Table 1. Design and production details of 3D textiles

Design Code	Production method	Raw material	Material type	Production dimensions	Production time	Weight
Design I	FDM	PLA	Solid thermoplastic	234.5 x 234.5 x 1 mm	27 h 50 min	11.25 g
Design I	SLS	PA	Powder thermoplastic	234.5 x 234.5 x 1 mm	4 h	7.14 g
Design I	Poly-Jet	Opaque photopolymer resin (VeroWhite)	Liquid photopolymer	234.5 x 234.5 x 1 mm	4 h 40 min	13.71 g
Design II	FDM	PLA	Solid thermoplastic	202.6x 202.6 x 1 mm.	32 h 30 min	17.1 g
Design II	SLS	PA	Powder thermoplastic	202.6 x 202.6 x 1 mm	4 h	8.13 g
Design II	Poly-Jet	Opaque photopolymer resin (VeroWhite)	Liquid photopolymer	202.6 x 202.6 x 1 mm	10 h	16.25 g

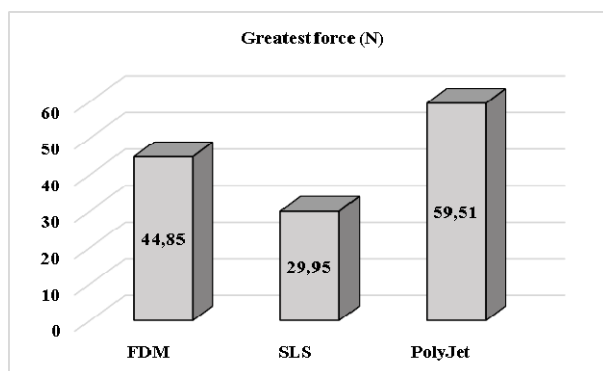


Figure 13. Design I, breaking strength, the greatest force

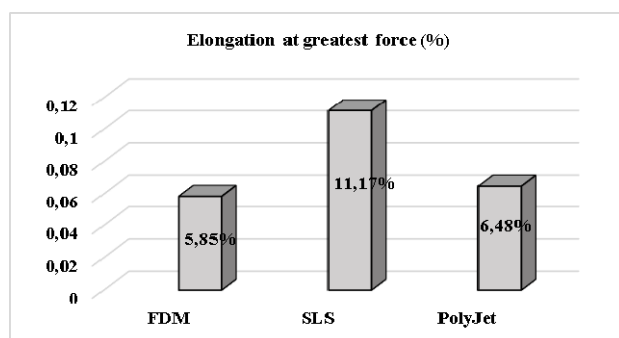


Figure 14. Design I, breaking strength, elongation at the greatest force

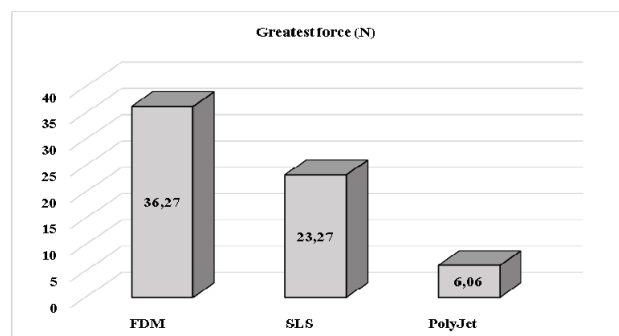


Figure 15 Design II, breaking strength, the greatest force

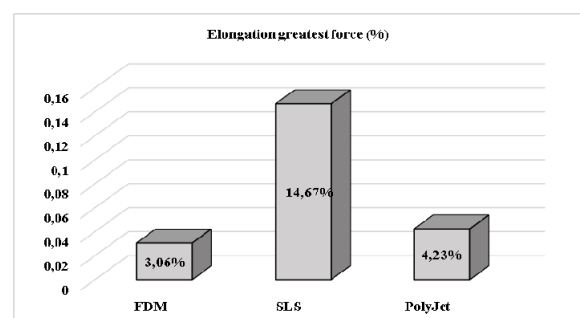


Figure 16. Design II, breaking strength, elongation at the greatest force

Design I and Design II were produced with FDM, SLS, Polyjet production methods using suitable materials. The charts below show the bursting strength measurement results of the samples and their mean values. The results of the burst strength pressure values are given as N/mm<sup>2</sup>.

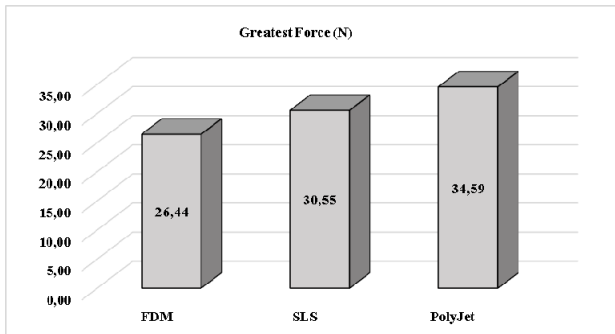


Figure 17. Design I, bursting strength, the greatest force

The charts shown in Figure 17 and 18 demonstrates that the surface structure and the material used have an effect on the burst strength pressure values. According to these results, the bursting strength is highest in Design I produced using the Polyjet method. This was followed by surfaces produced by SLS and FDM method, respectively. Although slight differences due to the material were observed for the design with the same tightness setting, these surfaces are considered to be weak in terms of burst strength.

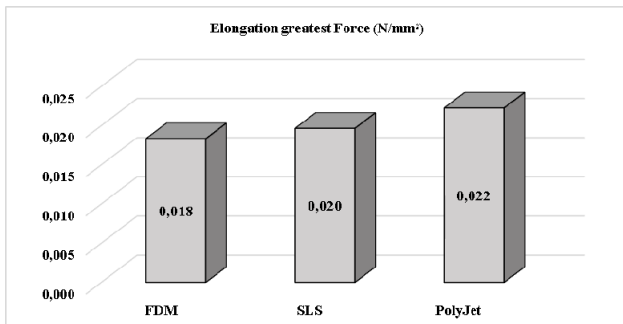


Figure 18. Design I, bursting strength, elongation at the greatest force

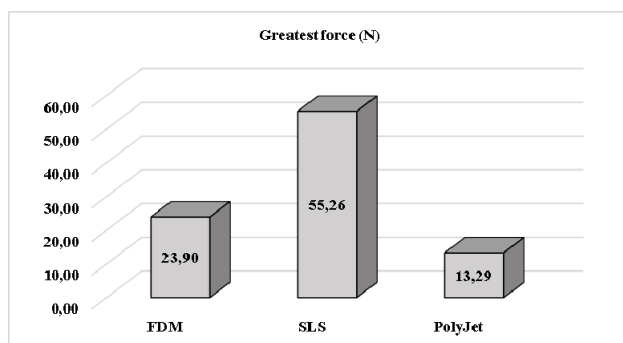


Figure 19. Design II, bursting strength, the greatest force

Evaluation of the Design II in terms of bursting strength showed that the strength value of the surface produced by the SLS method is higher than the others. The strength of

the surfaces produced by the FDM and Polyjet method was observed to be lower.

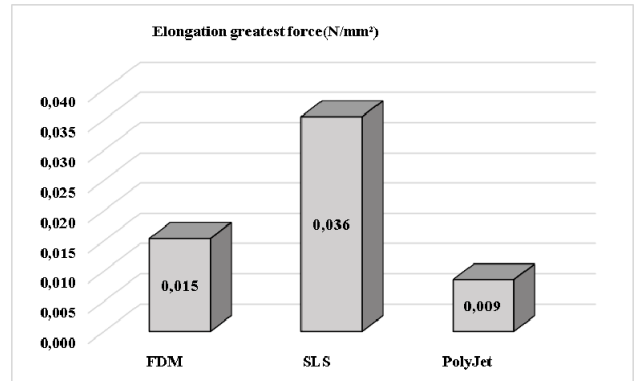


Figure 20. Design II, bursting strength, elongation at the greatest force

The materials used in the production of Design I and Design II have been subjected to various tests by their manufacturers and the performance of these materials has been evaluated as high. However, the performance values of the textile surfaces produced for this study are quite low. It was considered that this situation is caused by the design and the structural properties of the design substantially affect the performance properties of 3D textiles.

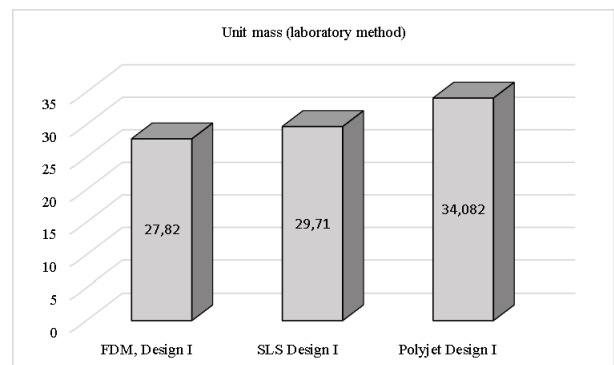


Figure 11. Design I, test results of weight determination

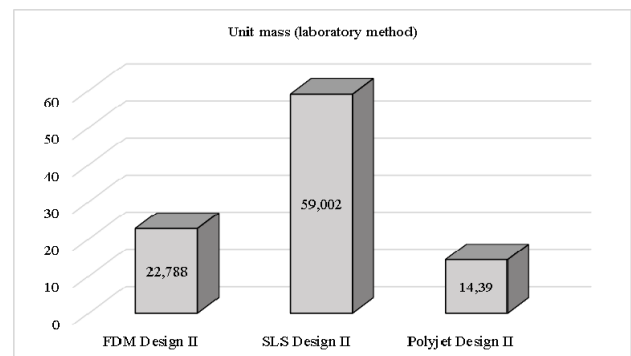


Figure 12. Design II, test results of weight determination

According to the weight test results applied to Design I, the lowest weight textile surface was produced with FDM method and PLA material. This was followed by SLS



production and Polyjet production, respectively. In the weight tests of Design II, the lowest weighted textile was produced with the Polyjet method and VeroWhite. This 3D textile surface was followed by the textile surfaces produced by the PolyJet method and the FDM method, respectively (Figure 22).

The weight test results of 3D textiles advise the surfaces from their area of use to performance characteristics. Weight tests are important for the area of use of textile surfaces. According to standards established in conventional textiles (TSE 251, EN ISO 3801, ASTM D 3776, BS EN 12127, BS 2471); the weights are expected to be as 30 g/m<sup>2</sup> for gauze patches, 80-120 g/m<sup>2</sup> for combed cotton fabric, 200-250 g/m<sup>2</sup> for dress fabrics and around 400 g/m<sup>2</sup> for coated fabric. Based on the weight determination test results of 3D textiles that are produced with different methods and materials, these textiles were found to be heavier than conventional textiles.

### 3.2. Comparison Analysis

In this study, comparison tests were also needed to test the hypotheses and the fracture, burst and weight values of designs 1 and 2 of FDM, SLS and Polyjet production methods were compared. Breaking, bursting and weight variables have not been distributed normally in a group. The in-group values of kurtosis and skewness of variables should be between -1.5 and +1.5 [40]. As can be seen from Table 1, there is no normal distribution by kurtosis and skewness values.

As the normal distribution in the group was not provided, the nonparametric Kruskal Wallis test was used instead of the One-Way Anova test, which is a parametric difference test for variables with more than two groups. In variables where test results are significant ( $p < 0.05$ ) from which groups the difference originates was tested with Tamhane T<sub>2</sub>, which is one of the nonparametric post-hoc tests. The results are as in Table 3 below.

**Table 2.** Kurtosis and Skewness Values

Test		FDM	FDM	SLS	SLS	POLYJET	POLYJET
		Design I	Design II	Design I	Design II	Design I	Design II
Breaking Strength	Kurtosis	-1.534	0.241	-0.609	-1.280	1.643	0.62
	Skewness	2.682	0.123	-3.077	0.895	3.018	-1.81
Bursting Strength	Kurtosis	0.486	-0.386	1.763	-0.632	1.806	-0.15
	Skewness	-3.112	-2.908	3.336	-3.048	3.719	-1.89
Weight Determination	Kurtosis	0.609	2.135	0.299	-1.736	-0.503	-1.84
	Skewness	-3.333	4.635	-2.718	3.251	-3.146	3.61

**Table 3.** Comparison of Test Results

Test	Method	Design	M	SD	Z	P
Tensile Strength Test Result (N)	FDM	Design I	43.05 N	5.90	25.71	0.000
	SLS	Design I	29.95 N	5.90		
	Poly-Jet	Design I	59.11 N	15.63		
	FDM	Design II	36.27 N	4.32		
	SLS	Design II	23.27 N	2.43		
	Poly-Jet	Design II	6.06 N	2.45		
Bursting Strength Test Result (N)	FDM	Design I	27.82 N	5.12	21.98	0.000
	SLS	Design I	29.71 N	4.63		
	Poly-Jet	Design I	34.08 N	10.27		
	FDM	Design II	22.79 N	4.16		
	SLS	Design II	59.00 N	19.18		
	Poly-Jet	Design II	14.39 N	4.43		
Weight Determination Test Result (g)	FDM	Design I	11.25 g	0.04	28.31	0.000
	SLS	Design I	7.14 g	0.032		
	Poly-Jet	Design I	13.708 g	0.14		
	FDM	Design II	17.06 g	0.29		
	SLS	Design II	8.128	0.016		
	Poly-Jet	Design II	16.254	0.04		

When Table 1, Table 2 and Table 3 are examined, the breaking, bursting and weight values of the measurements in different methods and designs are seen to differentiate significantly ( $p < 0.05$ ). The group in which this differentiation occurs was tested by Tamhane's T2.

The significant difference in breaking test is among the Polyjet method Design II and all other designs and the SLS method Design II and the FDM method Design I and Design II. While the Polyjet method Design II has a lower mean breaking test than all other designs, the SLS method Design II have a lower mean of breaking test than FDM method Design I and Design II. There is no significant difference between other methods and designs for bursting test.

The significant difference in bursting test is between Design II of Polyjet method and Design I of FDM and SLS method. Design II of Polyjet method has a lower bursting test average compared to these two designs. There is no significant difference between other methods and designs for bursting test.

The significant difference in weight testing is between all designs. While SLS method Design I has the lowest weight value, it was respectively ranged as SLS method Design II, FDM method Design I, Polyjet method Design I, Polyjet method Design II and FDM method Design II.

The textiles produced with 3D printers are evaluated as a result of their performance tests in terms of application areas. The Design I and Design II was found to be ineligible for the production of a complete garment. The material must be flexible so that the textiles to be transformed into an adaptable garment to body movements. However, the flexibility in conventional textiles was not attained currently with materials that are used in 3D printers and failed to resist the stretching caused by body movements. Multi-piece designs were also determined to perform poorly in terms of strength requirement, although they provide a certain degree of freedom of movement and drape. Therefore, the use of these textiles as accessories in part of garments produced with conventional textiles can be the best way to be recommended to the designers in the short run. Besides, better performance characteristics of

single-piece textile with 3D printers are considered to be used in shoe production, provided that the thinness parameters of this technology are not kept low. The research that was done by Spahiu and his colleagues in the shoe production with 3D printers in 2016 and the fact that Nike Company has focused its innovation efforts on the production of runner shoes with 3D printers since 2016 reinforce our thought.

#### 4. CONCLUSION

This article provides designers with a roadmap for 3D design and 3D print textile production; creates a comprehensive framework to evaluate the relationship between design, 3D printing, material and performance. 3D printed textiles have shown low resistance in the performance tests. Despite the successful performance of the materials used in printing in strength tests, *Design I* and *Design II* failed to resist the force they were exposed to and broken and torn in low force. When a one-piece design to be produced by 3D printing is printed by using hard materials, it will be difficult to use and won't be drapable like conventional textile surfaces. From this aspect, better results can get from designs in this structure by using soft and flexible material. Lack of flexibility in commonly used materials, inability to attain the appropriate fiber thinness in 3D printing for textile are disadvantages for the designers. Also, the speed is of the utmost importance in textile production, however, 3D printing is incomparably slow than the conventional technologies. But from a design point of view, allowing the production forms that cannot be attained through conventional production methods, introducing new initiatives to designers, consumers, and thus the textile industry are considered as the advantage of this technology.

#### Acknowledgement

This study was produced from the doctoral dissertation on "Investigation of the Performance and Comfort Properties of Textile Surfaces Obtained by Three Dimensional Printers" completed by Fatma Bulat in 2019; It was supported with the project number 58 / 2017-06 within the scope of Gazi University Scientific Research Projects.

#### REFERENCES

1. Hearle, J.W.S. (2015). *Mechanical Properties of Textile Reinforcements For Composites. Advances In Composites Manufacturing and Process Design*. Woodhead Publishing.
2. Tobler-Rohr, M.I. (2011). *Handbook of sustainable textile production*, Woodhead Publishing
3. Bulat, F., & Başaran, F.N. (2018). Tekstil Tasarımında Yenilikçi Yaklaşımlar: 3B Yazıcılarla Deneysel Çalışmalar [Innovative Approaches in Textile Design: Experimental Practices with 3d Printers]. *The Journal of Kesit Academy*, 4(14), 257-273
4. Önlü, N. (2004). Tasarımda Yaratıcılık ve İşlevsellik, Tekstil Tasarımındaki Konumu [Creativity and Functionality in Design, Its Position in Textile Design]. *Atatürk University Social Sciences Institute Journal*, 3(1), 86.
5. Meriç, D., & Üreyen, M. E. (2019). Akıllı Tekstil Malzemelerinin Tekstil ve Moda Tasarımına Katkıları [Contribution of Smart Textile Materials to Textile and Fashion Design], *International Social Sciences Studies Journal*, 5(30), 535-545.
6. Gürcüm, H. B., & Bulat, F. (2016). Tekstil Tasarımında İnovatif Bir Yaratıcılık Aracı Olarak Lazer Kesim [Laser Cutting as An Innovative Creativity Tool in Textile Design], *Idil Journal of Art and Language*, 6(28), 107-130.
7. Leigh, S.J., Bradley, R.J., Purssell, C.P., Billson, D.R., & Hutchins, D.A. (2012). A Simple, Low-Cost Conductive Composite Material for 3D Printing of Electronic Sensors. *PLOS ONE* 7(11), 1-14.
8. Lehmann, A., Ehrmann, A., & Finsterbusch, K. (2017). Optimization Of 3D Printing with Flexible Materials. *International textile conference*, Stuttgart.

9. Cali, J., Calian, A.D., Amati, C., Kleinberger, R., Steed, A., Kautz, J., & Weyrich, T. (2012). 3D-Printing of Non-Assembly, Articulated Models. *ACM Transactions on Graphics (TOG)- Proceedings of ACM, Siggrapy Asia*, 31(6), 1-8.
10. Kim, H., Park, E., Kim, S., Park, B., Kim, N., & Lee, S. (2017). Experimental Study on Mechanical Properties of Single- and Dual-Material 3D Printed Products. *Elsevier B.V. Procedia Manufacturing*, 10, 887-897.
11. Çelik, İ. Karakoç, F., Çakır, C.M., & Duysak, A. (2013). Hızlı Prototipleme Teknolojileri ve Uygulama Alanları [Rapid Prototyping Technologies and Application Areas]. *Journal of Science and Technology of Dumlupınar University*, 31, 53-70.
12. Özsoy, K., & Duman, B. (2017). Eklemeli İmalat (3 Boyutlu Baskı) Teknolojilerinin Eğitimde Kullanılabilirliği [Usability of Additive Manufacturing (3D Printing) Technologies in Education]. *International Journal of 3D Printing Technologies and Digital Industry*, 1(1), 36-48.
13. Reiss, D. (2013). Complex processes and 3D printing. BSC. Project. Imperial Collage London.
14. Gross, C. B., Erkal, L. J., Lockwood, Y. S., Chen, C., & Spence, M. D. (2014). Evaluation of 3D Printing and Its Potential Impact on Biotechnology and the Chemical Sciences. *Analytical Chemistry*, 86, 3240-3253.
15. Kara, N. (2013). Havacılıkta Katmanlı İmalat Teknolojisinin Kullanımı [Use of Additive Manufacturing Technology in Aviation Industry]. *Engineer and Machine Journal*, 54(636),
16. Zhang, L.C., Han, M., & Huang, S.H. (2003). CS File – An Improved Interface Between CAD and Rapid Prototyping Systems. *International Journal of Advanced Manufacturing Technology*, 21, 15-19.
17. Çelebi, A., Tosun, H., & Önçağ, Ç.A. (2017). “Hasarlı Bir Kafatasının Üç Boyutlu Yazıcı ile İmalatı ve İmplant Tasarımı [Manufacturing A Damaged Skull With 3d Printer an Implant Design], *International Journal Of 3D Printing Technologies and Digital Industry*, 1((1), 27-35.
18. Ege Bölgesi Sanayi Odası Raporu. (2015), Sanayi 4 [Industry 4]. URL: <https://docplayer.biz.tr/26361764-Ege-bolgesi-sanayi-odasi-sanayi-4-0-arastirma-mudurlugu.html>, Last accessed: 13.06.2019.
19. Bulat, F. (2019). Üç Boyutlu Yazıcılarla Elde Edilen Tekstil Yüzeylerinin Performans ve Konfor Özelliklerinin Belirlenmesi [Research on The Performance and Comfort Properties of Textile Surfaces Printed Out from Three-Dimensional Printers]. Unpublished doctoral thesis, Gazi University, Ankara.
20. Başaran, F.N. (2019). *Basit Yapılı Dokuma Teknikleri* [Simple Structured Weaving Techniques]. Karınca Publishing.
21. Başer, G. (2005). *Dokuma Tekniği ve Sanatı* [Weaving Technique and Art]. Punto Publishing.
22. Bulat, F., & Başaran, F.N. (2018). 3B Yazıcılarla Tekstil Tasarımında FDM Yöntemi [FDM Method in Textile Surface Design With 3D Printers]. III. *International Multidisciplinary Studies Congress*, Ankara.
23. Black Panther's Oscar-winning costumes include 3D-printed designs. (2021, August 19). <https://www.dezeen.com/2019/02/27/black-panther-best-costume-design-oscar-3d-printing/>.
24. 3D Printing Wins Big At The Oscars With Black Panther And Materialise. (2021, August 19). <https://3dprintingindustry.com/news/3d-printing-wins-big-at-the-oscars-with-black-panther-and-materialise-149884/>.
25. Davis, F. (2012). 3D Printed Textiles from Textile Code: Structural Form and Material Operations, *Proceedings of the 16th Iberoamerican Congress of Digital Graphics*, Brasil.
26. Palz, N., & Thomsen M. R. (2009). Computational material: rapid prototyping of knitted structures. *In Proceedings of Architecture and Stages in the Experience City*, Aalborg University.
27. Melnikova, R., Ehrmann, A., & Finsterbusch, K., (2014). 3D Printing of Textile-Based Structures by Fused Deposition Modelling (FDM) With Different Polymer Materials, *Global Conference on Polymer and Composite Materials*, China.
28. Lussenburg, K., Velden, V.D.N., Doubrovski, Z., Geraedts, J. & Karana, E., (2014, Ocak). Designing with 3D Printed Textiles. Conference: *International Conference on Additive Technologies*, Vienna.
29. Partsch, N.L., Vassiliadis, S., & Papageorgas, P. (2015). 3D Printed Textile Fabrics Structures. *International Istanbul Textile Congress*. Innovative Technologies “Inspire to Innovate”, İstanbul.
30. Spahiu, T., Piperi, E., Grimmelsmann, N., Ehrmann, A., & Shehi, E. (2016). 3D Printing as A New Technology for Apparel Designing and Manufacturing. *International Textile Conference*, Dresden.
31. Safka, J., Ackermann, M., & Martis, D. (2016). Chemical Resistance of Materials Used in Additive Manufacturing, *MM Science Journal*, (12), 1573-1578.
32. Rivera, M. L., Moukperian, M., Daniel-Ashbrook, D., Mankoff, J., Scott, E., & Hudson, S. E. (2017). Stretching the Bounds of 3D Printing with Embedded Textiles, CHI 2017, Denver, CO, *International Symposium*, USA.
33. Ayyıldız, Ç., & Koç, E. (2004). Denim Kumaşlarda Performans Analizi I-Kumaş Mukavemeti ve Aşınma Dayanımı Değerlendirmesi [Performance Analysis of Denim Fabrics I-Fabric Strength and Abrasion Resistance Evaluation]. Çukurova University, *Journal of the Faculty of Engineering and Architecture*, 19(2), 69-82.
34. Demirci, İ. H., Şen, Ş., & Sekban, B. (2016, 5-7 Mayıs). 3B Yazıcıda Farklı Baskı Yöntemleriyle Üretilen Çıktıların Mekanik Özelliklerinin İncelenmesi [Investigation of Mechanical Properties of Printouts Produced with Different Printing Methods in a 3D Printer]. *International 3D Print Technologies Symposium*, İstanbul.
35. Fodran, E., Koch, M., & Menon, U. (1996). Mechanical and Dimensional Characteristics of Fused Deposition Modeling Build Styles. *In Solid Freeform Fabrication Proc*, 419-442.
36. PLA cartridge filament material. (2021, August 19). <https://www.xyzprinting.com/en-US/material/pla-for-original>.
37. PA 2200 powder material. (2021, August 19). [https://www.alibaba.com/product-detail/Easy-processing-PA2200-powder-selective-laser\\_60507099149.html](https://www.alibaba.com/product-detail/Easy-processing-PA2200-powder-selective-laser_60507099149.html).
38. VeroWhite plus resin material. (2021, August 19). <https://store.goengineer.com/products/verowhite-plus-rgd835-3-6kg>.
39. Hassan, N.M., Mondol, S.M., & Hossain, S. (2018). Effect of Yarn Count on Single Jersey Knitted Fabric Properties, *IOSR Journal of Polymer and Textile Engineering*, 5 (5), 21-24.70-75. Tabachnick, B. G. & Fidell, L.S. (2013) B.G. Tabachnick, L.S. Fidell Using Multivariate Statistics (sixth ed.) Pearson, Boston (2013)
40. Tabachnick, B. G. & Fidell, L.S. (2013) B.G. Tabachnick, L.S. Fidell Using Multivariate Statistics (sixth ed.) Pearson, Boston (2013)

# The Usage of Carbon-Based Filament Yarns in Different Forms in the Design of Textile Reinforced Concrete Structures

Mutlu Kurban<sup>1</sup>  0000-0001-9132-0349

Osman Babaarslan<sup>2</sup>  0000-0002-1606-3431

İsmail Hakkı Çağatay<sup>3</sup>  0000-0001-5182-776X

<sup>1</sup>Cukurova University/ Adana Organize Industrial Region of Vocational School Technical Sciences/ Textile Technology, Adana, Türkiye

<sup>2</sup>Cukurova University/ Faculty of Engineering/ Department of Textile Engineering, Adana, Türkiye

<sup>3</sup>Cukurova University/ Faculty of Engineering/ Department of Civil Engineering, Adana, Türkiye

**Corresponding Author:** Mutlu Kurban, mkurban@cu.edu.tr

## ABSTRACT

Textile reinforced concrete (TRC) is an innovative building material that has been used in recent years and consist of textile components with high tensile strength and concrete produced from fine-grained aggregates. Textile components can be used in the form of raw yarn, coated with various polymers, and recently, in the form of hybrid yarn. There are many hybrid yarn production methods used in the textile industry, and in this study, the braiding technique, which is suitable for the material used, is emphasized. In the study, samples were produced by positioning two different textile surfaces produced from three different yarn structures with carbon roving in three different positions in the concrete. Compared to the raw filament use, it was observed that the flexural strength increased by 23% with the use of hybrid yarn, while it increased by 167% with the use of epoxy coated filament.

## 1. INTRODUCTION

Various materials such as straw, clay, stone, and wood have been used in the production of buildings since the first periods of history for accommodation, which is one of the basic needs of human beings. Building materials have changed with the developments throughout history. Concrete is one of them, and with the discovery of cement in the 1800s, the use of concrete increased and it has become one of the most widely used construction materials today. The reason for this is that high compressive strength concrete is low cost and abundant. However, besides these advantages of concrete, it also has some disadvantages. For example, concrete with high compressive strength has high shrinkage and cracking and gives low tensile and bending strength. In addition, the weak toughness, high fragility and low impact strength of concrete led researchers to new searches for concrete [1-2].

Due to these disadvantages of concrete, which is widely used today because there is no alternative, studies have been

carried out on its reinforcement with various materials, as was done in the first periods of concrete history. In particular, studies on composite structures created by combining concrete mortar and textile structures have gained intensity in the last quarter-century. These materials, called textile reinforced concrete (TRC), are composite materials that have been used as building material recently. TRC is known as innovative building materials with various uses such as sandwich panels, roofs, and outdoor furniture [3-4]. TRC is a composite material and consists of fine-grained concrete and textile materials with high tensile and alkali resistance such as alkali-resistant glass, basalt, and carbon filament. These high-strength materials are transformed into different textile structure forms to transfer their technical properties to concrete. The textile structures with a hollow structure that such as leno woven fabrics, knitted fabrics with bidirectional or multidirectional warp, or sandwich knitted fabrics can be used to allow the passage of the prepared concrete mortar [4-7]. Technical textile materials used in concrete reinforcement consist of materials that do not have the risk of corrosion. For

## ARTICLE HISTORY

Received: 26.01.2021

Accepted: 14.09.2021

## KEYWORDS

Buildtech, hybrid yarn, braiding yarn, epoxy resin, textile reinforced concrete (TRC), flexural behavior

**To cite this article:** Kurban M, Babaarslan O, Çağatay İH. 2022. The usage of carbon-based filament yarns in different forms in the design of textile reinforced concrete structures, *Tekstil ve Konfeksiyon*, 32(2), 173-182.

---

this reason, it is not necessary to create thick structures in order to prevent rusting as in classical reinforced concrete production. Thanks to these structures, thin, high-strength, and long-lasting structures that do not carry the risk of corrosion can be obtained [4, 8].

Concrete mortar has a high alkaline environment and this environment affects the strength of textile fibers to be used in concrete reinforcement [9]. Despite alkaline-resistant filaments are mostly used as a textile component, and coating these filaments with various materials in order to further increase their alkali and tensile strength is one of the common methods used recently [10]. Due to the high cost of the coating materials used and the complex process steps of the coating process, alternative methods have been sought in the composite industry. With this quest, intensive studies have been carried out on hybrid yarn production technologies in which the main reinforcement component and thermoplastic material are combined. Thermoplastic composites are preferred because they can be processed at low pressure with temperature. In addition, it provides the possibility of production suitable for automation according to thermoset composites. However, there are problems in the impregnation process due to the high viscosity of the thermoplastic material in the melt. Therefore, the necessity of close contact between the reinforcement component and the thermoplastic component arises [11]. Hybrid yarn production technologies can provide this desired close contact. There are different hybrid yarn production techniques available and these methods aim to reduce the damage applied to the reinforcement component during the process [12].

Based on this, an alternative to the textile structures commonly used in concrete reinforcement was sought. Despite the disadvantages of the coating process applied in TRC production, the use of hybrid yarn production technologies is becoming widespread.

Halvaei et al. 2020, used carbon woven textiles for TRC production. These textile structures have gaps to allow concrete flowing. These gaps' sizes are changing from 0 to 20 mm. Since the reinforcement components contribute to the flexural direction, the performance of the samples was examined with the four-point flexural test. When the textile gap size was reduced, the samples gave higher flexural load and toughness. When the gap size was chosen as 2 mm instead of 20 mm, the flexural strength increased approximately 4 times, the toughness increased 8 times. It is thought that the more textile volume percentages causes this. When the gap size is zero, the infiltration of the concrete matrix into the textile material decreases in the samples and therefore shows a weaker performance. As a result of the study, it was found that the gap size of the textile structure is an important component in the flexural behavior of TRC [13].

Kravaev et al. 2009, developed and produced hybrid yarn with commingling technique. Thanks to this yarn, TRC was able to carry more loads. It was used AR-Glass fibers and water-soluble PVA yarns to produce hybrid yarn. At the

end of production, the strength of hybrid yarns is 30% lower than conventional roving. Despite this, the hybrid structures is still twice as much as the strength of the composite structure that its strength is 500 N/mm<sup>2</sup> [14].

Merter et al. 2016, their study have showed the influences of hybrid yarn preparation method and fiber sizing type on the mechanical properties of composites that consist of glass and PP fibre. The air-jet and direct twist method were selected to produce composite material from hybrid yarn. When they produced fabrics with the air-jet hybrid yarn preparation method, they achieved the best glass fiber orientation. The tensile strength test was applied to investigate to the influences of production parameters on the mechanical properties of composites. Composite panels with similar fiber volume ratios were produced with both hybrid yarn production methods and their mechanical properties were compared. The best mechanical properties were obtained with the usage of air-jet hybrid yarn. PP resin and PES resin were used as sizing agents. It has been observed that the PP resin sizing agent contributes more to the bending and shear properties [15].

Hengstermann et al. 2016, have produced the hybrid spun yarns with reinforcement and thermoplastic component. They have used staple CF (Carbon fibre) as a reinforcement component and PA6 fibre as a thermoplastic component. Two different fibre length have used as a 40 mm and 60 mm. The length of used fibers, their mixing ratio, and their orientation in the card web are crucial factors in the carding process. Fibers with a length of 60 mm provide better carding effect and therefore better orientation. Consequently, if 60 mm fibers have used, the sliver quality has found to be better owing to the excellent orientation of fibers. In order to increase the strength of hybrid yarns, 60 mm fiber should be used as fiber length, yarn twist and CF ratio should be increased [16].

Funke et al. 2013, created a new superior-performance hybrid material for construction applications. For this, they combined textile reinforced concrete (TRC) and glass fiber reinforced plastic (GFRP). When TRC has high strength and durability, GFRP has high strength and design flexibility. The advantage of these two materials is combined in the hybrid material obtained. In comparison, while the tensile strength of fiber reinforced concretes is 12 MPa, ultra-high performance concretes 15 MPa, and textile reinforced concretes 44 MPa, the designed hybrid material has 165 MPa tensile strength. The test results showed that the usage of this hybrid structure as a building material is possible. The high tensile strength, low density and high design flexibility of the hybrid material increase the usage of the material in the construction industry [17].

Kurban and Babaarslan 2020, produced hybrid yarns to use at TRC production. AR-Glass and PP filament were combined with the commingling technique. They utilized the Taguchi orthogonal design to optimize the parameters of commingling yarn production. When the effect of hybrid yarn production parameters on breaking strength was

examined, it was determined that the machine speed with 62.6%, air pressure with 15.4%, and the amount of feed with 9.6% had the effect [18].

The braiding technique, which is one of the hybrid yarn production techniques, has been used in textile production for about two centuries. A structure is formed by braiding three or more threads crosswise over each other [19-20]. In the braiding machines, which have two main types as a fixed and variable cross-section, only three-dimensional braiding machines allow the production of products with variable cross-sections [20]. With the technological developments in braiding machines, the usage areas of the products have expanded and their usage in technical applications has increased [21].

Kurban et al. 2017, in their study, alkali-resistant glass filament yarn was used for concrete reinforcement such as raw roving, epoxy resin coated, and hybrid yarn that was produced with the braiding technique. The yarns were not converted to the surface but placed in the concrete in the direction of bending. As a result of the study, samples produced from epoxy coated yarn contributed 78% to flexural strength compared to samples using raw filament yarn, while samples produced using hybrid yarn contributed 12% [22].

In this study, it is focused on whether the braiding technique, which has different applications in the textile industry but has not been studied in concrete reinforcement, can be used to create a textile structure for concrete reinforcement.

## 2. MATERIAL AND METHOD

### 2.1 Material

Carbon roving fibers are used as reinforcement materials in this study. Three different patterns of these materials were used in this investigation: (i) raw yarn, (ii) epoxy resin coated yarn, and (iii) hybrid yarn. Carbon fiber roving (DowAksa) was used as raw yarn for the first pattern. For

the second pattern, carbon fiber roving was coated with epoxy resin (SR 8500/ SD 8605 from Sicomin). For the last pattern, carbon fiber roving for reinforcement material and polypropylene (PP) filament yarn (Aker Textile Yarn) for thermoplastic matrix material were combined to obtain hybrid yarn. Braiding technique, which has different application areas, such as shoelaces and ship rope, was chosen to obtain hybrid yarn. Hybrid yarns were produced by combining reinforcement and matrix components on a tubular braiding machine consisting of 16 spindles (Figure 1). The obtained hybrid yarn is a compact yarn structure in which the reinforcement and thermoplastic component is combined into a single yarn. In order to obtain hybrid yarn with braiding technique, continuous carbon filament was placed in the center where braiding is performed, and PP filaments were placed in the 16 spindles around the center. In the hybrid yarn production process, while the continuous carbon filament moves, the PP filaments on the spindles, rotate around the carbon filament, and thermoplastic component are braided on the reinforcement component. Properties of carbon roving and PP filament yarn were shown in Table 1.



Figure 1. Braiding machine

### 2.2 Method

Three different yarns were transformed into two different textile structures. Each textile structures have 10x40 yarns or 10x8 yarns (Figure 2). The first pattern (raw carbon roving) is wound to a special mold with noches getting textile surface (Figure 3).

Table 1. Properties of hybrid yarn materials

	Linear density (tex)	Density (g/cm <sup>3</sup> )	Tensile strength (MPa)	Young's modulus (GPa)
Carbon	1600	1,78	4200	240
PP	66,6	0,9	550	3,5

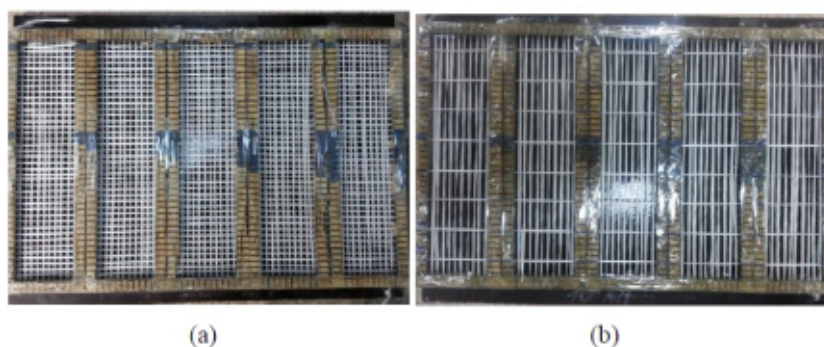


Figure 2. Textile forms using raw roving: (a) 10x40, (b) 10x8



Raw carbon rovings are wound in the mold to form textile structures in two different forms.

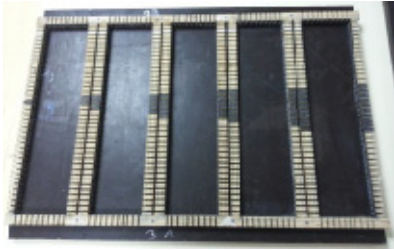


Figure 3. Special molds with notches

For the second pattern, carbon roving coated epoxy resin and they were wound to a frame getting a textile structure. After coated carbon rovings were formed textile structures, all textile structures were put the oven for curing epoxy resin. The epoxy resin coated textile structures were pre-heated and fixed at the appropriate temperature and time as specified in the technical data sheet (TDS).

For the last pattern, hybrid yarns are wound in a frame to form a textile structure (Figure 4). Next, these structures were put in a hot compression device. Matrix fibers (PP filament) melted between hot compression molders. Then the molten thermoplastic component covers the reinforcement component which is the carbon roving. After hot compression, textile structures with hybrid yarns were obtained (Figure 5).

Contrary to molds in which raw carbon filaments are wound, textile surfaces obtained from the epoxy resin coated filament or hybrid yarn are put in different molds (Figure 6). These molds have holes and the strands to be used to fix the structures are passed through these holes. After the concrete pouring process, the structure fixing strands are removed. The textile structures were placed at three different distances from the bottom of the sample: (a) 3 mm, (b) 5 mm, and (c) 10 mm.

TRC is produced from high workability concrete. In order to meet this requirement, fine-grained concrete was chosen as the matrix in the study. Aggregates with a maximum particle size of 0.5 mm were used to obtain fine-grained concrete. In this way, it is ensured that the concrete matrix passes easily through the gaps of the textile structures and settles in the mold homogeneously. After all textile components were prepared, concrete was prepared as shown mix proportions in Table 2.

After the prepared concrete mortar was poured into the lubricated molds, a vibrator was used to better settle the concrete in the mold and to reduce the number of air bubbles. The dried samples were removed from the mold after 1 day and placed in the pool in the curing chamber to be cured according to the TS EN 12390-2 standard [23].

The prepared fine-grained concrete mixture is poured into molds of 150x150x150 mm and 400x100x20 mm. While 150x150x150 mm cubes are used for the compression test, 400x100x20 mm beams were used for the four-point flexural test. According to TS EN 12390-3 standard [24], the compression tests were carried on the 150x150x150mm cubes out in UTEST compression test machine (Type UTC-5750) (Figure 7, a). The loading rate was chosen at 4 kN/sec. The average compressive strength of a cube specimen was measured as 52,3 MPa. According to TS EN 12390-5 standard [25], the four-point flexural tests were carried on the 400x100x20mm beams out in ELE flexural test machine (Model 37-6330) (Figure 7, b). The loading rate was chosen at 0,05 kN/sec.

A comparator was attached in the mid-span (Figure 7b). During the test, when the deflection was measured from the comparator, the load was measured by the load cell in the test machine, too. The placement of the sample in the flexural test machine is seen in Figure 8.

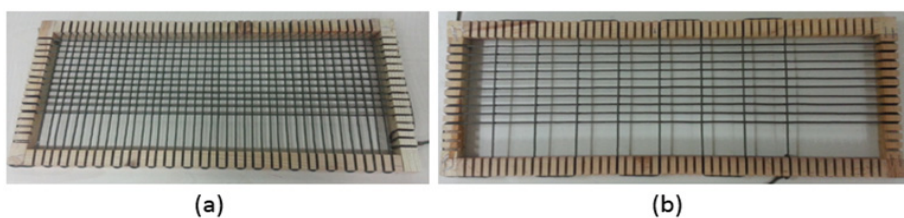


Figure 4. Frames to form textile structures from hybrid yarns: (a) 10x40, (b) 10x8

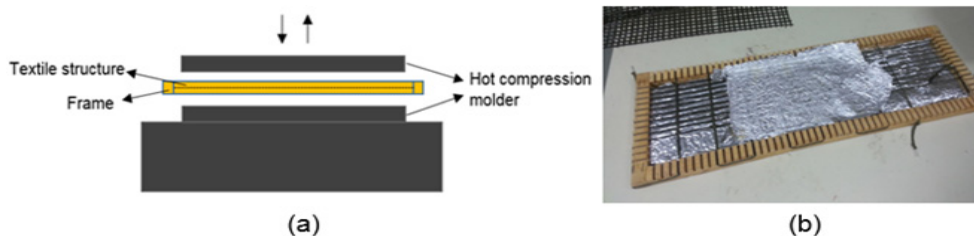


Figure 5. (a) Hot compression device, (b) Textile structure after hot compression



Figure 6. Special molds with holes for structure production from epoxy resin coated filament or hybrid yarn

Table 2. Fine-grained concrete matrix composition

Material	Cement CEM I 42,5 R	Fly ash	Siliceous fines (0-0.3 mm)	Siliceous sand (0.2-0.5 mm)	Superplasticiser	Water
Content (kg/m <sup>3</sup> )	480	240	642	503	10,8	284



(a)

(b)

Figure 7. (a) Compression test machine (b) Flexural strength test machine

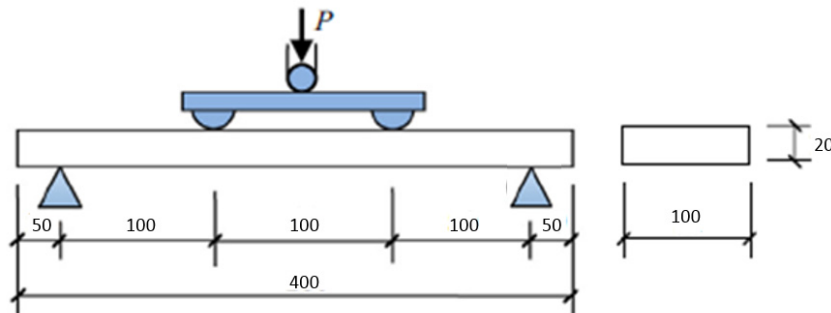


Figure 8. Four-point bending test setup and sample sizes

The flexural behavior of the different test specimens were compared according to TS EN 12390-5. According to the test standard, the deflection and flexural stress was expressed [25]. The results of the experiment are described as flexural strength and load-deflection curves. The flexural strength is calculated by Equation (1).

$$\sigma = \frac{(Pl)}{(bh^2)} \quad (1)$$

Where  $\sigma$  is the flexural strength,  $P$  is the load,  $l$  is the span of the specimen,  $b$  is the width of the cross-section, and  $h$  is the height of the cross-section.

The area under the load-deflection curve gives the flexural toughness. The evaluation of the flexural toughness of the

TRC specimens was carried out by adopting the energy method. The energy absorption is calculated by Equation (2).

$$W = \int_0^{\delta} F d\delta \quad (2)$$

$W$  is the energy absorbed by the specimen, N mm;  $\delta$  is the mid-span deflection, mm;  $F$  is the load, N.

### 3. RESULTS AND DISCUSSION

#### 3.1 Flexural strength

The flexural strength of samples are shown in Figure 9. The use of carbon roving as a reinforcement component

contributed to the flexural strength for each reinforcement type, on both textile structures and at all distances. There are different parameters in the study such as reinforcement type, reinforcement location, and textile structure type. The effect of these parameters were explained in the next sections. The unreinforced concrete sample was coded as WR (without reinforced). The samples with raw carbon roving were coded as RC. The samples with epoxy resin coated carbon roving were coded as EC. The samples with hybrid yarn were coded as HY.

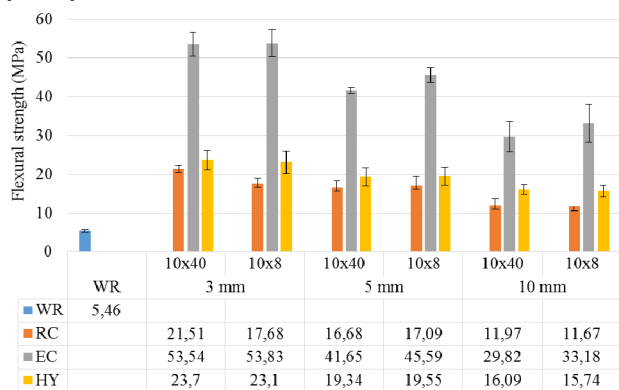


Figure 9. Flexural strength of TRC samples

### 3.1.1 Effect of reinforcement type

The flexural strength of all samples with reinforcement is higher than that of without reinforcement. As seen in Figure 9, the greatest contribution to the flexural strength was obtained in the samples where epoxy-coated textile structures were used. The lowest contribution was obtained in the samples using raw carbon filament. Based on the highest mean flexural strength values, the reinforced samples showed an increase in flexural strength of approximately 9.8 times with epoxy resin coated carbon roving, 4.3 times with hybrid yarn, and 3.6 times with raw carbon roving compared to the unreinforced sample. Even at its lowest flexural strength values, epoxy resin coated carbon roving contributed 446%, hybrid yarn 188%, and raw carbon roving 114% according to the unreinforced sample. Each reinforcement component contributed to the flexural strength thanks to its mechanical properties. With the contribution of the thermoplastic structure in the hybrid yarn structure, the flexural strength increased compared to the raw filament samples. In the use of epoxy resin, a high flexural strength has been obtained due to the superior mechanical properties of the material. For example, when the 10x8 reinforcement component is used at 3 mm, hybrid yarn contributed 30.7% and epoxy coated contributed 204.4% according to the raw carbon roving.

### 3.1.2 Effect of reinforcement location

As seen in Figure 9, flexural strength increases as the textile structure get closer to the sample base. As the textile reinforcement structures approached the sample bottom, they contributed more to the flexural strength as more stress was created in the sample bottom during bending. In the

10x40 textile structures, for raw carbon roving, when the textile structures are placed 5 mm, it gives 39,3% better flexural strength than 10 mm, when the textile structures are placed 3 mm, it gives 29% better flexural strength than 5 mm. For epoxy resin coated carbon roving when the textile structures are placed 5 mm, it gives 39,7% better flexural strength than 10 mm, when the textile structures are placed 3 mm, it gives 28,5% better flexural strength than 5 mm. For hybrid yarn, when the textile structures are placed 5 mm, it gives 20.2% better flexural strength than 10 mm, when the textile structures are placed 3 mm, it gives 22.5% better flexural strength than 5 mm. In the 10x8 textile structures, for raw carbon roving, when the textile structures are placed 5 mm, it gives 46,4% better flexural strength than 10 mm, when the textile structures are placed 3 mm, it gives 3,5% better flexural strength than 5 mm. For epoxy resin coated carbon roving when the textile structures are placed 5 mm, it gives 37,4% better flexural strength than 10 mm, when the textile structures are placed 3 mm, it gives 18,1% better flexural strength than 5 mm. For hybrid yarn, when the textile structures are placed 5 mm, it gives 24,2% better flexural strength than 10 mm, when the textile structures are placed 3 mm, it gives 18,2% better flexural strength than 5 mm.

### 3.1.3 Effect of textile structure type

In this study, two different textile structures such as 10x40 and 10x8 were used. While the number of yarns in the bending direction was kept constant, the number of yarns in the other direction was changed. In the use of epoxy resin coated carbon roving, the flexural strength of 10x8 textile structures is higher than 10x40 textile structures. The flexural strength of samples with 10x8 textile structure placed at 3 mm, 5 mm, and 10 mm increased by approximately 1%, 9,5%, and 11,3%, respectively, compared to samples with 10x40 textile structure. In the raw carbon roving and hybrid yarn, the flexural strength of both textile structures is similar, except raw carbon roving at 3 mm. In the raw carbon roving at 3 mm, 10x40 textile structure contributed 21,6% according to the 10x8 textile structure.

### 3.2 Load-deflection curve

In order to explain the flexural strength of textile reinforced concrete, the bending state of composite structures should be examined. The bending behavior of textile reinforced concrete under load can be modeled as the load-deflection curve shown in Figure 10. The load-deflection curve technically consists of two main regions and is defined as Case I: Uncracked concrete and Case II: Crack stabilization [5, 26].

State I corresponds to the elastic state of the textile-reinforced concrete element without cracks, where the stiffness is purely a function of the concrete matrix. It consists of a linear slope in this region. The first cracking

occurs when the tensile strength of the concrete is reached, and then the stress in the crack area initiates the stresses in the textile component used as reinforcement. At the end of crack formation it stabilizes in State II, where stress reinforcement of the concrete is said to be effective. In this region, it consists of a linear but lower slope than in State I. Finally, in the end of State II, when the reinforcement component in the textile-reinforced concrete reaches its final limit load, the test sample breaks when the filament breaks or the filament is pulled out [5, 26].

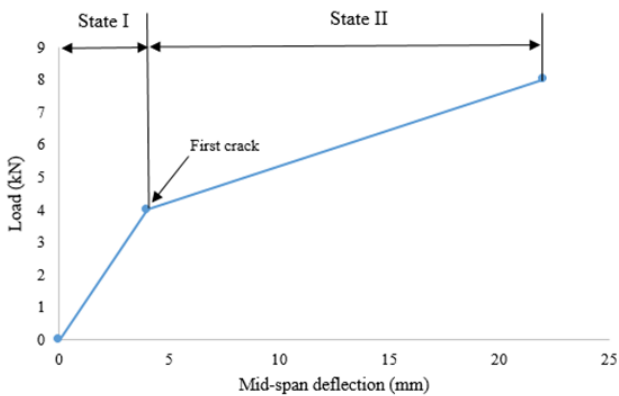


**Figure 10.** Load versus mid-span deflection for TRC under four-point bending, with indicated stages

The load-deflection curves of the samples produced from different reinforcement types are shown in Figure 11. In order to observe the effect of the reinforcement type, the load-deflection curves of the samples with 10x40 or 10x8 textile structures which give the highest load value, are placed at 3 mm, were examined. To compare the load-deflection curves, the load and direction axis values are kept constant. All curves were plotted up to the maximum load. As seen in Figure 11, all samples showed similar behavior up to the part where the first crack occurred. After the first crack formation, the slope of the load-deflection curve decreases. However, samples with raw filament and hybrid yarn have a similar and low slope, while epoxy resin

coated samples have a greater slope. Hybrid yarn samples gave greater load and deflection value according to samples with raw carbon roving. It is thought that the thermoplastic reinforcement in the hybrid yarn protects the reinforcement filament and contributes more to the flexural strength, causing an increase in load and deflection. For example, in the use of 10x40 textile structure at 3 mm, for 2 kN load, a deflection value of 3,2 mm was obtained by raw filament, while a deflection value of approximately 4,3 mm was obtained in the use of hybrid yarn.

The load-deflection curves of the samples obtained when the textile structures are placed at different distances are shown in Figure 12. In order to observe the effect of the reinforcement location, the load-deflection curves of the epoxy resin coated samples with 10x40 or 10x8 textile structures were examined. In order to compare the load-deflection curves, the load and direction axis values are kept constant. All curves were plotted up to the maximum load. Since the highest flexural strengths were obtained in epoxy resin coated samples, the effect of reinforcement location was investigated in these samples. As can be seen in Figure 12, the first crack formation in all samples took place a bit later than in the unreinforced sample. After the first crack formation, the slope of the load-deflection curve increases from 10 mm to 3 mm. A greater load is required to achieve the same deflection value as the reinforcement component approaches the bottom of the sample. For example, in the use of 10x8 textile structure, for 4 mm deflection, a load value of 6 kN was obtained at 3 mm, a load value of 4,5 kN was obtained at 5 mm, and a load value of 3,5 kN was obtained at 10 mm. Textile reinforcement components should be placed close to the sample bottom in order to obtain greater flexural strength for a constant deflection value. In addition, when Figure 12 is analyzed, it is seen that 10x8 textile structures give higher load and deflection values than 10x40 textile structures. It is thought that the reason for this is that the 10x8 textile structures allow the concrete to flow more due to the hollow structure and the concrete matrix-textile reinforcement bonding is more.

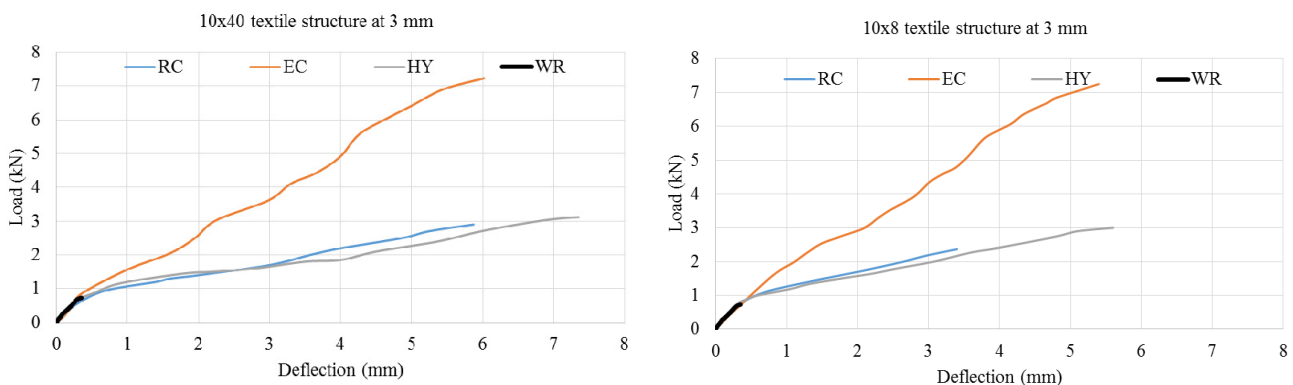


**Figure 11.** Load-deflection curves of the samples with 10x40 and 10x8 textile structure at 3 mm



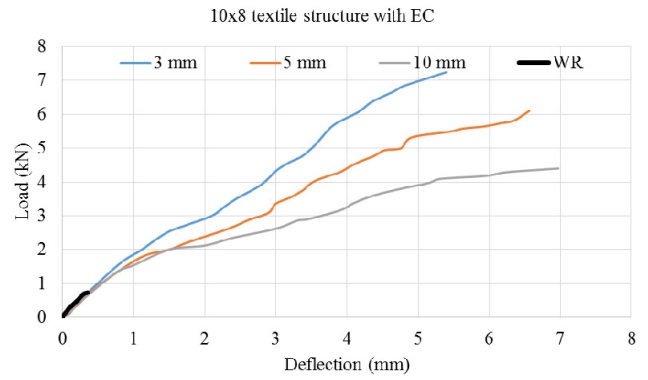
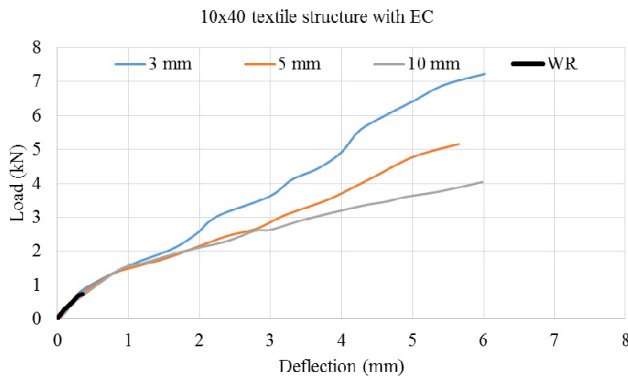


Figure 12. Load-deflection curves of the epoxy resin coated samples with 10x40 and 10x8 textile structure

### 3.3 Flexural Toughness

The energy absorptions of samples are shown in Figure 13. The effect of reinforcement types, reinforcement location, and textile structure type on energy absorption is seen in Figure 13.

The use of epoxy resin coated or hybrid yarn as a reinforcement component contributed to the energy absorption for each textile structure and at all distances according to samples with raw carbon roving. In the use of epoxy resin coated yarn, the energy absorption of 10x8 textile structures is higher than that of 10x40 textile structures. This is a similar result to that of the flexural strength graph.

When the energy absorption and flexural strength graphs are examined, it is seen that they are similar to each other. While samples with epoxy resin coated to give the highest values, samples with raw filament give the lowest values. For 10x40 textile structures, while the flexural strength of samples with hybrid yarn textile structures placed at 3 mm, 5 mm, and 10 mm increased by approximately 10,2%, 16%, and 34,4% respectively, compared to samples with raw filaments, the energy absorption of samples with hybrid yarn textile structures placed at 3 mm, 5 mm, and 10 mm increased by approximately 73,4%, 115,1%, and 253,6% respectively. For 10x8 textile structures, while the flexural strength of samples with hybrid yarn textile structures placed at 3 mm, 5 mm, and 10 mm increased by approximately 30,7%, 14,4%, and 34,9% respectively, compared to samples with raw filaments, the energy absorption of samples with hybrid yarn textile structures placed at 3 mm, 5 mm, and 10 mm increased by approximately 100%, 97,3%, and 92,4% respectively. The use of hybrid yarn instead of raw filament made a greater contribution to energy absorption according to flexural

strength. The reason for this is that the thermoplastic structure in the hybrid yarn contributes more to the deflection as well as the increase in flexural strength.

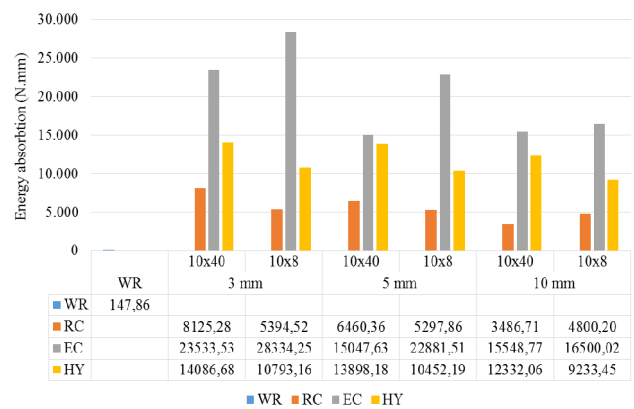


Figure 13. Energy absorption of samples

### 3.4 Failure Modes

In this section, crack images of the samples after the flexural test are given in Figure 14. The fracture images of raw, epoxy resin-coated and hybrid-fiber carbon filament reinforced samples placed at a distance of 3 mm from the base after the flexural test are given. When Figure 14 is examined, it has been observed that fractures occur in the vertical and diagonal directions to the bending axis in the samples where raw filament structures are used. In the samples where epoxy resin coated and hybrid yarn structures were used, fractures occurred along the bending axis and in the diagonal direction. Fracture formations show that the bond between the textile structure and the concrete is good or moderate in samples where raw filament textile surfaces are used. The fractures in the samples where epoxy resin coated and hybrid yarn structures are used show that

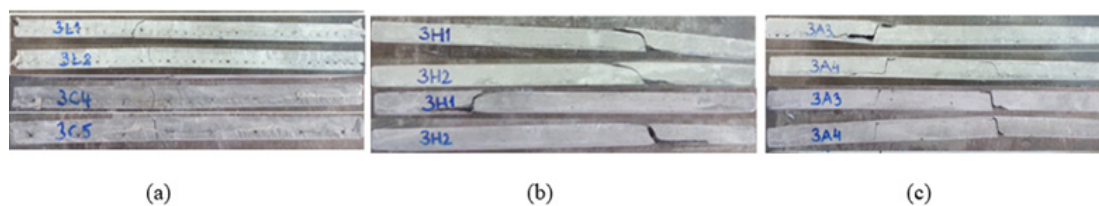


Figure 14. Failure modes of specimens with different materials (a) RC, (b) EC, (c) HY

the connection between the textile structure and the concrete is moderate or weak. While covering the raw filament with epoxy resin or using it in the form of hybrid yarn increases the flexural strength of the structure, it reduces the textile structure-concrete bond.

#### 4. CONCLUSION

This article has shown the effect of the reinforcement types, reinforcement location, and textile structures on the flexural behavior of TRC by analyzing the results of four-point flexural tests. The main conclusions are as follows:

- All reinforcements contributed to the flexural strength according to unreinforcement sample. While epoxy resin coated samples provided the highest contribution, the lowest contribution was obtained in raw roving samples.
- The textile reinforcement structures contributed more to the flexural strength as they approached the sample bottom, as it better accommodated the stress on the sample bottom during bending.
- When 10x40 textile structures were placed at 3 mm for all reinforcement types, it gave more deflection than 10x8 textile structures. When the flexural strengths are examined, 10x40 textile structures in the use of raw carbon roving and hybrid yarn have higher values at other usage distances except 5 mm. In the use of epoxy

resin coated yarn, 10x8 textile structures showed better flexural strength than 10x8 textile structures.

- The toughness distribution is similar to the flexural strength distribution of the samples. However, since the melted thermoplastic structure increased the deflection in the hybrid yarn samples, its contribution to the toughness was more.
- While the textile structure-concrete connection is good and moderate in raw filament samples, the connection is moderate and weak in epoxy resin and hybrid yarn samples.
- Although the hybrid yarn samples did not show sufficient flexural strength compared to the epoxy coated samples, it contributed to the flexural strength compared to the raw filament use. It has been observed that hybrid yarn structures have the potential to be used in concrete reinforcement.

#### Acknowledgement

This research is supported by “Scientific Research Projects Governing Unit of Çukurova University” with the project number of FDK-2016-6682. Also, the authors wish to thank to Kord Industrial Rope and Yarn Industry and Trade Inc for hybrid yarn production, Çimsa Cement Industry and Trade Inc. that we used their materials and laboratory.

#### REFERENCES

1. Bagherzadeh R, Sadeghi AH, Latifi M. 2011. Utilizing polypropylene fibers to improve physical and mechanical properties of concrete. *Textile Research Journal* 82(1), 88-96.
2. Yao W, Li J, Wu K. 2003. Mechanical properties of hybrid fiber-reinforced concrete at low fiber volume fraction. *Cement and Concrete Research* 33, 27-30.
3. Holler S, Butenweg C, Noh SY, Meskouris K. 2004. Computational model of textile-reinforced concrete structures. *Computers and Structures* 82, 1971–1979.
4. Du Y, Zhang, X, Liu L, Zhou F, Zhu D, Pan W. 2018. Flexural Behaviour of Carbon Textile-Reinforced Concrete with Prestress and Steel Fibres. *Polymers* 10 (98), 1-19.
5. Brameshuber W. 2006. *Textile Reinforced Concrete, In State-of-the-art Report of RILEM Technical Committee 201-TRC*. Bagnaux, France: RILEM Publications S.A.R.L.
6. Scholzen A, Chudoba R, Hegger J. 2015. Thin-walled shell structures made of textile-reinforced concrete Part I: Structural design and construction. *Structural Concrete* 16 (1), 106-114.
7. Sharei E, Scholzen A, Hegger J, Chudoba R. 2017. Structural behavior of a lightweight, textile-reinforced concrete barrel vault shell. *Composite Structures* 171, 505–514.
8. Häußler-Combe U, Harting J. 2007. Bond and failure mechanisms of textile reinforced concrete (TRC) under uniaxial tensile loading. *Cement & Concrete Composites* 29, 279–289.
9. Gao SL, Mäder E, Plonka R. 2007. Nanostructured coatings of glass fibers: Improvement of alkali resistance and mechanical properties, *Acta Mater* 55 (3), 1043–1052.
10. Scheffler C, Gao SL, Plonka R, Mäder E, Hempel S, Butler, M, Mechtcherine V. 2009. Interphase modification of alkali-resistant glass fibres and carbon fibres for textile reinforced concrete I: Fibre properties and durability. *Composites Science and Technology* 69, 531–538.
11. Golzar M, Brünig H, Mäder E. 2007. Commingled Hybrid Yarn Diameter Ratio in Continuous Fiber-reinforced Thermoplastic Composites. *Journal of Thermoplastic Composite Materials* Vol. 20, 17-25.
12. Alagirusamy R, Figueiro R, Ogale V, Padaki N. 2006. Hybrid Yarns and Textile Preforming for Thermoplastic Composites. *Textile Progress* 38:4, 1-71.
13. Halvaei M, Jamshidi M, Latifi M, Ejtemaei M. 2020. Experimental investigation and modelling of flexural properties of carbon textile reinforced concrete. *Construction and Building Materials* 262, 120877.
14. Kravaev P, Janetzko S, Gries T, Kang B, Brameshuber W, Zel M, Hegger J. 2009, June. Commingling Yarns for Reinforcement of Concrete. 4th Colloquium on Textile Reinforced Structures (CTRS4), 17 – 28. Dresden, Germany.
15. Merter NE, Başer G, Tanoğlu M, 2016. Effects of hybrid yarn preparation technique and fiber sizing on the mechanical properties of continuous glass fiber-reinforced polypropylene composites. *Journal of Composite Materials* Vol. 50(12),1697–1706.
16. Hengstermann M, Raithel N, Abdkader A, Hasan MMB, Cherif C. 2016. Development of new hybrid yarn construction from recycled carbon fibers for high performance composites. Part-I: basic processing of hybrid carbon fiber/polyamide 6 yarn spinning from virgin carbon fiber staple fibers. *Textile Research Journal* Vol. 86(12), 1307–1317.



- 
17. Funke H, Gelbrich S, Ehrlich A. 2013. Development of a new hybrid material of textile reinforced concrete and glass fibre reinforced plastic. *Procedia Materials Science* 2, 103 – 110.
  18. Kurban M, Babaarslan O. 2020. High Performance Hybrid Yarn Development and Optimization of Production Parameters for Using in Textile Reinforced Concrete Production. *Journal of Textiles and Engineer* 27: 120, 292- 298.
  19. Ayranci C, Carey J. 2008. 2D braided composites: A review for stiffness critical applications. *Composite Structures* 85, 43–58.
  20. Kyosev Y. 2015. *Braiding Technology for Textiles*. Cambridge: Woodhead Publishing Limited.
  21. Gries T, Veit D, Wulfhorst B. 2015. *Textile Technology*. München: Hanser Publishers.
  22. Kurban M, Babaarslan O, Çağatay İ.H, 2017. Hybrid Yarn Composites for Construction. Kumar B and Thakur S, Editor, *Textiles for Advanced Applications* London: InTech Open, 135-160.
  23. TS EN 12390-2. 2019. Testing hardened concrete - Part 2: Making and curing specimens for strength tests, Ankara.
  24. TS EN 12390-3. 2010. Testing hardened concrete-Part 3: Compressive strength of test specimens, Ankara.
  25. TS EN 12390-5. 2010. Testing hardened concrete - Part 5: Flexural strength of test specimens, Ankara.
  26. Williams Portal, N, Nyholm Thrane, L, Lundgren, K. 2017. Flexural behaviour of textile reinforced concrete composites: experimental and numerical evaluation. *Mater Struct* 50, 4.